Investigation of Novel Screen-Printed Electrochemical Sensors for Measuring 17β-estradiol in an Aqueous Environment

By

Auwal Muhammad Musa

A thesis submitted in partial fulfilment of the requirements of the University of The West of England, Bristol, for the degree of

Doctor of Philosophy

Faculty of Environment and Technology,

University of the West of England

May 2024

Dedication

To my father, Musa Muhammad; my mother, Aisha Musa; and siblings, for their support throughout my life.

Acknowledgement

In the name of Allah, the Most Gracious and the Most Merciful.

"It takes a whole village to raise a child" - African proverb. So, it is safe to say, "it took a whole village to produce this thesis".

Thanks to my wonderful supervisor, Professor Janice Kiely, for the opportunity to pursue this educational journey and tremendous learning throughout the past years. Your professionalism and kindness made the journey memorable, starting with the first email and ending with this dissertation. Next is Professor Richard Luxton; your apt feedback and guidance are appreciated. Thanks to Dr Kevin Honeychurch for your kindness, prompt feedback, scientific talks, and helpful suggestions that widened my horizon.

I want to express my gratitude to Nigeria's Government Petroleum Technology Fund Scholarship (PTDF/ED/OSS/PHD/AMM/1519/19) programme gratefully acknowledged; thank you for allowing me to do this PhD programme for development knowledge and support. I want to express my gratitude to Palintest Limited and the University of the West of England for the opportunity to use their facilities and various support that made this PhD project possible. Thanks to Dr James Iacobini and Dr Samantha Lunn of Palintest for their help. I want to thank Dr David Patton for the SEM analysis. Thanks to Dr David Ferrier for brainstorming, the beautiful lab and discussion times, and Dr Paul Worgan for your tremendous support and help.

Abstract

The hormone 17β-estradiol (E2) is increasingly prevalent in environmental waters globally, posing a significant threat to human and animal health due to its adverse effects on endocrine functions. Traditional methods of analysing E2 are complex and time-consuming, lacking the ability to provide real-time analysis. Electrochemical sensors that utilize screen-printed electrodes present a cost-effective, uncomplicated, and portable alternative for conducting on-site analyses. There is a research gap regarding using nanomaterials as modifiers for screen-printed electrodes in developing electrochemical sensors to monitor environmental estradiol. This thesis examines modifying screen-printed electrode surfaces with carbon-based materials to provide cost-effective materials for electroanalysis of the E2 hormone. This study emphasises the employment of carbon materials in the electrochemical analysis of E2. Various techniques are utilized to study the sensors' electrochemical properties and structural characteristics, including cyclic voltammetry (CV), amperometry, and differential pulse voltammetry (DPV). In addition, methods such as scanning electron microscopy (SEM), ultraviolet-visible absorption spectroscopy (UV-Vis), Fourier-transform infrared (FTIR), and Raman spectroscopy are employed to elucidate the physical and chemical structures of materials. Chapter 2 presents foundational information on this thesis's fundamental electrochemistry and conventional electrochemical methods. Additionally, this chapter provides an extensive survey of prior research concerning using screen-printed electrodes for E2 analysis. Chapter 3 results illustrate that a carbon spherical shell material modified screen-printed electrode (CSSM/SPE) has two linear plots within concentration ranges of 0.83 – 2.49 μM (8.3×10^{-7} – 2.49×10^{-6} M) and 3.31 –

4.98 μM (3.31×10^{-6} - 4.98×10^{-6} M). The limit of detection (LOD) was calculated as (n = 3), the standard deviation of the signal response against the slope of the calibration plot. For lower and higher concentration ranges, the sensitivities were 0.273 $\mu A \mu M^{-1}$ cm^{-2} and 0.118 $\mu A \mu M^{-1}$ cm^{-2} for CSSM/SPE and 0.244 $\mu A \mu M^{-1}$ cm^{-2} for bare SPE, respectively.

Chapter 4 explores the use of graphene-based electrodes in the electrochemical determination of E2 using an amperometric method and illustrates that the direct electrooxidation of E2 offers advantages. These include cost-effectiveness, eliminating the need for expensive enzymes, and stability against temperature and pH changes. Graphene has remarkable properties such as high electron transfer, high conductivity, robust mechanical characteristics, and a large surface-to-volume ratio. Although many electrochemical sensors suffer from electrode fouling due to the electrochemical oxidation of E2's phenolic group, which forms an insoluble layer on the working electrode and affects performance, graphene-based electrodes can overcome this challenge. In this study, graphene screen-printed electrodes (GHSPE), electrochemically exfoliated graphene-modified electrodes (EEFGHSPE), and 3D graphene foam screen-printed electrodes (3D-GFSPE) were compared. The analytical performance of these sensors was observed at an applied potential of +0.65 V (vs. Ag/AgCl) across the concentration range of 0.83 to 4.98 μM (8.3×10^{-7} - 4.98×10^{-6}) estradiol. Sensitivities of 0.495 $\mu A \mu M^{-1} cm^{-2}$, 0.121 $\mu A\ \mu M^{-1} cm^{-2}$, and 0.264 $\mu A\ \mu M^{-1} cm^{-2}$ were determined for GHSPE, 3D-GFSPE, and EEFGHSPE, respectively, with detection limits (LODs) of 0.71 μM (7.1×10^{-7} M), 0.41 μM (4.1×10^{-7} M), and 0.33 μM (3.3×10^{-7} M) (n=3). Subsequently, the possibility of determining E2 levels in a potable tap water sample by amperometry was investigated over the

concentration range of 0.83 – 4.98 µM (8.3×10^{-7} - 4.98×10^{-6}) M. In Chapter 5, a screen-printed electrode (SPE) modified with gold nanoparticles decorated within reduced graphene oxide carbon nanotubes (rGO-AuNP/CNT/SPE) was studied for E2 determination. The AuNPs were produced through an eco-friendly method utilizing a plant extract, eliminating the need for less environmentally friendly chemicals and reagents, and removing the requirements of sophisticated fabrication methods and tedious procedures. Additionally, rGO-AuNP serves as a dispersant for the CNT to improve the dispersion stability of CNTs. The composite rGO-AuNP/CNT/SPE exhibited a notable improvement compared to bare/SPE and GO-CNT/SPE, as evidenced by the relative peak currents. The optimized E2 sensor offers linear sensitivity from 0.05 - 1.00 µM (5×10^{-8} - 1×10^{-6} M) with an LOD of 3.4 nM (3.4×10^{-9} M) based on three times the standard deviation (3σ). Notably, this sensing approach yields stable, repeatable, and reproducible outcomes. Assessment of drinking water samples indicates an average percentage recovery of 97.5% for samples fortified with E2 at concentrations as low as 0.5 µM, with a coefficient of variation (% CV) value of 2.7%. Chapter 6 investigated the use of a disposable electrochemical sensor that utilised a deep eutectic solvent (DES), molecularly imprinted polymer (MIP), and carbon paste printed electrode (CPE). The DES served as a solvent binder for MIP and for the homogenization of the carbon paste. The MIP was made conductive with carbon paste for electrochemical transduction. This method addresses the slow diffusion and rebinding kinetics of analytes and the cavities of the MIP for use in electrochemical sensors as disposable sensors that afford simplicity, ease of production, and low cost.

Contents

List of Figures

List of Tables

Acronyms and Abbreviations

AFM	Atomic force microscopy
Ag/AgCl	Silver/Silver chloride
AU	Arbitrary units
AuNP	Gold nanoparticle
BPPG	Basal plane pyrolytic graphite
BRB	Britton Robinson Buffer
CA	Chronoamperometry
CE	Counter electrode
CP	Carbon paste
CNT	Carbon nanotube
CV	Cyclic voltammetry
DI	Deionized water
DES	Deep eutectic solvent
DMSO	Dimethyl sulfoxide
DPV	Differential pulse voltammetry
E2	Estradiol
EDX	Electron dispersive X-ray

EEDC	Estrogenic endocrine-disrupting chemicals
EDCs	Endocrine disruptors
EPPG	Edge plane pyrolytic graphite
EIS	Electrochemical impedance spectroscopy
EF	Electrolytic exfoliation
FTIR	Fourier transform infrared spectroscopy
GCE	Glassy carbon electrode
GO	Graphene oxide
rGO-AuNP	reduced graphene oxide-gold nanoparticle
LOD	Limit of Detection
LOQ	Limit of quantification
LR	Linear Range
MIT	Molecularly Imprinting technology
MIP	Molecularly Imprinted polymer
MWCNT	Multi-walled carbon nanotubes
NIP	Non-imprinted polymer
NPs	Nanoparticles
PBS	Phosphate buffer solution
PSS	Polystyrene sulfonate

RE	Reference electrode
rGO	Reduced graphene oxide
SEM	Scanning electron microscopy
SPGP	Screen-printed graphene paste
SPCE	Screen-printed carbon electrode
SPE	Screen printed electrode
SPGE	Screen-printed graphene electrode
SP	Screen-printing
UV-Vis	Ultraviolet-visible spectroscopy
WE	Working electrode

List of Symbols

β	Beta
Ipa	Anodic current peak
Epa	Anodic peak potential
Ipc	Cathodic current peak
Epc	Cathodic peak potential
Ip	Current peak
Ep	Peak Potential
D	Diffusion coefficient
ψ	Dimensionless rate parameter
k^0	Heterogeneous rate constant
ΔEp	Peak to peak separation
A	Area of electrode
C	Concentration of the bulk solution
F	Faraday's constant
R	Molar gas constant

Chapter 1 Introduction

This chapter introduces the thesis, delving into its motivation, aims and scope. It presents background on environmental monitoring with a focus on 17β-estradiol hormone, the research objectives, and an outline of the structure of the thesis.

1.1 Motivation

The supply of safe drinking water is paramount for the health and well-being of people across the globe [1]. Unfortunately, various anthropogenic activities, particularly industrialisation, have strained our available water resources. Industries produce waste in many forms, including hormonal pollutants that find their way into the environment and pose significant threats to water supplies [2]. Confidence in our water supply is imperative as it helps us accurately trace pollution sources through water testing. Regular testing makes this possible, ensuring we maintain high safety levels and identify potential risks before they escalate into more significant problems [2-3].

Despite the advancements in water testing technology, current measurement techniques still have significant challenges. It often takes several days and requires multiple steps, such as sample collection, storage, transportation, and treatment, before analysis can be conducted at centralised laboratories; this contributes to higher costs. This has created an urgent need for rapid testing methods that offer stand-alone devices positioned remotely in various locations throughout the modern water industry. This solution would provide more efficient results and increase safety measures [4].

In the early 21st century, there was a significant increase in interest in using screen-printing technology to fabricate screen-printed electrodes (SPEs), which are miniature sensors ideal for point-of-use applications [5]. These devices offer simplicity, affordability and portability compared to laboratory-based analytical instruments. This makes it possible to analyse outside of traditional laboratories at point-of-use sites while achieving accurate results from low-cost devices due to the mass production capabilities inherent in this technology [5]. By integrating electroanalytical techniques, SPEs have been successfully applied to various environmental and clinical monitoring analytes.

The glucose sensor is one of the most prized achievements, surpassing traditional and mercury electrodes in electroanalysis. Screen-printed electrodes have ushered in a new era of cost-effective miniaturisation that can be mass-produced for use with portable instruments in the field. The current trend towards designing sensitive, specific, continuous monitoring, wash-free and calibration-free sensors aims to overcome existing screen-printed electrode technology limitations.

This has brought forth a new golden age of screen-printed sensing platforms, which could be applied across various domains such as the food industry, healthcare systems or environmental assessments where versatility plays an important role [5]. To enhance their performance, it would be highly beneficial if the sensitivity of this platform was improved, thereby providing enhanced results from these sensing devices [6-7].

1.2 Environmental Monitoring of 17β-estradiol

The monitoring of trace quantities of 17-β-estradiol (E2) in drinking water is imperative from an environmental standpoint owing to the possible health hazards associated with it, such as a heightened likelihood of breast and ovarian cancer as well as alterations to reproductive, immune, and nervous systems [1]. The suggested maximum level for E2 in surface water is 1.47×10^{-12} M [2]. E2 is the most potent of all estrogens produced by the ovaries. It is responsible for developing and maintaining the female and male reproductive systems. However, E2 has also been identified as an endocrine-disrupting compound by humans and domestic animals. It has high estrogenic activity and has been identified on the European Water Framework Directive Watch List [2]. Methods such as high-performance liquid chromatography (HPLC) [3], various spectroscopic [4], electrochemiluminescence [5], colourimetry [6], and surface-enhanced Raman spectroscopy [7] have been reported for E2 determination. These all suffer from setbacks related to their need for complex instrumentation, time-consuming analysis processes, the need for highly trained personnel, an inability to perform real-time analysis, and high cost. In addition, determining E2l in water requires complex laboratory protocols, from sample collection to transportation and preparation.

In contrast, electroanalysis offers simplified operation, miniaturised, portable tools, quick analysis time, and analytical proficiency. For many years, mercury electrodes set the standard in electroanalysis, especially for detecting heavy metals via stripping voltammetry, until they were phased out by other alternatives, such as ultramicroelectrodes, rotating disk electrodes, and boron-doped diamonds. Following these, the advent of screen-printed electrodes (SPE)

emerged as a cost-effective and versatile alternative to traditional solid electrodes. Consequently, SPEs serve as an outstanding non-laboratory-based analytical platform that can fulfil the demand for low-cost, on-site devices capable of measuring E2 in water while eliminating costly laboratory techniques.

1.3 Aim of the work

This PhD study aims to investigate the application of screen-printed electrochemical sensors for the measurement of estradiol in water to enable rapid, low-cost environmental monitoring.

To achieve this, the following objectives were formulated:

1. To comprehensively review existing literature on screen-printed sensors used in E2 detection, emphasising, and identifying gaps within the body of research gaps in electrode materials, surface modifications, and measurement techniques.
2. To design and fabricate screen-printed sensors using carbon spherical shell synthesised hydrothermally, electrolytically synthesised graphene using a graphite rod and compare its sensing performance to the commercially available graphene-based sensor and carbon nanotubes in composite materials to improve electron transfer and sensitivity of screen-printed sensors for electroanalytical applications.
3. To understand the electrochemical oxidation of E2 on novel carbon electrode materials (carbon spherical shell material (CSSM), electrochemically exfoliated graphene (EEFGH), reduced graphene oxide decorated with gold nanoparticles and carbon nanotubes composite (rGO-AuNP/CNT.) modified

SPEs using cyclic voltammetry, differential pulse voltammetry and amperometry.

4. Integrate electrode materials and molecularly imprinted polymers (MIPs) into a sensor and evaluate their analytical selectivity towards E2. This will involve exploring amperometric methods for achieving optimal performance and reliability in selective sensor design, ultimately resulting in an enhanced understanding of MIP applications.

1.4 Structure of the Thesis

The thesis is organised into seven chapters.

This chapter provides the general introduction, motivation, and context for the research work, as well as the structure of the thesis and an outline of the dissemination of the research findings via presentations at conferences and publications in peer-reviewed journals.

Chapter 2 provides an extensive literature review on the current state-of-the-art research about utilising SPEs in analysing E2, including a brief discussion on various electrochemistry methods such as amperometry, cyclic voltammetry and differential pulse voltammetry employed within this thesis. The broad applications of SPEs and their use within electrochemistry are described, and their status, drawbacks, and future opportunities are summarised. In addition, it highlights the multiple materials used in the electroanalysis of estradiol.

Chapter 3 explores the application of carbon spherical shell material (CSSM) on screen-printed electrodes for E2 determination. In addition, solvent pre-treatment of the SPEs was tested as a facile mean of activating SPEs (pre-treatment techniques have been discussed in section 2.7.1 in detail). These preliminary

results led to further development with carbon spherical shell material used for modifying the SPEs, which were synthesized hydrothermally and characterized based on their amperometric performance and other properties analysed.

Chapter 4 investigates the process of electrochemical synthesis of graphene and its application as a modifier on bare SPE. The chapter details a simple method for synthesizing uniform graphene through electrolytic exfoliation of graphite rods, avoiding harsh chemicals commonly used in other methods. A comparison between commercially available electrodes (EFFGH-SPE, GHP-SPE, and 3DGF-SPE) and those obtained by electrochemical exfoliation is presented to evaluate their efficacy in detecting E2. Morphological, structural, and electrochemical properties are analysed using SEM, TEM, FT-IR and DLS techniques.

Chapter 5 introduces a novel electrochemical screen-printed sensor for detecting E2 based on a composite material of reduced graphene oxide-carbon nanotubes decorated with gold nanoparticles. The process involves using an eco-friendly method for fabricating a composite material based on reduced graphene oxide decorated with gold nanoparticles via a single-step method without requiring intricate processes or harsh chemicals. This approach involves employing plant extracts to synthesize AuNPs and bio-reducing graphene oxide in conjunction with rGO acting as a dispersant for CNTs. Additionally, this methodology adheres to non-toxic standards aligned with the principles of green chemistry to optimize sensor performance.

Chapter 6 explores an approach for developing sensors that utilise amperometry, which has been introduced to selectivity. To create this sensor, a molecularly

imprinted polymer (MIP) and a non-imprinted polymer (NIP) were synthesised using methacrylic acid (MAA) as the functional monomer. The resulting MIP and NIP were then used to prepare a disposable carbon paste sensor for an imprinted E2 sensor.

Chapter 7 provides an overall conclusion and outlines possible work for future research in the field. The research findings were disseminated through presentations at international conferences and articles published in peer-reviewed journals as contributions to the field of study.

Publications

1. Musa, A.M.; Kiely, J.; Luxton, R.; Honeychurch, K.C. Recent Progress in Screen-printed Electrochemical Sensors and Biosensors for the Detection of Estrogens. TrAC Trends in Analytical Chemistry, 139, 2021, 116254
2. Musa, A.M.; Kiely, J.; Luxton, R.; Honeychurch, K.C. An Electrochemical Screen-Printed Sensor Based on Gold-Nanoparticle-Decorated Reduced Graphene Oxide–Carbon Nanotubes Composites for the Determination of 17-β Estradiol. Biosensors 2023, 13, 491.
3. Musa, A.M.; Kiely, J.; Luxton, R.; Honeychurch, K.C. Graphene-based electrodes for monitoring of estradiol. Chemosensors 2023, 2227-9040.
4. Musa, A.M.; Kiely, J.; Luxton, R.; Honeychurch, K.C. Synthesis, and electrochemical performance of Carbon Spherical Shell Modified Screen-Printed Electrode for Estradiol Detection, *in preparation to Chemosensor.*

Conferences and Communications

1. Musa, A.M.; Kiely, J.; Luxton, R.; Honeychurch, K.C, Next generation screen-printed electrochemical platforms: Tailoring graphene, the Swiss Army Knife of nanomaterials in sensing Endocrine Disrupting Hormonal Pollutants in Water. STEM for BRITAIN (2021)
2. Musa, A.M.; Kiely, J.; Luxton, R.; Honeychurch, K.C, "A simple ratiometric electrochemical sensor based on electrochemical pre-treatment of Glassy carbon electrode modified functionalised multi-walled carbon nanotube for detection of endocrine disruptor." 30th Anniversary World Congress on Biosensors, Busan, South Korea (2020)
3. Musa, A.M.; Kiely, J.; Luxton, R.; Honeychurch, K.C, "Imprinting" Makes "Sensing" Simple: A Tailor-Made Receptor Based on Molecularly Imprinted Polymers (MIPs)". 8th Graduate Student Symposium on Molecular Imprinting, Berlin, Germany (2019)
4. Musa, A.M.; Kiely, J.; Luxton, R.; Honeychurch, K.C, "Smart Materials: Sensing by "Fitting" and "Imprinting" based on aptamer and molecularly imprinted polymers (MIPs)." C3Bio conference on Biosensors, Bath, UK (2019).

References

[1] M. Masikini, M.E. Ghica, P.G.L. Baker, E.I. Iwuoha, C.M.A. Brett, Electrochemical Sensor Based on Multi-walled Carbon Nanotube/Gold Nanoparticle Modified Glassy Carbon Electrode for Detection of Estradiol in Environmental Samples, Electroanalysis. 31 (2019) 1925–1933. https://doi.org/10.1002/elan.201900190.

[2] M. Farré, L. Kantiani, S. Pérez, D. Barceló, Sensors and biosensors in support of EU Directives, TrAC - Trends Anal. Chem. 28 (2009) 170–185. https://doi.org/10.1016/j.trac.2008.09.018.

[3] F.C. Moraes, B. Rossi, M.C. Donatoni, K.T. de Oliveira, E.C. Pereira, Sensitive determination of 17β-estradiol in river water using a graphene based electrochemical sensor, Anal. Chim. Acta. 881 (2015) 37–43. https://doi.org/10.1016/j.aca.2015.04.043.

[4] H. Pu, Z. Huang, D.W. Sun, H. Fu, Recent advances in the detection of 17β-estradiol in food matrices: A review, Crit. Rev. Food Sci. Nutr. 59 (2019) 2144–2157. https://doi.org/10.1080/10408398.2019.1611539.

[5] J.M. Díaz-Cruz, N. Serrano, C. Pérez-Ràfols, C. Ariño, M. Esteban., Electroanalysis from the past to the twenty-first century: Challenges and perspectives. Journal of Solid State Electrochemistry, 24 (2020) 2653-2661.

[6] D. Zhang, W. Zhang, J. Ye, S. Zhan, B. Xia, J. Lv, H. Xu, G. Du, L. Wang, A label-free colorimetric biosensor for 17β-estradiol detection using nanoparticles assembled by aptamer and cationic polymer, Aust. J.

Chem. 69 (2016) 12–19. https://doi.org/10.1071/CH14735.

[7] H. Pu, X. Xie, D.W. Sun, Q. Wei, Y. Jiang, Double strand DNA functionalized Au@Ag Nps for ultrasensitive detection of 17β-estradiol using surface-enhanced raman spectroscopy, Talanta. 195 (2019) 419–425. https://doi.org/10.1016/j.talanta.2018.10.021.

Chapter 2 Literature Review

This chapter provides a comprehensive overview of screen-printed electrodes (SPEs) and their application as electrochemical sensors and biosensors for estradiol (E2) analysis. It critically examines the current state of research in this field, identifies key challenges, and highlights future perspectives to set the stage for subsequent sections within this thesis. Furthermore, it is crucial to emphasise that despite significant advancements in research on SPEs' potential application in determining E2 levels accurately, research gaps still require attention. Chapter 2 has been published in the journal “Trends in Analytical Chemistry titled: Recent Progress in Screen-Printed Electrochemical Sensors and Biosensors for The Detection of Estrogens” [1].

2.1 Introduction

The last two decades have witnessed increased awareness regarding the dangers of pollutants resulting from various human activities. A growing body of literature recognizes that anthropogenic activities, including those from agriculture, pharmaceuticals, and other chemical-intensive industries, substantially contribute to environmental pollution. A list of up to 1,000 priority substances has been identified as emerging pollutants (EPs), which require close monitoring by world regulatory bodies [2]. Among these emerging pollutants are estrogenic endocrine-disrupting chemicals (EEDCs), which affect the endocrine system's normal functioning, even at low concentrations [3].

The endocrine system comprises hormone-producing glands that play a critical role in growth, metabolism, and reproduction [4]. These estrogens, including estrone (E1), 17β-estradiol (E2), estriol (E3), and 17-α-ethinylestradiol (EE2),

shown in Figure 2.1, are part of the EU watch list of emerging substances to be monitored (European decision EU 2015/495) [5]. Additionally, 17β-estradiol (E2) is a biologically active hormone (both natural and synthetic) that interferes with estrogen receptors [6].

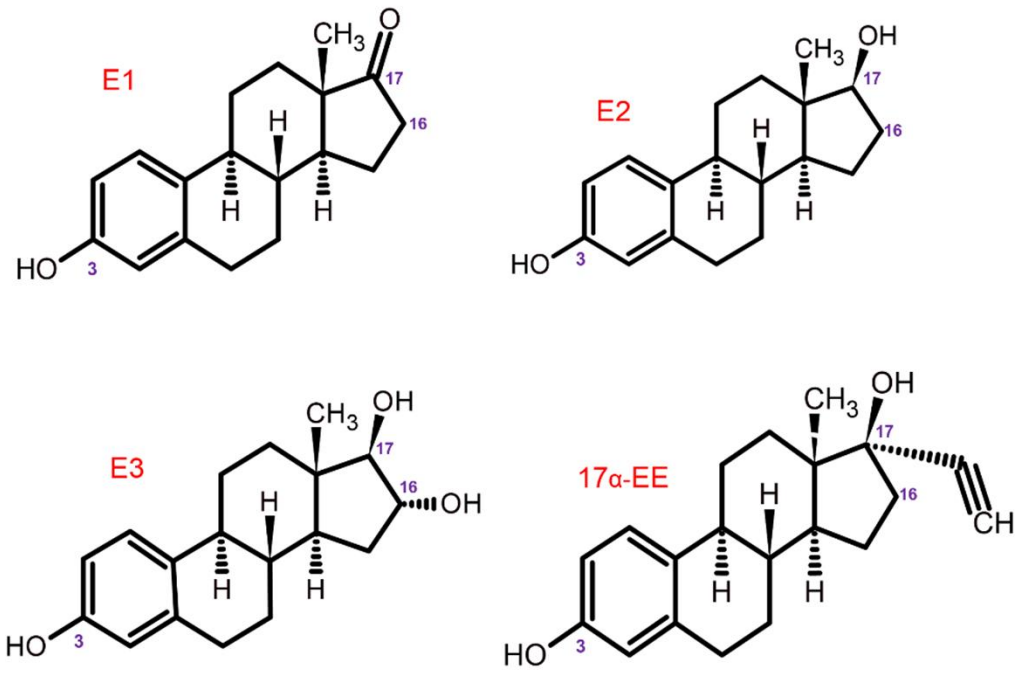

Figure 2.1 Chemical structure of estrogenic compounds. Key: E1, estrone; E2, 17β-estradiol; E3, estriol; 17α-EE2, ethinyl estradiol.

17β-estradiol (E2) is primarily produced by the ovaries but plays a significant role in both males and females [7,8]. Among these roles are brain structure, neuronal arrangement, behavioural sex differences, puberty, adulthood, pregnancy, and other vital human physiological processes [9,10]. Estrogens (also known as the C18 steroidal group) share the same structural framework of four rings: one phenolic group, two cyclohexane, and one cyclo-pentane ring (Figure 2.1), with differences only in the configuration of the D-ring at positions C16 and C17. 17β-estradiol (E2) has a single hydroxyl group at the C17 position either downward or upward on the molecular symmetry, creating α-estradiol or β-estradiol [11].

Methods for detecting estradiol typically involve techniques such as liquid chromatography-mass spectrometry (LC-MS), biological assays, immunoassays [12], and electrochemiluminescence (ECL) [13]. However, these approaches require complex sample preparation, have protracted assay times, require expertise, and are costly, all of which impede their potential application in routine environmental monitoring. Another challenge is the low concentration of these pollutants in complex environmental matrices. Analytical approaches generally require off-line pre-concentration and clean-up steps, followed by chromatographic or electrophilic separation. The low limits of detection require advanced and sensitive detection systems, such as tandem mass spectrometry and LC-MS, which are commonly used.

The benchmark for measuring estrogenic endocrine disruptors in water was carried out using an offline-online solid phase extraction concentration coupled with high-performance liquid chromatography-tandem mass spectrometry (HPLC-MS/MS) and negative electrospray ionization (ESI) [5]. However, presently, there are no reported electroanalytical methods capable of measuring these compounds at linearity values of 1.29 x 10^{-13} M to 8.22 x 10^{-12} M and limit of quantification (LOQ) levels of 1.28 x 10^{-13} M to 3.67 x 10^{-13} M [5]. Estrogens have been detected in effluents of sewage treatment plants (STPs) in different countries at concentrations ranging up to 2.57 x 10^{-10} M for E1, 2.35 x 10^{-10} M for E2, 6.61 x 10^{-11} M for E3, and 1.54 x 10^{-10} M for EE2. An investigation in Italian STPs reported values of 2.94 x 10^{-10} M, 4.41 x 10^{-11} M, 1.1 x 10^{-11} M, and 1.9 x 10^{-10} M for E1, E2, E3, and EE2, respectively. In Japan, the values of E2 in influents of Japanese STPs range from 1.1 x 10^{-10} M to 3.3 x 10^{-10} M in autumn and 7.3 x 10^{-11} M to 3.5 x 10^{-10} M in summer seasons, respectively [14].

In China, Zhou et al. [15] reported that more than 40% of natural estrogens and 60% of EE2 in wastewater might be entering receiving water, with average concentrations ranging from 1.76 x 10^{-10} M to 2.57 x 10^{-10} M for E1, E2, E3, and EE2 in the receiving water, respectively [15]. Other wastewater treatment plants (WWTPs) in Beijing have maximum concentrations of E1 at 2.7 x 10^{-10} M, E2 at 1.4 x 10^{-11} M, E3 at 1.8 x 10^{-11} M, and EE2 at 1.7 x 10^{-11} M, respectively [14]. In North America, E2 in WWTPs, rivers, and freshwater ranged from 3.6 x 10^{-12} µM to 8.1 x 10^{-11} M and 0 to 1.6 x 10^{-11} M, respectively [16]. Kolodziej et al. reported that estrogens in California, USA, were observed in 86% of samples from pasture surface water, with a maximum of 1.6 x 10^{-11} M recorded during the winter wet season [17].

E2 concentrations in river waters from Japan, Germany, Italy, and the Netherlands ranged from 9.9 x 10^{-11} M to 2.4 x 10^{-11} M, while groundwater in Arkansas, USA, was 2.2 x 10^{-11} M. The UK Drinking Water Inspectorate has set the benchmark value for the endocrine-disrupting E2 at 3.6 x 10^{-12} M [18]. Consequently, the research area is very active, with numerous publications [2, 5, 15–24] to fulfil the stringent requirements for monitoring estrogens in surface water. This demonstrates how far the research in this area has matured and points to the literature gap for a holistic synopsis of the state-of-the-art research [28–31].

2.2 Toxic Effects of Estrogens and Their Environmental Recalcitrance

As knowledge of the endocrine-disrupting activities of estrogens in the environment has increased, methods capable of monitoring low concentrations

in environmental samples have become increasingly important. For example, EE2 is widely used in contraceptive pills and hormone replacement therapy and is resistant to degradation; hence, it accumulates in aquatic bodies [32]. Therefore, these compounds threaten our food chain as they can be present in soil, water, and plants [11, 32]. In addition, a well-documented aspect is the feminization of fish, as their physiology and reproductive development are adversely affected by increased levels of environmental estrogens [11, 33].

The toxic effects associated with these compounds are not fully understood [11]. As a result, they are referred to as pollutants of emerging concern or contaminants of emerging concern that require monitoring [32]. For example, the work of Celik et al. reported the attachment of endocrine-disrupting compounds (EDCs), including E2 and E3, to the endocrine receptor in tissues, causing problems in the endocrine, metabolism, and reproductive systems [33]. Other health issues, such as the hindrance of sulfotransferase enzyme by EDCs, have been linked to a possible increase in E2 levels in humans [36]. Other studies have reported the link between excess estrogens and metabolic disturbances [37], Parkinson's disease [38], breast cancer [39], and the risk of Alzheimer's disease [40]. These issues reinforce the platform requirement to monitor these pollutants [41].

Figure 2.2 shows the potential sources of estrogens, their release into water resources, and their accumulation. Due to the persistence of estrogens in the environment and their potential toxicity via the food chain, these compounds should be monitored [11]. Estrogens have hydrophobic and lipophilic characteristics that help facilitate their passage through plant membranes,

leading to their accumulation in plant roots and shoots. The accumulation of estrogens in animals and humans is a health concern [11,16].

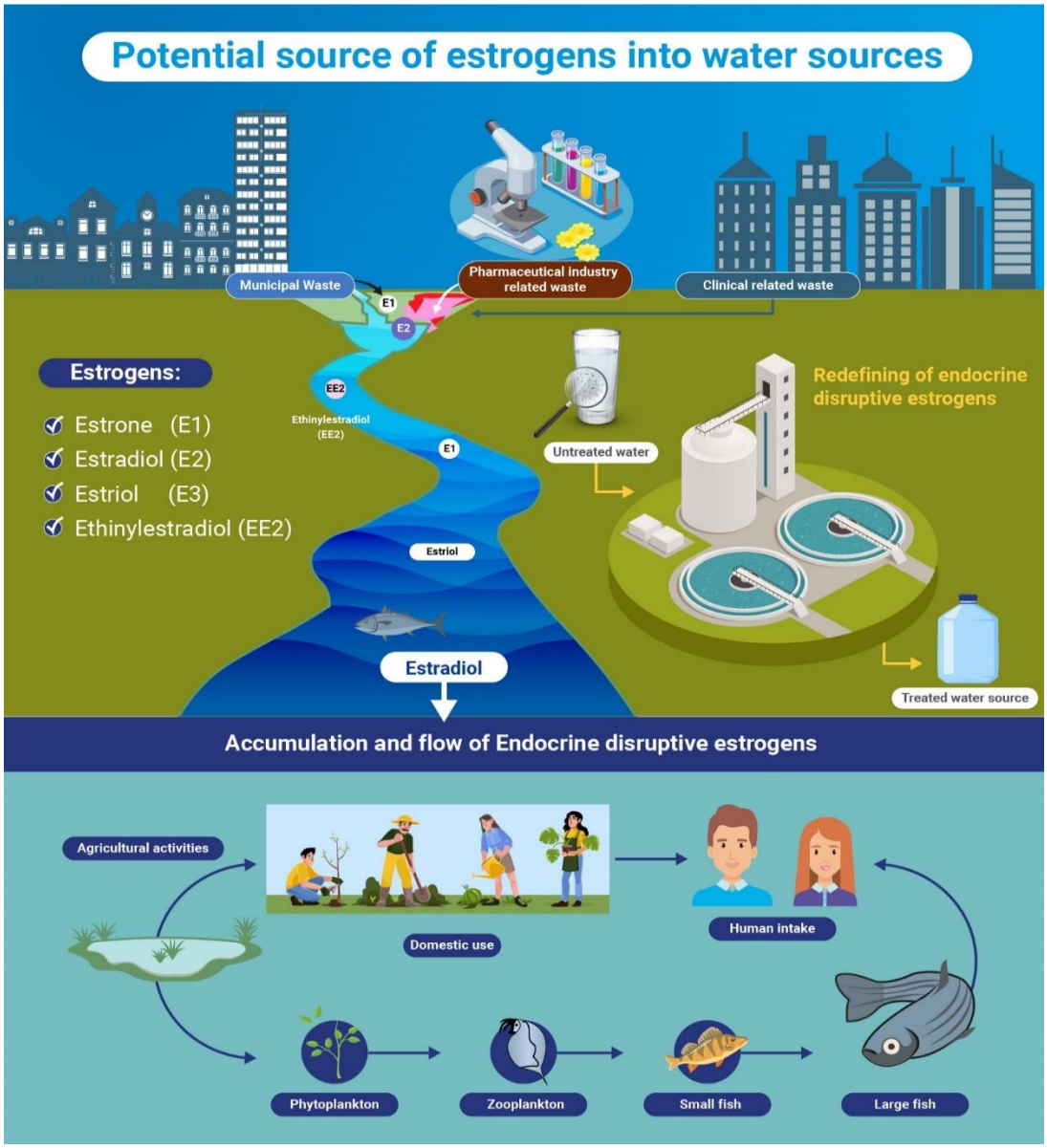

Figure 2.2 Possible sources of estrogens and their release into water supplies. The lower part shows the accumulation of estrogens.

2.3 Electrochemical Sensors and Biosensors

An electrochemical sensor is any device used to gain insight into the electrochemical information resulting from transformation (reaction) into a readable signal. These are a form of chemical sensors that provide real-time

analytical data, such as chemical species concentration [42]. Chemical sensors consist of two significant parts: one for recognition through the interaction with the analyte and a second for transduction, i.e. translating the interaction into a readable signal [42]. The recognition or sensing element must be sensitive and specific to the analyte of interest. Several strategies have been reported utilising various transducers and detection techniques in each electrochemical sensor and biosensor category. The electrochemical sensor consists of two or three-electrode systems attached to a potentiostat, depending on the setup. The most common setup is the three-electrode system, which consists of working (WE), counter (CE), and reference electrodes (RE) in an electrolytic solution. Screen-printed electrochemical sensors, like SPEs, facilitate on the spot monitoring and point-of-care testing in biomedical, pharmaceutical, and environmental sectors. They also eliminate pre-treatment and cleaning steps in routine measurements [43]. Figure 2.3 shows two sensor arrangements [42].

Electrochemical biosensors are integrated devices that provide specific quantitative or semi-quantitative analytical information. They achieve this by utilising a biological recognition element close to an electrochemical transduction component [42]. Several electrochemical techniques, such as potentiometric, amperometric, conductometric, impedimetric and field effect, have been used to determine various analyte types [42]. The success of the technique is evidenced by the growth in the biosensors market, particularly for blood glucose measurement, which recorded a revenue of USD 12.8 billion in 2018 with a projection of USD 23.7 billion by 2025 [44].

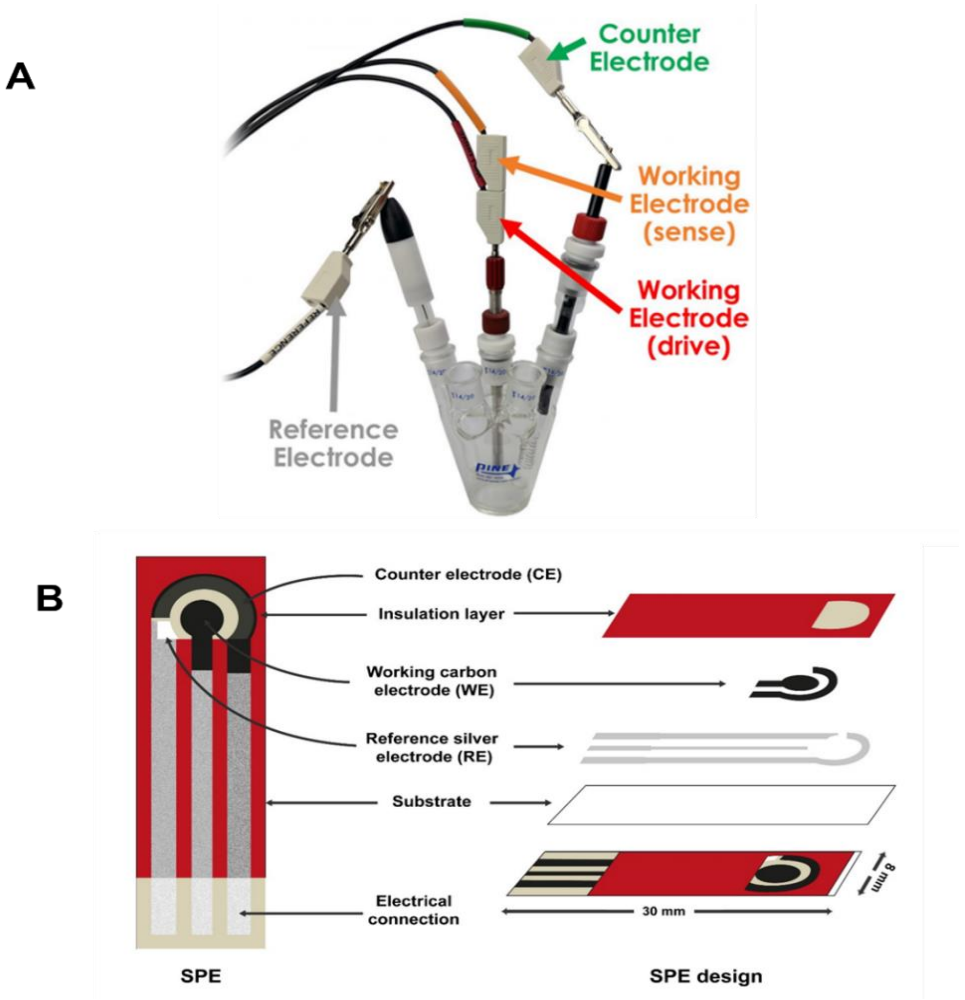

Figure 2.3 Schematic illustrations of the (A) standard three-electrode system using Solid electrodes, (B) the integrated working electrodes and counter and reference electrodes on a single screen-printed strip [54].

The ideal chemical sensor should have the following properties: (i) inexpensive, (ii) portable, and (iii) a simple/easy-to-use device that can respond sensitively and instantly to a target chemical substance (analyte) with good selectivity in any medium. In addition, it must produce a quantifiable signal output for that required analyte. Such sensors are needed for the growing number of applications for rapid, *in situ* analysis [45]. The viability of electrochemical devices in measuring various analytes is already evidenced in some applications, such as stripping voltammetry for heavy metals, lactate, and glucose measurements [46–50].

2.4 Electroanalytical Techniques

These are the techniques used to study the concentration of analytes in electrochemistry, as well as understanding the electrochemical behaviour of analytes under investigation through the generation of readable signals such as potential (V), current (A), charges (C) and impedance (Ω) in an electrochemical cell [51,52]. Generally, in an electrochemical measurement (electroanalytical), one or more of the following parameters are measured – potential (E), current (i), charge (Q) and time (t). Electroanalysis methods, like voltammetry and amperometry, detect a range of analytes by measuring the change in the oxidation state of electroactive species. This change directly correlates with the analyte's concentration [53].

The derived information is formed by plotting the above parameters in several ways. The electroanalytical systems employing techniques such as (1) amperometry, in which changes in output current are measured [31,54], (2) voltammetric techniques, such as differential pulse voltammetry (DPV) [55,56], square wave voltammetry (SWV) [23,27,57], cyclic voltammetry (CV) and linear sweep voltammetry (LSV) [58–60], potentiometric [61] and (3) impedance spectroscopy [62]. Analytes of interest are oxidised or reduced at the working electrode's (WE) surface based on their redox potentials [47,63]. Electrochemical techniques employed in this project include cyclic voltammetry (CV), differential pulse voltammetry (DPV), and amperometry, briefly discussed below.

2.4.1 Amperometry

Amperometry is a technique to probe electrochemical reactions and mechanisms resulting from electron transfer [42]. At the same time, the potential

is controlled, and the current resulting from the response is measured. As a controlled-potential technique, the potential can be constant (single step) carried out by applying a fixed potential at which no faradaic reaction is occurring, then stepping the potential to a value at which the electrochemical reaction occurs, and the resultant current is measured. The applied potential can be single-potential or multiple-potential applied. A typical amperometric plot is depicted in Figure 2.4. Using amperometry, a potential is stepped at an appropriate value where the analyte oxidises at the electrode by introducing the sample via batch or flow injection system. As a result of the peculiar oxidation or reduction potential, the resultant current generated is proportional to the concentration of the sample analyte [64].

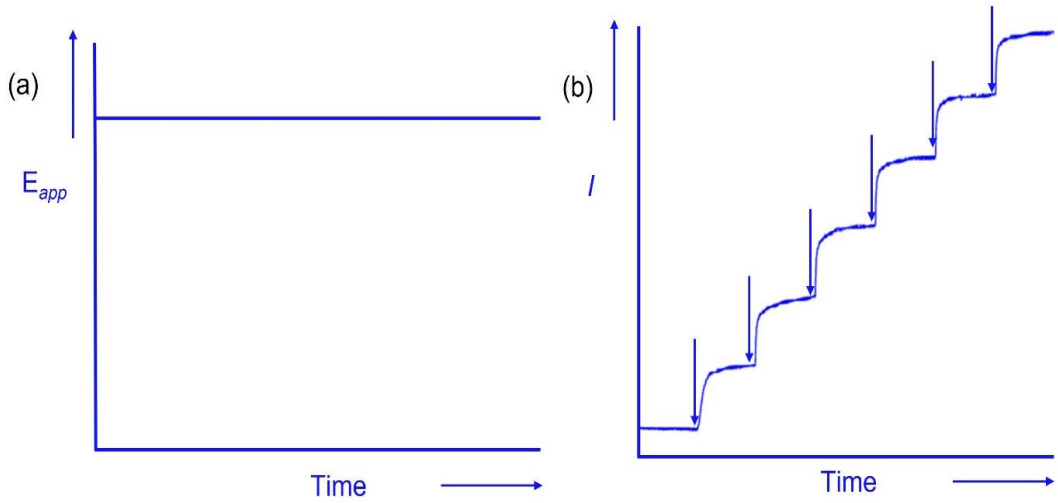

Figure 2.4 (a) Current waveform for amperometry (b) amperometric plot under stirring and subsequent injections (illustrated by the vertical arrows) of the target analyte

2.4.2 Cyclic Voltammetry

One of the most used means of understanding the electrochemical process is to set a programmed voltage or current and to measure the resultant current response or voltage. Cyclic voltammetry is commonly employed to

explore an electrode’s reactions and interfacial properties as properties of an analyte or system [65,66]. Cyclic Voltammetry (CV) is a widely applied technique in acquiring an electrode’s reactions and interfacial properties [67]. It gives qualitative analytical information about the response at the electrode-electrolyte interface (redox process) as an analyte’s or system’s properties [65,66]. It is easy to perform and offers a non-destructive approach to any electrode material. In cyclic voltammetry, the working electrode’s potential is ramped linearly over time [65] in a triangular waveform, and potential is scanned in both the cathodic and anodic directions. Figure 2.5 shows the potential-excitation signal. The first scan potential to more positive values, oxidizing R to O, then to reverse directions and scan to more negative potentials, reducing O to R. As the cyclic voltammetry is performed in an unstirred solution, the cyclic voltammogram (Figure 2.6) has peak currents instead of limiting currents. The voltammogram has separate peaks for the oxidation and reduction reactions, each characterise by a peak potential and a peak current. Electron transfer rates depend on several factors: the electrode material's energy barrier, surface area, and potential, as well as the electrolyte's conductivity. Impurities can also slow down the process.

In addition to the technique employed, the electron transfer rate at electrode surfaces is influenced by factors such as mass transfer of ions, electron transfer kinetics at the electrode surface, chemical reactions, adsorption/desorption processes, electrode area, and surface concentration of reactants [65]. The conductivity of an electrode surface influences the heterogeneous electron transfer kinetics in an electrochemical system. If the surface is more conductive, electrons move freely, which leads to faster standard rate constants and minimal peak separations. Overall, high conductivity allows electrons to transfer more

readily across the electrode-solution interface by facilitating electron flow in the electrode itself and reducing kinetic barriers, iR distortions, and impedance. iR distortion is caused by the internal resistance in an electrode, which impacts electrochemical processes by causing non-uniform current distribution [66]. It can be mitigated using conductive materials, a larger surface area, and geometry. Thus, choosing electrode materials with good conductivity is necessary to understand electron transfer rates [66].

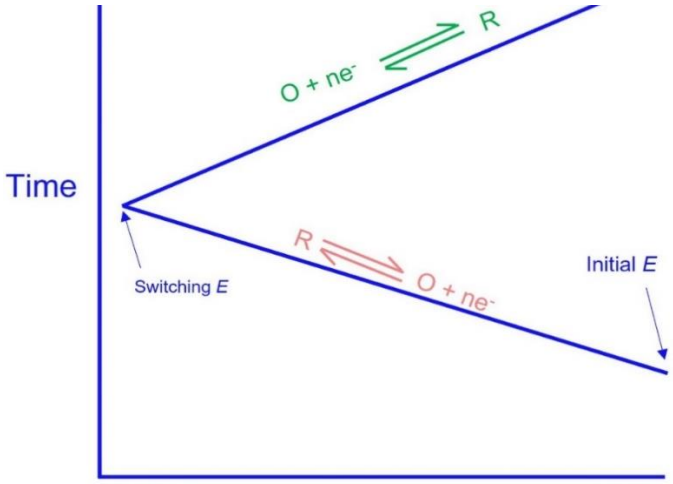

Figure 2.5 shows the potential-excitation signal.

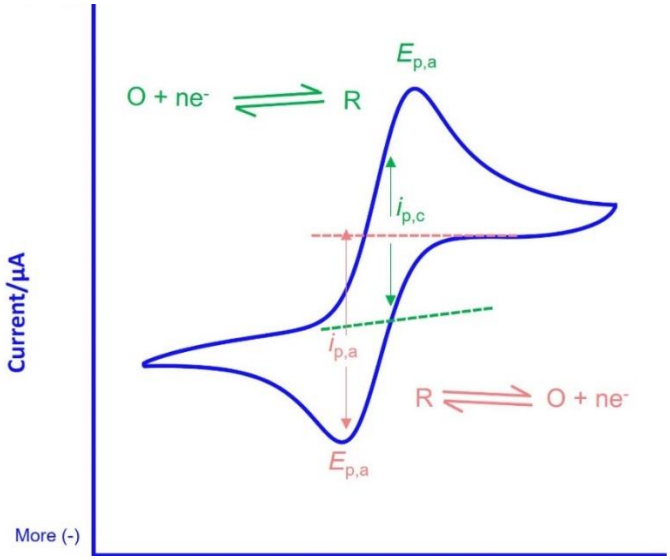

Figure 2.6 A typical cyclic voltammogram

2.4.3 Differential Pulse Voltammetry

Differential pulse voltammetry (DPV) is a pulse technique used for quantitatively monitoring analytical signals, providing information on chemical reaction mechanisms, kinetics, and thermodynamics. It can distinguish between background and faradaic current due to its short pulse time and differential nature. It can measure analytes directly at parts per billion (ppb) levels. Unlike cyclic voltammetry, based on the continuous application of a potential to the working electrode, DPV applies the potential in pulses that can be tightly controlled. When a potential is applied to the working electrode, a charge is generated called the double layer, which brings about significant background signals because of its capacitance. By applying the short pulsing, the applied potential allows this current to decay, which prevents the building up of background capacitive current, thus enhancing the redox signals [68].

The short pulse time increases the measured currents, while the differential measurement discriminates against background processes. In DPV, the first current is subtracted from the second. The difference is plotted versus the applied potential, giving a differential pulse voltammogram with current peaks and heights directly proportional to the concentration of the analyte. In contrast, peak potential (Ep) can be used to identify the species (Figure 2.7).

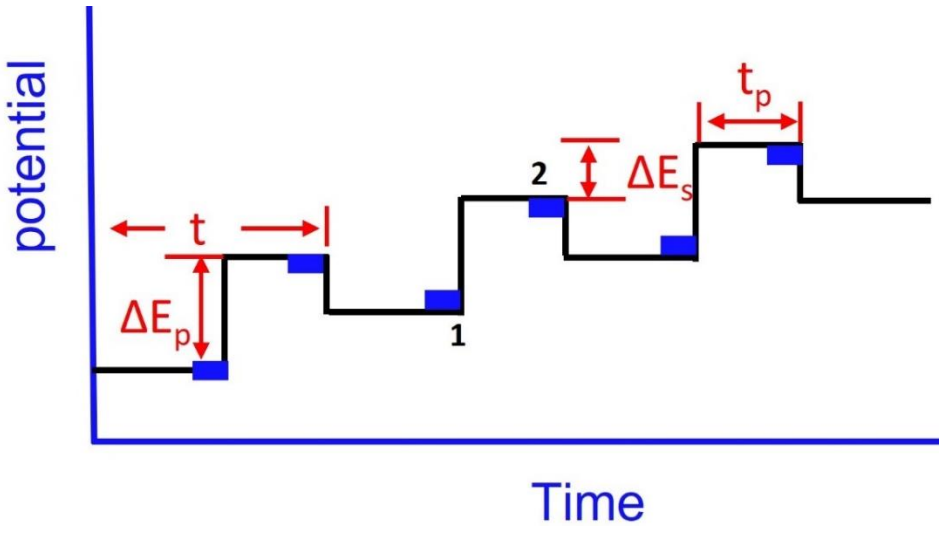

Figure 2.7 The potential waveform in DPV (2 cycles are shown)

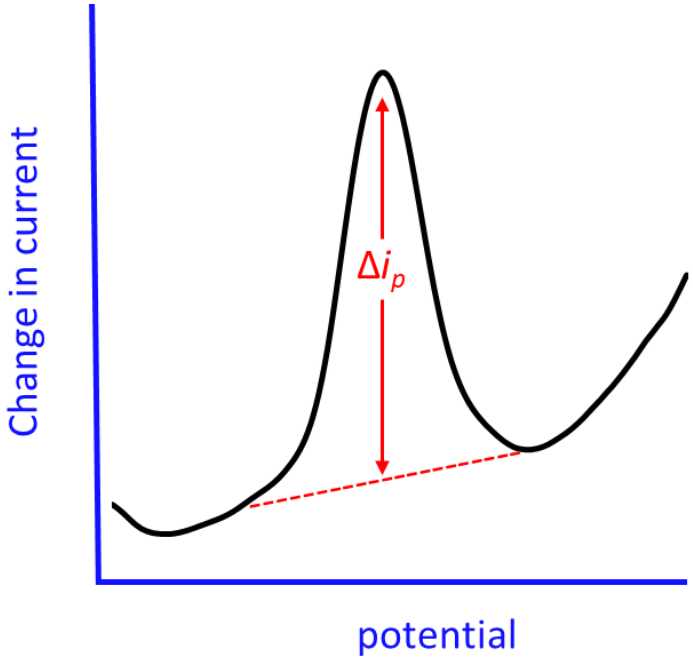

Figure 2.8 A typical differential pulse voltammogram.

2.5 Applications of Electrochemical Sensing for E2

Estradiol (E2) is of great concern and is the target analyte in 80% of the publications on analysing estrogens. It is the most potent of all estrogens [69,70].

Estrogens have been measured using mercury-based electrodes, such as the dropping mercury electrode (DME) and the hanging mercury drop electrode (HMDE). These were replaced by graphitic and metallic macro electrodes [71] and carbon paste electrodes [72], which then led to the current configuration of macro electrodes constructed from ordered pyrolytic graphite, glassy carbon and boron-doped diamond electrodes with various modifications [73,74]. Sensitivity and selectivity are the hallmarks of any electroanalytical technique when designing any sensor. In addition, mass production is a hallmark of the screen-printing of electrodes vital in fabricating (bio)chemical sensors [75]. This approach allows a cost-effective device to be produced in large volumes with a customised sensitivity and selectivity for a particular application.

Screen-printed electrodes (SPEs) are suitable for electrode modification due to their versatile design, ease of mass production, and compatibility with various electrochemical techniques. Their structure allows for easy surface modifications, enhancing both performance and selectivity. Drop-casting, spin-coating, and inkjet printing have been employed to deposit modifying materials on SPEs for various applications. This screen-printing process facilitates the production of cost-effective devices in bulk, tailored for sensitivity and selectivity for specific applications [50]. Electrode modification is driven by the necessity to enhance the effectiveness of the sensor's performance in terms of sensitivity, specificity, durability, and cost-effectiveness in meeting environmental monitoring standards and ensuring reliability in various matrices [50]. Despite the volume of published literature, the development of miniaturised tools to replace the routine analytical means of measuring estrogens is still a subject of investigation. The features of electrochemical sensors can deliver point-of-interest or point-of-care

measurements in various real matrices, possibly transforming the whole sector [76]. Recent work by Lu et al. highlighted research from 2017 - 2019, which reported using biosensors for estrogen measurement in food and the environment using various electrode surfaces [28]. They concluded that applying nanomaterials to enhance biosensor performance is standard, using multiple materials such as carbon nanomaterials. Various methods and techniques have been reported for estrogen sensing. Electrochemical sensing employs electrodes to detect electrical signals produced from a chemical reaction. Some of these methods and techniques frequently used for electrochemical sensing of estrogen are discussed in Sections 2.7 and 2.8, in addition to an overview of materials used, emphasising carbon-based.

2.5.1 Electrode Materials

Carbon is a vital area in modern material nanoscience research [77]. For example, carbon-based nanomaterials cover 50% of commonly reported nanomaterials in sensing applications [78]. This is due to electrical and thermal conductivity, high mechanical strength and chemical stability, and a high surface-to-volume ratio [79]. These characteristics are vital for electroanalytical applications because they are less prone to sensing surface passivation and broader electrochemical potential [78–81]. Another feature of carbon-based materials is that they can be produced in various dimensions and sizes into (1) zero-0D; an example of the materials is fullerene, having a C60 molecule is around 1 nm in range and atomic clusters, which has three dimensions in the nanometers size range; (2) first-1D, consists of two dimensions in the nanometre size range, examples are carbon nanotubes, nanorods, nanowires and nanofibers [82]. These are the common materials in this category with features

of high mechanical strength, high chemical stability, tunability, and a combination of unique electrical properties that make them ideal candidates in many applications [83]; (3) second-2D materials have one dimension in the nanometre size range. Graphene is a 2D material with high thermal stability, decomposition temperature, and optical and mechanical features. Moreover, features such as large surface area, high electron and mass transfer ability make it an ideal candidate in sensor fabrication [78]; (4) third-3D dimensions have axes of approximately the same length (equiaxed) in a nanometre-sized grains format; examples are carbon sponges and carbon aerosols. Carbon base- materials' features such as mechanical strength, electrical conductivity, and superb thermal, chemical, and electrochemical stability [81] help make economical devices as they are readily available from various sources [82].

2.6 Design and Fabrication of Screen-printed Electrodes

Screen printing techniques were a subset of thick-film technology believed to have originated in China during the Song dynasty [49,50]. They originated from the construction of the Great Wall of China and ancient Egyptian cloth. Screen printing technology has recently produced ‘thick film’ printed electronic circuits [84]. Moreover, this technology was part of the “New frontier in the Renaissance of electroanalysis” [85]. In addition to screen-printing, printed sensors have been produced by other fabrication methods, such as lithography and ink-jet printing. Recently, Honeychurch et al. [205] reported the application of three-dimensional (3D) printing technology (rapid prototyping) as an alternative means of fabricating electrodes using carbon nanofiber–graphite–polystyrene electrodes with a carbon pseudo-reference electrode [86]. In addition, the Rotogravure printing process has been used by [87,88]. All these technologies are helping to

revolutionise the field of low-cost and mass-produced sensors as effective routes for the environmental monitoring of emerging pollutants.

Since the 1990s, screen-printing technology, adapted from the microelectronics industry, has offered high-volume production of inexpensive yet highly reproducible and reliable sensors [89,90]. Screen-printing technology allows the production of various forms of SPEs to be used as transducers in electrochemical sensors [91–93]. Screen printing enables the printing of working, counter and reference electrodes in different geometries, using inks modified with various catalysts, mediators, and other materials. The technique facilitates the fabrication of low-cost electrochemical sensors, thus offering economic and practical benefits, as it is viable for the sensor to be disposable.

Generally, the screen-printing technique to produce SPEs involves forcing suitable ink formulations as a paste through a patterned stencil or screened mesh of a specific size and shape onto a planer substrate [43]. The formulation paste can contain graphite, carbon, gold, silver, platinum, binders, polymers, plasticizers and solvents, additives such as metals, metal oxides, enzymes, and ion exchange resins [94]. In the screen-printing process, ink is forced through the open regions of a mesh screen, using a squeegee to form the desired design on a substrate surface (see Figure 2.9a). The screen is detached from the substrate, leaving the ink in the desired format. This process produces electrodes with a thickness typically 10-20 µm. Subsequently, the printed electrodes are cured under various regimes, for example, at approximately 60 °C for 30-60 min. Depending on the proposed application of the electrode, different types of meshes can be used to print the electrodes. Substrate materials usually are either ceramic or plastic-based [95]. The process is amendable to fabricating many

sensors on a single sheet. Additionally, the process can then be repeated to produce many reproducible devices. An in-depth description of the screen-printing process is given by Fletcher et al., in which the physical and chemical properties of the screen-printing of a carbon electrode are discussed [96].

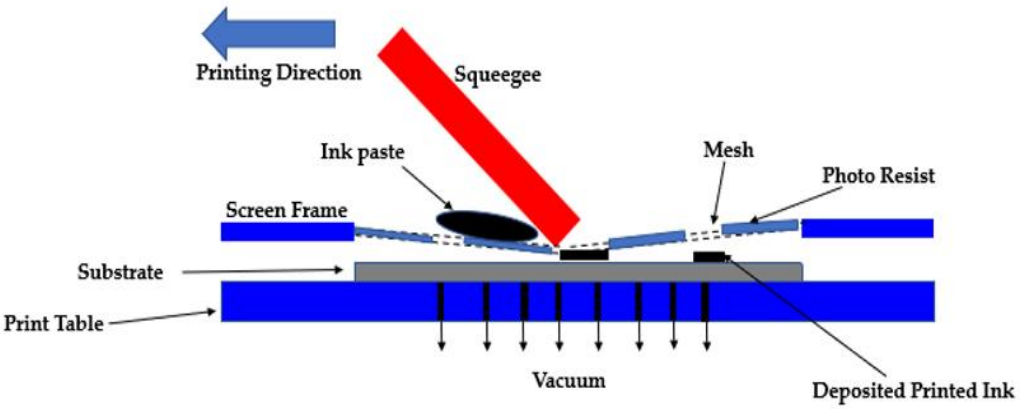

Figure 2.9. Representation of the screen-printing process for the fabrication of SPEs.

Three essential features of the screen-printed process make it an attractive fabrication technique: (1) the ability to control the electrode area, thickness, and composition; (2) Reproducible results can be obtained and statistically validated; and (3) almost any materials, such as biologically compatible materials, e.g., carbon, metallic nanoparticles, and polymers, can be incorporated into the screen-printing process. An SPE consists of a solid support with two, three or more electrodes, *viz* a working electrode (WE), a pseudo reference electrode (RE) and a counter electrode (CE) [73,75], as shown in the representation in Figure 2.3.

2.7 Screen-printed Electrochemical Sensors

Recent progress in electrochemical sensor design uses various materials to modify electrode surfaces to improve performance. Among these carbonaceous

nanomaterials in electrochemical sensing are carbon nanotubes (CNTs) and graphene (Gr) and their various derivatives [79]. These materials are explored in the performance of electrochemical sensors [97]. Furthermore, SPEs from graphite and graphene conductive inks allow fast adsorption kinetics, selectivity, a sizeable binding capacity and reusability [45].

All carbon materials, such as carbon black (activated form inclusive), graphite nanotubes, graphene, fullerenes, and quantum dots, have been screen-printed. Different SPEs, modified with various materials, such as enzymes and nanomaterials, have been characterised and compared as sensing platforms for environmental applications (Figure 2.10). A common challenge in improving sensor performance includes the near-identical electrochemical behaviour of different analytes on SPE surfaces, which can be solved by incorporating materials that can be selective towards the target analyte. The second challenge comes from the ink composition because of the various components of the ink, such as insulating organic polymeric substances that hinder the conductivity in the fabrication of the SPE. A conductive binder can help with the problem, or different approaches that see abandoning the binder altogether, such as laser scribing, as discussed in Chapter 4, can be used as an alternative. Many studies have already been reported using commercial ink supplied by multiple companies [94,98], with each fabricated electrode giving a different response to various analytes. This is due to the variety of compositions, printing techniques and curing process protocols. Active surface area and roughness factors are contributors to the performance of SPEs. Calculating the surface area has been tricky due to non-uniform material composition and printing processes. Redox systems [99] are used to include both inner-sphere and outer-sphere redox

probes, such as potassium ferricyanide (III), ascorbic acid (AA), and NADH. McCreery et al. [99] results revealed that the nature of an SPE's response in various redox systems is linked to the amount of graphite in the ink composition, the functionalisation of the surface, the curing process, the binder, and the wettability of the surface. Honeychurch et al. looked at redox characteristics of lead (Pb) at modified screen-printed carbon electrodes (SPCEs) [100].

The roughness contributes to the edge plane sites available; thus, the higher the roughness, the more edge plane sites, leading to better reversibility performance [94]. This is a subject of debate as other researchers hold different views on this [101–104]. There is yet to be a clear prevailing view on this. However, we tend to support Kadara et al. [94] based on the study currently being undertaken in our laboratory. Screen-printed electrodes have been modified using various materials to adapt the sensing element to respond specifically to the analytes of interest. Nanomaterials such as gold nanoparticles (AuNPs), for example, are easy to synthesize, functionalised with good stability, and are employed as a detection label for lateral flow assay [105]. Gold nanoparticles (AuNPs) can be tailored with molecules that specifically bind to a target analyte, enhancing sensor selectivity and ensuring the analyte is more likely to attach to the AuNPs than other solution components. It has been demonstrated that nanomaterial surfaces can be coated with various biological receptors, such as antibodies, aptamers and molecularly imprinted polymers, to increase the sensitivity and the selectivity of various sensor designs to overcome general sensing challenges [106].In the case of the immobilization of biomolecules, the analyte-specific part of the sensor functions as the sensing element of the system. Various immobilisation techniques, including adsorption, entrapment, micro-encapsulation, crosslinking,

or covalent attachment [107], are used to immobilised different bio-molecules onto the surface of the electrode; analyte-specific as part of the sensor functioning as the sensing element [108]. Peveler et al. [106] highlighted the advantages and disadvantages of selectivity and specificity in sensing approaches in the two domains for specific and selective sensing [106]. Diverse materials have been employed to modify SPEs, boosting conductivity and stability, improving biocompatibility and electron transfer, providing selective recognition sites, and increasing surface area and mechanical strength. Thus enhancing sensor performance, as shown in Figure 2.10 [1].

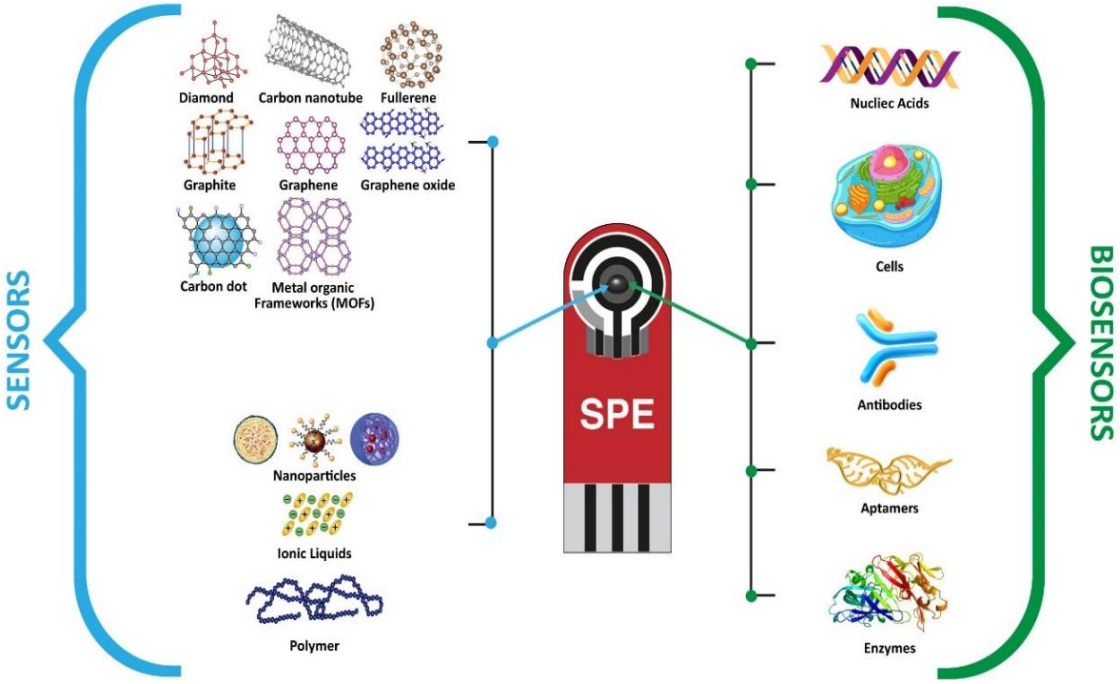

Figure 2.10 Schematic representation of various materials that modify SPEs [1].

2.7.1 Graphene-based Screen-printed electrodes

Features such as a large surface area and high electrical conductivity are among the attributes of graphene, making it an excellent electrode modifier for promoting

fast electron transfer between a target analyte and the electrode. Karuwan et al. reported adding graphene to the ink formulation in screen printing [109]. In another study [110], SPCE was modified using multi-walled carbon nanotubes (MWCNTs) and graphene (GP) [110]. A dedicated review based on applying graphene-carbon nanotube-modified electrochemical sensors can be found elsewhere [111]. Cinti et al. [139] provided an overview of the modification of SPEs using graphene-based materials [112].

Barton et al. [140] demonstrated the analysis of E1, E2, and EE2 using graphene screen-printed electrodes (G-SPEs). The PANI/graphene-SPE devices displayed linear responses to estrogenic substances in EIS assays over a 3.58 x 10^{-19} M concentration range to 7.34 x 10^{-13} M in water samples. Detection limits (LODs) of 1.59 x 10^{-22} M for E1, 6.98 x 10^{-16} M for E2, and 2.36 x 10^{-22} M for EE2 were lower than other techniques such as commercial ELISA [113].

2.7.2 Carbon Nanotubes (CNTs)-based Screen-printed Electrode

Carbon nanotubes (CNTs) are well-reported electrode modifiers that increase the electrocatalytic activity of several analytes in sensor design [114]. Ochiai and co-workers used a microflow device and an SPE modified with CNTs to measure E3, producing a device that combines low sample usage and a fast amperometric technique [115]. A linear response was observed for a concentration range of 1 x 10^{-6} to 1 x 10^{-3} M, with LOD and LOQ of 5.3 x 10^{-7} M and 1.77 x 10^{-6} M, respectively. The proposed methodology was applied to determine estriol in commercial samples, and the results were compared with those provided by spectrophotometric methods. The obtained results agreed at a 95% confidence level [142].

Wang et al. reported a novel disposable electrochemical film doped with MWNTs/Al_2O_3/Poly-L-Lysine to measure E2 in clinical samples. Under optimized conditions, the sensor detected E2 with a linear range of 1.0 x 10^{-10} M to 5 x 10^{-8} M and a low LOD of 1.4 x 10^{-11} M [70]. The authors reported the use of cyclic voltammetry for this sensitive sensor. This requires a look into the contributions made by changes in the double-layer capacitance since CV does not have background correction ability for changes in the capacitive layer [116]. Gan et al. employed CNTs to enhance the oxidation signal for 17α-ethinylestradiol determination. The screen-printed modified electrodes achieved high sensitivity under optimized conditions [117]. Hao and his co-workers produced a layer-by-layer assembly of Polyethyleneimine (PEI), Polyacrylic acid (PAA), F-MWCNT with graphite clay, and a pencil graphite electrode with an LOD of 1 x 10^{-8} M [118].

2.7.3 Other Material-modified Screen-printed Electrode

Other forms of carbon-based nanomaterials have been incorporated into various sensor platforms [119]. For example, Sanati et al. [102] reviewed the modification of SPEs with carbonaceous materials in electrochemical biosensing for bioelectrochemical platforms, including materials such as mesoporous carbon, carbon nanofibers, and carbon nanospheres [79]. Cesarino et al. applied tristimulus analysis to measure two estrogens based on differential pulse voltammetry measurement to overcome the lack of specificity of the sensor to a single chemical species [120].

In addition, carbon nanostructures, namely graphene oxide, reduced graphene oxide, and reduced graphene oxide doped with antimony nanoparticles, were utilized for E2 and E3 detection in water [120]. Mazzaracchio et al. [121] investigated various carbon nanomaterials as modifiers to improve SPE

performance. The work also explored multiple forms of carbon black as an inexpensive modifier for this purpose. A notable increase in analytical performance was reported compared with an unmodified bare electrode. Additionally, the authors reported improvements such as lower applied potential, greater peak-to-peak separation, and increased peak signal intensity. This resulted from enhanced material properties, including high electron transfer, onion-like carbon structure, and the availability of increased numbers of defect sites [121].

A rapid, efficient, and sensitive sensor based on adsorptive stripping voltammetry (AdSV) was reported to determine E2 and EE2 in pharmaceutical formulations and urine samples [69]. The work compared different electrodes, namely HMDE, SPE and screen-printed carbon nanotube electrodes (SPCNTE). The LODs were 1.10×10^{-12} M for E2, 4.99×10^{-11} M for EE2 at −0.23 V, and 3.27×10^{-11} M for EE2 for HMDE at −1.20 V. Whilst the LOD was 8.88×10^{-10} M for E2, 1.02×10^{-9} M, 6.68×10^{-10} M, and 7.01×10^{-10} M for SPE and SPCNTE at 0.30, 0.31, 0.32, and 0.33 V potentials [69]. These results supported the claim of Barek et al. that mercury-based electrodes “are probably the best sensors for the determination of trace amounts of electrochemically reducible organic compounds” [122].

Wong et al. developed an E2 electrochemical sensor using an SPE modified with copper phthalocyanine (CuPc), carbon nanoballs (Printex 6L carbon), and Nafion film. The authors compared various SPEs (SPE, acid functionalised SPE-SPE_F, CuPc-P6LC-Nafion/SPE_F) before and after modification with different materials. The electrochemical oxidation of E2 was evaluated using cyclic voltammetry, where a single oxidation peak was observed during anodic potential scanning at a potential of 0.39 V. After optimizing experimental conditions, a more sensitive

DPV technique was used to evaluate the sensor over a linear concentration range of 8 x 10^{-8} M to 7.3 x 10^{-8} M, and a LOD of 5 x 10^{-9} M was achieved. Synthetic urine sample analysis revealed the sensor's application in different matrices [123]. Mesoporous carbon was among the materials employed for electrochemical sensor development [135]. This study combined materials to determine E1, E2, and E3. The deposition of each material was used to fabricate the sensor at a concentration of 0.1 mg/ml in phosphate buffer (pH 7). Factors such as the influence of pH, electrodeposition cycles, and accumulation time were optimized when designing the sensor. Square wave voltammetry was utilized as the method for the determination of E2 in human serum. A linear range of 5 x 10^{-9} M to 2 x 10^{-6} M and a 2 x 10^{-9} M LOD were obtained [124].

Electrochemically pre-treated SPEs have been proposed to increase their sensitivity towards numerous analytes. The pre-treatment of the SPE can be performed electrochemically or by soaking it in various solutions that dissolve the binder and solvent remaining on the surface after the final product of the screen-printing process. Electron and charge resistance transfer are typically compared between pre-treated and untreated SPEs using inner and outer-sphere redox systems. These pre-treatment methods condition the electrode surface to enhance fast reaction kinetics such as electron and proton transfer. [125] This makes them known as activated or pre-treated electrodes. The electrocatalytic activity of pre-treated screen-printed electrodes, as compared to untreated ones, is influenced by edge plane activity. Several methods suggest that the edge and basal planes of treated SPEs behave differently, with the former showing better activity towards biological compounds [89]. Little information on the behaviour of estrogen at pre-treated SPEs has been reported [126]. Raymundo-Pereira et al.

demonstrated the simple electrochemical pre-treatment of SPEs using cyclic voltammetry by employing a potential range of -2.5 to 2.5 V at 100 mV/s in 0.5 M H_2SO_4 (two scans) for the treatment of a sensor for the determination of the emerging pollutants: E2, hydroquinone (HQ), and paracetamol (PARA). Their simultaneous determination in tap water gave LODs of 1.85 x 10^{-7}, 2.18 x 10^{-7}, and 8.88 x 10^{-7} M, respectively, within a linear range between 5 x 10^{-7} M and 1 x 10^{-5} M. The results of this study were compared with HPLC, showing the validity of the pre-treated sensor as an economical, rapid, and sensitive method for environmental protection [91]. Pradela-Filho et al. investigated the suitability of incorporating glass varnish, an alkyd resin, into carbon conductive inks for disposable electrochemical SPE sensors. The SPE sensors measured a range of analytes, including estriol, in the linear range of 1 x 10^{-7} - 8 x 10^{-6} M, with an LOD of 8 x 10^{-8} M. The new material can be inexpensive when designing disposable SPEs to enhance analytical performance. This is because of the efficient dispersion of the graphite particles with the functional groups of the glass varnish (alkyd resin) as a suitable binder, leading to high electrical conductivity and excellent adhesion without aggregation [127].

Moreira et al. reported the application of a carbon paste electrode modified with magnetite nanoparticles and the ionic liquid, 1-butyl-3-methylimidazolium hexafluorophosphate, in the electroanalytical determination of E2 and E3. Due to the irreversible nature of E2 and E3, peaks at +0.32 V and +0.4 V were observed, which were triple the unmodified SPE values. Optimizing the measurement parameters, i.e., scan increment, amplitude, and frequency, was possible using the box-behnken factorial design for each estrogen. For 17β-estradiol, the calibration plot was linear from 1 x 10^{-7} to 1 x 10^{-6} M, with a LOD of 5.0 x 10^{-8} M.

At the same time, for estriol, the range was 1 x 10^{-7} to 1 x 10^{-6} M, with a LOD of 3 x 10^{-7} M. A statistical comparison was made between these results and those obtained using ultraviolet-visible (UV/Vis) spectrometry with no significant difference, demonstrating the quality of the modified sensors [23].

2.8 Screen-printed Biosensors for Estradiol

Electrochemical biosensors are electrochemical sensors that provide analytical information using an analyte's biological recognition element (biochemical or biological mechanisms). In a biosensor device, the key features that determine the performance include the bioreceptor, which is responsible for interacting with the target analyte. The performance of a biosensor depends on the interaction between its components, such as the bioreceptor and the transducer. These components affect the device's sensitivity, selectivity, and stability [28]. The bioreceptor, an enzyme, antigen, antibody, or aptamer, allows for specific interaction with the target analyte, providing selectivity. The transducer converts this interaction into a measurable signal, which can be electrochemical, optical, or based on EIS, as mentioned in section 2.4 [64]. The sensitivity of the biosensor relies on the transducer's ability to amplify and measure the signal effectively. Therefore, a highly sensitive bioreceptor paired with an efficient transduction mechanism can detect analytes at low concentrations, making the biosensor suitable for trace detection. The stability of the biosensor is influenced by both the bioreceptor and the transducer, which must maintain their integrity under operational conditions [64].

Electrochemical biosensors are already used in diagnostic, agri-food, and environmental applications [128]. Therefore, the application of biosensors in detecting estrogenic EDCs has received significant interest. A review presented

by Lu et al. in 2019 updated the recent progress (2017-2019) concerning biosensors for monitoring estrogens in the environment and food. The study covered all biosensor transduction methods, not only electrochemical sensors, and briefly referred to SPEs [28].

On the other hand, Jaiswal et al. reviewed recent advancements in biosensor technology based on carbon nanomaterial modified SPEs [64] but only briefly mentioned the detection of estrogens. Generally, the LOD, analysis time, sensitivity and selectivity are vital when designing an electrochemical sensor or biosensor. Furthermore, a trade-off is required between signal improvement and the time taken for measurement. Therefore, careful consideration of the application is needed when deciding whether to use an electrochemical sensor or a biosensor, in addition to portability, cost, and ease of operation (with or without sample preparation). Most of the relevant studies in the literature on sensor developments are based on CNTs and graphene platforms. Table 2.1 presents a range of reported approaches for detecting estrogens employing electrochemical sensors and screen-printed biosensors. The table provides the sensors and biosensors for estrogens analysis and the various modifying materials used in the design, with sensitivity evidently at the heart of improving the performance of the sensors. The table shows that carbon materials are predominantly used in constructing E2 sensors, offering several advantages since they are relatively inexpensive, versatile, and chemically inert [99,129]. However, there are fewer reports on SPEs. Most of the most relevant studies on sensor developments in the literature are based on CNTs and graphene platforms. In addition, carbon-based species in both modified and unmodified forms, including graphene, graphite, and CNTs, are commonly employed in

detecting E2 in various matrices. From the reported E2 sensors in Table 2.1, the LODs are generally 1 x 10^{-7} M. Reduced graphene oxide, graphene, and carbon nanotubes, combined with other materials such as conductive polymers, have been reported. Despite the noted work, little detailed research has been done on screen-printed electrodes, perhaps the most common approach used in other electrode systems, such as glassy carbon electrodes, to fully assess the capability of this electroanalytical approach for detecting E2.

2.8.1 Enzyme-Modified Screen-printed Electrode

Enzymatic biosensors are a well-developed group of sensors in health, environmental, and food analysis applications [130]. Recombinant techniques have revolutionized enzyme production, offering alternatives to traditional methods of isolating enzymes from natural sources [131]. This has particularly benefited amperometric biosensors, which rely on enzyme-catalysed reactions to measure electrical current [132, 133]. This is applied to enhance the SPE development as a simple and effective technique for electrochemical enzyme-based biosensors [132, 133]. Despite this, enzyme-based biosensors still face various challenges, such as sensitivity to temperature and pH, enzyme degradation, and issues like E2 oxidation fouling and the use of electrochemical mediators in enzyme electrodes. Other obstacles include interference from other substances and environmental factors affecting enzyme stability, cost, and attachment to transducer surfaces [35]. Aromatase enzymes have been involved in the biosensing of various analyses since the first work by [134]. Laccase has also been exploited for estrogen estradiol detection [135, 136]. Using SPE as a transducer, the Kuzikov group [137] described the electrocatalytic activity of CYP19A1 (aromatase) on screen-printed electrodes modified by di-dodecyl

dimethylammonium bromide (DDAB). The reaction pathways of CYP19A1 produce products (estrone and estradiol) of the induced CYP19A1 reactions, determined by direct electrochemical oxidation on the electrode. Sensitivity values obtained were 0.1 A/M for estrone and 0.12 A/M for estradiol, respectively. Detection limits were calculated to be 1.1 x 10^{-8} M and 3.4 x 10^{-9} M for estrone and estradiol [137].

2.8.2 Antibody-Modified Screen-printed Electrode

Immunosensors are among the most reported biosensors, using antigens or antibodies specific to a target. A transducer measures the binding of a complementary target with the bioreceptor in a sample under investigation. This can be carried out as labelled or label-free assays, as shown in Figure 2.11 [105]. The antibody/antigen binding interaction is specific and selective and can be determined by electrochemical, optical, and mass techniques. Immunoassay kits are available to detect many environmental pollutants [138]. Combining screen-printing production methods and immunoassay allows for low-cost, high-volume production required for environmental analysis. In 2005, Pemberton et al. [139] conducted one of the first studies investigating the possibility of integrating immunoassay with an electrochemical method for rapid analysis of E2. They recorded a LOD of 1.8 x 10^{-10} M for an E2 concentration range of 9.17 x 10^{-11} - 1.83 x 10^{-9} M [139]. Kanso et al. described using magnetic beads attached to a carboxylic or amine-functionalized estrogen derivative on SPEs for sensitive detection of E2 and EE2 with immunosensors. They used SWV as the electrochemical technique for quantification.

The electrochemical immunosensors showed a highly sensitive response to E2 and EE2, with LODs of 3.67 × 10^{-12} M and 3.67 × 10^{-11} M. The sensors offer an

easy and rapid assay protocol, with an assay time of 120 minutes compared to 280 minutes for conventional immunoassays [27]. Scala-Benuzzi et al. reported a paper-based immunocapture assay (EPIA) for ethinyl estradiol (EE2) determination in water samples. The sensor combined paper microzones on an SPE modified with electrochemically reduced graphene (rGO). LOD and linear range values of 3.67 x 10^{-13} M and 1.830 x 10^{-12} M - 4.4 x 10^{-10} M, respectively, were obtained [140]. Disposable immunosensors based on SPEs were used as a direct enzyme-linked immunosorbent assay (ELISA) for estradiol detection in bovine serum. A polyclonal antibody was used to compete with 17β-estradiol-alkaline phosphatase conjugate (17β-E2-AP) [141]. The prototype sensors recorded a LOD below the action limit of 1.46 x 10^{-10} M for E2, as EU criteria (2002/657/EC) described for qualitative and quantitative screening methods. Ma et al. employed a multiplexed immunoassay method to determine DES and E2 using disposable SPE. The immunosensors had different antibodies attached to the SPE with platinum nanoparticle-functionalized mesoporous silica nanoparticles (Pt@SBA-15) as the label for the secondary antibodies. Platinum catalytic properties and mesoporous silica (SBA-15) allowed a strong signal towards the analytical antigens. The sensor response to DES and E2 showed wide linear ranges with LODs of 1.03 x 10^{-12} M and 4.40 x 10^{-12} M, respectively [142].

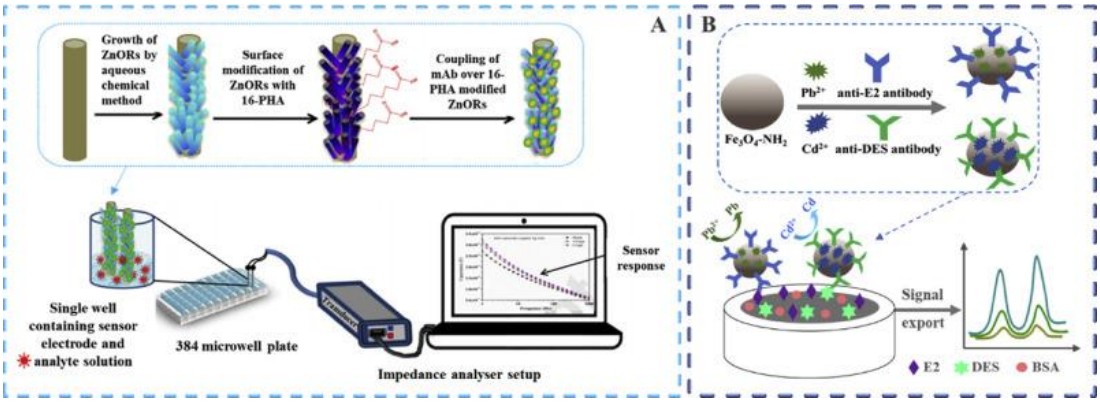

Figure 2.11 Schematic diagram of electrochemical immunosensors. A. Label-free immunosensor based on ZnONRs modified silver wire electrode [10]. B. Immunosensor based on Fe_3O_4–NH_2–Cd_{2+} and Fe_3O_4–NH_2–Pb_{2+} labelled antibodies (Reproduced with permission from Elsevier ref. [28]**. Copyright 2021 Elsevier).**

An immunosensor for estradiol was reported based on forming a biotin-streptavidin linkage using a p-aminobenzoic acid-modified screen-printed carbon electrode [143]. Covalently bound streptavidin serves as the bridge for the biotinylated anti-estradiol. A competitive immunoassay was analysed with peroxidase-labelled estradiol (HRP–estradiol) using amperometry at -0.2 V with hydroquinone (HQ) as a redox mediator. The calibration curve was linear between 3.67 x 10^{-12} M to 9.17 x 10^{-10} M and 2.83 x 10^{-12} M LOD. The fabricated immunosensor was tested in serum and urine samples with promising results [143]. Mistry et al. provide a valuable review of amperometric detection techniques for immunosensors based on SPEs. They explicitly explain the measurement principle, design of the sensors, and modifications, highlighting the strengths and weaknesses. However, estrogen detection is not covered [144].

2.8.3 Aptamer-based Screen-printed Electrode

Aptamers are an alternative bio-recognition element synthesised chemically with the target. Their advantages over other biological recognition elements, such as antibodies, peptides, and enzymes, include high stability and exceptional affinity

to various targets, overcoming drawbacks (highlighted in section 2.8.1) of short shelf-life, poor stability, decreased catalytic activity and limited analytical response [44]. (Three independent research groups discovered aptamers almost simultaneously, paving the way for the active engagement in nucleic acid research we are witnessing now [145,146].)

Aptamers are single-stranded DNA/RNA produced by an in-vitro process known as the Systematic Evolution of Ligands by Exponential Enrichment (SELEX), as shown in Figure 2.13. They comprise 20 to 120 nucleotides with a nitrogenous base, a five-carbon sugar (ribose or deoxyribose), and a phosphate group [147]. SELEX allows for generating aptamers that bind with high affinity and specificity to the compound. The process starts with generating an extensive oligonucleotide library consisting of randomly generated sequences of specific lengths with a constant sequence at positions 5' and 3' ends, which serve as primers, as shown in Figure 2.12. Nezami et al. [30] provided an overview of the applications of aptamer-based biosensors and bioaffinity sensors in the analysis and monitoring of estradiol [30]. Gatel et al. [148] published a detailed report on nucleic acid sensor technology to detect EDCs in the environment [148].

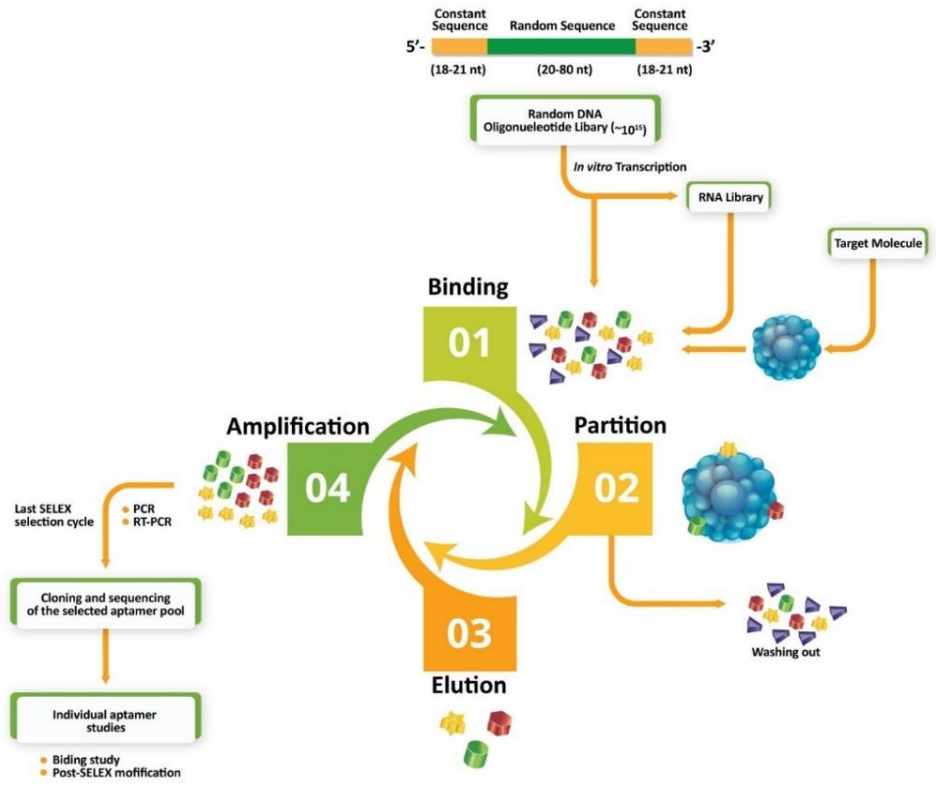

Figure 2.12 Schematic of the Systematic evolution of ligands by Exponential Enrichments (SELEX) process [1].

Kim and his group reported the first aptamer (a 76-mer and 23 kDa sequence) for 17β-estradiol, produced using the SELEX process [149]. Since 2007, the sequence has been extensively studied with modifications [13, 150–155] on various electrode surfaces and using different transduction techniques. Zaid et al. utilized the same sequence, aminated at the 5'-end with $–NH_2$, to develop an electrochemical aptamer sensor on a screen-printed electrode (SPCE) modified by electrodeposition of carbon nanodots as an immobilization platform and probe for the detection of E2. The E2 aptamer-based biosensors were tested at various concentrations of E2 with a linear range of 1.0×10^{-10} M to 7×10^{-7} M and a LOD of 5.0×10^{-13} M. Furthermore, it was used to measure actual river water samples. The selectivity of the fabricated sensor was tested against bisphenol A (BPA), estriol (E3), and progesterone (P4), with good selectivity toward E2 and excellent

discrimination, respectively. E2-spiked water samples were recovered from 98.2% - 103.8%, relative standard deviations (RSD) of 1.1% - 3.8%, revealing the feasibility of applying the aptamer sensor for E2 measurement in water samples [156].

The immobilization of aptamers on gold substrates allows for various sequence modifications, such as thiol-Au bond formation and EDC/NHS attachments. These are ways to combine aptamers on transducer surfaces with other emerging strategies, even without a secondary aptamer [157]. No aptamer development has been reported for estrogens E1, E3, and EE2 due to the limited molecular diversity of libraries [158, 159].

2.8.4 Molecularly Imprinted Polymer (MIP)-Modified Screen-printed Electrode

Molecularly imprinted polymers (MIPs) are among the most promising alternatives for investigating natural receptors [160]. Molecular imprinting technology (MIT) was first reported by Polyakov more than 80 years ago. However, its applications remain in immunoassays, affinity separation, and sensors, making it relevant to date [161]. Molecular imprinting is a technique for creating binding sites within a polymer network with the same shape, size, and functional groups as the target (template). A template (target analyte), monomer, initiator, and cross-linker undergo polymerization in MIP synthesis to form a polymer complex between the target molecule and functional monomers in a solvent. Template removal, after polymerization, leaves a vacant site in the porogen, which is utilized for mimicking the molecular recognition ability of natural receptors within the polymer network [162, 163], making it selective to the template (analyte of interest).

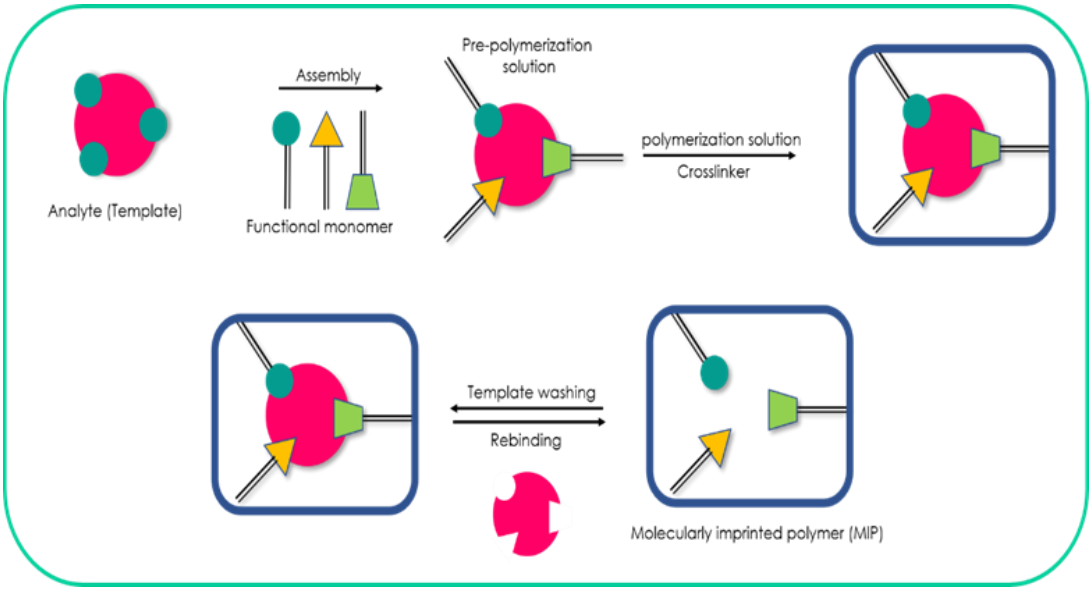

Figure 2.13 Schematic representation of molecularly imprinted polymers (MIPs) synthesis.

Combining MIP and electrochemistry to produce molecularly imprinted electrochemical sensors (MIECs) has improved sensor capabilities [164]. Different analytical methods have been used, such as amperometry, potentiometry, conductometry, and voltammetry. Figure 2.14 illustrates the various analytical methods reported for MIECs, allowing direct and indirect redox probe methods to be used as the basis for detection. Furthermore, Beluomini et al. reviewed the application of molecularly imprinted polymers on nanostructured carbon materials, such as carbon nanotubes and graphene, due to the increasing sensitivity, selectivity, and stability achieved by combining the properties of the two materials, as opposed to their use individually [165].

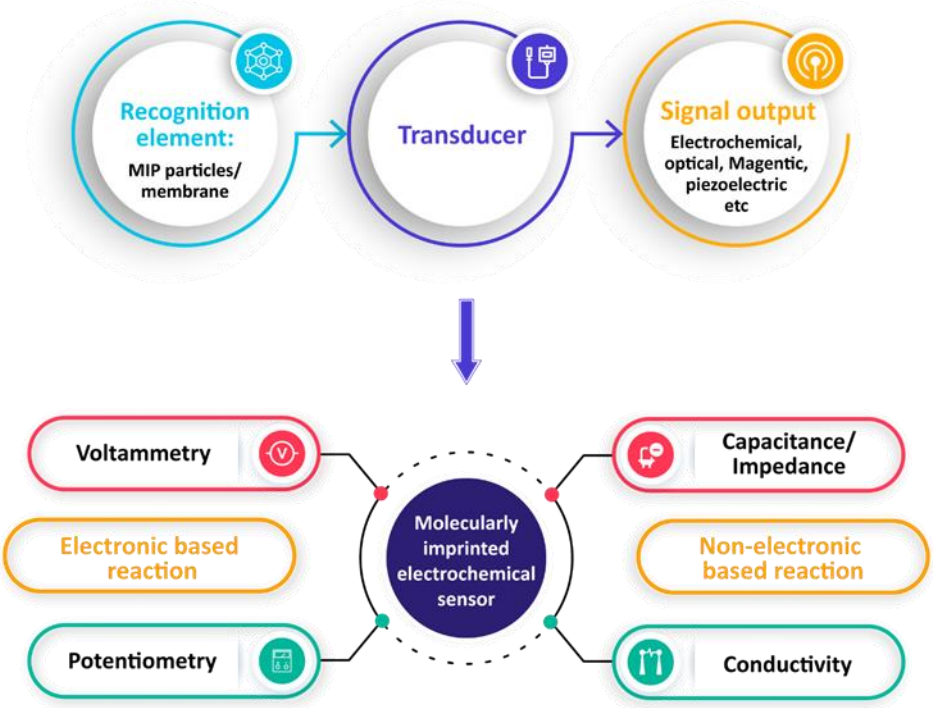

Figure 2.14 Mechanisms of molecularly imprinted electrochemical sensors (MIECS) [1].

As reported in various works in the literature, hybrid materials are essential in environmental monitoring applications [166]. MIPS has continued to attract researchers' attention, with over 16,000 review articles [167]. This hybrid polymer combines the advantages of organic and inorganic materials. It exhibits unique properties, such as structural flexibility and thermal and mechanical stability. MIPS are considered to complement polyclonal antibodies as bio-inspired materials for sensors [167–169].

Synthetic receptors have been explored to replace biological receptors [147]. The main drivers include reducing costs, increasing sensor shelf-life, and eliminating denaturation issues to make the sensors more suitable for measuring complex environmental matrices [170–172]. In a molecularly imprinted electrochemical sensor (MIECS), the rule of thumb is to have selective and sensitive recognition

for the analyte of interest, which is the template. This gives molecularly imprinted polymers (MIPs) the upper hand as an alternative due to their unique properties, appreciable potential detection range, cost, high sensitivity, ease of preparation, and compatibility with various analyte templates. Lahcen and coworkers [173] developed a MIP sensor (Fe_3O_4-MIP) using aniline and dimethacrylate (EGDMA) as monomers for the detection of estradiol. Iron nanoparticles (Fe_3O_4) were utilized as part of the pre-polymerization mixture for signal amplification due to the high surface area.

The MIP-based sensor increased the oxidation current using square wave voltammetric measurements, delivering a linear range of 5×10^{-8} –11×10^{-5} M and a LOD of 2×10^{-8} M [173]. Futra et al. [182] developed a molecularly imprinted polymeric microsphere MWNT–gold nanoparticle (AuNP) modified SPE to detect the E2 hormone in serum samples rapidly. MWCNT and AuNPs aid the acceleration of electron transfer, while the microspheres were designed to bind specifically to E2. A photopolymerization technique was employed to deposit the MIP on SPCE. Under optimal conditions, the sensor could detect the concentrations of 17β-estradiol from 1×10^{-9} M to 1×10^{-6} M with a LOD of 2.5×10^{-11} M [174]. A similar polymerization method for antibiotics was reported by [175]. Thermocouples were used for thermal measurements of the MIP sensors. Screen-printed electrodes were doped with gold nanoparticles to provide a suitable platform for developing an MIP receptor for E2 detection. The rationale was to create a platform with high surface areas stable enough to generate a uniform polymer matrix on the electrode surface. Truong et al. reported the electrodeposition of AuNPs onto SPEs followed by electropolymerisation of functional monomer for E2 analysis. The rationale was to increase the specific

area of the membrane MIP electrode, thus increasing the imprinted site. They reported a LOD of 2 x 10^{-15} M. This demonstrates that using gold nanoparticles instead of gold ink on the carbon SPE platform results in the simplicity of manufacture and high reproducibility [176]. Recently, Jiang et al. [177] reported a signal-on type electrochemiluminescence (ECL) hybrid sensor for diethylstilbestrol (DES), a synthetic form of the E2 employing a magnetic surface. The surface comprised a magnetic molecular imprinted polymer (MMIP) coupled with aptamer-labelled cadmium selenide quantum dots (CdS QDs) conjugated probe [177]. The MMIPs-DES-CdS-apt composite was attached to an SPE using an external magnetic field. The sensor emitted an electrochemical luminescence signal at a potential of -1.1 V. The signal intensity was proportional to the DES concentrations in the range of 1.1 x 10^{-12} M to 3.67 x 10^{-17} M, with the LOD of 3.67 x 10^{-13} M. The rationale behind using the E2 aptamer was not given, just the statement that it served as a tag. However, the E2 to aptamer binding is assumed to have higher affinity than the antibody to antigen [177]. This is the first concept of a hybrid Apta-MIP sensor for estrogen. However, we have seen MIP combined with other materials, such as a peptide-polymer hybrid system for lipopolysaccharide [179], and previously reported novel biomimetic Apta-MIP hybrid to detect cocaine [180]. Lee and his group reported the integration of MIPs and screen-printed gold electrodes for the electrochemical determination of steroidal hormones cortisol, progesterone, testosterone, and E2 in urine simultaneously. They established a four-channel system to determine the hormones by CV simultaneously. The concentration range and the LOD were 3.67 x 10^{-21} to 3.67 x 10^{-18} M and 3.31 x 10^{-22} M, respectively [181].

Moreover, a MIP-SPE sensor based on a tungsten disulfide coating formed by electropolymerisation of aniline and a metanilic acid-conductive polymer SPE was created to detect 17β-estradiol. As a transition metal dichalcogenide (TMD) type, tungsten is a dopant due to its direct band gaps, improving the electrochemical signal. The MIP-SPE sensor was applied to eel serum samples with various concentrations of E2 in the 2.67×10^{-10} - 3.83×10^{-10} M range, and an LOD of 2.20×10^{-16} M was obtained [182]. The commercial viability of MIPs in sensors has still not been proven. However, separation methods have successfully applied the technology [147]. Recent focus has been on developing Molecularly Imprinted Polymers (MIPs) for sensors, but still behind traditional biosensors due to the need for further optimization. Despite active research, commercial MIP sensors are still in the early stages. Similarly, their use in environmental monitoring is developing, with much potential for future exploration [183].

Table 2.1. Summaries of recent developments in the application of screen-printed electrochemical sensors & biosensors for the determination of estrogens [1].

SPE-Design	Modifier	Applied Technique	Sensor type	Linear range	LOD	Estrogens	Samples	Ref.
Screen-printed carbon electrode	Aptamer/Carbon Nanodots	electrochemical impedance spectroscopy	Impedimetric biosensor	1.0 x 10^{-7} to 1.0 x 10^{-12} M	5.0 x 10^{-13} M	Estriol (E3)	River water samples	[156]
Screen-printed carbon electrode	Reduced graphene oxide/silver nanowires (AgNWs) and silver nanoparticles (AgNPs)	differential pulse voltammetry	Electrochemical sensor	1.0 x 10^{-6} to 9.0 x 10^{-5} M	5.8 x 10^{-7} M	Estriol (E3)	Urine	[184]
Screen-printed carbon electrode	Glass varnish-based carbon conductive ink	square wave voltammetry	Electrochemical sensor	1.0 x 10^{-7} to 8.0 x 10^{-6} M	8.0 x 10^{-8} M	Estriol (E3)	Water, Vaginal cream	[127]

Table 2.1. Summaries of recent developments in the application of screen-printed electrochemical sensors & biosensors for the determination of estrogens [1].

SPE-Design	Modifier	Applied Technique	Sensor type	Linear range	LOD	Estrogens	Samples	Ref.
Screen-printed carbon electrode		Square wave voltammetry	Electrochemical sensor	1.7 x 10^{-3} M	2.42 x 10^{-4} M	Estradiol (E2)	urine	[69]
Screen-printed carbon electrode		Square wave voltammetry	Electrochemical sensor	2 x 10^{-6} M	2.77 x 10^{-4} M	Ethinylestradiol (EE2)	urine	[69]
Screen-printed carbon nanotube electrode (SPCNTE)	carbon nanotubes	Square wave voltammetry	Electrochemical sensor	4.41 x 10^{-6} M	6.68 x 10^{-7} M	Estradiol (E2)	urine	[69]
Screen-printed carbon nanotube electrode (SPCNTE)	carbon nanotubes	Square wave voltammetry	Electrochemical sensor	5.40 x 10^{-6} M	6.44 x 10^{-7} M	Ethinylestradiol (EE2)	urine	[69]

Table 2.1. Summaries of recent developments in the application of screen-printed electrochemical sensors & biosensors for the determination of estrogens [1].

SPE-Design	Modifier	Applied Technique	Sensor type	Linear range	LOD	Estrogens	Samples	Ref.
Gold-Screen printed electrode (Au-SPE)	MIP Coated poly (ANIco-MSAN) s	cyclic voltammetry	Electrochemical sensor	1 x 10^{-18} - 1 x 10^{-12} M	9 x 10^{-18} M	Estradiol (E2)	urine	[181]
Gold-Screen printed electrode (Au-SPE)	(TSMEIPs) poly (AN-*co*-MSAN)	cyclic voltammetry	Electrochemical sensor	1.32 x 10^{-11} - 2.68 x 10^{-10} M	9 x 10^{-18} M	Estradiol (E2)	serum	[182]
Screen-printed electrode	antibody	differential pulse voltammetry	Immunosensor	9.18 x 10^{-11} - 1.84 x 10^{-9} M	1.84 x 10^{-10} M	Estradiol (E2)	serum	[139]
Screen-printed electrodes	Electrochemical pre-treatment	differential pulse voltammetry	Electrochemical sensor	5 x 10^{-7} - 1 x 10^{-5} M	8.88 x 10^{-7} M	Estradiol (E2)	Tap water	[185]
Screen-printed electrodes	CuPc-P6LC-Nafion/SPE_F	differential pulse voltammetry	Electrochemical sensor	8.0×10^{-8} to 7.3×10^{-6} M	5.0×10^{-9} M	Estradiol (E2)	River Water samples	[123]
Screen-printed electrodes	Fe_3O_4-MIP/SPCE	Square wave voltammetry	Electrochemical sensor	5 x 10^{-8} - 1 x 10^{-5} M	2 x 10^{-8} M	Estradiol (E2)	River water samples	[173]
Screen-printed electrodes	MIP-AuNPs-SPCE	EIS	Electrochemical sensor	1 x 10^{-10} - 1 x 10^{-8} M	2 x 10^{-12} M	Estradiol (E2)	PBS Buffer	[176]

Table 2.1. Summaries of recent developments in the application of screen-printed electrochemical sensors & biosensors for the determination of estrogens [1].

SPE-Design	Modifier	Applied Technique	Sensor type	Linear range	LOD	Estrogens	Samples	Ref.
Screen-printed electrodes	MWNTs/Al2O3/poly-L-lysine	cyclic voltammetry	Electrochemical sensor	5×10^{-10} - 5×10^{-8} M	1.4×10^{-11} M	Estradiol (E2)	Blood and urine samples	[70]
Screen-printed electrodes	MWCNT–AuNP-SPE	differential pulse voltammetry	Electrochemical sensor	1.0×10^{-15} - 1.0×10^{-6} M	2.5×10^{-16}M	Estradiol (E2)	serum	[186]
Screen printed electrode	E2-HexaMagnetic Beads	square wave voltammetry	Immunosensor	3.67×10^{-10} - 3.67×10^{-7} M.	3.67×10^{-8} M	Estradiol (E2)	Water samples	[27]
Screen printed electrode	EE2-Hexa-Magnetic Beads	square wave voltammetry	Immunosensor	3.37×10^{-10} - 3.37×10^{-7} M.	3.37×10^{-8} M	Ethinylestradiol (EE2)	Water samples	[27]
Screen printed electrode	Anti-estradiol-Biotin/Strept-ABA-g-SPCE.	Electrochemical impedance spectroscopy	Immunosensor	3.67×10^{-12} - 9.18×10^{-10} M.	2.82×10^{-12} M.	Estradiol (E2)	human serum and urine.	[143]
Screen printed electrode	Anti-17ß-estradiol antibody Au-protein-SPCE	cyclic voltammetry	Immunosensor	3.67×10^{-10} - 7.34×10^{-8} M.	1.28×10^{-10} M	Estradiol (E2)	Serum	[187]

Table 2.1. Summaries of recent developments in the application of screen-printed electrochemical sensors & biosensors for the determination of estrogens [1].

SPE-Design	Modifier	Applied Technique	Sensor type	Linear range	LOD	Estrogens	Samples	Ref.
Screen printed electrode	Anti-rabbit IgG-17ß-estradiol antibody-SPCE	differential pulse voltammetry	Immunosensor		5.51 x 10^{-11} M.	Estradiol (E2)	Serum	[141]
Screen printed electrode	Anti-17ß-estradiol antibody-SPCE	amperometry	immunosensor	3.67 x 10^{-11} - 3.67 x 10^{-8} M	9.18 x 10^{-13} M.	Estradiol (E2)	serum	[188]
Screen-printed electrodes	[C8py][PF6]-MWCNTs	Linear sweep voltammetry	Electrochemical sensor	5 x 10^{-5} - 2 x 10^{-3} M	2 x 10^{-9} M	Ethinylestradiol (EE2)	phosphate buffer solution (pH 7.0)	[117]
screen-printed electrodes	Pt@SBA-15-Ab2	cyclic voltammetry	immunosensor	1.84 x 10^{-12} - 2.94 x 10^{-9} M.	4.40 x 10^{-12} M	Estradiol (E2)	River water samples	[142]
screen-printed electrodes	Pt@SBA-15-Ab2	cyclic voltammetry	immunosensor	3.37 x 10^{-12} - 3.37 x 10^{-9} M	9.44 x 10^{-13} M	Ethinylestradiol (EE2)	River water samples	[142]
screen-printed electrodes	MMIPs-QDs-Apt	Electrochemiluminescence (ECL)		1.04 x 10^{-9} - 3.47 x 10^{-4} M	3.47 x 10^{-10} M	diethylstilbesterol	Serum	[177]

Table 2.1. Summaries of recent developments in the application of screen-printed electrochemical sensors & biosensors for the determination of estrogens [1].

SPE-Design	Modifier	Applied Technique	Sensor type	Linear range	LOD	Estrogens	Samples	Ref.
screen-printed electrodes	Enzyme electrodes (SPE/DDAB/CYP19A1)	square wave voltammetry	Biosensor		1.1×10^{-8} M	Estradiol (E2)	Buffer	[137]
screen-printed electrodes	Reduced-Graphene oxide-SPCE	square wave voltammetry	Biosensor	1.69×10^{-12} - 4.1×10^{-10} M	3.37×10^{-13} M	ethinyl estradiol (EE2)	water samples	[140]
screen-printed electrodes	Multiwalled Carbon nanotube	Amperometry	Electrochemical sensor	1×10^{-6} - 1×10^{-3} M	5.3×10^{-7} M	Estriol (E3)	pharmaceutical sample	[115]
Screen-printed electrodes	Anti-E1/ Polyaniline (PANI)/Gr-SPE	Electrochemical Impedance Spectroscopy (EIS)	Biosensor	3.57×10^{-13} - 7.33×10^{-10} M	1.57×10^{-13} M	Estrone (E1)	River water samples	[113]
screen-printed electrodes	Anti-E1/ Polyaniline (PANI)/Gr-SPE	Electrochemical Impedance Spectroscopy (EIS)	Biosensor	3.58×10^{-13} 7.34×10^{-10} M	6.97×10^{-13} M	Estradiol (E2)	River water samples	[113]
screen-printed electrodes	Anti-EE2/ Polyaniline (PANI)/Gr-SPE	Electrochemical Impedance Spectroscopy (EIS)	Biosensor	3.29×10^{-13} 6.74×10^{-10} M	2.36×10^{-13} M	ethinyl estradiol (EE2)	River water samples	[113]
screen-printed electrodes	Graphene quantum dots (GQD)/SPE	Linear Sweep voltammetry	Electrochemical sensor	5×10^{-8} - 7.5×10^{-6} M	8.8×10^{-9} M	diethylstilbesterol (DES)	Urine and tap water	[189]

2.9 Summary

Electrochemical sensors have been studied extensively, and efforts to enhance their performance remain ongoing. This chapter provided an overview of the current literature in this domain. Various nanomaterials, including carbon-based materials, metal oxides, ionic liquids, and metals, have been identified as beneficial for sensor enhancement [1]. While they have demonstrated superior performance in detecting a range of analytes compared to traditional techniques, there is a noticeable lack of research on screen-printed electrode (SPE)-based methods. A rising area of interest is the SPE-based immunosensors, especially given the prevalent use of commercial immunoassay kits and antibodies.

However, it is essential to recognise that SPE-based sensors are primarily in the research phase and not commercially available. Despite this, there is potential for academic growth through refining current methods. The development of high-performing SPEs may necessitate the integration of multiple materials. Nevertheless, this endeavour is not without its challenges. For instance, conventional drop-coating methods suitable for other electrodes may not be directly transferable to SPEs. This discrepancy is partly because of the unique nature of the SPE's reference electrode, known as a pseudo-reference electrode, which can degrade prematurely. Such degradation can lead to inconsistencies in results obtained from electrochemical oxidation processes. Nonetheless, recent studies, like those by [91], indicate that pre-treated SPEs can rival the performance of their nanomaterial-based counterparts. Designing SPE-based electrochemical sensors using diverse nanomaterials remains a complex task due to challenges related to sensitivity, specificity, and the need for ongoing real-

time analysis on wash-free platforms with antifouling features and calibration-free sensing systems.

The recent literature suggests that the current fabrication of E2 sensors has limitations in terms of specificity, sensitivity, and variability due to the fabrication processes. However, various nanomaterials and pre-treatment techniques can significantly improve their performance. The added complexity and additional steps involved in electrode pre-treatment directly defeat the purpose of plug-and-play. Thus, there is a need to develop more effective, simple, and specific electrochemical sensors for E2, emphasising using carbon materials that are easy to synthesise. As reported, E2 sensor designs often have limited sensitivity, posing difficulty detecting lower concentrations. Moreover, sensor materials and designs can be costly to fabricate, limiting their practicality for widespread use in environmental monitoring due to cost considerations.

This study aims to develop an electroanalytical method for monitoring E2 levels in water. The method employed here utilised the direct anodic oxidation current of E2 using carbonaceous electrode materials, thereby eliminating the need for complex mechanism and material preparation steps, unlike other electrochemical approaches that require specialized bioreceptors such as enzymes, antibodies and complex preparation techniques in the case of graphene synthesis using chemical vapour deposition. The method proposed here serves as an alternative analytical tool with several advantages. These advantages include the simplicity of hydrothermal synthesis and the use of readily available precursors like glucose. Additionally, the method utilizes plant extracts for the dual reduction of reduced-graphene-oxide-gold nanoparticle-carbon nanotube-modified screen-

printed electrodes (rGO-AuNP/CNT) at room temperature, further simplifying the material preparation process by eliminating the need for specialized equipment.

Furthermore, these materials offer several advantages, such as eliminating the need for strong oxidants, cost-effectiveness, and achieving stable dispersions without solvents like DMSO or DMF. This stability is crucial for straightforward electrode modification via drop-casting. Although previous research has emphasized their remarkable electroanalytical capabilities for various analytes, including dopamine, catechol and estriol [21], gaps remain in understanding their electrochemical behaviour specific to E2.

References

[1] A.M. Musa, J. Kiely, R. Luxton, K.C. Honeychurch, Recent progress in screen-printed electrochemical sensors and biosensors for the detection of estrogens, TrAC - Trends Anal. Chem. 139 (2021) 116254. https://doi.org/10.1016/j.trac.2021.116254.

[2] V. Geissen, H. Mol, E. Klumpp, G. Umlauf, M. Nadal, M. van der Ploeg, S.E.A.T.M. van de Zee, C.J. Ritsema, Emerging pollutants in the environment: A challenge for water resource management, Int. Soil Water Conserv. Res. 3 (2015) 57–65. https://doi.org/10.1016/J.ISWCR.2015.03.002.

[3] E. Özgür, E. Yılmaz, G. Şener, L. Uzun, R. Say, A. Denizli, A new molecular imprinting-based mass-sensitive sensor for real-time detection of 17β-estradiol from aqueous solution, Environ. Prog. Sustain. Energy. 32 (2013) 1164–1169. https://doi.org/10.1002/ep.11718.

[4] G. Csaba, The Immuno-Endocrine System: Hormones, Receptors and Endocrine Function of Immune Cells. The Packed-Transport Theory, Adv. Neuroimmune Biol. 1 (2011) 71–85. https://doi.org/10.3233/NIB-2011-007.

[5] S. Barreca, M. Busetto, L. Colzani, L. Clerici, D. Daverio, P. Dellavedova, S. Balzamo, E. Calabretta, V. Ubaldi, Determination of estrogenic endocrine disruptors in water at sub-ng L −1 levels in compliance with Decision 2015/495/EU using offline-online solid phase extraction concentration coupled with high performance liquid chromatography-

tandem mass spectrometry, Microchem. J. 147 (2019) 1186–1191. https://doi.org/10.1016/j.microc.2019.04.030.

[6] A. Pillon, A.M. Boussioux, A. Escande, S. Aït-Aïssa, E. Gomez, H. Fenet, M. Ruff, D. Moras, F. Vignon, M.J. Duchesne, C. Casellas, J.C. Nicolas, P. Balaguer, Binding of estrogenic compounds to recombinant estrogen receptor-α: Application to environmental analysis, Environ. Health Perspect. 113 (2005) 278–284. https://doi.org/10.1289/ehp.7522.

[7] P. Busayapongchai, S. Siri, Sensitive detection of estradiol based on ligand binding domain of estrogen receptor and gold nanoparticles, Anal. Biochem. 518 (2017) 60–68. https://doi.org/10.1016/J.AB.2016.11.003.

[8] A. Florea, C. Cristea, F. Vocanson, R. Săndulescu, N. Jaffrezic-Renault, Electrochemical sensor for the detection of estradiol based on electropolymerized molecularly imprinted polythioaniline film with signal amplification using gold nanoparticles, Electrochem. Commun. 59 (2015) 36–39. https://doi.org/10.1016/J.ELECOM.2015.06.021.

[9] D. deCatanzaro, Sex steroids as pheromones in mammals: The exceptional role of estradiol, Horm. Behav. 68 (2015) 103–116. https://doi.org/10.1016/J.YHBEH.2014.08.003.

[10] M. Amatoury, J.W. Lee, A.M. Maguire, G.R. Ambler, K.S. Steinbeck, Utility of salivary enzyme immunoassays for measuring estradiol and testosterone in adolescents: a pilot study, Int. J. Adolesc. Med. Health. 0 (2016). https://doi.org/10.1515/ijamh-2015-0126.

[11] M. Adeel, X. Song, Y. Wang, D. Francis, Y. Yang, Environmental impact

of estrogens on human, animal and plant life: A critical review., Environ. Int. 99 (2017) 107–119. https://doi.org/10.1016/j.envint.2016.12.010.

[12] L. Zhao, J.-M. Lin, Z. Li, X. Ying, Development of a highly sensitive, second antibody format chemiluminescence enzyme immunoassay for the determination of 17β-estradiol in wastewater, Anal. Chim. Acta. 558 (2006) 290–295. https://doi.org/10.1016/J.ACA.2005.11.034.

[13] K.J. Huang, Y.J. Liu, J.Z. Zhang, J.T. Cao, Y.M. Liu, Aptamer/Au nanoparticles/cobalt sulfide nanosheets biosensor for 17β-estradiol detection using a guanine-rich complementary DNA sequence for signal amplification, Biosens. Bioelectron. 67 (2015) 184–191. https://doi.org/10.1016/j.bios.2014.08.010.

[14] G.G. Ying, R.S. Kookana, Y.J. Ru, Occurrence and fate of hormone steroids in the environment, Environ. Int. 28 (2002) 545–551. https://doi.org/10.1016/S0160-4120(02)00075-2.

[15] Y. Zhou, J. Zha, Y. Xu, B. Lei, Z. Wang, Occurrences of six steroid estrogens from different effluents in Beijing, China, Environ. Monit. Assess. 184 (2012) 1719–1729. https://doi.org/10.1007/s10661-011-2073-z.

[16] A. Pal, K.Y.H. Gin, A.Y.C. Lin, M. Reinhard, Impacts of emerging organic contaminants on freshwater resources: Review of recent occurrences, sources, fate and effects, Sci. Total Environ. 408 (2010) 6062–6069. https://doi.org/10.1016/j.scitotenv.2010.09.026.

[17] E.P. Kolodziej, D.L. Sedlak, Rangeland grazing as a source of steroid

hormones to surface waters, Environ. Sci. Technol. 41 (2007) 3514–3520. https://doi.org/10.1021/es063050y.

[18] Z. Syed, M. Sogani, A. Dongre, A. Kumar, K. Sonu, G. Sharma, A.B. Gupta, Bioelectrochemical systems for environmental remediation of estrogens: A review and way forward, Sci. Total Environ. 780 (2021) 146544. https://doi.org/10.1016/j.scitotenv.2021.146544.

[19] X. Liu, K. Deng, H. Wang, C. Li, S. Zhang, H. Huang, Aptamer based ratiometric electrochemical sensing of 17β-estradiol using an electrode modified with gold nanoparticles, thionine, and multiwalled carbon nanotubes, Microchim. Acta. 186 (2019). https://doi.org/10.1007/s00604-019-3465-y.

[20] H. Pu, Z. Huang, D.W. Sun, H. Fu, Recent advances in the detection of 17β-estradiol in food matrices: A review, Crit. Rev. Food Sci. Nutr. 59 (2019) 2144–2157. https://doi.org/10.1080/10408398.2019.1611539.

[21] A. Azzouz, S.K. Kailasa, P. Kumar, E. Ballesteros, K.-H. Kim, Advances in functional nanomaterial-based electrochemical techniques for screening of endocrine disrupting chemicals in various sample matrices, TrAC Trends Anal. Chem. 113 (2019) 256–279. https://doi.org/10.1016/J.TRAC.2019.02.017.

[22] P. Gamache, I. Acworth, Measurement of Environmental Estrogens in Water Using a Gradient HPLC-EC-UV Method, (2014). https://assets.thermofisher.com/TFS-Assets/CMD/Application-Notes/AB-160-HPLC-EC-UV-Estrogens-Water-AB71224-EN.pdf (accessed June

20, 2020).

[23] F. Moreira, E.R. Santana, A. Spinelli, Ionic liquid-supported magnetite nanoparticles as electrode modifier materials for estrogens sensing, Sci. Rep. 10 (2020) 1–11. https://doi.org/10.1038/s41598-020-58931-6.

[24] A. Nezami, R. Nosrati, B. Golichenari, R. Rezaee, G.I. Chatzidakis, A.M. Tsatsakis, G. Karimi, Nanomaterial-based aptasensors and bioaffinity sensors for quantitative detection of 17β-estradiol, TrAC Trends Anal. Chem. 94 (2017) 95–105. https://doi.org/10.1016/J.TRAC.2017.07.003.

[25] C.L. Waller, T.I. Oprea, K. Chae, H.K. Park, K.S. Korach, S.C. Laws, T.E. Wiese, W.R. Kelce, L.E. Gray, Ligand-based identification of environmental estrogens, Chem. Res. Toxicol. 9 (1996) 1240–1248. https://doi.org/10.1021/tx960054f.

[26] M. Česen, E. Heath, Disk-based solid phase extraction for the determination of diclofenac and steroidal estrogens E1, E2 and EE2 listed in the WFD watch list by GC–MS, Sci. Total Environ. 590–591 (2017) 832–837. https://doi.org/10.1016/j.scitotenv.2017.02.222.

[27] H. Kanso, L. Barthelmebs, N. Inguimbert, T. Noguer, Immunosensors for estradiol and ethinylestradiol based on new synthetic estrogen derivatives: Application to wastewater analysis, Anal. Chem. 85 (2013) 2397–2404. https://doi.org/10.1021/ac303406c.

[28] X. Lu, J. Sun, X. Sun, Recent advances in biosensors for the detection of estrogens in the environment and food, Trends Anal. Chem. (2020) 115882. https://doi.org/10.1016/j.trac.2020.115882.

[29] C. Li, Y. Wei, S. Zhang, W. Tan, Advanced methods to analyze steroid estrogens in environmental samples, Environ. Chem. Lett. (2020). https://doi.org/10.1007/s10311-019-00961-2.

[30] A. Nezami, R. Nosrati, B. Golichenari, R. Rezaee, G.I. Chatzidakis, A.M. Tsatsakis, G. Karimi, Nanomaterial-based aptasensors and bioaffinity sensors for quantitative detection of 17β-estradiol, TrAC Trends Anal. Chem. 94 (2017) 95–105. https://doi.org/10.1016/J.TRAC.2017.07.003.

[31] L. Barreiros, J.F. Queiroz, L.M. Magalhães, A.M.T. Silva, M.A. Segundo, Analysis of 17-β-estradiol and 17-α-ethinylestradiol in biological and environmental matrices - A review, Microchem. J. 126 (2016) 243–262. https://doi.org/10.1016/j.microc.2015.12.003.

[32] I. Cabas, S. Liarte, A. García-Alcázar, J. Meseguer, V. Mulero, A. García-Ayala, 17α-Ethynylestradiol alters the immune response of the teleost gilthead seabream (Sparus aurata L.) both in vivo and in vitro, Dev. Comp. Immunol. 36 (2012) 547–556. https://doi.org/10.1016/j.dci.2011.09.011.

[33] K.E. Arnold, A.R. Brown, A.R. Brown, G.T. Ankley, J.P. Sumpter, Medicating the environment: Assessing risks of pharmaceuticals to wildlife and ecosystems, Philos. Trans. R. Soc. B Biol. Sci. 369 (2014). https://doi.org/10.1098/rstb.2013.0569.

[34] L. Celik, J.D.D. Lund, B. Schiøtt, Exploring interactions of endocrine-disrupting compounds with different conformations of the human estrogen receptor α ligand binding domain: A molecular docking study, Chem. Res.

Toxicol. 21 (2008) 2195–2206. https://doi.org/10.1021/tx800278d.

[35] G.C. Mauruto de Oliveira, E. P. de Palma, M.H. Kunita, R. Antigo Medeiros, R. de Matos, K.R. Francisco, B.C. Janegitz, Tapioca Biofilm Containing Nitrogen-doped Titanium Dioxide Nanoparticles for Electrochemical Detection of 17-β Estradiol, Electroanalysis. 29 (2017) 2638–2645. https://doi.org/10.1002/elan.201700392.

[36] A.. Kester, M.H., Bulduk, S., Tibboel, D., Meinl, W., Glatt, H., Falany, C.N., Coughtrie, M.W., Bergman, A.K.E., Safe, S.H., Kuiper, G.G. and Schuur, Potent inhibition of estrogen sulfotransferase by hydroxylated PCB metabolites: a novel pathway explaining the estrogenic activity of PCBs, Endocrinology. 141 (2000) 1897–1900.

[37] R.P.A. Barros, J.Å. Gustafsson, Estrogen receptors and the metabolic network, Cell Metab. 14 (2011) 289–299. https://doi.org/10.1016/j.cmet.2011.08.005.

[38] M. Nitkowska, R. Tomasiuk, M. Czyzyk, A. Friedman, Prolactin and sex hormones levels in males with Parkinson’s disease, Acta Neurol. Scand. 131 (2015) 411–416. https://doi.org/10.1111/ane.12334.

[39] C. Schairer, J. Lubin, R. Troisi, S. Sturgeon, L. Brinton, R. Hoover, Menopausal estrogen and estrogen-progestin replacement therapy and breast cancer risk, J. Am. Med. Assoc. 283 (2000) 485–491. https://doi.org/10.1001/jama.283.4.485.

[40] S.C. Janicki, N. Schupf, Hormonal influences on cognition and risk for Alzheimer’s disease, Curr. Neurol. Neurosci. Rep. 10 (2010) 359–366.

https://doi.org/10.1007/s11910-010-0122-6.

[41] M. Farré, L. Kantiani, S. Pérez, D. Barceló, Sensors and biosensors in support of EU Directives, TrAC - Trends Anal. Chem. 28 (2009) 170–185. https://doi.org/10.1016/j.trac.2008.09.018.

[42] G.S.W. Daniel R.Thevenot, Klara Toth, Richard A. Durdt, ELECTROCHEMICAL BIOSENSORS : RECOMMENDED Electrochemical biosensors : Recommended definitions and classification (Technical Report), Pure Appl. Chem. 71 (1999) 2333–2348. https://doi.org/10.1016/S0956-5663(01)00115-4.

[43] H.M. Mohamed, Screen-printed disposable electrodes: Pharmaceutical applications and recent developments, TrAC - Trends Anal. Chem. 82 (2016) 1–11. https://doi.org/10.1016/j.trac.2016.02.010.

[44] A. Villalonga, A.M. Pérez-Calabuig, R. Villalonga, Electrochemical biosensors based on nucleic acid aptamers, Anal. Bioanal. Chem. 412 (2020) 55–72. https://doi.org/10.1007/s00216-019-02226-x.

[45] R.A.S. Couto, J.L.F.C. Lima, M.B. Quinaz, Recent developments, characteristics and potential applications of screen-printed electrodes in pharmaceutical and biological analysis, Talanta. 146 (2016) 801–814. https://doi.org/10.1016/j.talanta.2015.06.011.

[46] K.C. Honeychurch, J.P. Hart, Screen-printed electrochemical sensors for monitoring metal pollutants, TrAC - Trends Anal. Chem. 22 (2003) 456–469. https://doi.org/10.1016/S0165-9936(03)00703-9.

[47] K.C. Honeychurch, Review of electroanalytical-based approaches for the determination of benzodiazepines, Biosensors. 9 (2019). https://doi.org/10.3390/bios9040130.

[48] K.C. Honeychurch, M. Piano, Electrochemical (bio) sensors for environmental and food analyses, Biosensors. 8 (2018) 2–4. https://doi.org/10.3390/bios8030057.

[49] K.C. Honeychurch, Screen-printed Electrochemical Sensors and Biosensors for Monitoring Metal Pollutants, Insciences J. 2 (2012) 1–51. https://doi.org/10.5640/insc.020101.

[50] J.P. Hart, A. Crew, E. Crouch, K.C. Honeychurch, R.M. Pemberton, Some Recent Designs and Developments of Screen-Printed Carbon Electrochemical Sensors/Biosensors for Biomedical, Environmental, and Industrial Analyses, Anal. Lett. 37 (2004) 789–830. https://doi.org/10.1081/AL-120030682.

[51] T. Cho, J. Wang, Selective Voltammetric Measurements of Epinephrine and Norepinephrine in Presence of Common Interferences Using Cyclic Square-voltammetry at Unmodified Carbon Electrodes, Electroanalysis. 30 (2018) 1028–1032. https://doi.org/10.1002/elan.201700823.

[52] M. Mascini, S. Gaggiotti, F. Della Pelle, J. Wang, J.M. Pingarrón, D. Compagnone, Hairpin DNA-AuNPs as molecular binding elements for the detection of volatile organic compounds, Biosens. Bioelectron. (2018). https://doi.org/10.1016/j.bios.2018.07.028.

[53] A. García-Miranda Ferrari, S.J. Rowley-Neale, C.E. Banks, Screen-

printed electrodes: Transitioning the laboratory in-to-the field, Talanta Open. 3 (2021) 100032. https://doi.org/10.1016/j.talo.2021.100032.

[54] K. Yamanaka, M.C. Vestergaard, E. Tamiya, Printable electrochemical biosensors: A focus on screen-printed electrodes and their application, Sensors (Switzerland). 16 (2016) 1–16. https://doi.org/10.3390/s16101761.

[55] D. Ji, N. Xu, Z. Liu, Z. Shi, S.S. Low, J. Liu, C. Cheng, J. Zhu, T. Zhang, H. Xu, X. Yu, Q. Liu, Smartphone-based differential pulse amperometry system for real-time monitoring of levodopa with carbon nanotubes and gold nanoparticles modified screen-printing electrodes, Biosens. Bioelectron. 129 (2019) 216–223. https://doi.org/10.1016/j.bios.2018.09.082.

[56] M. Franco Guzmán, G.A. Álvarez-Romero, L.H. Mendoza-Huizar, C.A. Galán-Vidal, G. Roa Morales, M.T. Ramírez-Silva, M.G. Montes de Oca Yemha, Optimization of a Differential Pulse Voltammetric Methodology for the Quantification of Diclofenac Using Paste Electrodes and Carbon Nanotubes, ECS Trans. 76 (2017) 9–18. https://doi.org/10.1149/07601.0009ecst.

[57] K.L. Westmacott, A. Crew, O. Doran, J.P. Hart, A novel electroanalytical approach to the measurement of B vitamins in food supplements based on screen-printed carbon sensors, Talanta. 181 (2018) 13–18. https://doi.org/10.1016/j.talanta.2017.12.074.

[58] A. Morrin, A.J. Killard, M.R. Smyth, Electrochemical characterization of

commercial and home-made screen-printed carbon electrodes, Anal. Lett. 36 (2003) 2021–2039. https://doi.org/10.1081/AL-120023627.

[59] X. Lin, Y. Li, A sensitive determination of estrogens with a Pt nano-clusters/multi-walled carbon nanotubes modified glassy carbon electrode, Biosens. Bioelectron. 22 (2006) 253–259. https://doi.org/10.1016/j.bios.2006.01.005.

[60] A. Florea, C. Cristea, F. Vocanson, R. Səndulescu, N. Jaffrezic-Renault, Electrochemical sensor for the detection of estradiol based on electropolymerized molecularly imprinted polythioaniline film with signal amplification using gold nanoparticles, Electrochem. Commun. 59 (2015) 36–39. https://doi.org/10.1016/j.elecom.2015.06.021.

[61] Mahboubeh Vafi, G.H. Rounaghi, Z. Es'haghi, Chemometrically-Assisted Fabrication of a Potentiometric Sensor for Potassium Ion Based on Kryptofix 22 Ionophore, Russ. J. Phys. Chem. A. 92 (2018) 2795–2801. https://doi.org/10.1134/S0036024418130320.

[62] X. Liu, P.A. Duckworth, D.K.Y. Wong, Square wave voltammetry versus electrochemical impedance spectroscopy as a rapid detection technique at electrochemical immunosensors, Biosens. Bioelectron. 25 (2010) 1467–1473. https://doi.org/10.1016/j.bios.2009.10.047.

[63] K.C. Honeychurch, J.P. Hart, N. Kirsch, Voltammetric, chromatographic and mass spectral elucidation of the redox reactions of 1-hydroxypyrene occurring at a screen-printed carbon electrode, Electrochim. Acta. 49 (2004) 1141–1149. https://doi.org/10.1016/j.electacta.2003.10.025.

[64] N. Jaiswal, I. Tiwari, Recent build outs in electroanalytical biosensors based on carbon-nanomaterial modified screen printed electrode platforms, Anal. Methods. 9 (2017) 3895–3907. https://doi.org/10.1039/c7ay01276d.

[65] D. Mandler, Fritz Scholz (Ed.): Electroanalytical methods. Guide to experiments and applications, 2nd ed., Anal. Bioanal. Chem. 398 (2010) 2771–2772. https://doi.org/10.1007/s00216-010-4195-5.

[66] Marken, F.; Neudeck, A.; Bond, A. M. , Scholz, F.; Bond, A. M.; Compton, R. G.; Fiedler, D. A.; Inzelt, G.; Kahlert, H.; Komorsky-Lovrić, Š.; Lohse, H.; Lovrić, M.; Marken, F.; Neudeck, A.; Retter, U.; Scholz, F.; Stojek, Z., Eds.; Springer Berlin Heidelb, In Electroanalytical Methods: Guide to Experiments and Applications, 2010.

[67] W R, S. and Chemical Instrumentation: A systematic approach., No Place Wiley. (1989).

[68] E.P. Randviir, D.A.C. Brownson, J.P. Metters, R.O. Kadara, C.E. Banks, The fabrication, characterisation and electrochemical investigation of screen-printed graphene electrodes, Phys. Chem. Chem. Phys. 16 (2014) 4598–4611. https://doi.org/10.1039/c3cp55435j.

[69] J.J. Triviño, M. Gómez, J. Valenzuela, A. Vera, V. Arancibia, Determination of a natural (17B-estradiol) and a synthetic (17A-ethinylestradiol) hormones in pharmaceutical formulations and urine by adsorptive stripping voltammetry, Sensors Actuators, B Chem. 297 (2019) 126728. https://doi.org/10.1016/j.snb.2019.126728.

[70] Y. Wang, Y. Xiong, H. Tian, S. Wang, Q. Zhang, M. Zhang, H. Ding, Y. Gu, A. Peng, Application of sensitive sensor modified with MWNTs/Al2O3/poly-L-lysine composite for 17β -estradiol determination in pregnant woman blood, Int. J. Electrochem. Sci. 13 (2018) 147–158. https://doi.org/10.20964/2018.01.20.

[71] V.K. Gupta, R. Jain, K. Radhapyari, N. Jadon, S. Agarwal, Voltammetric techniques for the assay of pharmaceuticals-A review, Anal. Biochem. 408 (2011) 179–196. https://doi.org/10.1016/j.ab.2010.09.027.

[72] M.M. Charithra, J.G. Manjunatha, Poly (l-Proline) modified carbon paste electrode as the voltammetric sensor for the detection of Estriol and its simultaneous determination with Folic and Ascorbic acid, Mater. Sci. Energy Technol. 2 (2019) 365–371. https://doi.org/10.1016/j.mset.2019.05.002.

[73] J.P. Metters, E.P. Randviir, C.E. Banks, Screen-printed back-to-back electroanalytical sensors, Analyst. 139 (2014) 5339–5349. https://doi.org/10.1039/c4an01501k.

[74] G. Liu, Y. Lin, Nanomaterial labels in electrochemical immunosensors and immunoassays, Talanta. 74 (2007) 308–317. https://doi.org/10.1016/j.talanta.2007.10.014.

[75] J.P. Metters, R.O. Kadara, C.E. Banks, New directions in screen printed electroanalytical sensors: An overview of recent developments, Analyst. 136 (2011) 1067–1076. https://doi.org/10.1039/c0an00894j.

[76] L.E. Sofen, A.L. Furst, Perspective—Electrochemical Sensors to Monitor

Endocrine Disrupting Pollutants, J. Electrochem. Soc. 167 (2020) 037524. https://doi.org/10.1149/2.0242003jes.

[77] C.M. Lieber, C.-C. Chen, Preparation of Fullerenes and Fullerene-Based Materials, in: Solid State Phys. - Adv. Res. Appl., 1994: pp. 109–148. https://doi.org/10.1016/S0081-1947(08)60578-0.

[78] E.M. Kirchner, T. Hirsch, Recent developments in carbon-based two-dimensional materials: synthesis and modification aspects for electrochemical sensors, Microchim. Acta. 187 (2020). https://doi.org/10.1007/s00604-020-04415-3.

[79] A. Sanati, M. Jalali, K. Raeissi, F. Karimzadeh, M. Kharaziha, S.S. Mahshid, S. Mahshid, A review on recent advancements in electrochemical biosensing using carbonaceous nanomaterials, Microchim. Acta. 186 (2019). https://doi.org/10.1007/s00604-019-3854-2.

[80] M. Zhou, Y. Zhai, S. Dong, Electrochemical sensing and biosensing platform based on chemically reduced graphene oxide, Anal. Chem. 81 (2009) 5603–5613. https://doi.org/10.1021/ac900136z.

[81] M. Ferreira, H. Varela, R.M. Torresi, G. Tremiliosi-Filho, Electrode passivation caused by polymerization of different phenolic compounds, Electrochim. Acta. 52 (2006) 434–442. https://doi.org/10.1016/j.electacta.2006.05.025.

[82] S. Afreen, R.A. Omar, N. Talreja, D. Chauhan, M. Ashfaq, Carbon-Based Nanostructured Materials for Energy and Environmental Remediation Applications, Nanotechnol. Life Sci. (2018) 369–392.

https://doi.org/10.1007/978-3-030-02369-0_17.

[83] S. Nalini, C. Divya, Studies on the use of novel nano composite (CNT/chitosan/Fe(0)) towards arsenate removal., J. Environ. Res. Dev. 8 (2014) 594–599. http://www.jerad.org/dispabstract.php?vID=1132.

[84] K. Grennan, A.J. Killard, M.R. Smyth, Physical characterizations of a screen-printed electrode for use in an amperometric biosensor system, Electroanalysis. 13 (2001) 745–750. https://doi.org/10.1002/1521-4109(200105)13:8/9<745::AID-ELAN745>3.0.CO;2-B.

[85] A. Escarpa, Food electroanalysis: Sense and simplicity, Chem. Rec. 12 (2012) 72–91. https://doi.org/10.1002/tcr.201100033.

[86] K.C. Honeychurch, Z. Rymansaib, P. Iravani, Anodic stripping voltammetric determination of zinc at a 3-D printed carbon nanofiber–graphite–polystyrene electrode using a carbon pseudo-reference electrode, Sensors Actuators, B Chem. 267 (2018) 476–482. https://doi.org/10.1016/j.snb.2018.04.054.

[87] O. Bagel, E. L'Hostis, G. Lagger, M.D. Osborne, B.J. Seddon, H.H. Girault, D. Brack, U. Loyall, H. Schäfer, Rotograved carbon electrodes for amperometric cadmium and lead determination, J. Electroanal. Chem. 469 (1999) 189–195. https://doi.org/10.1016/S0022-0728(99)00226-0.

[88] O. Bagel, G. Lagger, H.H. Girault, D. Brack, U. Loyall, H. Schäfer, Mercury free determination of lead by differential pulse anodic stripping voltammetry onto silver-plated rotograved carbon electrodes, Electroanalysis. 13 (2001) 100–103. https://doi.org/10.1002/1521-

4109(200102)13:2<100::AID-ELAN100>3.0.CO;2-I.

[89] X. Ji, C.E. Banks, A. Crossley, R.G. Compton, Oxygenated edge plane sites slow the electron transfer of the ferro-/ferricyanide redox couple at graphite electrodes, ChemPhysChem. 7 (2006) 1337–1344. https://doi.org/10.1002/cphc.200600098.

[90] A.G. Tummala, R., Rymaszewski, E. J., & Klopfenstein, Microelectronics Packaging Handbook:Subsystem Packaging, 2nd ed., Springer US, 1997. https://www.springer.com/gp/book/9780412084515.

[91] P.A. Raymundo-Pereira, N.O. Gomes, S.A.S. Machado, O.N. Oliveira, Simultaneous, ultrasensitive detection of hydroquinone, paracetamol and estradiol for quality control of tap water with a simple electrochemical method, J. Electroanal. Chem. 848 (2019) 113319. https://doi.org/10.1016/j.jelechem.2019.113319.

[92] K. Tyszczuk-Rotko, K. Pietrzak, A. Sasal, Adsorptive stripping voltammetric method for the determination of caffeine at integrated three-electrode screen-printed sensor with carbon/carbon nanofibers working electrode, Adsorption. 25 (2019) 913–921. https://doi.org/10.1007/s10450-019-00116-3.

[93] X. Cetó, A.M. O'Mahony, J. Wang, M. Del Valle, Simultaneous identification and quantification of nitro-containing explosives by advanced chemometric data treatment of cyclic voltammetry at screen-printed electrodes, Talanta. 107 (2013) 270–276. https://doi.org/10.1016/j.talanta.2012.12.042.

[94] R.O. Kadara, N. Jenkinson, C.E. Banks, Characterisation of commercially available electrochemical sensing platforms, Sensors Actuators, B Chem. 138 (2009) 556–562. https://doi.org/10.1016/j.snb.2009.01.044.

[95] M. Li, Y.T. Li, D.W. Li, Y.T. Long, Recent developments and applications of screen-printed electrodes in environmental assays-A review, Anal. Chim. Acta. 734 (2012) 31–44. https://doi.org/10.1016/j.aca.2012.05.018.

[96] S. Fletcher, Screen-Printed Carbon Electrodes, Adv. Electrochem. Sci. Eng. 16 (2016) 425–443. https://doi.org/10.1002/9783527697489.ch12.

[97] W. Xin, Y. Song, Mesoporous carbons: recent advances in synthesis and typical applications, RSC Adv. 5 (2015) 83239–83285. https://doi.org/10.1039/c5ra16864c.

[98] J. Barton, M.B.G. García, D.H. Santos, P. Fanjul-Bolado, A. Ribotti, M. McCaul, D. Diamond, P. Magni, Screen-printed electrodes for environmental monitoring of heavy metal ions: a review, Microchim. Acta. 183 (2016) 503–517. https://doi.org/10.1007/s00604-015-1651-0.

[99] R.L. McCreery, Advanced carbon electrode materials for molecular electrochemistry, Chem. Rev. 108 (2008) 2646–2687. https://doi.org/10.1021/cr068076m.

[100] K.C. Honeychurch, D.M. Hawkins, J.P. Hart, D.C. Cowell, Voltammetric behaviour and trace determination of copper at a mercury-free screen-printed carbon electrode, Talanta. 57 (1999) 565–574. https://doi.org/10.1016/S0039-9140(02)00060-7.

[101] M.I. González-Sánchez, B. Gómez-Monedero, J. Agrisuelas, J. Iniesta, E. Valero, Highly activated screen-printed carbon electrodes by electrochemical treatment with hydrogen peroxide, Electrochem. Commun. 91 (2018) 36–40. https://doi.org/10.1016/j.elecom.2018.05.002.

[102] D.M. Anjo, M. Kahr, M.M. Khodabakhsh, S. Nowinski, M. Wanger, Electrochemical activation of carbon electrodes in base: Minimization of dopamine adsorption and electrode capacitance, Anal. Chem. 61 (1989) 2603–2608. https://doi.org/10.1021/ac00198a004.

[103] J. Wang, B.A. Freiha, Extractive Preconcentration of Organic Compounds at Carbon Paste Electrodes, Anal. Chem. 56 (1984) 849–852. https://doi.org/10.1021/ac00268a069.

[104] A.N. Patel, M.G. Collignon, M.A. OConnell, W.O.Y. Hung, K. McKelvey, J. V. MacPherson, P.R. Unwin, A new view of electrochemistry at highly oriented pyrolytic graphite, J. Am. Chem. Soc. 134 (2012) 20117–20130. https://doi.org/10.1021/ja308615h.

[105] K. Mahato, S. Kumar, A. Srivastava, P.K. Maurya, R. Singh, P. Chandra, Electrochemical immunosensors: Fundamentals and applications in clinical diagnostics, Elsevier Inc., 2018. https://doi.org/10.1016/B978-0-12-811762-0.00014-1.

[106] W.J. Peveler, M. Yazdani, V.M. Rotello, Selectivity and Specificity: Pros and Cons in Sensing, ACS Sensors. 1 (2016) 1282–1285. https://doi.org/10.1021/acssensors.6b00564.

[107] T.W.B. Lo, L. Aldous, R.G. Compton, The use of nano-carbon as an

alternative to multi-walled carbon nanotubes in modified electrodes for adsorptive stripping voltammetry, Sensors Actuators, B Chem. 162 (2012) 361–368. https://doi.org/10.1016/j.snb.2011.12.104.

[108] R.A.S. Couto, J.L.F.C. Lima, M.B. Quinaz, Recent developments, characteristics and potential applications of screen-printed electrodes in pharmaceutical and biological analysis, Talanta. 146 (2016) 801–814. https://doi.org/10.1016/j.talanta.2015.06.011.

[109] C. Karuwan, A. Wisitsoraat, D. Phokharatkul, C. Sriprachuabwong, T. Lomas, D. Nacapricha, A. Tuantranont, A disposable screen printed graphene-carbon paste electrode and its application in electrochemical sensing, RSC Adv. 3 (2013) 25792–25799. https://doi.org/10.1039/c3ra44187c.

[110] P. Pasakon, J.P. Mensing, D. Phokaratkul, C. Karuwan, T. Lomas, A. Wisitsoraat, A. Tuantranont, A high-performance, disposable screen-printed carbon electrode modified with multi-walled carbon nanotubes/graphene for ultratrace level electrochemical sensors, J. Appl. Electrochem. 49 (2019) 217–227. https://doi.org/10.1007/s10800-018-1268-1.

[111] S. Radhakrishnan, J. Mathiyarasu, Graphene-carbon nanotubes modified electrochemical sensors, Elsevier Inc., 2018. https://doi.org/10.1016/B978-0-12-815394-9.00008-X.

[112] S. Cinti, F. Arduini, Graphene-based screen-printed electrochemical (bio)sensors and their applications: Efforts and criticisms, Biosens.

Bioelectron. 89 (2017) 107–122. https://doi.org/10.1016/j.bios.2016.07.005.

[113] H. Barton, W.M. Berbel-Filho, S. Consuegra, L. Francis, C. Tizaoui, R.S. Conlan, S.R. Teixeira, Ultrasensitive environmental assessment of xeno-estrogens in water samples using label-free graphene immunosensors, Anal. Biochem. 548 (2018) 102–108. https://doi.org/10.1016/j.ab.2018.02.027.

[114] T. Rasheed, F. Nabeel, M. Adeel, K. Rizwan, M. Bilal, H.M.N. Iqbal, Carbon nanotubes-based cues: A pathway to future sensing and detection of hazardous pollutants, J. Mol. Liq. 292 (2019). https://doi.org/10.1016/j.molliq.2019.111425.

[115] L.M. Ochiai, D. Agustini, L.C.S. Figueiredo-Filho, C.E. Banks, L.H. Marcolino-Junior, M.F. Bergamini, Electroanalytical thread-device for estriol determination using screen-printed carbon electrodes modified with carbon nanotubes, Sensors Actuators, B Chem. 241 (2017) 978–984. https://doi.org/10.1016/j.snb.2016.10.150.

[116] A. Allagui, T.J. Freeborn, A.S. Elwakil, B.J. Maundy, Reevaluation of Performance of Electric Double-layer Capacitors from Constant-current Charge/Discharge and Cyclic Voltammetry, Sci. Rep. 6 (2016). https://doi.org/10.1038/srep38568.

[117] P. Gan, J.S. Foord, R.G. Compton, Ionic liquid-carbon nanotube modified screen-printed electrodes and their potential for adsorptive stripping voltammetry, Electroanalysis. 26 (2014) 1886–1892.

https://doi.org/10.1002/elan.201400214.

[118] G. Hao, D. Zheng, T. Gan, C. Hu, S. Hu, Development and application of estradiol sensor based on layer-by-layer assembling technique, J. Exp. Nanosci. 6 (2011) 13–28. https://doi.org/10.1080/17458081003752988.

[119] J.N. Tiwari, V. Vij, K.C. Kemp, K.S. Kim, Engineered carbon-nanomaterial-based electrochemical sensors for biomolecules, ACS Nano. 10 (2016) 46–80. https://doi.org/10.1021/acsnano.5b05690.

[120] I. Cesarino, I.A. Hümmelgen, An additional tool towards overcoming absence of specificity of carbon nanostructure-based electrochemical sensors—application to estriol and estradiol detection and distinction, J. Solid State Electrochem. 19 (2015) 3045–3050. https://doi.org/10.1007/s10008-015-2923-7.

[121] V. Mazzaracchio, M.R. Tomei, I. Cacciotti, A. Chiodoni, C. Novara, M. Castellino, G. Scordo, A. Amine, D. Moscone, F. Arduini, Inside the different types of carbon black as nanomodifiers for screen-printed electrodes, Electrochim. Acta. 317 (2019) 673–683. https://doi.org/10.1016/j.electacta.2019.05.117.

[122] J. Barek, Possibilities and limitations of mercury and mercury-based electrodes in practical electroanalysis of biologically active organic compounds, Port. Electrochim. Acta. 31 (2013) 291–295. https://doi.org/10.4152/pea.201306291.

[123] A. Wong, A.M. Santos, E.L. Fava, O. Fatibello-Filho, M.D.P.T. Sotomayor, Voltammetric determination of 17β-estradiol in different

matrices using a screen-printed sensor modified with CuPc, Printex 6L carbon and Nafion film, Microchem. J. 147 (2019) 365–373. https://doi.org/10.1016/j.microc.2019.03.052.

[124] Y. Zhu, X. Liu, J. Jia, Electrochemical detection of natural estrogens using a graphene/ordered mesoporous carbon modified carbon paste electrode, Anal. Methods. 7 (2015) 8626–8631. https://doi.org/10.1039/c5ay01833a.

[125] G.M. Swain, Handbook of Electrochemistry, Handb. Electrochem. (2007) 111–V. https://doi.org/10.1016/B978-044451958-0.50006-9.

[126] N. Karikalan, P. Sundaresan, S.-M. Chen, R. Karthik, Exploring the Electrocatalytic Edge Plane Activity of Screen Printed Carbon Electrode and Various Carbonaceous Materials towards the Catecholic Derivatives, J. Electrochem. Soc. 165 (2018) H969–H978. https://doi.org/10.1149/2.1081814jes.

[127] L.A. Pradela-Filho, I.A.A. Andreotti, J.H.S. Carvalho, D.A.G. Araújo, L.O. Orzari, A. Gatti, R.M. Takeuchi, A.L. Santos, B.C. Janegitz, Glass varnish-based carbon conductive ink: A new way to produce disposable electrochemical sensors, Sensors Actuators, B Chem. 305 (2020) 127433. https://doi.org/10.1016/j.snb.2019.127433.

[128] G. Hughes, K. Westmacott, K.C. Honeychurch, A. Crew, R.M. Pemberton, J.P. Hart, Recent advances in the fabrication and application of screen-printed electrochemical (bio)sensors based on carbon materials for biomedical, agri-food and environmental analyses, Biosensors. 6 (2016). https://doi.org/10.3390/bios6040050.

[129] R.L. McCreery, M.T. McDermott, Comment on electrochemical kinetics at ordered graphite electrodes, Anal. Chem. 84 (2012) 2602–2605. https://doi.org/10.1021/ac2031578.

[130] E. Eltzov, A. Kushmaro, R.S. Marks, Biosensors for endocrine disruptors, Woodhead Publishing Limited, 2009. https://doi.org/10.1533/9781845695743.2.183.

[131] A. Economou, Enzymatic biosensors, Portable Biosensing Food Toxicants Environ. Pollut. (2013) 123–159. https://doi.org/10.1201/b15589.

[132] M. Nurul Karim, H.J. Lee, Amperometric phenol biosensor based on covalent immobilization of tyrosinase on Au nanoparticle modified screen printed carbon electrodes, Talanta. 116 (2013) 991–996. https://doi.org/10.1016/j.talanta.2013.08.003.

[133] C.C. Mayorga-Martinez, M. Cadevall, M. Guix, J. Ros, A. Merkoçi, Bismuth nanoparticles for phenolic compounds biosensing application, Biosens. Bioelectron. 40 (2013) 57–62. https://doi.org/10.1016/j.bios.2012.06.010.

[134] G. Di Nardo, S. Castrignanò, S.J. Sadeghi, R. Baravalle, G. Gilardi, Bioelectrochemistry as a tool for the study of aromatization of steroids by human aromatase, Electrochem. Commun. 52 (2015) 25–28. https://doi.org/10.1016/j.elecom.2015.01.007.

[135] A. Wang, Y. Ding, L. Li, D. Duan, Q. Mei, Q. Zhuang, S. Cui, X. He, A novel electrochemical enzyme biosensor for detection of 17β-estradiol by

mediated electron-transfer system., Talanta. 192 (2019) 478–485. https://doi.org/10.1016/j.talanta.2018.09.018.

[136] E. Povedano, F.H. Cincotto, C. Parrado, P. Díez, A. Sánchez, T.C. Canevari, S.A.S. Machado, J.M. Pingarrón, R. Villalonga, Decoration of reduced graphene oxide with rhodium nanoparticles for the design of a sensitive electrochemical enzyme biosensor for 17β-estradiol, Biosens. Bioelectron. 89 (2017) 343–351. https://doi.org/10.1016/j.bios.2016.07.018.

[137] A. V. Kuzikov, R.A. Masamrekh, T.A. Filippova, Y.I. Haurychenka, A.A. Gilep, T. V. Shkel, N. V. Strushkevich, S.A. Usanov, V. V. Shumyantseva, Electrochemical oxidation of estrogens as a method for CYP19A1 (aromatase) electrocatalytic activity determination, Electrochim. Acta. 333 (2020) 135539. https://doi.org/10.1016/j.electacta.2019.135539.

[138] J. Castro-Jiménez, C. Gonzalez, Immunoassay-based screening of polychlorinated biphenyls (PCB) in sediments: Requirements for a new generation of test kits, J. Environ. Monit. 13 (2011) 894–900. https://doi.org/10.1039/c0em00569j.

[139] R.M. Pemberton, T.T. Mottram, J.P. Hart, Development of a screen-printed carbon electrochemical immunosensor for picomolar concentrations of estradiol in human serum extracts, J. Biochem. Biophys. Methods. 63 (2005) 201–212. https://doi.org/10.1016/j.jbbm.2005.05.002.

[140] M.L. Scala-Benuzzi, J. Raba, G.J.A.A. Soler-Illia, R.J. Schneider, G.A.

Messina, Novel Electrochemical Paper-Based Immunocapture Assay for the Quantitative Determination of Ethinylestradiol in Water Samples, Anal. Chem. 90 (2018) 4104–4111. https://doi.org/10.1021/acs.analchem.8b00028.

[141] G. Volpe, G. Fares, F. delli Quadri, R. Draisci, G. Ferretti, C. Marchiafava, D. Moscone, G. Palleschi, A disposable immunosensor for detection of 17β-estradiol in non-extracted bovine serum, Anal. Chim. Acta. 572 (2006) 11–16. https://doi.org/10.1016/j.aca.2006.05.008.

[142] H. Ma, K. Mao, H. Li, D. Wu, Y. Zhang, B. Du, Q. Wei, Ultrasensitive multiplexed immunosensors for the simultaneous determination of endocrine disrupting compounds using Pt@SBA-15 as a non-enzymatic label, J. Mater. Chem. B. 1 (2013) 5137–5142. https://doi.org/10.1039/c3tb20932f.

[143] I. Ojeda, J. López-Montero, M. Moreno-Guzmán, B.C. Janegitz, A. González-Cortés, P. Yáñez-Sedeño, J.M. Pingarrón, Electrochemical immunosensor for rapid and sensitive determination of estradiol, Anal. Chim. Acta. 743 (2012) 117–124. https://doi.org/10.1016/j.aca.2012.07.002.

[144] K.K. Mistry, K. Layek, A. Mahapatra, C. RoyChaudhuri, H. Saha, A review on amperometric-type immunosensors based on screen-printed electrodes, Analyst. 139 (2014) 2289–2311. https://doi.org/10.1039/c3an02050a.

[145] L. Gold, SELEX: How It Happened and Where It will Go, J. Mol. Evol. 81

(2015) 140–143. https://doi.org/10.1007/s00239-015-9705-9.

[146] T. Mairal, V. Cengiz Özalp, P. Lozano Sánchez, M. Mir, I. Katakis, C.K. O'Sullivan, Aptamers: Molecular tools for analytical applications, Anal. Bioanal. Chem. 390 (2008) 989–1007. https://doi.org/10.1007/s00216-007-1346-4.

[147] M. Menger, A. Yarman, J. Erdossy, H.B. Yildiz, R.E. Gyurcsányi, F.W. Scheller, MIPs and aptamers for recognition of proteins in biomimetic sensing, Biosensors. 6 (2016). https://doi.org/10.3390/bios6030035.

[148] L. Gatel, A. Cuprys, P. Kumar, G. Suresh, F. Bendourou, M. Chaali, K. Hegde, S.K. Brar, Recent advances in oligonucleotide-based sensor technology for detection of endocrine-disrupting chemicals (EDC) in the environment, Elsevier Inc., 2019. https://doi.org/10.1016/b978-0-12-814679-8.00007-8.

[149] Y.S. Kim, H.S. Jung, T. Matsuura, H.Y. Lee, T. Kawai, M.B. Gu, Electrochemical detection of 17β-estradiol using DNA aptamer immobilized gold electrode chip, Biosens. Bioelectron. 22 (2007) 2525–2531. https://doi.org/10.1016/j.bios.2006.10.004.

[150] R.A. Olowu, O. Arotiba, S.N. Mailu, T.T. Waryo, P. Baker, E. Iwuoha, Electrochemical aptasensor for endocrine disrupting 17β-estradiol based on a Poly(3,4-ethylenedioxylthiopene)-gold nanocomposite platform, Sensors (Switzerland). (2010). https://doi.org/10.3390/s101109872.

[151] H. Ke, M. Liu, L. Zhuang, Z. Li, L. Fan, G. Zhao, A Fetomolar Level 17β-estradiol Electrochemical Aptasensor Constructed On Hierachical

Dendritic Gold Modified Boron-Doped Diamond Electrode, Electrochim. Acta. 137 (2014) 146–153. https://doi.org/10.1016/J.ELECTACTA.2014.06.014.

[152] D. Zhang, W. Zhang, J. Ye, S. Zhan, B. Xia, J. Lv, H. Xu, G. Du, L. Wang, A label-free colorimetric biosensor for 17β-estradiol detection using nanoparticles assembled by aptamer and cationic polymer, Aust. J. Chem. 69 (2016) 12–19. https://doi.org/10.1071/CH14735.

[153] G. Zhang, T. Li, J. Zhang, A. Chen, A simple FRET-based turn-on fluorescent aptasensor for 17B-estradiol determination in environmental water, urine and milk samples, Sensors Actuators, B Chem. 273 (2018) 1648–1653. https://doi.org/10.1016/j.snb.2018.07.066.

[154] K. Vanschoenbeek, J. Vanbrabant, B. Hosseinkhani, V. Vermeeren, L. Michiels, Aptamers targeting different functional groups of 17β-estradiol., J. Steroid Biochem. Mol. Biol. 147 (2015) 10–16. https://doi.org/10.1016/j.jsbmb.2014.10.013.

[155] K.J. Huang, Y.J. Liu, G.W. Shi, X.R. Yang, Y.M. Liu, Label-free aptamer sensor for 17β-estradiol based on vanadium disulfide nanoflowers and Au nanoparticles, Sensors Actuators, B Chem. 201 (2014) 579–585. https://doi.org/10.1016/j.snb.2014.05.055.

[156] M.H.M. Zaid, J. Abdullah, N. Rozi, A.A.M. Rozlan, S.A. Hanifah, A sensitive impedimetric aptasensor based on carbon nanodots modified electrode for detection of 17ß-estradiol, Nanomaterials. 10 (2020) 1–14. https://doi.org/10.3390/nano10071346.

[157] Z. Li, M.A. Mohamed, A.M. Vinu Mohan, Z. Zhu, V. Sharma, G.K. Mishra, R.K. Mishra, Application of electrochemical aptasensors toward clinical diagnostics, food, and environmental monitoring: Review, Sensors (Switzerland). 19 (2019). https://doi.org/10.3390/s19245435.

[158] H.Y. Kong, J. Byun, Nucleic acid aptamers: New methods for selection, stabilization, and application in biomedical science, Biomol. Ther. 21 (2013) 423–434. https://doi.org/10.4062/biomolther.2013.085.

[159] O. Rabal, F. Pastor, H. Villanueva, M.M. Soldevilla, S. Hervas-Stubbs, J. Oyarzabal, In Silico Aptamer Docking Studies: From a Retrospective Validation to a Prospective Case Study'TIM3 Aptamers Binding, Mol. Ther. - Nucleic Acids. 5 (2016) e376. https://doi.org/10.1038/mtna.2016.84.

[160] M. Hussain, J. Wackerlig, P.A. Lieberzeit, Biomimetic strategies for sensing biological species, Biosensors. 3 (2013) 89–107. https://doi.org/10.3390/bios3010089.

[161] R. Viveiros, S. Rebocho, T. Casimiro, Green Strategies for Molecularly Imprinted Polymer Development, Polymers (Basel). 10 (2018) 306. https://doi.org/10.3390/polym10030306.

[162] O.S. Ahmad, T.S. Bedwell, C. Esen, A. Garcia-Cruz, S.A. Piletsky, Molecularly Imprinted Polymers in Electrochemical and Optical Sensors, Trends Biotechnol. 37 (2019) 294–309. https://doi.org/10.1016/J.TIBTECH.2018.08.009.

[163] F. Canfarotta, J. Czulak, A. Guerreiro, A.G. Cruz, S. Piletsky, G.E.

Bergdahl, M. Hedström, B. Mattiasson, A novel capacitive sensor based on molecularly imprinted nanoparticles as recognition elements, Biosens. Bioelectron. 120 (2018) 108–114. https://doi.org/10.1016/j.bios.2018.07.070.

[164] C. Zhong, B. Yang, X. Jiang, J. Li, Current Progress of Nanomaterials in Molecularly Imprinted Electrochemical Sensing., Crit. Rev. Anal. Chem. 48 (2018) 15–32. https://doi.org/10.1080/10408347.2017.1360762.

[165] M.A. Beluomini, J.L. da Silva, A.C. de Sá, E. Buffon, T.C. Pereira, N.R. Stradiotto, Electrochemical sensors based on molecularly imprinted polymer on nanostructured carbon materials: A review, J. Electroanal. Chem. 840 (2019) 343–366. https://doi.org/10.1016/j.jelechem.2019.04.005.

[166] A. Nezhadali, M. Mojarrab, Fabrication of an electrochemical molecularly imprinted polymer triamterene sensor based on multivariate optimization using multi-walled carbon nanotubes, J. Electroanal. Chem. 744 (2015) 85–94. https://doi.org/10.1016/j.jelechem.2015.03.010.

[167] M. Weller, Immunoassays and Biosensors for the Detection of Cyanobacterial Toxins in Water, Sensors. 13 (2013) 15085–15112. https://doi.org/10.3390/s131115085.

[168] M. Peeters, P. Linton, A. Hidalgo-Bastida, Bioinspired Materials 2018: Conference Report, Biomimetics. 4 (2019) 4. https://doi.org/10.3390/biomimetics4010004.

[169] R. Peltomaa, E. Benito-Peña, M.C. Moreno-Bondi, Bioinspired recognition

elements for mycotoxin sensors, Anal. Bioanal. Chem. 410 (2018) 747–771. https://doi.org/10.1007/s00216-017-0701-3.

[170] J.K. Stroble, R.B. Stone, S.E. Watkins, An overview of biomimetic sensor technology., Sens. Rev. Pp. 29 (2009) 112–119.

[171] M.F. Frasco, L.A.A.N.A. Truta, M.G.F. Sales, F.T.C. Moreira, Imprinting technology in electrochemical biomimetic sensors, Sensors (Switzerland). 17 (2017). https://doi.org/10.3390/s17030523.

[172] G. Díaz-Díaz, D. Antuña-Jiménez, M. Carmen Blanco-López, M. Jesús Lobo-Castañón, A.J. Miranda-Ordieres, P. Tuñón-Blanco, New materials for analytical biomimetic assays based on affinity and catalytic receptors prepared by molecular imprinting, TrAC - Trends Anal. Chem. (2012). https://doi.org/10.1016/j.trac.2011.09.011.

[173] A.A. Lahcen, A.A. Baleg, P. Baker, E. Iwuoha, A. Amine, Synthesis and electrochemical characterization of nanostructured magnetic molecularly imprinted polymers for 17-β-Estradiol determination, Sensors Actuators, B Chem. 241 (2017) 698–705. https://doi.org/10.1016/j.snb.2016.10.132.

[174] D. Futra, L.Y. Heng, M.Z. Jaapar, A. Ulianas, K. Saeedfar, T.L. Ling, A novel electrochemical sensor for 17β-estradiol from molecularly imprinted polymeric microspheres and multi-walled carbon nanotubes grafted with gold nanoparticles, Anal. Methods. 8 (2016) 1381–1389. https://doi.org/10.1039/c5ay02796a.

[175] O. Jamieson, T.C.C. Soares, B.A. de Faria, A. Hudson, F. Mecozzi, S.J. Rowley-Neale, C.E. Banks, J. Gruber, K. Novakovic, M. Peeters, R.D.

Crapnell, Screen Printed Electrode Based Detection Systems for the Antibiotic Amoxicillin in Aqueous Samples Utilising Molecularly Imprinted Polymers as Synthetic Receptors, Chemosensors. 8 (2019) 5. https://doi.org/10.3390/chemosensors8010005.

[176] T.N.L. Truong, P. Van Toan, N.Q. Hao, Using AuNPs-modified screen-printed electrode in the development of molecularly imprinted polymer for artificial bioreceptor fabrication to improve biosensor sensitivity for 17 β - estradiol detection, Adv. Nat. Sci. Nanosci. Nanotechnol. 10 (2019) 015015. https://doi.org/10.1088/2043-6254/ab0d1b.

[177] Q. Jiang, D. Zhang, Y. Cao, N. Gan, An antibody-free and signal-on type electrochemiluminescence sensor for diethylstilbestrol detection based on magnetic molecularly imprinted polymers-quantum dots labeled aptamer conjugated probes, J. Electroanal. Chem. 789 (2017) 1–8. https://doi.org/10.1016/j.jelechem.2017.02.020.

[178] M.R. Gotrik, T.A. Feagin, A.T. Csordas, M.A. Nakamoto, H.T. Soh, Advancements in Aptamer Discovery Technologies, Acc. Chem. Res. 49 (2016) 1903–1910. https://doi.org/10.1021/acs.accounts.6b00283.

[179] J.L. Bowen, Detection of lipopolysaccharide pyrogens by molecularly imprinted polymers, PQDT - Glob. (2011) 226.

[180] A. Poma, H. Brahmbhatt, H.M. Pendergraff, J.K. Watts, N.W. Turner, Generation of novel hybrid aptamer-molecularly imprinted polymeric nanoparticles, Adv. Mater. 27 (2015) 750–758. https://doi.org/10.1002/adma.201404235.

[181] M.H. Lee, J.L. Thomas, W.C. Liu, Z.X. Zhang, B. Da Liu, C.H. Yang, H.Y. Lin, A multichannel system integrating molecularly imprinted conductive polymers for ultrasensitive voltammetric determination of four steroid hormones in urine, Microchim. Acta. 186 (2019). https://doi.org/10.1007/s00604-019-3797-7.

[182] M.H. Lee, J.L. Thomas, Z.L. Su, Z.X. Zhang, C.Y. Lin, Y. Sen Huang, C.H. Yang, H.Y. Lin, Doping of transition metal dichalcogenides in molecularly imprinted conductive polymers for the ultrasensitive determination of 17β-estradiol in eel serum, Biosens. Bioelectron. 150 (2020) 111901. https://doi.org/10.1016/j.bios.2019.111901.

[183] L. Uzun, A.P.F. Turner, Molecularly-imprinted polymer sensors: realising their potential., Biosens. Bioelectron. 76 (2016) 131–144. https://doi.org/10.1016/j.bios.2015.07.013.

[184] Q. Zhao, Y. Faraj, L.Y. Liu, W. Wang, R. Xie, Z. Liu, X.J. Ju, J. Wei, L.Y. Chu, Simultaneous determination of dopamine, uric acid and estriol in maternal urine samples based on the synergetic effect of reduced graphene oxide, silver nanowires and silver nanoparticles in their ternary 3D nanocomposite, Microchem. J. 158 (2020) 105185. https://doi.org/10.1016/j.microc.2020.105185.

[185] P.A. Raymundo-Pereira, N.O. Gomes, S.A.S. Machado, O.N. Oliveira, Simultaneous, ultrasensitive detection of hydroquinone, paracetamol and estradiol for quality control of tap water with a simple electrochemical method, J. Electroanal. Chem. 848 (2019).

https://doi.org/10.1016/j.jelechem.2019.113319.

[186] D. Futra, L.Y. Heng, M.Z. Jaapar, A. Ulianas, K. Saeedfar, T.L. Ling, A novel electrochemical sensor for 17β-estradiol from molecularly imprinted polymeric microspheres and multi-walled carbon nanotubes grafted with gold nanoparticles, Anal. Methods. 8 (2016) 1381–1389. https://doi.org/10.1039/c5ay02796a.

[187] D. YANG, Y., MU, J., DING, Y., WANG, J., LI, J., DU, X., & CHANG, An Immunosensor for Detection of 17β-Estradiol Based on Screen-Printed Electrode with Nano-Gold and Protein-A, Chinese J. Sensors Actuators. 4 (2012) 2.

[188] D. Butler, G.G. Guilbault, Disposable amperometric immunosensor for the detection of 17-β estradiol using screen-printed electrodes, Sensors Actuators, B Chem. 113 (2006) 692–699. https://doi.org/10.1016/j.snb.2005.07.019.

[189] A. Gevaerd, C.E. Banks, M.F. Bergamini, L.H. Marcolino-Junior, Graphene Quantum Dots Modified Screen-printed Electrodes as Electroanalytical Sensing Platform for Diethylstilbestrol, Electroanalysis. 31 (2019) 838–843. https://doi.org/10.1002/elan.201800838.

[190] M.B. Gholivand, A.R. Jalalvand, H.C. Goicoechea, T. Skov, Chemometrics-assisted simultaneous voltammetric determination of ascorbic acid, uric acid, dopamine and nitrite: Application of non-bilinear voltammetric data for exploiting first-order advantage, Talanta. 119 (2014) 553–563. https://doi.org/10.1016/j.talanta.2013.11.028.

[191] S. Campuzano, M. Pedrero, M. Gamella, V. Serafín, P. Yáñez-Sedeño, J.M. Pingarrón, Beyond sensitive and selective electrochemical biosensors: Towards continuous, real-time, antibiofouling and calibration-free devices, Sensors (Switzerland). 20 (2020) 1–22. https://doi.org/10.3390/s20123376.

Chapter 3 Detection of Estradiol by Screen-printed Electrodes Modified with Carbon Spherical Shell Material

This chapter examines the performance of unmodified screen-printed carbon electrodes and those modified with carbon spherical shell material (CSSM) in developing electrochemical sensors for detecting E2. The first part investigates the cyclic voltammetric behaviour of the E2 SPE sensor. In contrast, the second explores CSSM's application as a cost-effective alternative to expensive materials. This chapter describes a hydrothermal synthesis technique for producing carbon spherical material from glucose using an autoclave reactor. Hydrothermal synthesis offers precise control over morphology with minimal material loss within a wide temperature range [1]. The synthesised CSSM was explored to modify the electrode as an amperometric sensor.

3.1 Introduction

Several factors associated with SPE manufacture affect the electrode performance, including ink formulation/composition, properties, and particle size. These factors include printing loading, curing temperature, carbon surface structure, morphology, surface orientation, and choice of redox marker to characterize the SPEs [29]. As discussed in Chapter 2, various sensor platforms have integrated carbon nanomaterials as modifiers for sensors with improved sensitivity, LODs, and stability of SPEs [30]. Recently, there has been an increasing interest in a carbon material variant, which, although not commonly investigated as the graphitic allotrope of carbon, has garnered research attention

due to its superb conductive and electrocatalytic properties known as carbon spherical shells [31-32]. Many techniques have been developed to produce this material in the past few years, utilizing various carbon sources such as wood, fruit shells, and polymers at higher temperatures [37, 38]. These methods have proven to be cost-effective [39].

Conventional amorphous carbon materials, for example, carbon black (also known as acetylene black, channel black, furnace black, lamp black, and thermal black), have been employed in various sensor applications [27, 40-42]. Carbon black is produced by partially burning and pyrolyzing coal, coal tar, vegetable matter, or petroleum products, such as low-value oil residues, at high temperatures under controlled process conditions. Chemically, carbon black is a colloidal form of elemental carbon consisting of 90-98% carbon. Carbon black exhibits excellent electrical conductivity, is dispersible in solvents, has the potential for facile functionalization, and possesses numerous defect sites, fast electron transfer kinetics, large surface area, good electric conductivity, high thermal conductivity, high chemical stability, and low density [31, 43-47]. Carbon black's usage as an electrode material stems from its properties above. It can be made from various carbon sources, which are relatively low in cost, making it ideal as an electrode material in sensor applications [53].

Lo et al. reported the use of carbon black as a cheaper alternative to CNTs for determining nicotine [52]. Dong et al. reported the determination of E2 in water using carbon nanosized biochar as an economical, rapid, and sensitive method for environmental protection, with a LOD of 1.13×10^{-8} M [49]. In another report, using linear sweep voltammetry, carbon dot/polyaniline was utilized to modify

glassy carbon electrodes for E2 measurement. It achieved a LOD of 4.3 x 10^{-8} M [54]. Smajdor et al. reported using carbon black to detect E2 using voltammetry and a flow injection system, yielding a LOD of 9.2 x 10^{-8} M [33]. Meanwhile, Neves et al. used Printex 6L carbon with a deep eutectic solvent to modify screen-printed electrodes to quantify E2 in water samples. The screen-printed sensor had an LOD of 6.5 x 10^{-9} M compared to an unmodified SPE of 1.77 x 10^{-7} M, with recoveries between 92.15% and 102.10% [55]. Also, Wong et al. utilized Printex 6L carbon with Cupc and Nafion to fabricate a screen-printed sensor detecting E2 using DPV with a LOD of 5 x 10^{-9} M [56]. Zaid et al. described the application of aptamers and carbon nanodots to modify an SPE for E2 detection to develop an impedimetric sensor that demonstrated a linear concentration range of 1 x 10^{-9} - 1 x 10^{-7} M with a LOD of 5 x 10^{-11} M [57].

3.1.1 Pre-treatment of Screen-Printed Carbon Electrodes

Screen-printed-based electrochemical sensors are manufactured using various carbon ink materials that consist of several components such as graphite particles, solvents, and other proprietary materials to formulate ink [72]. The electrochemical performance of the SPEs can be affected by variations in ink composition, printing, and curing conditions [72,73]. Other factors are graphitic loading, electrochemical accessibility of the graphitic edges, and the nature of the graphite particles and functionalities [74,75]. In addition to these factors, most commercial SPEs lack accompanying information from the manufacturer regarding the exact composition and conditions required for use. Additionally, some desired electrode materials are not adequately conductive. Therefore, various pre-treatment strategies for screen-printed electrodes have been tested

to enhance their performance [72, 76, 77]. These pre-treatment techniques range from electrochemical approaches to cleaning with acids, bases, and solvents. Practical and economic issues have been considered, allowing the characteristics of the electrodes to be fine-tuned using appropriate surface pre-treatment methods [75]. One technique is to expose edge plane sites and remove the binder and other contaminants from the surface of the SPE during manufacturing. For example, the electrochemical pre-treatment method of Morrin et al. involves performing cyclic voltammetry on the screen-printed electrode in sulphuric acid (0.2 M), which strips the surface of the electrode of any residual materials [66].

On the other hand, the non-electrochemical pre-treatment method reported by Washe et al. is a facile and versatile approach of exposing SPE in N, N-dimethylformamide (DMF) for 5 minutes, followed by curing at 100°C for 20 minutes in an oven. The study reported that the DMF solvent dramatically improves the electrochemical characteristics of the electrodes [75]. This method allows mass surface activation in a simplified manner without the need for any special instrumentation requirements such as plasma [79] or laser equipment [80].

3.1.2 Carbon Spherical Shell Material as an electrode modifier

Carbon spherical material has been investigated as a cost-effective alternative material in sensor design. Carbon black has been utilized as a modifier for SPEs, specifically for detecting benzoquinone, ascorbic acid, cysteine, catechol, and caffeic acid [46]. Improving electrochemical sensors using different carbon black materials has been reported [53]. Portaccio et al. reported using thionine–carbon

black material for BPA detection [83]. This chapter explores the electrochemical performance of carbon spherical shell modified SPEs for E2. An amperometric technique eliminates the background current generally associated with other methods, such as CV/LSV [58-61]. Furthermore, amperometry has been frequently used as an electroanalytical approach for determining phenolic compounds to circumvent interference that might arise from other compounds in the sample [113].

The hydrothermal synthesis route employed in this research study was used to fabricate CSSM, which utilizes glucose as the carbon source. CSSM is a relatively new and unexplored material [52] that has not yet been used in electroanalysis for E2 sensing. The material is produced using hydrothermal green synthesis methods that provide uniform and low-cost material, producing an efficient, non-toxic, and affordable alternative material [52,84] for E2 sensing.

3.2 Materials and Methods

3.2.1 Materials

All the reagents and chemicals used were of analytical grade and used as received. 17β-estradiol (E2) standard, hexaammineruthenium chloride, potassium chloride (KCl), Sodium hydroxide (NaOH), Glacial acetic acid, Phosphoric acid, Boric acid, concentrated sulfuric acid (H_2SO_4), and nitric acid (HNO_3) were obtained from Fisher Scientific (Leicestershire, UK.). Silver nitrate ($AgNO_3$) was obtained from Acros Organics, UK. Deionised water was obtained from a Suez Select (Laboratory water purification system (SUEZ Water Purification Systems Ltd, U.K.) for solution preparation throughout the study. The standard stock solution of E2 0.05 M was prepared in absolute ethanol and stored

in a refrigerator at +4^{o}C. Phosphate buffer (0.1 M, pH 7.0) buffer solution was used throughout the study.

3.2.2 Instrumentation

Electrochemical measurements, including cyclic voltammetry (CV) and amperometry, were carried out using a PalmSens EmStat^{3} Potentiostat (Palmsens BV Houten, the Netherlands) connected to a PC controlled by software PSTrace 5.8 (Windows version). Palintest Limited (Newcastle, U.K.) supplied screen-printed electrodes consisting of a working electrode, a carbon counter electrode, and a silver reference electrode.

3.2.3 Voltammetric Measurements

Voltammetric measurements were performed by cyclic voltammetry (CV) using a redox probe, 5 mM ($[Ru(NH_3)_6]^{3+}$) or $[Fe(CN)_6]^{-3/-4}$ in 0.1 M KCl as a supporting electrolyte for the electrochemical behaviour of CSSM/SPE, across a potential range of −0.3 to +0.6 V. The effect of scan rate was investigated between 50 - 250 mV s^{-1}. The analytical measurement was undertaken by amperometry at +0.66 V in PBS 0.1 M (pH 7) through sequential additions of the E2 standard solution aliquots. Data analysis methodology employed in this thesis is fully discussed is in section 7.1.3 appendix E (Figure E3-E9) with corresponding calibration plot showing the error bars represent standard error of the mean.

3.2.4 Scanning Electron Microscopy (SEM)

Surface morphology and structure characterisation were carried out using an FEI Quanta 650 field emission scanning electron microscope with energy dispersive X-ray microanalysis (EDX) Oxford Instruments Aztec Energy (version 3.3) EDX system using an X-Max 50 detector, sputter coater Emscope SC500 gold sputter

coating unit. X-Max 50 detector - detector active area = 50 mm^2 to characterise the working electrodes.

3.2.5 Attenuated Total Reflection Fourier Transform infrared spectroscopy (ATR-FTIR)

Attenuated total reflection Fourier-transform infrared spectroscopy (ATR-FTIR) was performed using a Perkin-Elmer ATR-IR spectrometer (model Spectrum 1000). Both modified and unmodified electrodes were analysed over the 4000 to 400 cm^{-1} wavelength range. A minute quantity of the CSSM particles was dropped directly on the ATR crystal and clamped against the vertical face of the crystal without further preparation. As a result, the IR spectra of the samples, in transmittance mode, were obtained in the spectral region of 400–4000 cm^{-1}.

3.2.6 Dynamic Light Scattering

Dynamic light scattering (DLS) measurements were carried out using Zetasizer Nano Series and data analysis (Malvern Instruments Ltd, UK). 1 mg/mL concentration solutions of CSSM were further diluted (1:9) v/v then loaded into disposable cells, and data collected at 25°C. All the samples were prepared in deionised water/methanol (9:1) v/v.

3.2.7 Transmission Electron Microscopy

Carbon spherical shell material was used for modified electrode surface characterisation using an F.E.I. Tecnai 12 BioTwin transmission electron microscope (T.E.M.) with a 120 kV accelerating voltage with images captured on an FEI CETA camera (Thermo Fisher Scientific, Waltham, USA). Dried samples were suspended and diluted 200 times with a methanol/water mixture (final concentration of 0.1 % by wt). The samples were sonicated for 5 minutes, and 5

µL of the sample drop was cast on a glow-discharged carbon/pioloform-coated E.M. mesh grid and incubated for 1-2 mins. The excess was wicked away after air drying the sample.

3.2.8 Synthesis of Carbon Spherical Shell Material (CSSM)

CSSM were synthesised according to the procedure proposed by Campos et al. and Gan et al. [51,85] with some modifications. Briefly, in synthesising the CSSM hydrothermally, 6.5 g of glucose was added to 72 mL of DI water in a beaker and stirred at 300 rpm to obtain a clear solution. Next, 2 mL of 0.03 M $AgNO_3$ was added dropwise into the glucose solution under vigorous stirring [85]. This was followed by transferring the solution to a Teflon-sealed autoclave (100 mL), placing it in an oven at 180 °C for 4 hours and cooling it in natural air afterwards. Next, the prepared material was centrifuged at 4,032 × g (5000 rpm) for 30 minutes. Finally, the prepared material underwent a cleaning step consisting of centrifugation, washing, and resuspension in triplicate using water and ethanol and oven drying at 80 °C for 4 hours.

3.2.9 Preparation and Modification of the SPE Sensor

The CSSM/SPE was fabricated as follows. The electrode modification step involves the dispersion of the above-prepared materials to obtain a modified SPE sensor (CSSM/SPE). First, 1 mg of the material was sonicated in 10 mL DMF/water (1:1v/v). After that, 0.6 µL of the suspension was drop-casted on the working electrode and dried for 2 hours at room temperature, completing the electrode modification. Further concentrations were also tested (0.5, 1.0, 1.5 mg/mL).

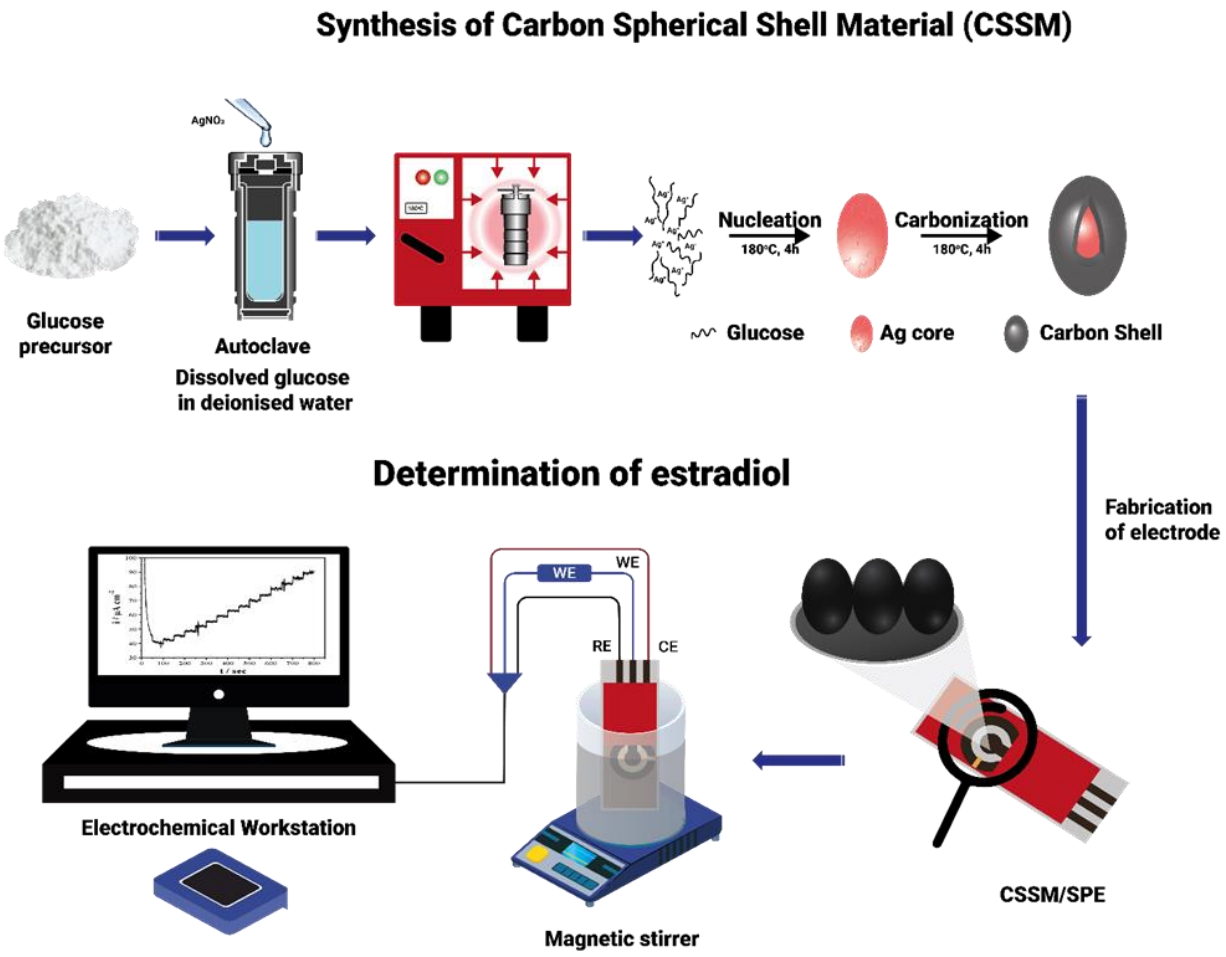

Figure 3.1 Schematic representation for synthesising carbon spherical shell (CSSM), construction and electrochemical detection of CSSM/SPE modified screen-printed electrode

3.3 Results and Discussion

CSSM electrodes were fabricated by drop-coating with a well-dispersed suspension of CSSM on the surface of the working electrode to produce the modified screen-printed surfaces. This method has been the fastest and simplest reported means of modifying electrodes in electrochemical sensor design [86].

3.3.1 Characterisation of carbon spherical shell material (CSSM)

Scanning electron microscopy (SEM) was employed to evaluate the topographical features of the surface of unmodified and modified SPEs. The electrode surface texture is vital in a sensor's performance, thus providing insight into the material compositions [29]. Figure 3.2 depicts the SEM image of a bare SPE, which indicates a compact graphitic flake-like layer in an irregular form, together with agglomerated flakes. In the image, the slight whitish edge of the flakes is visible, illustrating that they are distributed across the electrode surface. This can be attributed to the excellent dispersion of various components within the binder to formulate the graphite ink. Figure 3.3 shows the SEM image of carbon spherical shell coated SPE. The surface is covered by an even homogenous carbon powder layer uniformly adhered to the electrode surface with smooth surface morphology. It reveals a material consisting of multiple grains/particles of amorphous carbon; this nanoparticle material presents a high uniformity. No overlaying debris or remnants of other materials are visible; they are merely CSSM structures with well-defined large pores. Figure 3.4 shows a magnified image of CSSM-SPE at 20,000x magnification. The SEM image shows a less regular and more spherical amorphous powder-like material. The energy dispersive X-ray (EDS) spectra in Figure 3.5 (bare electrode) show carbon of 27 counts per second per electron-volt (cps/eV). In contrast, Figure 3.6 (CSSM) shows abundant carbon at 200 cps/eV, indicating varied surface structures with significantly different morphologies. Other materials, such as Au, come from the sample preparation step.

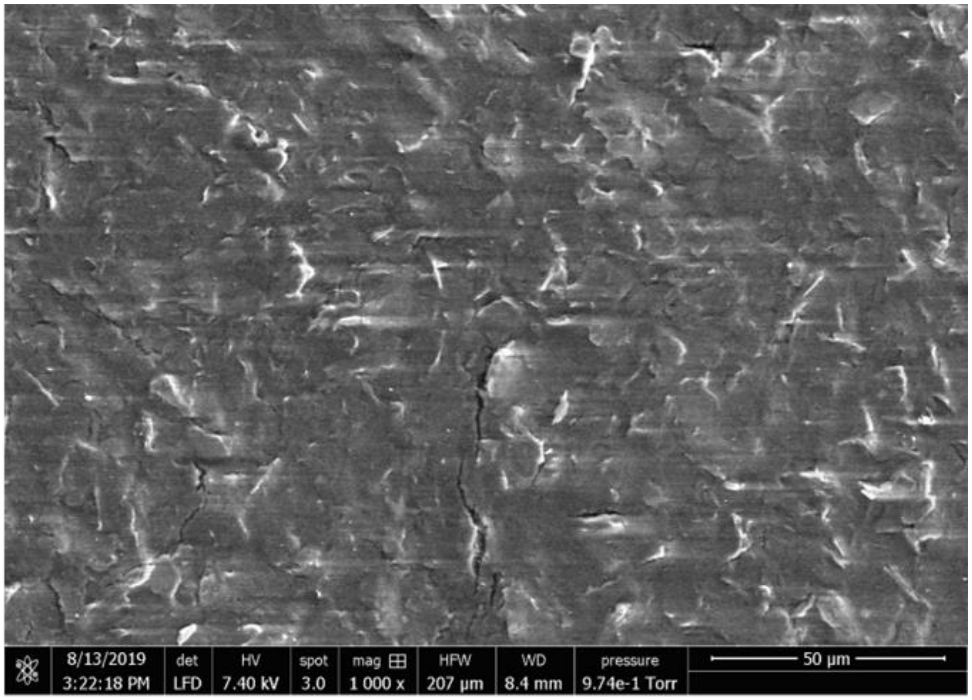

Figure 3.2 - SEM images of bare SPE surface at 1000x magnification.

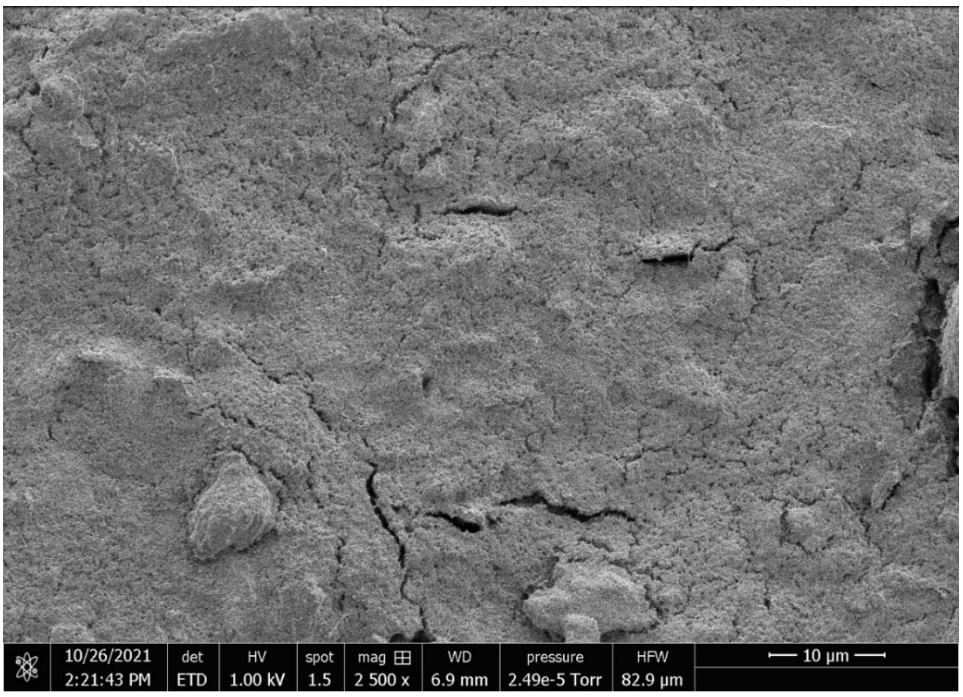

Figure 3.3 SEM images of CSSM modified SPE at 2 500x magnification.

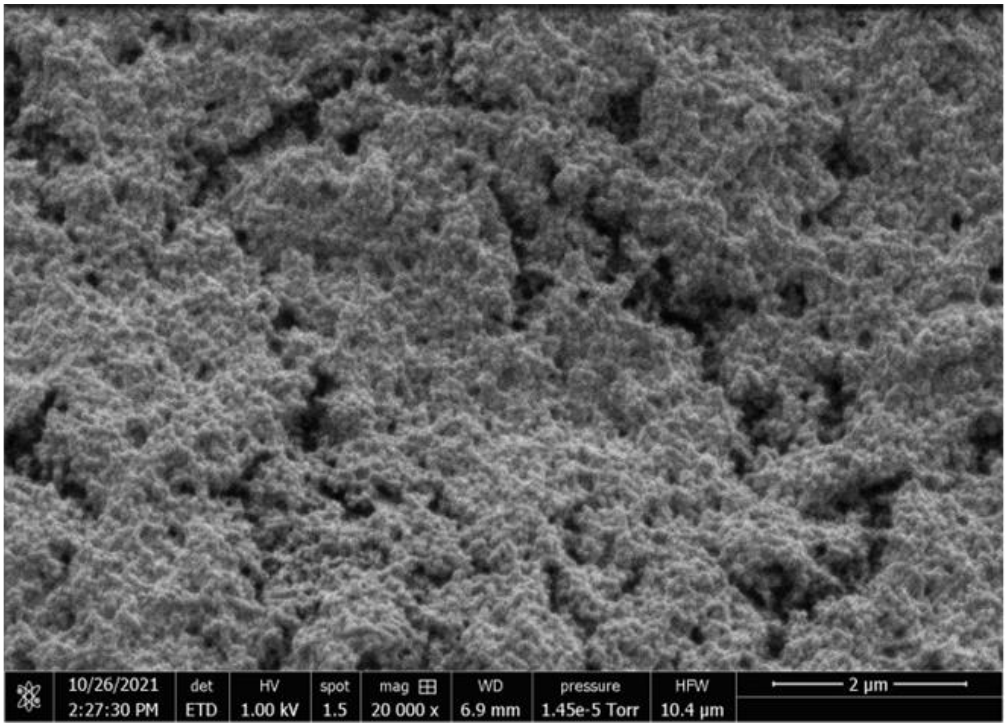

Figure 3.4 SEM images of CSSM/SPE at 20,000x magnification.

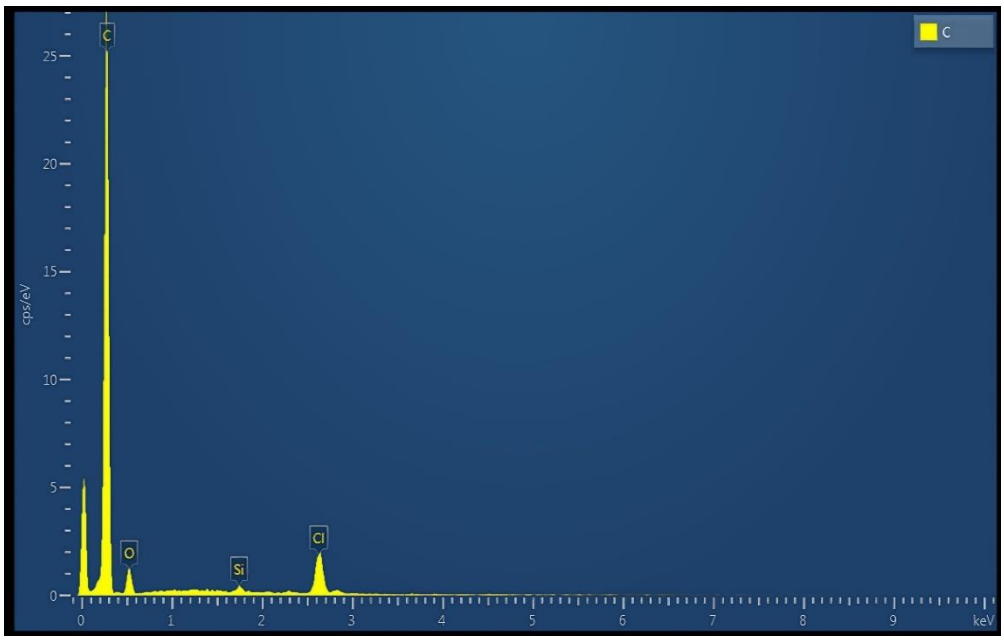

Figure 3.5 Energy-dispersive X-ray spectrometer (EDS) image Bare SPE

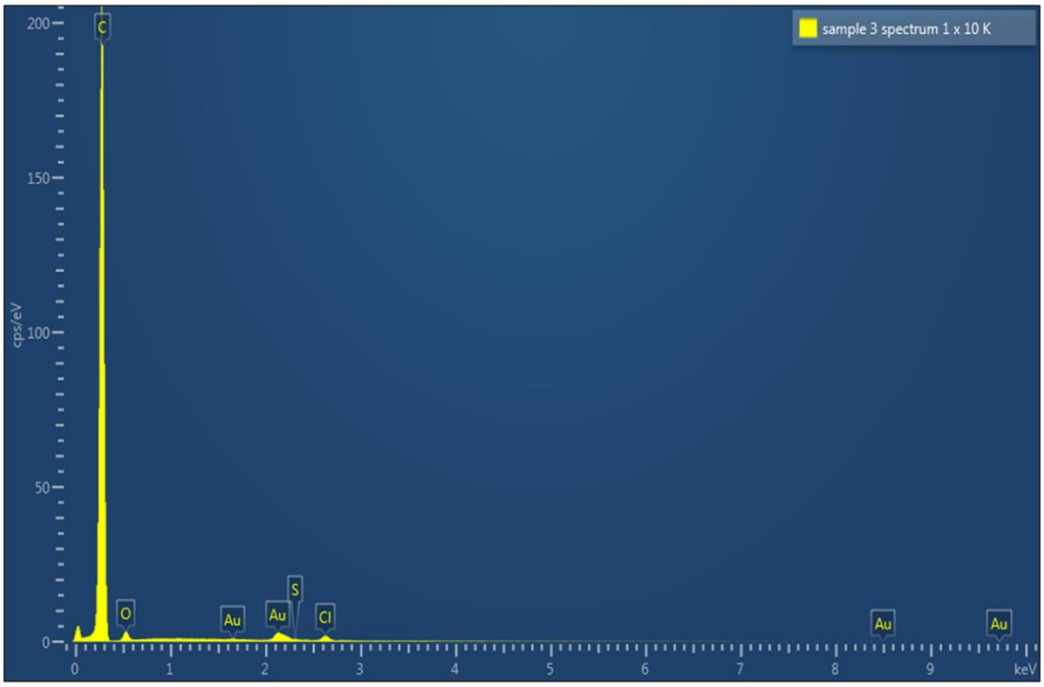

Figure 3.6 Energy-dispersive X-ray spectrometer (EDS) image CSSM.

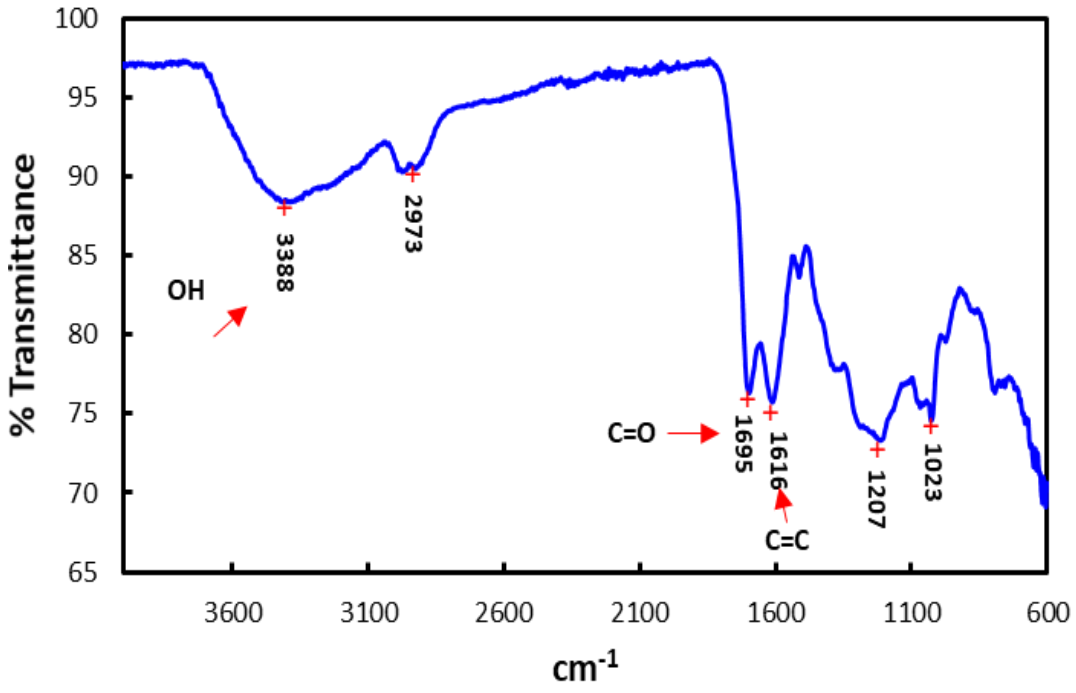

Figure 3.7 FTIR spectra of carbon spherical shell (CSSM).

The FTIR spectrum (Figure 3.7) depicts pronounced functional groups such as carbonyl (within 1000-1700 cm^{-1}) for C=O, C=C, C-O and hydroxyl -OH 3388 cm^{-1}) and C-H (2973 cm^{-1}), indicating the carbon-based nature of the synthesised materials [85]. The C=O and C=C are formed from the aromatisation of glucose (carbohydrate) synthesis [85]. The spectrum also evidences the presence of the hydroxyl group, which is consistent with other studies [51,85,87]. Also, the spectrum of Figure 3.7 contains bands in the region of 1650–1850 cm^{-1}, which were ascribed to C=O (1695 cm^{-1}) stretching vibrations (vC=O), and absorption at 1023 and 1207 $cm^{-1,}$ which were assigned to C–O–C stretching vibrations (vC–O). This indicates the presence of oxygen species on the electrode surface [88,89].

Dynamic light scattering (DLS) is a technique used to measure the size distribution of particles dispersed in a solution based on their Brownian motion [90]. Zetasizer measurements were examined, and synthesised CSSM was used to confirm the distribution of nanoparticle sizes, average particle size, and dispersion index. Figure 3.8 shows a dynamic light scattering analysis of the CSSM particles suspended within a liquid, showing nanoparticle aggregation from physical examination when the cuvette was allowed to settle before the measurement was taken. From Figure 3.8, the particle peak value size varies from 577 nm to 1265 nm, with an average of 711 nm indicating two distinct diffusing species in the solution. The size distribution by the intensity of the samples exhibited multimodal distributions with two principal modes. Despite the average particle size being outside the nanometre range (1-100 nm), most particles were over 400 nm. This suggests that the material aggregates primarily

into larger structures. This means that all the material aggregates into the large structures. Thus, the hydrodynamic diameters of the CSSM increase to a micrometre scale. In addition, the polydispersity indices (PdI) and z-average for the CSSM were 0.354 and 774, respectively, indicating that the material is polydisperse with large sedimenting particles. In contrast, [91] has demonstrated that carbon black (CB) obtained industrially is a manufactured colloidal material consisting of approximately spherical carbon primary particles with a diameter of 15 to 100 nm, typically forming fused aggregates with sizes below 1000 nm [91].

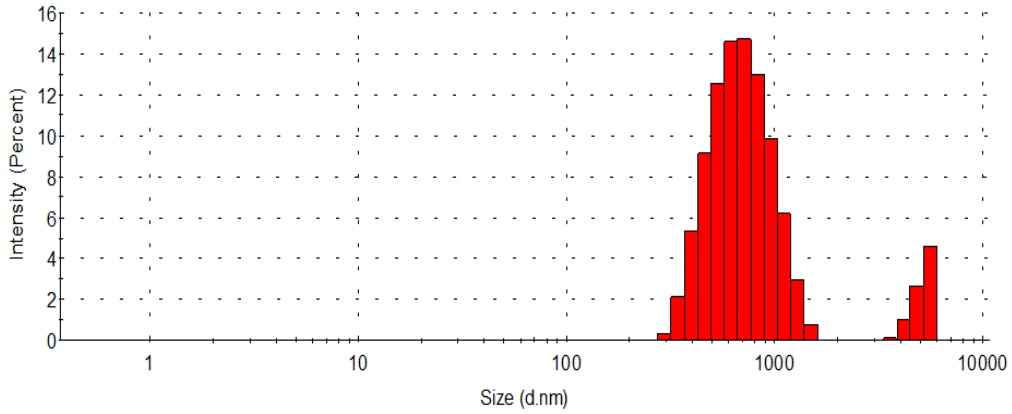

Figure 3.8 DLS analysis; Size distribution of CSSM by intensity.

DLS measures the hydrodynamic radius based on an ensemble average within a suspension related to the diffusive movement of particles [92,93]. The sample's particle size is indirectly determined through particle movement rather than direct measurement. Hydrodynamic diameter describes the size of smooth, spherical particles that diffuse at a rate equivalent to that of the sample particles [93]. DLS does not give the size of an individual particle but the cumulative particles in suspension. From the DLS results, the average particle size indicates large particles, which may be due to aggregation or contamination, leading to the

noticed imprecisions of the DLS analysis. Carbon-based nanomaterials are known for their high hydrophobicity when in dispersion. They are typically characterised by wide size distribution and large aggregates [93]. TEM analysis for the size and shape of the prepared CSSM TEM results (Figure 3.9) confirmed that the synthesised CSSM were more than 500 nm and had an irregular shape (Figure 3.9). The difference between the TEM and DLS particle diameters was probably due to material swelling, as reported by [93].

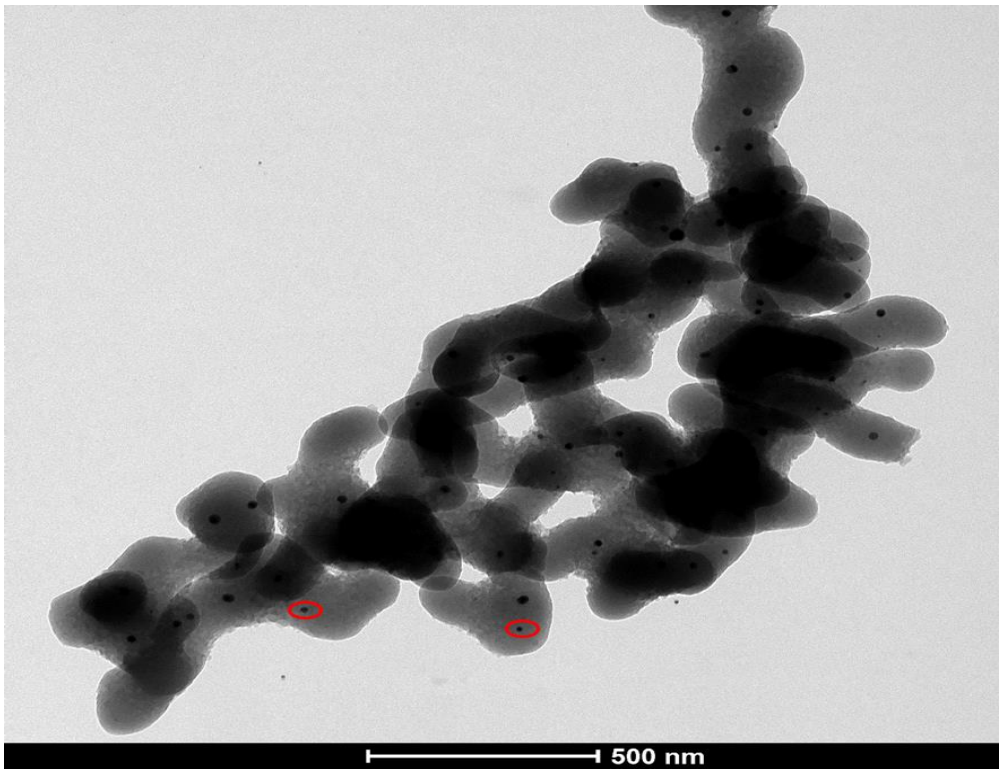

Figure 3.9 TEM image of carbon spherical shell material (CSSM).

A connection exists between the Polydispersity Index (PDI) and Transmission Electron Microscopy (TEM). PDI serves as an indicator of sample heterogeneity based on particle size. It offers insights into the size distribution within a sample. Conversely, TEM is a microscopic technique for visualizing particle size and

shape. Analysis of TEM images allows for the determination of particle size distribution, thereby facilitating the calculation of the PDI.

3.3.2 Electrochemical Characterisation

The electrochemical characterisation was performed on modified and unmodified electrodes using ferri/ferrocyanide and hexaammine ruthenium (III) chloride, as outlined in the following sections. Figures 3.10 - 3.12 depict the fabricated CSSM/SPE characterisation that was carried out using electrochemical redox probes. Electrochemical processes at the electrode surface are benchmarked using an outer sphere 5 mM ($[Ru(NH_3)_6]^{3+}$) redox system [94–98], an inner sphere redox was employed for carbonaceous materials and an inner-sphere redox probe 5 mM $[Fe(CN)_6]^{3-/4-}$. Some carbon-based materials exhibit fast electro-kinetics with this redox marker [94]. The reaction rate can be determined using peak current and peak-to-peak separation [94]. There are inner and outer sphere redox mediators for the characterisation of electrodes. For an outer-sphere probe, electron transfer is fast because the redox probes come close enough to the electrode surface for electrons to tunnel/hop across a monolayer of solvent but do not directly interact with the electrode surface. Such redox probes are influenced only by the electronic structure of the electrode surface. For inner-sphere redox probes, the electronic structure and electrode surface influence its behaviour, i.e., surface functional groups (adsorption sites)/surface chemistry. From Figure 3.10A, the results obtained for CSSM in $[FeCN_6]^{-3/-4}$ has a peak-to-peak separation (Δ_{EP}), 552 - 720 mV as an inner-sphere redox couple, showing a pronounced quasi-reversible process compared to bare SPE in $[FeCN_6]^{-3/-4}$ (Figure 3.11A) with Δ_{EP}, 320 - 580 mV, which also is not entirely irreversible

process. As anticipated for a quasi-reversible reaction, there was also an observed change in the peak potential with increasing scan rates. The quasi-reversible nature of a reaction, where the rate of electron transfer is comparable to the rate of diffusion, increases peak-to-peak separation with scan rate (v). This phenomenon reflects the complex interplay between electron-transfer kinetics and mass transport within the system beyond the visual voltammogram, also demonstrated in Chapter 4.

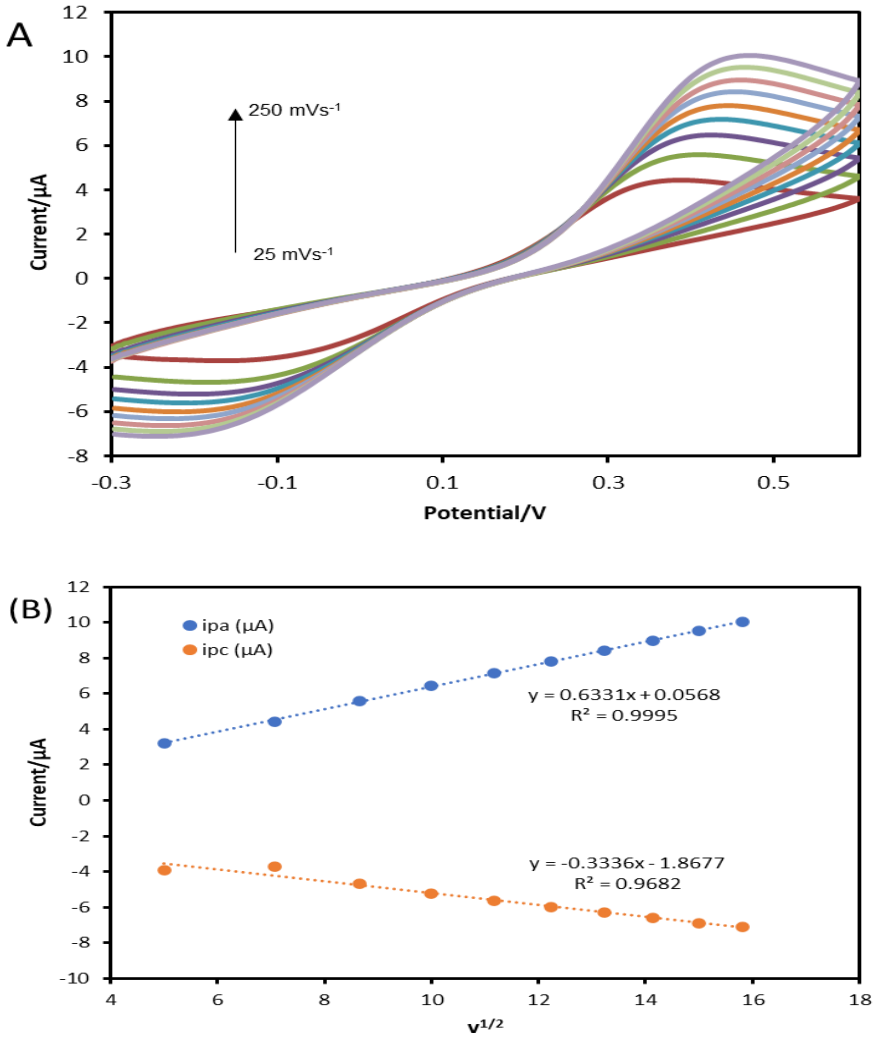

Figure 3.10 Cyclic voltammograms of (A) CSSM/SPE at 25 - 250 mVs^{-1} scan rates in 5 mM $[Fe(CN)_6]^{-3/-4}$. (B) Plots of CSSM/SPE Ipa (µA) vs $v^{1/2}$ and Ipc (µA) vs $v^{1/2}$, respectively.

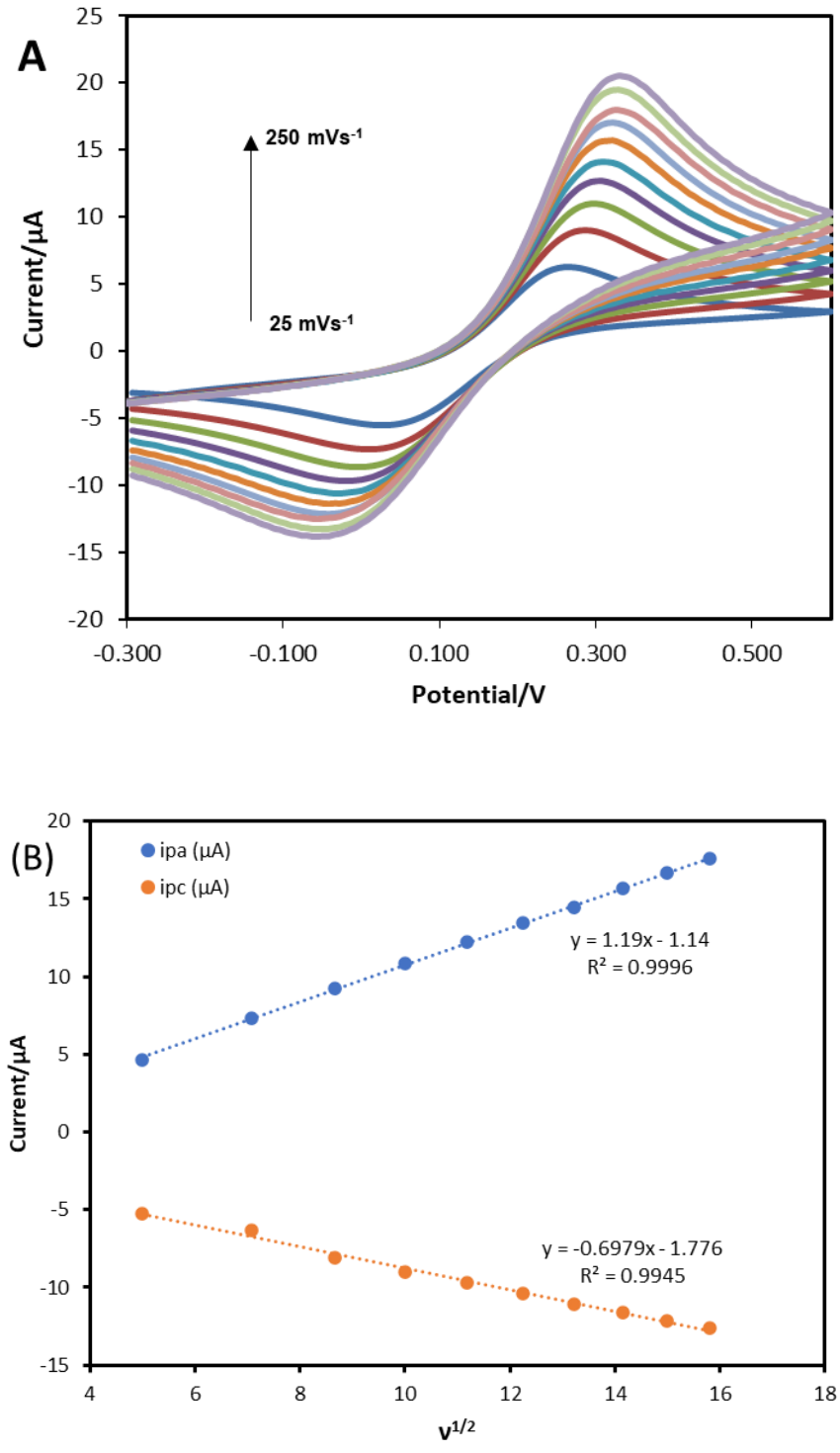

Figure 3.11 Cyclic voltammograms of (A) Bare SPE at 25 - 250 mVs^{-1} scan rates in 5 mM $[Fe(CN)_6]^{-3/-4}$. (B) Plots of bare SPE Ipa (µA) vs $v^{1/2}$ and Ipc (µA) vs $v^{1/2}$, respectively.

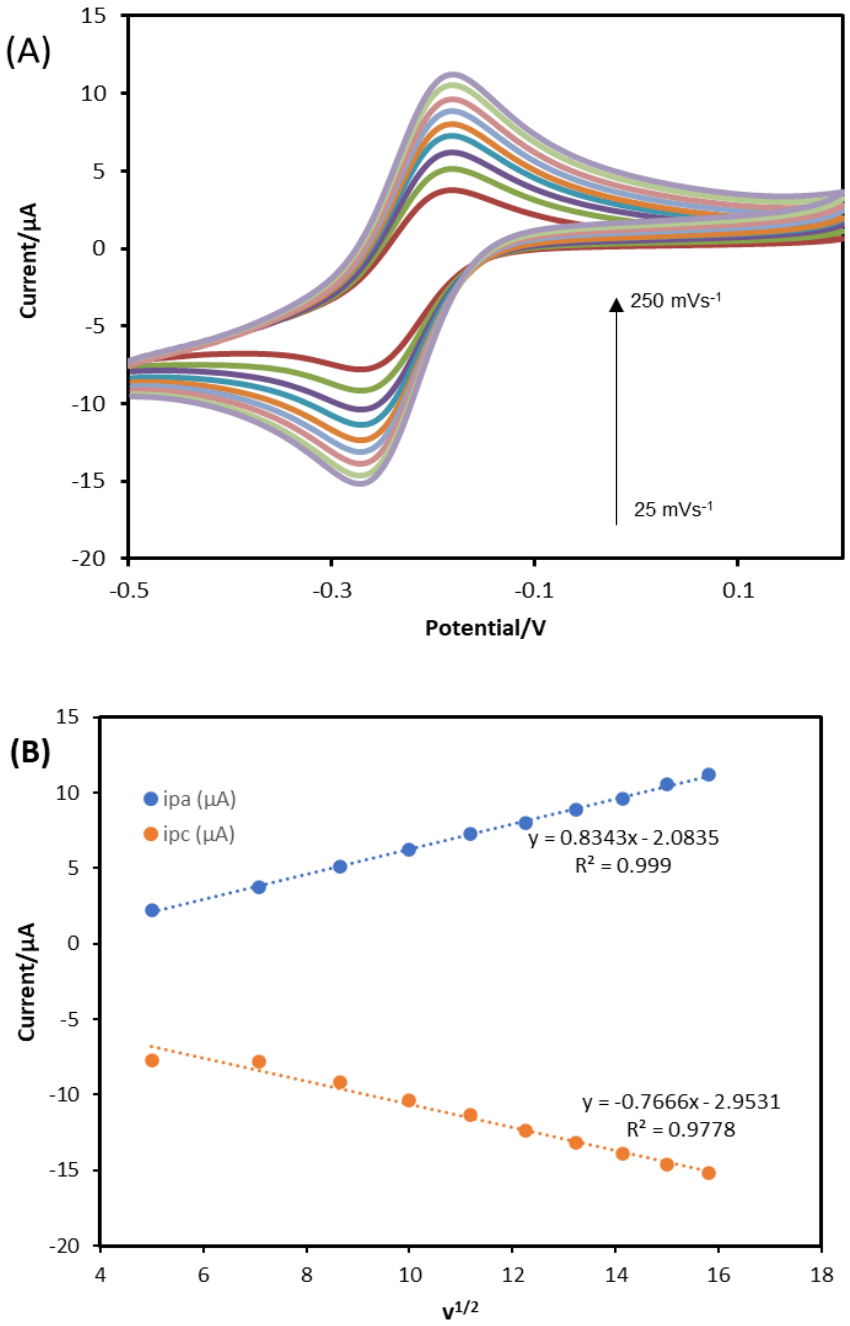

Figure 3.12 Cyclic voltammograms of (A) CSSM/SPE at 25 - 250 mVs^{-1} scan rates in 5 mM $[Ru(NH_3)_6]Cl_3$. (B) Plots of CSSM/SPE Ipa (µA) vs $v^{1/2}$ and Ipc (µA) vs $v^{1/2}$, respectively.

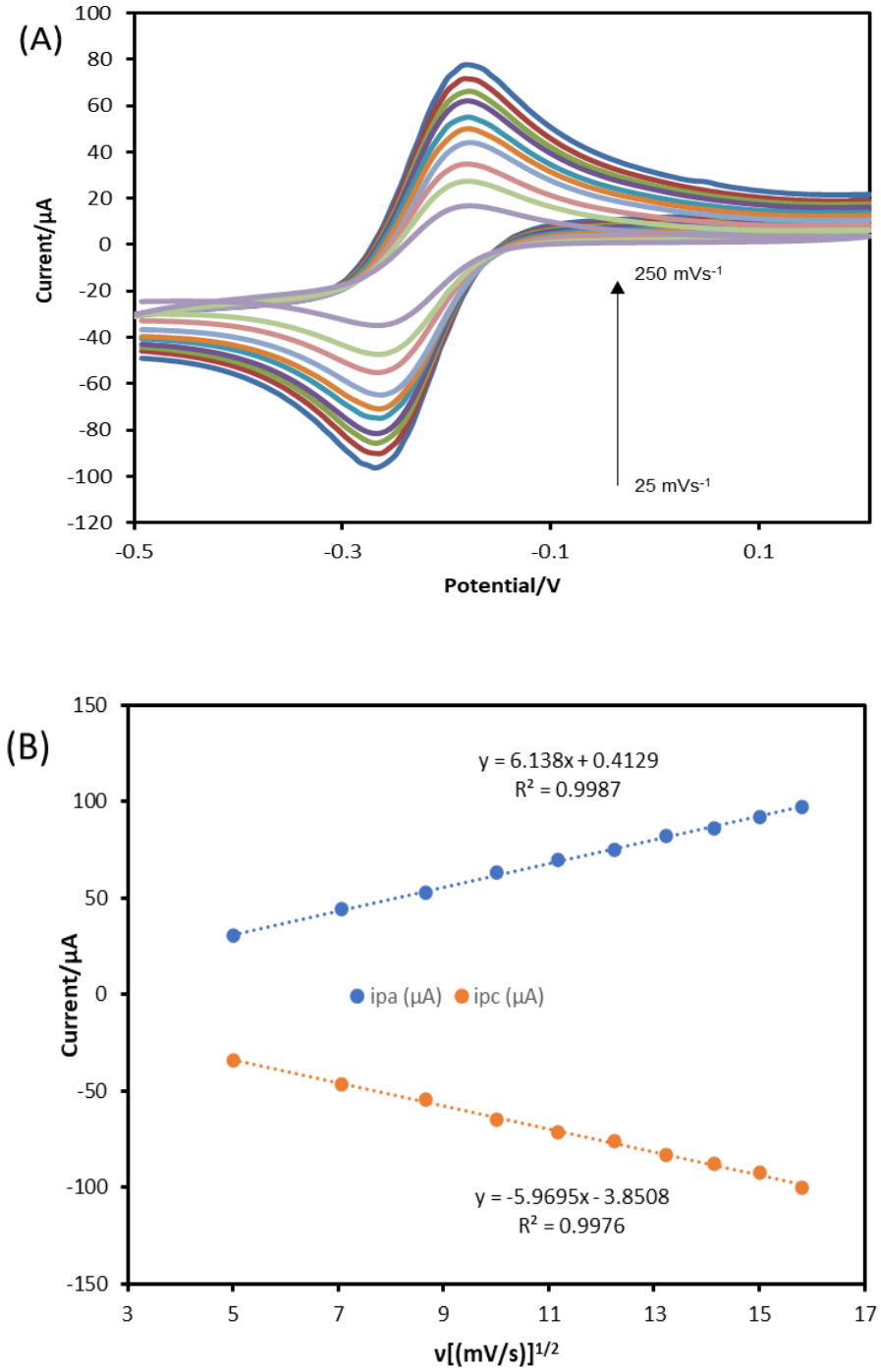

Figure 3.13 Cyclic voltammograms of (A) Bare SPE at 25 - 250 mVs^{-1} scan rates in 5 mM $[Ru(NH_3)_6]Cl_3$. (B) Plots of bare SPE Ipa (µA) vs $v^{1/2}$ and Ipc (µA) vs $v^{1/2}$, respectively.

Figure 3.10A indicates that surface chemistry does not significantly affect the electron transfer rates and depends only on the electrode's electronic structure with peak-to-peak separation (Δ_{EP}), between 552-720 mV across the scan rates. While looking at the $[FeCN_6]^{-3/-4}$, Figure 3.10A shows a difference between anodic and cathodic peak currents as the scan rate increases. The peak-to-peak separation (Δ_{EP}) is between 320 - 580 mV, considerably larger than Figure 3.10B, indicating the irreversible redox process. Bare SPEs (Figure 3.10A) show a large peak-peak separation with a typical quasi-reversible electron transfer characteristic, as generally observed for this redox couple at various types of carbon electrodes. Scan rate studies showed a linear relationship between peak current and the square root of scan rate, indicating a diffusion-limited response in all cases for both electrodes. A shift in peak potential with increasing scan rate was also observed, indicating slow electron transfer and a quasi-reversible reaction. Also, the theoretically ideal one-electron oxidation/reduction reaction was observed despite this shift. However, in the case of the $[Ru(NH_3)_6]Cl_3$, for CSSM-SPE (Figure 3.12A), there was an increase in both anodic and cathodic current and a peak-to-peak separation (Δ_{EP}) shift between 85.55 mV. Figure 3.12B also shows the dependence between peak current (I_p) and the square root of scan rate for CSSM-SPE (A). Figure 3.13A for bare SPE has peak-to-peak separation (Δ_{EP}) of 92 mV in contrast to the decrease observed for ferri/ferrocyanide. Figure 3.13B shows the plots of I_p against the square root of the scan rate for bare SPE (B). The lower slope might suggest the negligible or absence of thin layer effects. This is due to the smaller working area and the electrode's geometric and active surface area. Compared to ferricyanide, hexaammine ruthenium (III) chloride is not dependent on surface oxides [96]. The

slope of each plot shows that ideal diffusion-only behaviour is observed for hexaammine ruthenium (III) chloride, with slopes of 0.834 for CSSM/SPE compared with slopes of 1.2 for bare electrodes in $[Fe(CN)_6]^{3-/4-}$(Figure 3.11).

3.3.2.1 Calculation of active surface area

CV was employed to measure the electrochemically active surface areas of the electrode. From section 3.3.2 on characterisation, the electrodes displayed ideal behaviour for $[Ru(NH_3)_6]^{3+}$ than $[Fe(CN)_6]^{3-/4-}$. The surface area was calculated from the slope of peak current vs square root of scan rate to $2.69 \times 10^5\, n^{3/2} AD^{1/2}C$ [99]. The electroactive surface area of the working electrode was computed at scan rates of 25 - 250 mVs^{-1} using the Randles Sevcik equation [99] (Eq.(1):

$$Ip = \pm(2.69 \times 10^5)\, n^{3/2}\, AD^{1/2}\, Cv^{1/2} \qquad (1)$$

where I_p is the peak current, A is the electroactive area (cm^2), n refers to the number of electrons transferred, and D is the diffusion coefficient of hexaammine ruthenium (III) ($[Ru(NH_3)_6]^{3+}$) in 0.1 M KCl solution ($9.1 \times 10^{-6}\, cm^2\, s^{-1}$), C is the hexaammine ruthenium concentration (molarity). V is the potential scan rate ($V\, s^{-1}$). By rearranging Equation 1, A is calculated. The electroactive surface area of the electrodes was calculated by rearrangement of Equation 1 to give:

$A = Ip \div (v^{1/2} K\, n^{3/2}\, D^{1/2}\, C)$, where K is a constant (2.69×10^5).

Therefore, the estimated electroactive area was calculated to be 0.011 cm^2 for CSSM-SPE and 0.009 for the bare SPE. The difference of 0.002 between the two calculated surface area values is relatively small. It is important to point out that despite the small difference in surface area, there is still a significant change in material properties that can lead to improved adsorption capacity, reaction

kinetics, and other desirable properties for the desired application. Heterogeneous electron transfer rate constants (*k°*) were computed using Nicholson's equation [100] (Eq. (2)):

$$k^0 = \psi\sqrt{\frac{\pi D n \upsilon F}{RT}} \quad (2)$$

Where Ψ is the kinetic parameter, π=3.14, *F* is the Faraday constant (96,485 C mol^{-1}), *R is* the universal gas constant (8.31 J K^{-1} mol^{-1}), and *T* refers to the temperature (298.15 K).'

3.3.3 Pre-treated screen-printed Electrodes

First, the use of solvents, as has been described by Washe et al. as a simple, versatile approach for SPEs to enhance their electroanalytical response [75], was investigated. The methodology involved exposure of the SPEs to N, N-dimethylformamide (DMF) and dimethyl sulfoxide (DMSO), according to [75,101]. The SPE was covered with the solvents to expose all the electrodes entirely to the solvent [75].

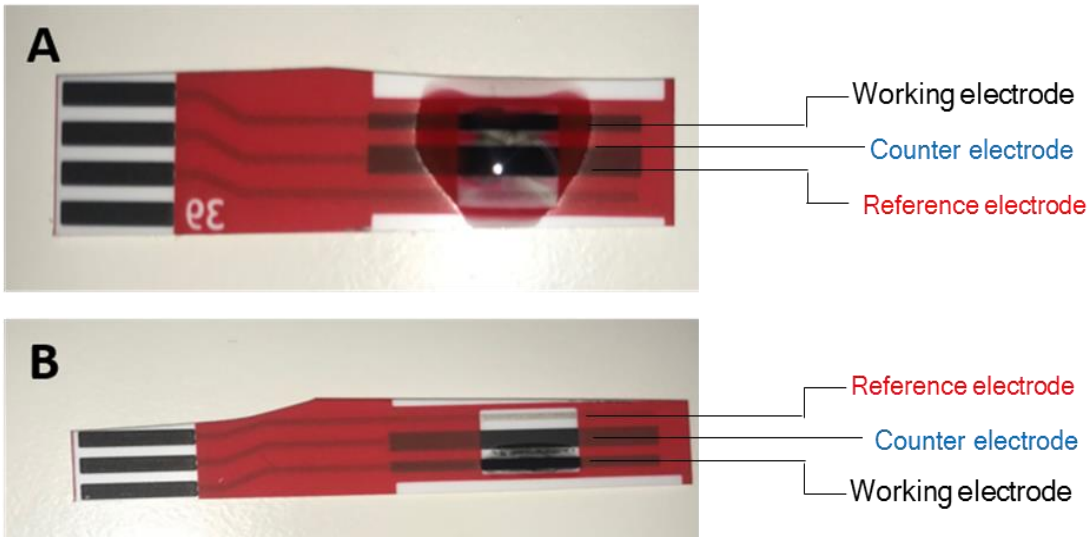

Figure 3.14 A photograph of the electrode and insulating layer after 30 minutes of exposure to (A) DMSO and (B) DMF, followed by curing in the oven at 60°C for 30 minutes.

The disadvantages of this technique included the dissolution of the carbon ink and the substrate and only marginal improvement in the electroanalytical sensitivity. Figure 3.14 shows the dissolution of the paste. This concurs with a study by Blanco et al. [101], where the group noticed that insulating layer crack/dissolution might be responsible for improved electrochemical performance [75]. Thus, the dissolution of the binder disrupts the SPE surface and leads to poor experimental outcomes. Furthermore, this process was designed to remove any organic compounds and other contaminants that may be present in the carbon ink from the screen-printing process. However, the observed results indicate that solvent treatment of these sensors leads to adverse effects. This approach was abandoned as a surface pre-treatment method.

3.4 Electrochemical Studies

3.4.1 Electrochemical oxidation of 17β-estradiol (E2)

The electrochemical activity of E2 at the electrode was measured to elucidate electrochemical behaviour at the screen-printed electrode and the mass transport mechanism of E2 on the electrode surface. CV studies were conducted in the potential range of 0.0 V to +0.8 V and at a scan rate of 100 mV s^{-1}. This is fundamental in a broader context of electrochemical sensor design. Before the target (E2) was added, a baseline was taken at 0.0 to +0.8 V in a blank buffer solution. Subsequently, E2 was added at a concentration of 100 µM (1 x 10^{-4} M), and a CV was recorded. Typical cyclic voltammetry responses of E2 are shown in Figure 3.15 (a-c) in a phosphate buffer solution (0.1 M, pH 7.0). In a blank buffer, no oxidation current was recorded (Figure 3.15a). However, with the addition of E2 in the buffer solution, a single anodic peak current was observed, as shown in Figure 3.15b.

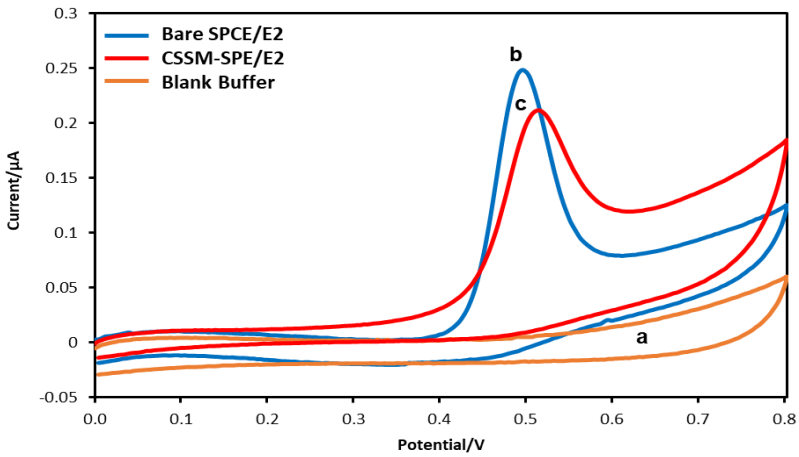

Figure 3.15. Cyclic voltammetry electrochemical profile of E2 in (a) blank Buffer on Bare SPE, (b) in the presence of 100 µM (1 x 10^{-4} M) E2 on Bare

SPE and (c) in 100 µM (1 x 10^{-4} M) E2 on CSSM-SPE. Analysis conditions: 0.1 M PBS (pH 7) at 0.1 Vs^{-1}.[1]

Figure 3.15b depicts the electrochemical behaviour of E2, showing an oxidation peak at +0.5V with a current of approximately 0.251 µA on the bare SPE. The modified CSSM-SPE (Figure 3.15c) showed an oxidation peak at +0.52V with a current of approximately 0.238 µA for E2 due to electron transfer on the electrode surface [102]. For both electrodes, no reduction peak was observed in the reversed scan, which is attributed to the irreversible oxidation nature of E2 [103]. This aligns with results from the literature, which indicate that the electrochemical activity of E2 at electrodes is irreversible [14-16]. The CV showed different electrochemical activity for the different electrode surfaces—the CSSM-modified electrode aimed to lower the background current significantly and generate a larger faradaic current. However, the CSSM electrode shows a poor electrochemical response to E2 (0.251 µA on the bare SPE compared to the modified CSSM-SPE (Figure 3.15c) at +0.52 V of 0.238 µA). This is somewhat unexpected since the modification should give a better peak current by incorporating the materials as modifiers in developing the sensor to improve performance [30]. This can be attributed to slow electron transfer. In this regard, bare SPE behaves like many other carbon-based electrodes for E2 [14-16].

[1]Micromolar (µM): Represents one micromole of solute per liter of solution (10^{-6} moles per liter). Molar (M): Represents one mole of solute per liter of solution. To convert from micromolar to molar, we divide by 1,000,000 (or multiply by 10^{-6}).

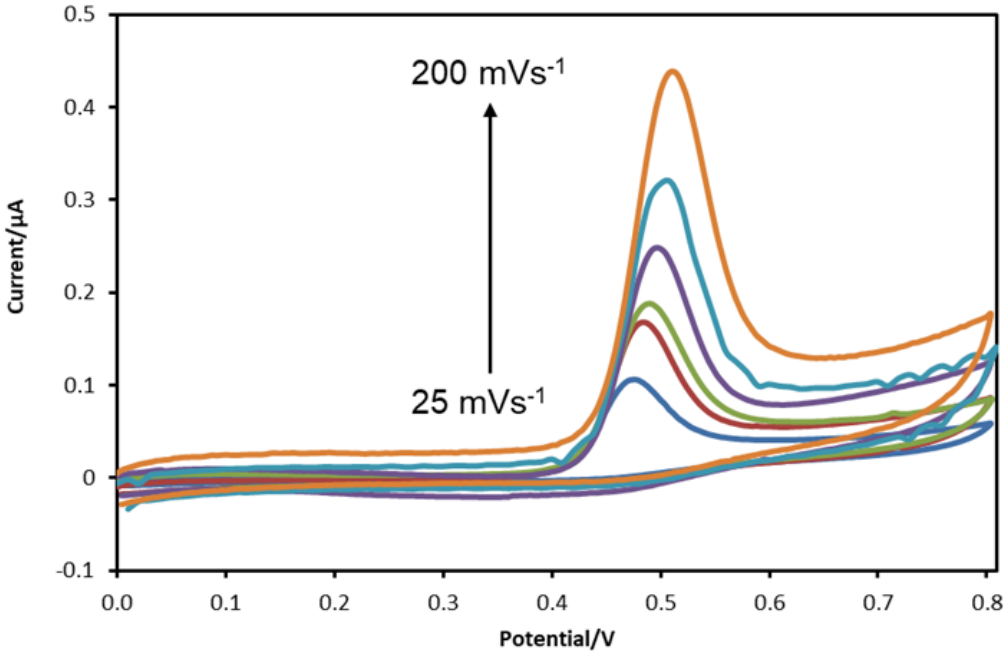

Figure 3.16 Cyclic voltammograms containing 0.1 M phosphate buffer and 1 x 10^{-4} M (100 µM) E2 at bare SPE with a 25 to 200 mVs-1 scan rate.

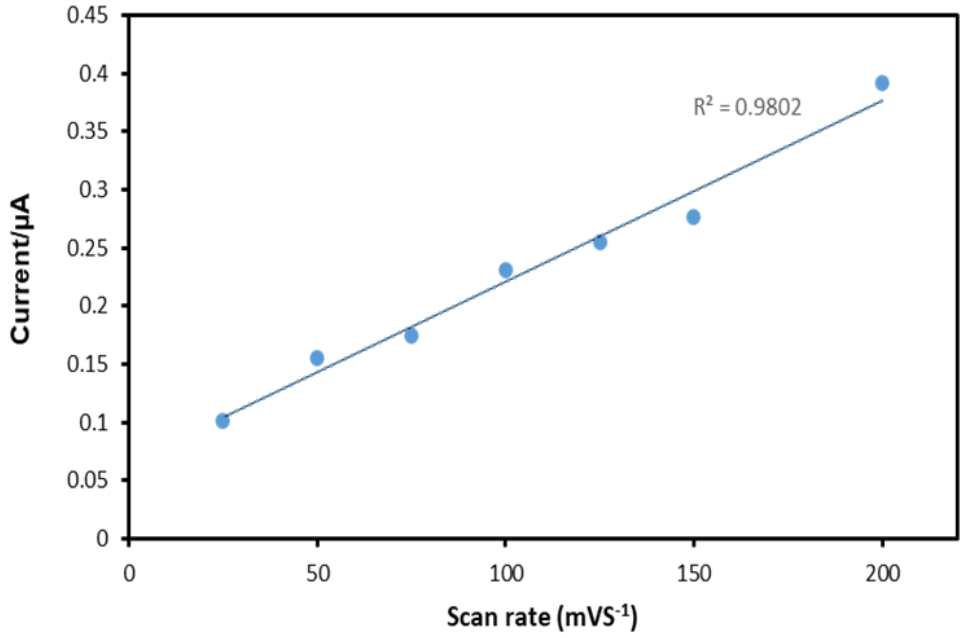

Figure 3.17 Plot of peak current vs the scan rate at bare SPE.

Figure 3.16 shows E2 oxidation at bare SPE as a function of scan rate. The dependence of peak current on the scan rates is depicted in Figure 3.17. From

Figure 3.17, as the scan rate increased, there was a linear increase in peak current for scan rates ranging from 25-200 mV s^{-1}. This yields a linear response of the equation of Ip = 0.0016x + 0.0651, with a correlation coefficient R^2 = 0.9802. This proportional relationship of peak current to scan rate indicates a simple electrode reaction of the adsorbed analyte. However, due to the complex reaction mechanisms for E2 oxidation, it is probably safer to view this result as an indicator that simple adsorption electrochemistry is observed. This does not agree with the diffusion of the analyte at the electrode for a Nernstian reaction [101]. Figure 3.18 depicts CSSM/SPE at 25 to 200 mVs^{-1} scan rates. The dependence of peak current versus scan rates is shown in Figure 3.19. The peak current versus scan rate is proportional to the 25 – 200 mVs^{-1} scan rate. The proportional relationship of peak current to scan rate represents an electrode reaction of an adsorbed species with the linear response having an equation of Ip = 0.0011x + 0.022 with a correlation coefficient R^2 = 0.9656.

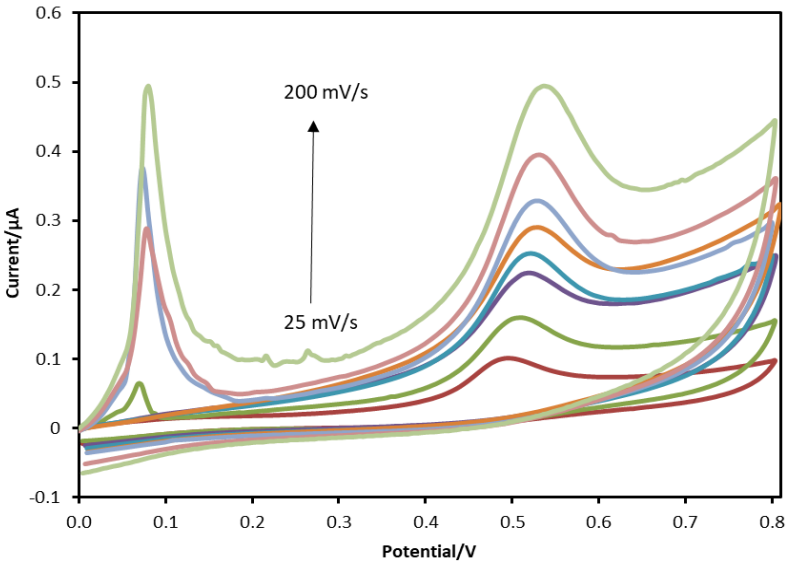

Figure 3.18. Cyclic voltammograms obtained in a solution containing 0.1 M phosphate buffer and 100 µM (1 x 10^{-4} M) E2 at CSSM/SPE with a scan rate of 25 to 200 mVs^{-1}.

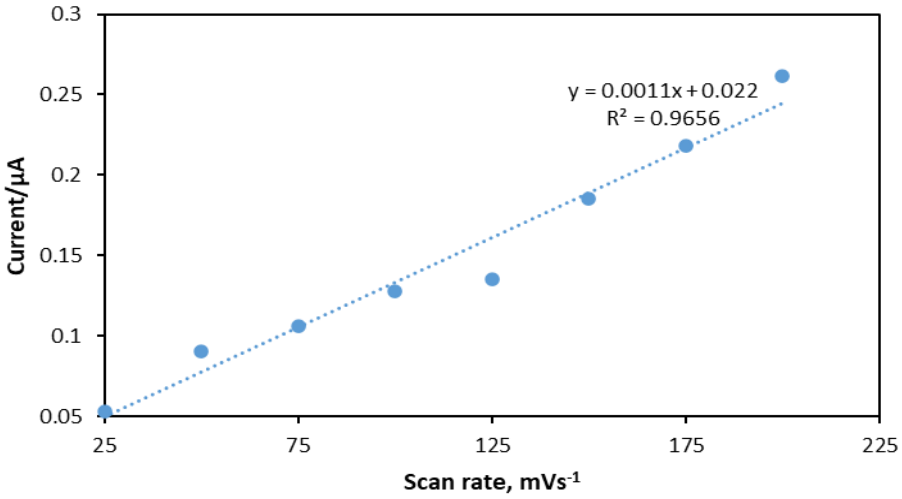

Figure 3.19 plot of peak current vs the scan rate at CSSM/SPE.

In Figure 3.18, a peak was also observed at 0.1 V at scan rates above 50 mv/s. This is in addition to the well-defined oxidation peak at 0.5 V attributed to the irreversible oxidation of estradiol, which is well-known and associated with the irreversible oxidation processes of phenolic compounds [16]. An additional

oxidation peak was observed when the scan rate was increased from 50 mV/s to 200 mV/s at 0.1 V, as shown in Figure 3.18. This secondary oxidative process exhibits voltammetric behaviour distinct from the primary estradiol oxidation peak at 0.5 V. The hypothesis for this observation can be attributed to the oxidation of other metabolites or a byproduct of estradiol, such as quinones. In addition, it can also be due to the specific experimental conditions, the electrolyte's composition, and the electrode's specific characteristics due to surface artefacts. The presence of Ag+ ion was reported by Lima et al., who noticed a similar peak and attributed that to silver ion in their work on the determination of the illicit nonsteroidal estrogen growth promoter, dienestrol [102].

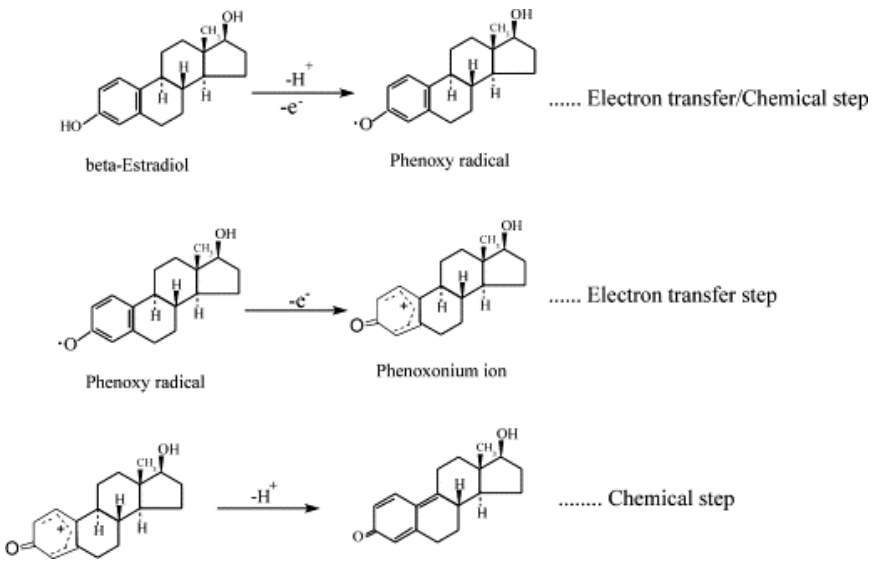

Figure 3.20. The proposed mechanism for the oxidation of estradiol (E2) [103].

Figure 3.20 shows the proposed electrochemical mechanism. The electrochemical oxidation of E2 and transformation to the electrochemical redox process involves a two-electron transfer – one-hydrogen ion transfer presented

in Figure 3.17. The mechanism for E2 on electrode surfaces has been studied by many authors [16,104–106]. Phenoxenium ion is a result of the formation of a dimer or quinone, which is the leading cause of fouling of carbon electrode surfaces, which results in the reduction of the E2 signal, as previously stated [107–109]. To overcome this problem, researchers use different carbon materials as a modifier with screen-printed carbon electrodes.

3.4.2 Analytical performance of the SPE electrode

Amperometry was performed to determine electrochemical performance for E2 detection and to estimate the analytical performance of the modified electrode. This was compared to the performance of a bare electrode. The amperometry experiments were carried out with a fixed potential of +0.65 V (vs Ag/AgCl); the results are shown in Figures 3.21 and 3.24. To investigate the influence of the applied potential in the amperometric measurements, voltages of 0.30, 0.40, 0.55 and 0.65 V (vs Ag/AgCl) were compared. A stable over-potential is observed for the potential selected, +0.65 V (vs Ag/AgCl). It was selected based on the oxidation peak obtained for the E2 oxidation in the cyclic voltammetry, where the oxidation peak is obtained (Figure 3.15) and ensures that the analyte is being oxidized efficiently during the amperometry. Thus, this potential was used for all amperometric experiments. Although this potential appears very high for a sensor, higher values (0.78 V [110] and 0.8 V [33,110]) have been reported in the literature for E2 measurements. The analytical characteristics of the sensors were established using amperometric measurements. After initial stabilisation, aliquots of E2 (from 0.5 mM concentration stock to give various concentrations in 30 mL PBS (pH 7)) were successfully added at 60-second intervals under stirring.

Figure 3.21 shows the amperometric response over the concentration range of 8.3×10^{-7} - 4.98×10^{-6} M. As the concentration increased, there was a decrease in the peak current generated due to the passivation of the modified electrode. Each point represents the mean value for three measurements. Figure 3.21 and figure 3.22 show the amperometric response for the CSSM/SPE and the corresponding calibration curve, plotted between current generated values and concentration, respectively. Figure 3.23 shows the amperometric response of the bare SPE at various concentrations of E2 and its corresponding calibration curve, plotted between current generated values and concentrations (Figure 3.24).

Analysing the raw amperometric signals is crucial to understanding the CSSM-SPE's electrochemical properties in terms of current generated from the amperometry. This establishes a baseline for assessing the effects of data processing techniques to be employed. Appendix B, Figure B1, displays the unprocessed data from three experiments. Also, the noise observed in the raw amperometric data of Bare SPE underwent cleaning and data processing. Appendix Figure B2 depicts the raw signal before any smoothing or baseline correction step. (Appendix B, Figure B2).

Figure 3.22 (CSSM/SPE) exhibits two linear plots: the concentration range 8.3×10^{-7} - 2.49×10^{-6} M and 3.31×10^{-6} - 4.98×10^{-6} M. The linear fit equations are $y = 0.003x + 0.066$; $R^2 = 0.992$, and $y = 0.0013x + 0.0106$, $R^2 = 0.9939$ (Figure 3.22). Figure 3.24 (bare SPE) again reveals a plot with a linear range of 8.3×10^{-7} - 4.98×10^{-6} M, with the best-fit line equation: $y = 0.0022x + 0.0009$, $R^2 = 0.9924$. The sensitivity of the electrodes was estimated from the calibration curve slope divided by the electrode's surface area in section 3.3.2. The limit of LOD is

calculated by (n = 3) standard deviation of the signal response against the slope of the calibration plot. For CSSM/SPE, the LODs were 1.82×10^{-6} M and 2.7×10^{-6} M for the first and second concentration ranges, respectively, with sensitivities of 0.273 $\mu A \mu M^{-1} cm^{-2}$ and 0.118 $\mu A \mu M^{-1} cm^{-2}$. The electrode sensitivity for the bare SPE was estimated to be 0.244 $\mu A \mu M^{-1} cm^{-2}$ with an LOD of 2.1×10^{-7} M. The performance of the CSSM/SPE sensor electrode was compared with other carbon-based modified electrodes, which are summarised in Table 3.1.

Although some publications presented a lower LOD than the CSSM electrode, the electrode presented in this work has a much more facile fabrication process. It offers a respectable LOD and linear range. Table 3.1 also indicates the various electrodes with modification steps used to compare them with the simple, direct application of the sensor as a practical approach, which was the focus of this study. Additionally, no other steps in the design and sensing protocol, such as the need for a Faraday cage or flow injection systems, have been reported with previous amperometric sensors [33]. It is difficult to compare measurements of different electrodes because of the fouling on bare SPE and CSSM/SPE. However, the result is comparable with the main body of the published literature. The reproducibility was estimated by performing amperometry measurements on an 8.3×10^{-7} M E2 solution in triplicate, gaining a %CV of 11.4%.

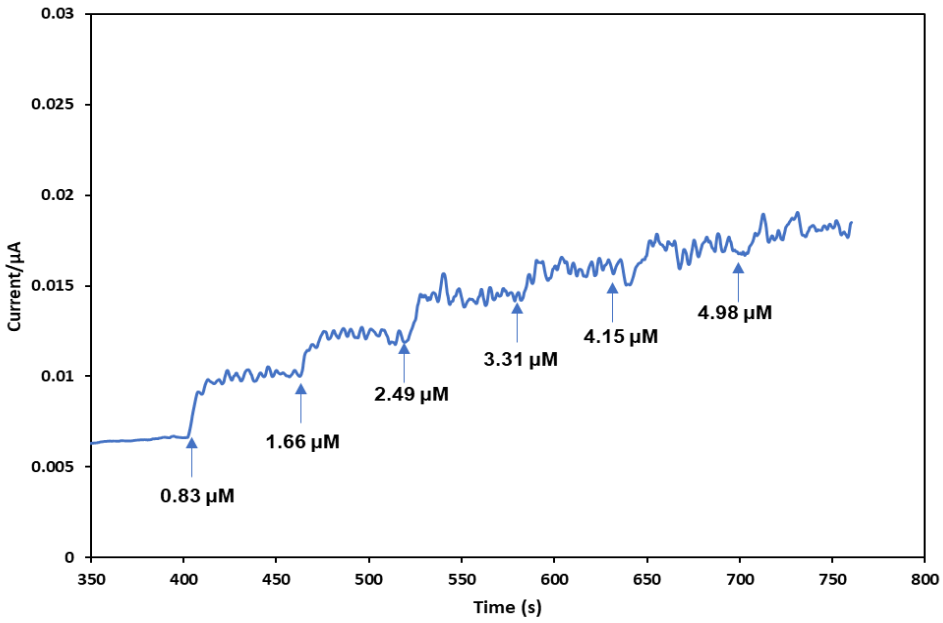

Figure 3.21. Amperometric response of estradiol (E2) sensor based on CSSM modified SPE (CSSM/SPE) with successive addition of estradiol (0.5 mM) at an operating potential of +0.65 V (vs Ag).

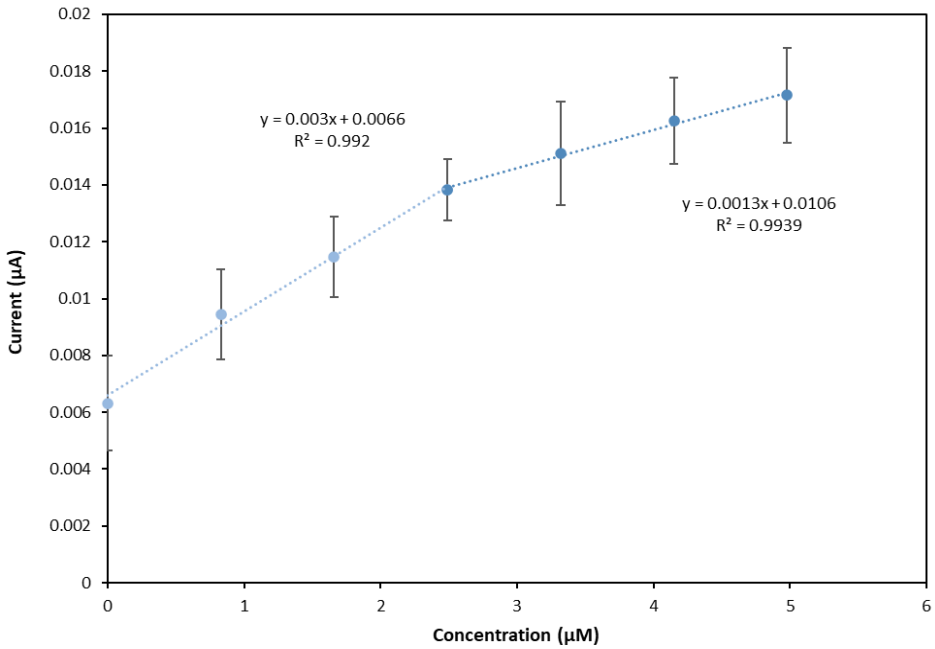

Figure 3.22. Shows the calibration plot of peak current vs concentration of CSSM/SPE. Error bars depict the standard deviation, representing the variability within triplicate measurements for each concentration point, n = 3.

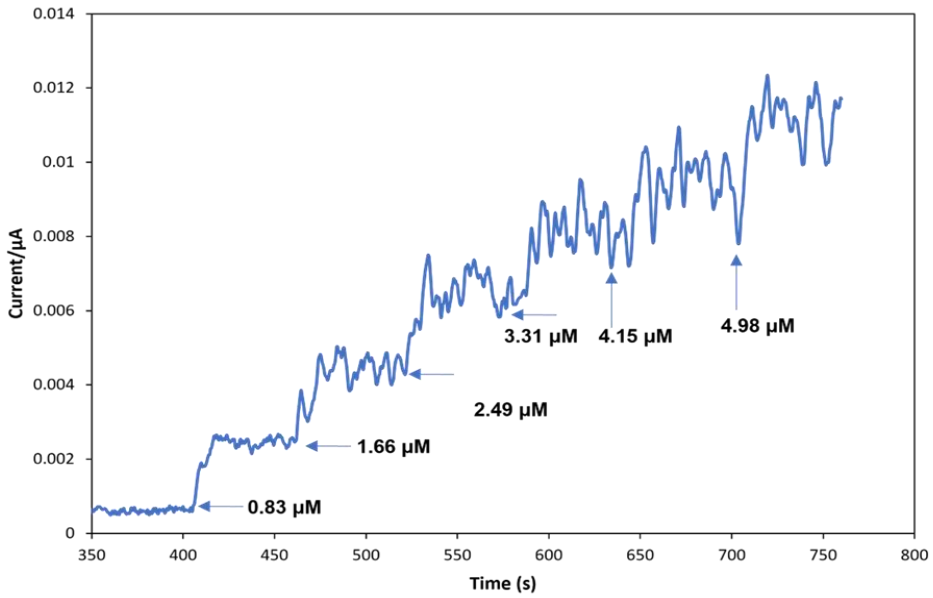

Figure 3.23. Amperometric response of estradiol (E2) sensor at bare SPE with successive addition of estradiol (E2) (concentration range of 0.83 – 4.98 µM (8.3 × 10^{-7} - 4.98 × 10^{-6} M) at an operating potential of +0.65 V (vs Ag).

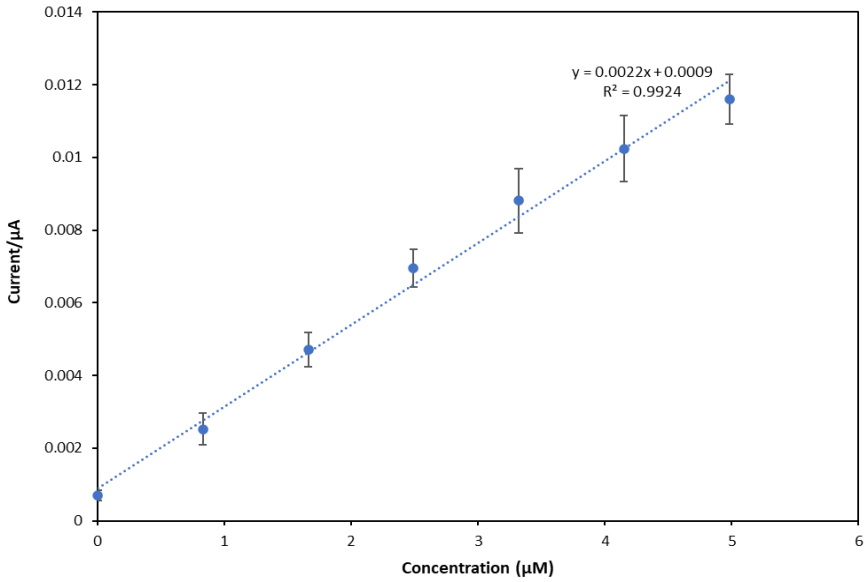

Figure 3.24 shows the calibration plot of peak current vs concentration of bare SPE. Error bars depict the standard deviation, representing the variability within triplicate measurements for each concentration point, n = 3.

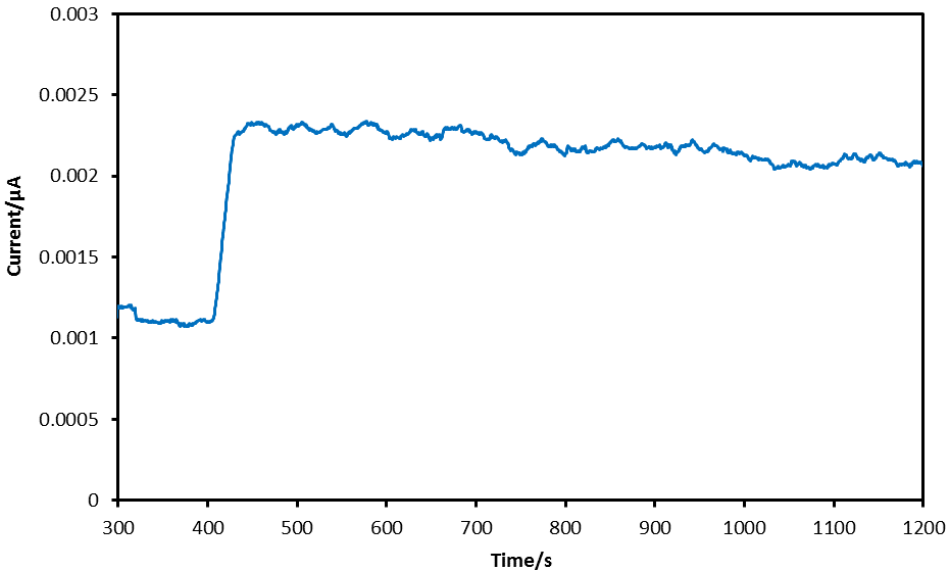

Figure 3.25 Stability test: steady oxidation current of 0.83 µM (8.3×10^{-7} M) estradiol addition over 1200 seconds using bare SPE.

Figure 3.25 shows the stability test results for the steady oxidation current with 8.3×10^{-7} M E2 addition only over 1200 seconds using a bare SPE to elucidate the noticed current reduction after injections of E2 in Figures 3.21 and 3.23. This resistance to fouling decrease (shown in the Figures) due to surface fouling may be caused by the amount of analyte in the solution, making the surface increasingly passivated. For Figure 3.25, the sensor retains a steady current over 1200 sec after adding 8.3×10^{-7} M E2 equivalent concentration, demonstrating surface polymerization has not covered the whole surface, thus the seen stability.

Figure 3.26A depicts the CVs of potential interferents examined. For ease of comparison, Figure 3.26B is the enlarged CV electrochemical profile of each interferent at 100 µM (1×10^{-4} M) in PBS buffer (pH 7.0), on CSSM-SPE: estrone (E1), estriol (E3), bisphenol A (BPA), Citric acid (CA), ibuprofen (Ibu) and Progesterone (P4). Combining the two figures makes the profile of E2 challenging to see, thus enlarging the two profiles.

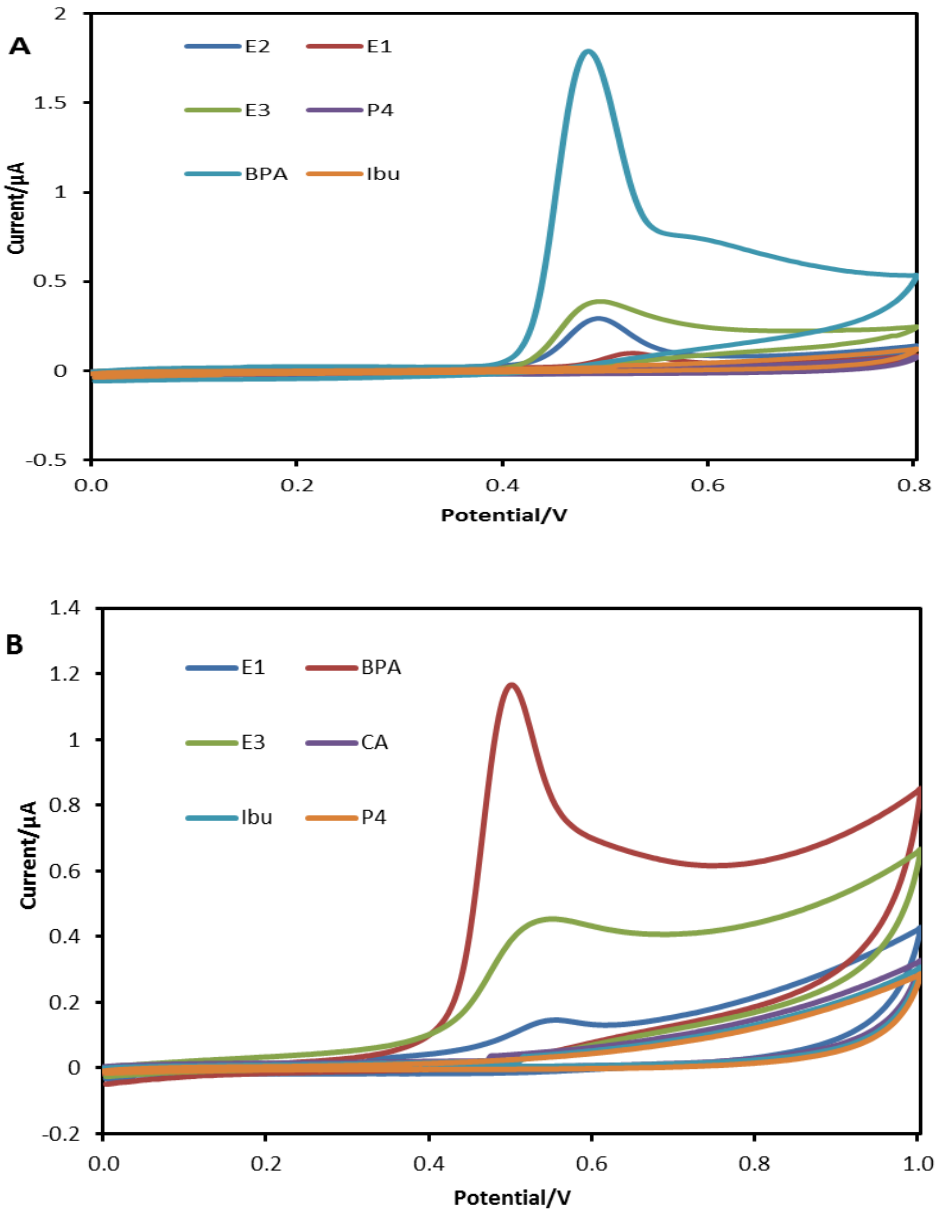

Figure 3.26 A). Cyclic voltammogram electrochemical profile of each interferent at 100 µM (1.0 × 10^{-4} M) in PBS buffer (pH 7.0), on bare SPE: estrone (E1), estriol (E3), bisphenol A (BPA), Citric acid (CA), ibuprofen (Ibu) and Progesterone (P4). B). Cyclic voltammogram electrochemical profile of each interferent at 100 µM (1.0 × 10^{-4} M) in PBS buffer (pH 7.0), on CSSM-SPE: estrone (E1), estriol (E3), bisphenol A (BPA), Citric acid (CA), ibuprofen (Ibu) and Progesterone (P4).

The studies indicate that fabricating screen-printed sensors using a facile strategy to prepare a carbon spherical shell does not significantly improve the

detection of E2 when used as a sensor modifier. Additionally, there seems to be variability in the baseline during amperometric measurement, indicating potential susceptibility to false positive and negative results despite the straightforward approach, as seen in figures 3.27-3.28 for interferent, where the fouling of the electrode is pronounced.

Table 3.1 Summary of Carbon-based nanomaterials reported for estradiol (E2) sensors.

Modifier	Linear range (M)	LOD	Electrode	Ref.
Fe_3O_4 /Nanoporous carbon	1×10^{-8} - 2×10^{-5} M	4.9×10^{-9} M.	Glassy carbon electrode (GCE)	[19]
Biochar nanosized particles (B.C.N.P.)	5×10^{-5} - 2×10^{-2} M	11.3×10^{-9} M	Glassy carbon electrode (GCE)	[49]
Polyaniline/carbon dot	1×10^{-6} - 1×10^{-1} M	4.3×10^{-8} M.	Glassy carbon electrode (GCE)	[54]
Printex 6L carbon/Deep eutectic solvent (D.E.S.)	9×10^{-7} - 2.1×10^{-4} M	6.5×10^{-9} M	Screen-printed carbon electrode (SPCE)	[55]
Nickel Ferrite Oxide/Mesoporous carbon	2×10^{-5} - 5.7×10^{-4} M	6.88×10^{-9} M	Glassy carbon electrode (GCE)	[111]
Cathodically pre-treated boron-doped diamond	1×10^{-4} - 3×10^{-3} M	1×10^{-7} M	Glassy carbon electrode (GCE)	[112]
Carbon spherical shell (CSSM)	3.31×10^{-3} - 5×10^{-3} M	4.4×10^{-7} M	Screen-printed carbon electrode (SPCE)	This work

3.4.3 Effect of Interferents

Water samples consist of a complex mixture of compounds. For example, several pharmaceuticals commonly found in water are associated with health concerns. Emerging pharmaceutical compounds structurally or in water were tested and reported for E2 (known). E2 was measured using the CSSM/SPE in the presence of other analytes, citric acid, ibuprofen, progesterone, and Bisphenol A (BPA) at the ratio 1:50 analyte: interferent, as a way of establishing the sensor applicability in a practical setting. Figure 3.28 shows a current signal after the injection of E2 but no signal generation upon the injection of citric acid.

Furthermore, the CSSM/SPE sensor shows no increase in current response at +0.65 V potential for ibuprofen and progesterone, suggesting interference-free determination of E2 at +0.65 V. In contrast, estrone, estriol and BPA, which behave like E2, show a current peak as they are oxidised at the same potential as E2. Figure 3.26 shows the cyclic voltammetry of these interferents and the potential at which they oxidised on the sensor surface. Figure 3.29 reveals the oxidation of some structural elements like E2. It provides information on the influence of these interferents on the electrochemical behaviour of E2. Water samples contain several compounds, including pharmaceuticals. Due to the complex nature of the water sample, we tested a few other compounds that might exist in water with E2. Some structurally compounds similar to E2 or in water were tested and reported for E2 (known). E2 was measured using the CSSM/SPE in the presence of other analytes, citric acid, ibuprofen, progesterone, and Bisphenol A (BPA) at the ratio 1:50 analyte: interferent, as a way of establishing the sensor applicability in a practical setting. Figure 3.28

shows a current signal after the injection of E2 but no signal generation upon the injection of citric acid.

Furthermore, the CSSM/SPE sensor shows no increase in current response at +0.65 V potential for ibuprofen and progesterone, suggesting interference-free determination of E2 at +0.65 V. In contrast, estrone, estriol and Bisphenol A (BPA), which behaves like estradiol, show a current peak as they are oxidised at the same potential as estradiol. Figure 3.27 shows the cyclic voltammetry of these interferents and the potential at which they oxidised on the sensor surface. Figure 3.28 reveals the oxidation of some structural elements like E2. It provides information on the influence of these interferents on the electrochemical behaviour of E2.

The approach adopted in this study was to measure E2 without using binding agents, such as antibodies or aptamers, which improve biosensor selectivity. Instead, the aim was to rely solely on carbon-based materials CSSM modified SPE, if possible, to provide an approach for sensor manufacture that was more straightforward and cost-effective and would remove the problems associated with instability and degradation of sensors known for binding agent. The aim of using CSSM is to find out if this carbon-based material is selective for estradiol. Different measurement techniques, such as differential pulse voltammetry, to distinguish the signal from E2 from the signals from interferents may be a possible solution to the interference problem. Other measurement techniques, such as differential pulse voltammetry, maybe a possible solution for distinguishing the electrochemical signal of estradiol from interferent species.

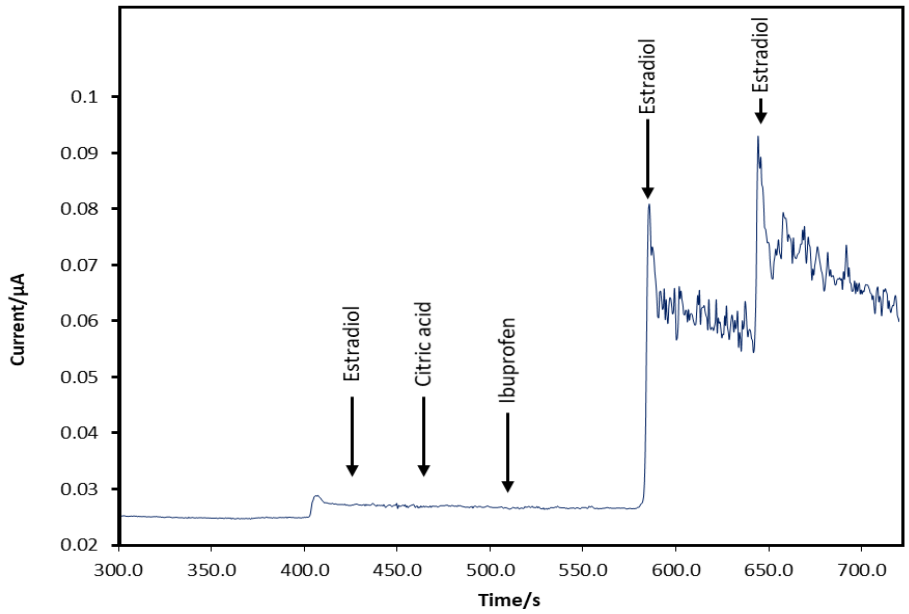

Figure 3.27 Amperometric response demonstrating the interference-free sensing of estradiol (E2). Citric acid, ibuprofen (10 mM each) last two injections of estradiol (E2) (10 mM) aliquot into 30 ml cell.

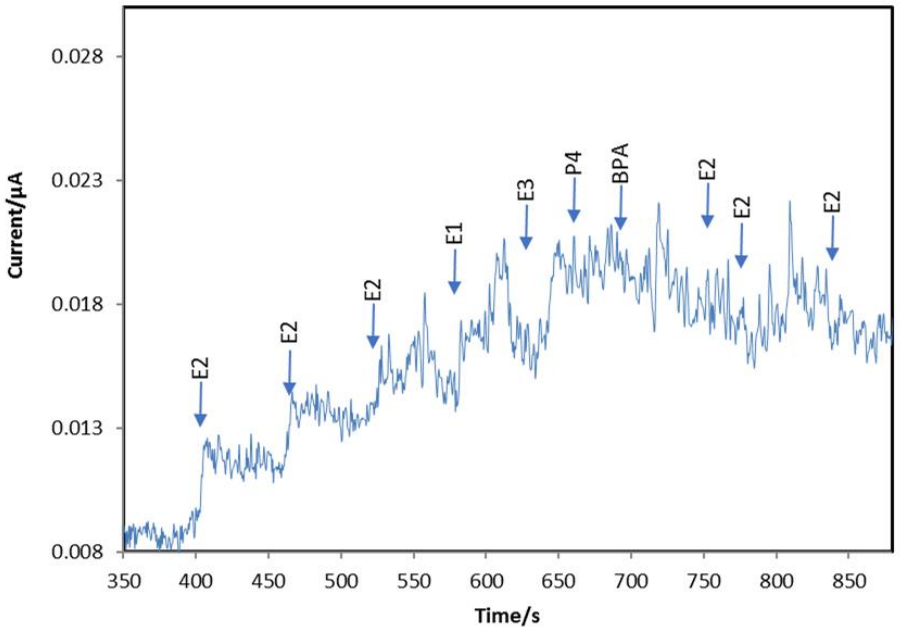

Figure 3.28 Amperometric response demonstrating the interference in sensing of estradiol (E2). Estrone (E1), Estriol (E3), progesterone (P4) and Bisphenol A (BPA) of 0.5 mM each aliquot into 30 ml cell.

3.5 Conclusion

This chapter described a simple hydrothermal synthesis of a carbon spherical shell as a suitable modifying material with no harsh reductant. The synthesis and characterisation of the carbon spherical shell material (CSSM) for application as a modifier in electrochemical sensors for E2 measurement has been demonstrated. These materials have been characterised by electron microscopy, spectroscopy, dynamic light scattering and electrochemically. The results of these studies have shown that a carbon spherical shell can be prepared in a simple process and can be applied to create screen-printed sensors (SPEs). However, using spherical carbon materials as a modifier for the sensor does not significantly enhance the detection of E2 relative to a bare electrode. Also, the reproducibility of the results does not appear to be satisfactory as there is variability in the baseline during the amperometric measurement, suggesting that this approach, even though straightforward, would be susceptible to false positive and negative results. Notably, what emerges from the Chapter are as follows:

- The amperometry technique determines E2 by applying fixed potential and measuring the current. CSSM/SPE has two linear plots within concentration ranges of 8.3×10^{-7} - 2.49×10^{-6} M and 3.31×10^{-6} - 4.98×10^{-6} M. CSSM/SPE has a sensitivity of 0.273 μA μM^{-1} cm^{-2} and 0.118 μA μM^{-1} cm^{-2} for the two linear concentrations. While for bare SPE, the electrode sensitivity was estimated to be 0.244 μA μM^{-1} cm^{-2}.
- CSSM-modified electrode indicates further strategy is required, such as doping with metallic particles, which is worthy of investigation in future

studies as the possibility of direct functionalisation during hydrothermal synthesis.

- DLS results of the materials seemed to aggregate and contain particles of various sizes, leading to larger particle sizes and less sphere-like shapes.

Further studies are needed to investigate a broader range of interferents besides the analytes tested in the current study, exploring other potential interferents, such as acetaminophen, naproxen, caffeine, and other substances such as pesticides. Future experimental design should be carried out on the interferents at different concentrations beyond the interferent ratio of 1:50 analyte: interferent, studied here, as interference effects are possible at higher or lower concentrations. Other interferent effects in more complex matrices, such as wastewater and surface water, should be investigated. Doing this will highlight the effect of the other compounds in the matrix and how that affects the interferents' electrochemical behaviour with E2. Overall, the experimental design should aim to characterise potential interferences under conditions that thoroughly mimic real-world water testing. As highlighted in the literature, it is common for the E2 electrochemical oxidation process to adhere to the electrode surface, creating a layer that decreases Ipa (peak current) and reduces the sensor's performance [25].

References

[1] Y.X. Gan, A.H. Jayatissa, Z. Yu, X. Chen, M. Li, Hydrothermal Synthesis of Nanomaterials, J. Nanomater. 2020 (2020). https://doi.org/10.1155/2020/8917013.

[2] M. Fleming, G. Achari, Q.K. Hassan, Modeling the loading and fate of estrogens in wastewater treatment plants, Cogent Environ. Sci. 2 (2016). https://doi.org/10.1080/23311843.2016.1222690.

[3] P. Busayapongchai, S. Siri, Sensitive detection of estradiol based on ligand binding domain of estrogen receptor and gold nanoparticles, Anal. Biochem. 518 (2017) 60–68. https://doi.org/10.1016/J.AB.2016.11.003.

[4] A. Florea, C. Cristea, F. Vocanson, R. Săndulescu, N. Jaffrezic-Renault, Electrochemical sensor for the detection of estradiol based on electropolymerized molecularly imprinted polythioaniline film with signal amplification using gold nanoparticles, Electrochem. Commun. 59 (2015) 36–39. https://doi.org/10.1016/J.ELECOM.2015.06.021.

[5] M. Farré, L. Kantiani, S. Pérez, D. Barceló, Sensors and biosensors in support of EU Directives, TrAC - Trends Anal. Chem. 28 (2009) 170–185. https://doi.org/10.1016/j.trac.2008.09.018.

[6] J. Barton, M.B.G. García, D.H. Santos, P. Fanjul-Bolado, A. Ribotti, M. McCaul, D. Diamond, P. Magni, Screen-printed electrodes for environmental monitoring of heavy metal ions: a review, Microchim. Acta. 183 (2016) 503–517. https://doi.org/10.1007/s00604-015-1651-0.

[7] A. Özcan, D. Topçuoğulları, Voltammetric determination of 17- β-estradiol by cysteamine self-assembled gold nanoparticle modified fumed silica decorated graphene nanoribbon nanocomposite, Sensors Actuators, B Chem. 250 (2017) 85–90. https://doi.org/10.1016/j.snb.2017.04.131.

[8] K. Yamanaka, M.C. Vestergaard, E. Tamiya, Printable electrochemical biosensors: A focus on screen-printed electrodes and their application, Sensors (Switzerland). 16 (2016) 1–16. https://doi.org/10.3390/s16101761.

[9] S. Cinti, F. Arduini, Graphene-based screen-printed electrochemical (bio)sensors and their applications: Efforts and criticisms, Biosens. Bioelectron. 89 (2017) 107–122. https://doi.org/10.1016/j.bios.2016.07.005.

[10] L.E. Platforms, Paper-Based Screen-Printed Electrodes : A New Generation of, (2021).

[11] A. García-Miranda Ferrari, S.J. Rowley-Neale, C.E. Banks, Screen-printed electrodes: Transitioning the laboratory in-to-the field, Talanta Open. 3 (2021) 100032. https://doi.org/10.1016/j.talo.2021.100032.

[12] A.C. de Sá, S.C. Barbosa, P.A. Raymundo-Pereira, D. Wilson, F.M. Shimizu, M. Raposo, O.N. Oliveira, Flexible carbon electrodes for electrochemical detection of bisphenol-a, hydroquinone and catechol in water samples, Chemosensors. 8 (2020) 1–11. https://doi.org/10.3390/chemosensors8040103.

[13] G.L. Marques, L.R. Rocha, M.C. Prete, F.A. Gorla, D. Moscardi dos

Santos, M.G. Segatelli, C.R. Teixeira Tarley, Development of Electrochemical Platform Based on Molecularly Imprinted Poly(methacrylic acid) Grafted on Iniferter-modified Carbon Nanotubes for 17β-Estradiol Determination in Water Samples, Electroanalysis. 33 (2021) 568–578. https://doi.org/10.1002/elan.202060270.

[14] P.A. Raymundo-Pereira, N.O. Gomes, S.A.S. Machado, O.N. Oliveira, Simultaneous, ultrasensitive detection of hydroquinone, paracetamol and estradiol for quality control of tap water with a simple electrochemical method, J. Electroanal. Chem. 848 (2019). https://doi.org/10.1016/j.jelechem.2019.113319.

[15] A. V. Kuzikov, R.A. Masamrekh, T.A. Filippova, Y.I. Haurychenka, A.A. Gilep, T. V. Shkel, N. V. Strushkevich, S.A. Usanov, V. V. Shumyantseva, Electrochemical oxidation of estrogens as a method for CYP19A1 (aromatase) electrocatalytic activity determination, Electrochim. Acta. 333 (2020) 135539. https://doi.org/10.1016/j.electacta.2019.135539.

[16] Y. Zhu, X. Liu, J. Jia, Electrochemical detection of natural estrogens using a graphene/ordered mesoporous carbon modified carbon paste electrode, Anal. Methods. 7 (2015) 8626–8631. https://doi.org/10.1039/c5ay01833a.

[17] R.M. Pemberton, T.T. Mottram, J.P. Hart, Development of a screen-printed carbon electrochemical immunosensor for picomolar concentrations of estradiol in human serum extracts, J. Biochem. Biophys. Methods. 63 (2005) 201–212. https://doi.org/10.1016/j.jbbm.2005.05.002.

[18] R. Shanmugam, K. Alagumalai, S.-M. Chen, T. Ganesan, Electrochemical evaluation of organic pollutant estradiol in industrial effluents, J. Environ. Chem. Eng. 9 (2021) 105723. https://doi.org/10.1016/j.jece.2021.105723.

[19] G.B. Braga, A.E.F. Oliveira, A.C. Pereira, Total Determination of Estrogenic Phenolic Compounds in River Water Using a Sensor Based on Reduced Graphene Oxide and Molecularly Imprinted Polymer, Electroanalysis. 30 (2018) 2176–2184. https://doi.org/10.1002/elan.201800238.

[20] Q. Jiang, D. Zhang, Y. Cao, N. Gan, An antibody-free and signal-on type electrochemiluminescence sensor for diethylstilbestrol detection based on magnetic molecularly imprinted polymers-quantum dots labeled aptamer conjugated probes, J. Electroanal. Chem. 789 (2017) 1–8. https://doi.org/10.1016/j.jelechem.2017.02.020.

[21] L. Fan, G. Zhao, H. Shi, M. Liu, A simple and label-free aptasensor based on nickel hexacyanoferrate nanoparticles as signal probe for highly sensitive detection of 17β-estradiol, Biosens. Bioelectron. 68 (2015) 303–309. https://doi.org/10.1016/j.bios.2015.01.015.

[22] Z. Wang, P. Wang, X. Tu, Y. Wu, G. Zhan, C. Li, A novel electrochemical sensor for estradiol based on nanoporous polymeric film bearing poly{1-butyl-3-[3-(N-pyrrole)propyl]imidazole dodecyl sulfonate} moiety, Sensors Actuators B Chem. 193 (2014) 190–197. https://doi.org/10.1016/J.SNB.2013.11.053.

[23] P.A. Raymundo-Pereira, N.O. Gomes, S.A.S. Machado, O.N. Oliveira,

Simultaneous, ultrasensitive detection of hydroquinone, paracetamol and estradiol for quality control of tap water with a simple electrochemical method, J. Electroanal. Chem. 848 (2019) 113319. https://doi.org/10.1016/j.jelechem.2019.113319.

[24] J.J. Triviño, M. Gómez, J. Valenzuela, A. Vera, V. Arancibia, Determination of a natural (17B-estradiol) and a synthetic (17A-ethinylestradiol) hormones in pharmaceutical formulations and urine by adsorptive stripping voltammetry, Sensors Actuators, B Chem. 297 (2019) 126728. https://doi.org/10.1016/j.snb.2019.126728.

[25] A.M. Santos, A. Wong, T.M. Prado, E.L. Fava, O. Fatibello-Filho, M.D.P.T. Sotomayor, F.C. Moraes, Voltammetric determination of ethinylestradiol using screen-printed electrode modified with functionalized graphene, graphene quantum dots and magnetic nanoparticles coated with molecularly imprinted polymers, Talanta. (2020) 121804. https://doi.org/10.1016/j.talanta.2020.121804.

[26] A. Wong, A.M. Santos, E.L. Fava, O. Fatibello-Filho, M.D.P.T. Sotomayor, Voltammetric determination of 17β-estradiol in different matrices using a screen-printed sensor modified with CuPc, Printex 6L carbon and Nafion film, Microchem. J. 147 (2019) 365–373. https://doi.org/10.1016/j.microc.2019.03.052.

[27] P.A. Raymundo-Pereira, A.M. Campos, F.C. Vicentini, B.C. Janegitz, C.D. Mendonça, L.N. Furini, N. V. Boas, M.L. Calegaro, C.J.L. Constantino, S.A.S. Machado, O.N. Oliveira, Sensitive detection of estriol

hormone in creek water using a sensor platform based on carbon black and silver nanoparticles, Talanta. 174 (2017) 652–659. https://doi.org/10.1016/j.talanta.2017.06.058.

[28] A.M. Musa, J. Kiely, R. Luxton, K.C. Honeychurch, Recent progress in screen-printed electrochemical sensors and biosensors for the detection of estrogens, TrAC - Trends Anal. Chem. 139 (2021) 116254. https://doi.org/10.1016/j.trac.2021.116254.

[29] J. Wang, B. Tian, V.B. Nascimento, L. Angnes, Performance of screen-printed carbon electrodes fabricated from different carbon inks, Electrochim. Acta. 43 (1998) 3459–3465. https://doi.org/10.1016/S0013-4686(98)00092-9.

[30] R. Cancelliere, A. Di Tinno, A.M. Di Lellis, Y. Tedeschi, S. Bellucci, K. Carbone, E. Signori, G. Contini, L. Micheli, An inverse-designed electrochemical platform for analytical applications, Electrochem. Commun. 121 (2020) 106862. https://doi.org/10.1016/j.elecom.2020.106862.

[31] F. Arduini, S. Cinti, V. Mazzaracchio, V. Scognamiglio, A. Amine, D. Moscone, Carbon black as an outstanding and affordable nanomaterial for electrochemical (bio)sensor design, Biosens. Bioelectron. 156 (2020) 112033. https://doi.org/10.1016/j.bios.2020.112033.

[32] D. Talarico, F. Arduini, A. Constantino, M. Del Carlo, D. Compagnone, D. Moscone, G. Palleschi, Carbon black as successful screen-printed electrode modifier for phenolic compound detection, Electrochem.

Commun. 60 (2015) 78–82. https://doi.org/10.1016/j.elecom.2015.08.010.

[33] J. Smajdor, R. Piech, M. Ławrywianiec, B. Paczosa-Bator, Glassy carbon electrode modified with carbon black for sensitive estradiol determination by means of voltammetry and flow injection analysis with amperometric detection, Anal. Biochem. 544 (2018) 7–12. https://doi.org/10.1016/j.ab.2017.12.025.

[34] F. Arduini, A. Amine, C. Majorani, F. Di Giorgio, D. De Felicis, F. Cataldo, D. Moscone, G. Palleschi, High performance electrochemical sensor based on modified screen-printed electrodes with cost-effective dispersion of nanostructured carbon black, Electrochem. Commun. 12 (2010) 346–350. https://doi.org/10.1016/j.elecom.2009.12.028.

[35] F.C. Vicentini, P.A. Raymundo-Pereira, B.C. Janegitz, S.A.S. Machado, O. Fatibello-Filho, Nanostructured carbon black for simultaneous sensing in biological fluids, Sensors Actuators, B Chem. 227 (2016) 610–618. https://doi.org/10.1016/j.snb.2015.12.094.

[36] J. dos Santos Fernandes, J.O. Fernandes, C.A.R. Bernardino, C.F. Mahler, B.F. Braz, R.E. Santelli, F.H. Cincotto, A New Electrochemical Sensor Based on Carbon Black Modified With Palladium Nanoparticles for Direct Determination of 17α-Ethinylestradiol in Real Samples, Electroanalysis. 34 (2022) 863–871. https://doi.org/10.1002/elan.202100474.

[37] C. Liang, Z. Li, S. Dai, Mesoporous carbon materials: Synthesis and modification, Angew. Chemie - Int. Ed. 47 (2008) 3696–3717.

https://doi.org/10.1002/anie.200702046.

[38] Y. Fang, D. Gu, Y. Zou, Z. Wu, F. Li, R. Che, Y. Deng, B. Tu, D. Zhao, A low-concentration hydrothermal synthesis of biocompatible ordered mesoporous carbon nanospheres with tunable and uniform size, Angew. Chemie - Int. Ed. 49 (2010) 7987–7991. https://doi.org/10.1002/anie.201002849.

[39] Y.P. Sun, B. Zhou, Y. Lin, W. Wang, K.A.S. Fernando, P. Pathak, M.J. Meziani, B.A. Harruff, X. Wang, H. Wang, P.G. Luo, H. Yang, M.E. Kose, B. Chen, L.M. Veca, S.Y. Xie, Quantum-sized carbon dots for bright and colorful photoluminescence, J. Am. Chem. Soc. 128 (2006) 7756–7757. https://doi.org/10.1021/ja062677d.

[40] N. Electrodes, Electrochemical Properties of Screen-Printed Carbon Nano-Onion Electrodes, (2020).

[41] J.C. Zuaznabar-Gardona, A. Fragoso, A wide-range solid state potentiometric pH sensor based on poly-dopamine coated carbon nano-onion electrodes, Sensors Actuators, B Chem. 273 (2018) 664–671. https://doi.org/10.1016/j.snb.2018.06.103.

[42] J. Breczko, M.E. Plonska-Brzezinska, L. Echegoyen, Electrochemical oxidation and determination of dopamine in the presence of uric and ascorbic acids using a carbon nano-onion and poly(diallyldimethylammonium chloride) composite, Electrochim. Acta. 72 (2012) 61–67. https://doi.org/10.1016/j.electacta.2012.03.177.

[43] S. Cinti, V. Mazzaracchio, I. Cacciotti, D. Moscone, F. Arduini, Carbon

black-modified electrodes screen-printed onto paper towel, waxed paper and parafilm m®, Sensors (Switzerland). 17 (2017) 1–12. https://doi.org/10.3390/s17102267.

[44] S. Cinti, D. Neagu, M. Carbone, I. Cacciotti, D. Moscone, F. Arduini, Novel carbon black-cobalt phthalocyanine nanocomposite as sensing platform to detect organophosphorus pollutants at screen-printed electrode, Electrochim. Acta. 188 (2016) 574–581. https://doi.org/10.1016/j.electacta.2015.11.069.

[45] S. Cinti, F. Arduini, M. Carbone, L. Sansone, I. Cacciotti, D. Moscone, G. Palleschi, Screen-Printed Electrodes Modified with Carbon Nanomaterials: A Comparison among Carbon Black, Carbon Nanotubes and Graphene, Electroanalysis. 27 (2015) 2230–2238. https://doi.org/10.1002/elan.201500168.

[46] V. Mazzaracchio, M.R. Tomei, I. Cacciotti, A. Chiodoni, C. Novara, M. Castellino, G. Scordo, A. Amine, D. Moscone, F. Arduini, Inside the different types of carbon black as nanomodifiers for screen-printed electrodes, Electrochim. Acta. 317 (2019) 673–683. https://doi.org/10.1016/j.electacta.2019.05.117.

[47] J. Tersoff, Emprical interatomic potential.pdf, (n.d.).

[48] Y. Li, R. Xu, H. Wang, W. Xu, L. Tian, J. Huang, C. Liang, Y. Zhang, Recent Advances of Biochar-Based Electrochemical Sensors and Biosensors, Biosensors. 12 (2022) 377. https://doi.org/10.3390/bios12060377.

[49] X. Dong, L. He, Y. Liu, Y. Piao, Preparation of highly conductive biochar nanoparticles for rapid and sensitive detection of 17β-estradiol in water, Electrochim. Acta. 292 (2018) 55–62. https://doi.org/10.1016/j.electacta.2018.09.129.

[50] M. Silva, S. Morante-Zarcero, D. Pérez-Quintanilla, I. Sierra, Simultaneous determination of pindolol, acebutolol and metoprolol in waters by differential-pulse voltammetry using an efficient sensor based on carbon paste electrode modified with amino-functionalized mesostructured silica, Sensors Actuators, B Chem. 283 (2019) 434–442. https://doi.org/10.1016/j.snb.2018.12.058.

[51] A.M. Campos, P.A. Raymundo-Pereira, C.D. Mendonça, M.L. Calegaro, S.A.S. Machado, O.N. Oliveira, Size Control of Carbon Spherical Shells for Sensitive Detection of Paracetamol in Sweat, Saliva, and Urine, ACS Appl. Nano Mater. 1 (2018) 654–661. https://doi.org/10.1021/acsanm.7b00139.

[52] T.W.B. Lo, L. Aldous, R.G. Compton, The use of nano-carbon as an alternative to multi-walled carbon nanotubes in modified electrodes for adsorptive stripping voltammetry, Sensors Actuators, B Chem. 162 (2012) 361–368. https://doi.org/10.1016/j.snb.2011.12.104.

[53] F.C. Vicentini, A.E. Ravanini, L.C.S. Figueiredo-Filho, J. Iniesta, C.E. Banks, O. Fatibello-Filho, Imparting improvements in electrochemical sensors: Evaluation of different carbon blacks that give rise to significant improvement in the performance of electroanalytical sensing platforms,

Electrochim. Acta. 157 (2015) 125–133. https://doi.org/10.1016/j.electacta.2014.11.204.

[54] P. Supchocksoonthorn, M.C. Alvior Sinoy, M.D.G. de Luna, P. Paoprasert, Facile fabrication of 17β-estradiol electrochemical sensor using polyaniline/carbon dot-coated glassy carbon electrode with synergistically enhanced electrochemical stability, Talanta. 235 (2021) 122782. https://doi.org/10.1016/j.talanta.2021.122782.

[55] C.G. Neves, A.L. Montiel, F.E.B. Junior, G.C. Paveglio, W.R.P. Barros, Application of a Screen-Printed Carbon Electrode Modified with Printex 6L and Deep Eutectic Solvent for Detection and Quantification of 17β-estradiol, J. Electrochem. Soc. 169 (2022) 057501. https://doi.org/10.1149/1945-7111/ac68a3.

[56] A. Wong, A.M. Santos, E.L. Fava, O. Fatibello-Filho, M.D.P.T. Sotomayor, Voltammetric determination of 17β-estradiol in different matrices using a screen-printed sensor modified with CuPc, Printex 6L carbon and Nafion film, Microchem. J. 147 (2019) 365–373. https://doi.org/10.1016/j.microc.2019.03.052.

[57] M.H.M. Zaid, J. Abdullah, N. Rozi, A.A.M. Rozlan, S.A. Hanifah, A sensitive impedimetric aptasensor based on carbon nanodots modified electrode for detection of 17ß-estradiol, Nanomaterials. 10 (2020) 1–14. https://doi.org/10.3390/nano10071346.

[58] M. Pohanka, H. Band'uchová, K. Vlčková, J.Ž. Karasová, K. Kuča, V. Damková, L. Pecková, F. Vitula, J. Pikula, Square wave voltammetry on

screen printed electrodes: Comparison to ferric reducing antioxidant power in plasma from model laboratory animal (grey partridge) and comparison to standard antioxidants, J. Appl. Biomed. 9 (2011) 103–109. https://doi.org/10.2478/v10136-009-0032-6.

[59] A. Chen, B. Shah, Electrochemical sensing and biosensing based on square wave voltammetry, Anal. Methods. 5 (2013) 2158–2173. https://doi.org/10.1039/c3ay40155c.

[60] D.C Ferrier, Kiely, J. and Luxton, R., 2022. Metal oxide decorated carbon nanocomposite electrodes for propofol monitoring. Biosensors and Bioelectronics: X, 12, p.100286.

[61] I. Süslü, M. Çelebier, S. Altinöz, Electrochemical behaviour investigation and square-wave voltammetric determination of rivaroxaban in pharmaceutical dosage forms, Anal. Methods. 6 (2014) 9397–9403. https://doi.org/10.1039/c4ay01871k.

[62] S. Singh, J. Wang, S. Cinti, Review—An Overview on Recent Progress in Screen-Printed Electroanalytical (Bio)Sensors, ECS Sensors Plus. 1 (2022) 023401. https://doi.org/10.1149/2754-2726/ac70e2.

[63] A. Wong, A.M. Santos, F.H. Cincotto, F.C. Moraes, O. Fatibello-Filho, M.D.P.T. Sotomayor, A new electrochemical platform based on low cost nanomaterials for sensitive detection of the amoxicillin antibiotic in different matrices, Talanta. 206 (2020) 120252. https://doi.org/10.1016/j.talanta.2019.120252.

[64] O.A. Farghaly, R.S.A. Hameed, A.- Alhakeem, H. Abu-Nawwas,

Analytical Application Using Modern Electrochemical Techniques, Int. J. Electrochem. Sci. 9 (2014) 3287–3318.

[65] Y. Saylan, S. Akgönüllü, H. Yavuz, S. Ünal, A. Denizli, Molecularly imprinted polymer based sensors for medical applications, Sensors (Switzerland). 19 (2019). https://doi.org/10.3390/s19061279.

[66] A. De Oliveira-Roberth, D.I.V. Santos, D.D. Cordeiro, F.M.D.A. Lino, M.T.F. Bara, E.D.S. Gil, Voltammetric determination of Rutin at Screen-Printed carbon disposable electrodes, Cent. Eur. J. Chem. 10 (2012) 1609–1616. https://doi.org/10.2478/s11532-012-0093-3.

[67] K.C. Honeychurch, Review of electroanalytical-based approaches for the determination of benzodiazepines, Biosensors. 9 (2019). https://doi.org/10.3390/bios9040130.

[68] A.A. Lahcen, A.A. Baleg, P. Baker, E. Iwuoha, A. Amine, Synthesis and electrochemical characterization of nanostructured magnetic molecularly imprinted polymers for 17-β-estradiol determination, Sensors Actuators, B Chem. 241 (2017) 698–705. https://doi.org/10.1016/j.snb.2016.10.132.

[69] Q. Zhao, Y. Faraj, L.Y. Liu, W. Wang, R. Xie, Z. Liu, X.J. Ju, J. Wei, L.Y. Chu, Simultaneous determination of dopamine, uric acid and estriol in maternal urine samples based on the synergetic effect of reduced graphene oxide, silver nanowires and silver nanoparticles in their ternary 3D nanocomposite, Microchem. J. 158 (2020) 105185. https://doi.org/10.1016/j.microc.2020.105185.

[70] L.A. Pradela-Filho, I.A.A. Andreotti, J.H.S. Carvalho, D.A.G. Araújo, L.O.

Orzari, A. Gatti, R.M. Takeuchi, A.L. Santos, B.C. Janegitz, Glass varnish-based carbon conductive ink: A new way to produce disposable electrochemical sensors, Sensors Actuators, B Chem. 305 (2020) 127433. https://doi.org/10.1016/j.snb.2019.127433.

[71] K.C. Honeychurch, M. Piano, Electrochemical (bio) sensors for environmental and food analyses, Biosensors. 8 (2018) 2–4. https://doi.org/10.3390/bios8030057.

[72] G. Cui, Jae Hyun Yoo, Joung Su Lee, J. Yoo, Jung Hee Uhm, Geun Sig Cha, H. Nam, Effect of pre-treatment on the surface and electrochemical properties of screen-printed carbon paste electrodes, Analyst. 126 (2001) 1399–1403. https://doi.org/10.1039/b102934g.

[73] Y.-J. Chen, T.-H. Yang, J.-L. Chang, W.-L. Cheng, A.S. Kumar, J.-M. Zen, A catholically pre-treated low cost screen-printed carbon electrode surface for metal compounds electrocatalyst like hydrogen evolution activity, J. Electroanal. Chem. 839 (2019) 59–66. https://doi.org/10.1016/J.JELECHEM.2019.02.038.

[74] P. Fanjul-Bolado, D. Hernández-Santos, P.J. Lamas-Ardisana, A. Martín-Pernía, A. Costa-García, Electrochemical characterization of screen-printed and conventional carbon paste electrodes, Electrochim. Acta. 53 (2008) 3635–3642. https://doi.org/10.1016/j.electacta.2007.12.044.

[75] A.P. Washe, P. Lozano-Sánchez, D. Bejarano-Nosas, I. Katakis, Facile and versatile approaches to enhancing electrochemical performance of screen printed electrodes, Electrochim. Acta. 91 (2013) 166–172.

https://doi.org/10.1016/j.electacta.2012.12.110.

[76] D.M. Anjo, M. Kahr, M.M. Khodabakhsh, S. Nowinski, M. Wanger, Electrochemical activation of carbon electrodes in base: Minimization of dopamine adsorption and electrode capacitance, Anal. Chem. 61 (1989) 2603–2608. https://doi.org/10.1021/ac00198a004.

[77] H. Wei, J.-J. Sun, Y. Xie, C.-G. Lin, Y.-M. Wang, W.-H. Yin, G.-N. Chen, Enhanced electrochemical performance at screen-printed carbon electrodes by a new pretreating procedure, Anal. Chim. Acta. 588 (2007) 297–303. https://doi.org/10.1016/J.ACA.2007.02.006.

[78] A.J. Killard, S. Zhang, H. Zhao, R. John, E.I. Iwuoha, M.R. Smyth, Development of an electrochemical flow injection immunoassay (FIIA) for the real-time monitoring of biospecific interactions, Anal. Chim. Acta. 400 (1999) 109–119. https://doi.org/10.1016/S0003-2670(99)00611-X.

[79] S.C. Wang, K.S. Chang, C.J. Yuan, Enhancement of electrochemical properties of screen-printed carbon electrodes by oxygen plasma treatment, Electrochim. Acta. 54 (2009) 4937–4943. https://doi.org/10.1016/j.electacta.2009.04.006.

[80] M.D. Osborne, B.J. Seddon, R.A.W. Dryfe, G. Lagger, U. Loyall, H. Schäfer, H.H. Girault, Excimer laser-induced electrochemical activity in carbon ink films, J. Electroanal. Chem. 417 (1996) 5–15. https://doi.org/10.1016/S0022-0728(96)04781-X.

[81] X. Liu, Y. Yao, Y. Ying, J. Ping, Recent advances in nanomaterial-enabled screen-printed electrochemical sensors for heavy metal

detection, TrAC - Trends Anal. Chem. 115 (2019) 187–202. https://doi.org/10.1016/j.trac.2019.03.021.

[82] L. Karadurmus, A. Cetinkaya, S.I. Kaya, S.A. Ozkan, Recent trends on electrochemical carbon-based nanosensors for sensitive assay of pesticides, Trends Environ. Anal. Chem. 34 (2022) e00158. https://doi.org/10.1016/j.teac.2022.e00158.

[83] M. Cammarota, M. Lepore, M. Portaccio, D. Di Tuoro, F. Arduini, D. Moscone, D.G. Mita, Laccase biosensor based on screen-printed electrode modified withthionine-carbon black nanocomposite, for Bisphenol A detection, Electrochim. Acta. 109 (2013) 340–347. https://doi.org/10.1016/j.electacta.2013.07.129.

[84] Y. Jiang, B. Tian, Inorganic semiconductor biointerfaces, Nat. Rev. Mater. 3 (2018) 473–490. https://doi.org/10.1038/s41578-018-0062-3.

[85] T. Gan, Z. Shi, K. Wang, Y. Chen, J. Sun, Y. Liu, Size-controlled core–shell-structured Ag@carbon spheres for electrochemical sensing of bisphenol A, J. Solid State Electrochem. 19 (2015) 2299–2309. https://doi.org/10.1007/s10008-015-2860-5.

[86] R. Smith, Characterisation and Surface Modification of Graphitic Felts, Univ. Liverpool. (2018).

[87] X. Xia, Y. Zhang, Z. Fan, D. Chao, Q. Xiong, J. Tu, H. Zhang, H.J. Fan, Novel Metal@CARBON spheres core-shell arrays by controlled self-assembly of carbon nanospheres: A stable and flexible supercapacitor electrode, Adv. Energy Mater. 5 (2015) 1–9.

https://doi.org/10.1002/aenm.201401709.

[88] K. Nakagawa, M.A. Yamagishi, H.A. Nishimoto, N.O. Ikenaga, T. Suzuki, T. Kobayashi, M. Nishitani-Gamo, T. Ando, Oxidized Diamond as a Simultaneous Production Medium of Carbon Nanomaterials and Hydrogen for Fuel Cell, Chem. Mater. 15 (2003) 4571–4575. https://doi.org/10.1021/cm0210997.

[89] T. Ando, K. Yamamoto, M. Ishii, M. Kamo, Y. Sato, Vapour-phase oxidation of diamond surfaces in O2 studied by diffuse reflectance Fourier-transform infrared and temperture-programmed desorption spectroscopy, J. Chem. Soc. Faraday Trans. 89 (1993) 3635–3640. https://doi.org/10.1039/FT9938903635.

[90] R. Berne, B.J. and Pecora, Dynamic light scattering: with applications to chemistry, biology, and physics, Dover Publications, 2000.

[91] A. Wang, Y. Ding, L. Li, D. Duan, Q. Mei, Q. Zhuang, S. Cui, X. He, A novel electrochemical enzyme biosensor for detection of 17β-estradiol by mediated electron-transfer system., Talanta. 192 (2019) 478–485. https://doi.org/10.1016/j.talanta.2018.09.018.

[92] L. Jitkang, Y.S. Pin, C.H. Xin, L.S. Chun, Characterization of magnetic nanoparticle by dynamic light scattering, Nanoscale Res. Lett. 8 (2013) 308–381. www.nanoscalereslett.com/content/8/1/381.

[93] M.L. Miglietta, G. Rametta, G. Di Francia, Characterization of carbon based nanoparticles dispersion in aqueous solution using dynamic light scattering technique, Macromol. Symp. 286 (2009) 95–100.

https://doi.org/10.1002/masy.200951212.

[94] A.N. Patel, M.G. Collignon, M.A. OConnell, W.O.Y. Hung, K. McKelvey, J. V. MacPherson, P.R. Unwin, A new view of electrochemistry at highly oriented pyrolytic graphite, J. Am. Chem. Soc. 134 (2012) 20117–20130. https://doi.org/10.1021/ja308615h.

[95] R.L. McCreery, Advanced carbon electrode materials for molecular electrochemistry, Chem. Rev. 108 (2008) 2646–2687. https://doi.org/10.1021/cr068076m.

[96] M. Velický, D.F. Bradley, A.J. Cooper, E.W. Hill, I.A. Kinloch, A. Mishchenko, K.S. Novoselov, H. V. Patten, P.S. Toth, A.T. Valota, S.D. Worrall, R.A.W. Dryfe, Electron transfer kinetics on mono- and multilayer graphene, ACS Nano. 8 (2014) 10089–10100. https://doi.org/10.1021/nn504298r.

[97] A.G.M. Ferrari, C.W. Foster, P.J. Kelly, D.A.C. Brownson, C.E. Banks, Determination of the electrochemical area of screen-printed electrochemical sensing platforms, Biosensors. 8 (2018) 1–10. https://doi.org/10.3390/bios8020053.

[98] S. Trasatti, O.A. Petrii, International Union of Pure and Applied Chemistry Physical Chemistry Division Commission on Electrochemistry: Real Surface Area Measurements in Electrochemistry, Pure Appl. Chem. 63 (1991) 711–734. https://doi.org/10.1351/pac199163050711.

[99] J. Moldenhauer, M. Meier, D.W. Paul, Rapid and Direct Determination of Diffusion Coefficients Using Microelectrode Arrays, J. Electrochem. Soc.

163 (2016) H672–H678. https://doi.org/10.1149/2.0561608jes.

[100] C.W. Foster, J.P. Metters, D.K. Kampouris, C.E. Banks, Ultraflexible screen-printed graphitic electroanalytical sensing platforms, Electroanalysis. 26 (2014) 262–274. https://doi.org/10.1002/elan.201300563.

[101] E. Blanco, C.W. Foster, L.R. Cumba, D.R. Do Carmo, C.E. Banks, Can solvent induced surface modifications applied to screen-printed platforms enhance their electroanalytical performance?, Analyst. 141 (2016) 2783–2790. https://doi.org/10.1039/c6an00440g.

[102] Lima Filho, M.M., Correa, A.A., Silva, F.D., Carvalho, F.A., Mascaro, L.H. and Oliveira, T.M., 2019. A glassy carbon electrode modified with silver nanoparticles and functionalized multi-walled carbon nanotubes for voltammetric determination of the illicit growth promoter dienestrol in animal urine. Microchimica Acta, 186, pp.1-10.

[103] Ngundi, M.M., Sadik, O.A., Yamaguchi, T. and Suye, S.I., 2003. First comparative reaction mechanisms of β-estradiol and selected environmental hormones in a redox environment. Electrochemistry communications, 5(1), pp.61-67.

[104] G.G. Ying, R.S. Kookana, Y.J. Ru, Occurrence and fate of hormone steroids in the environment, Environ. Int. 28 (2002) 545–551. https://doi.org/10.1016/S0160-4120(02)00075-2.

[105] F. Moreira, E.R. Santana, A. Spinelli, Ionic liquid-supported magnetite nanoparticles as electrode modifier materials for estrogens sensing, Sci.

Rep. 10 (2020) 1–11. https://doi.org/10.1038/s41598-020-58931-6.

[106] L. Luo, F. Li, L. Zhu, Y. Ding, D. Deng, Electrochemical sensing platform of natural estrogens based on the poly(l-proline)-ordered mesoporous carbon composite modified glassy carbon electrode, Sensors Actuators, B Chem. 187 (2013) 78–83. https://doi.org/10.1016/j.snb.2012.09.056.

[107] P. Rocha, Â. Vilas-Boas, N. Fontes, D. Geraldo, F. Bento, Evaluation of Polyphenols in Wine by Voltammetric Techniques with Screen Printed Carbon Electrodes, Electroanalysis. (2019) 1–8. https://doi.org/10.1002/elan.201900392.

[108] X. Liu, D.K.Y. Wong, Electrocatalytic detection of estradiol at a carbon nanotube|Ni(Cyclam) composite electrode fabricated based on a two-factorial design, Anal. Chim. Acta. 594 (2007) 184–191. https://doi.org/10.1016/j.aca.2007.05.043.

[109] A. Ghanam, A.A. Lahcen, A. Amine, Electroanalytical determination of Bisphenol A: Investigation of electrode surface fouling using various carbon materials, J. Electroanal. Chem. 789 (2017) 58–66. https://doi.org/10.1016/j.jelechem.2017.02.026.

[110] I. V. Batista, M.R.V. Lanza, I.L.T. Dias, S.M.C.N. Tanaka, A.A. Tanaka, M.D.P.T. Sotomayor, Electrochemical sensor highly selective for estradiol valerate determination based on a modified carbon paste with iron tetrapyridinoporphyrazine, Analyst. 133 (2008) 1692–1699. https://doi.org/10.1039/b804462g.

[111] E. Tanrıkut, İ. Özcan, E. Sel, S. Köytepe, E.K. Savan, Simultaneous

Electrochemical Detection of Estradiol and Testosterone Using Nickel Ferrite Oxide Doped Mesoporous Carbon Nanocomposite Modified Sensor, J. Electrochem. Soc. 167 (2020) 087509. https://doi.org/10.1149/1945-7111/ab927f.

[112] R.F. Brocenschi, R.C. Rocha-Filho, B. Duran, G.M. Swain, The analysis of estrogenic compounds by flow injection analysis with amperometric detection using a boron-doped diamond electrode, Talanta. 126 (2014) 12–19. https://doi.org/10.1016/j.talanta.2014.02.047.

[113] Hashemnia, S.; Khayatzadeh, S.; Hashemnia, M. Journal of Solid State Electrochemistry 2012, 16, 473.

[114] K. Kor, K. Zarei, Development and characterization of an amperometric sensor for triclosan detection based on electropolymerized molecularly imprinted polymer, Microchem. J. 146 (2016) 181–187. https://doi.org/10.1016/j.microc.2008.11.007.

[115] F.C. Moraes, B. Rossi, M.C. Donatoni, K.T. de Oliveira, E.C. Pereira, Sensitive determination of 17β-estradiol in river water using a graphene based electrochemical sensor, Anal. Chim. Acta. 881 (2015) 37–43. https://doi.org/10.1016/j.aca.2015.04.043.

[116] Barde, M.P. and Barde, P.J., 2012. What should be used to express the variability of data: Standard deviation or standard error of mean? Perspectives in clinical research, 3(3), pp.113-116.

Chapter 4 Graphene-based Electrodes for Monitoring of Estradiol

4.1 Introduction

This chapter builds upon the previous chapter's application of carbon-based spherical shells to investigate the use of graphene-based materials to enhance SPE for measuring E2.

Graphene is an attractive material for various applications, including electrochemical sensors, due to its thermal, electronic, mechanical, and electrochemical properties [1–18]. Researchers have extensively studied these beneficial characteristics for their potential as electrode materials [1-18]. Various methods exist to produce graphene, with the desired size and quality tailored to specific applications. These include bottom-up synthesis techniques [19] and top-down exfoliation methods [18]. While the mechanical exfoliation technique offers graphene with favourable physical attributes, it struggles with scalability [19–21]. On the other hand, the chemical vapour deposition technique facilitates graphene formation on substrates like nickel through hydrocarbon thermal decomposition [22]. This technique is conducive to bulk graphene production. Moreover, through the thermal decomposition method, graphene can be produced epitaxially. Unlike chemical vapour deposition, it mandates temperatures exceeding 1000˚C. At this temperature, silicon sublimates, leaving behind carbon atoms that configure themselves into graphene [23]. Several other techniques, with various modifications, are documented in existing literature [24–26]. Graphene's diverse forms are applicable in electrochemical sensor fabrication [27,28]. Table 4.1

highlights the deployment of graphene-based electrodes in E2 detection and the corresponding detection techniques. Only Barton et al. [29] reported using SPE as an electrode. However, it is worth mentioning that the fabrication steps are intricate; primarily, graphene is produced through chemical exfoliation.

Table 4.1 Some recent literature on E2 determination based on graphene-based materials.

Modifier/Electrode	Detection technique	Linear range (M)	Limit of detection(M)	Ref.
Graphene quantum dots with poly-sulfosalicylic (PSSA/GO)/GCE	DPV	1×10^{-6} - 6×10^{-6}	2.3×10^{-10}	[30]
Reduced graphene oxide/molecularly imprinted polymer/GCE	DPV	1.6×10^{-4} - 1.5×10^{-5}	2.7×10^{-8}	[31]
Reduced graphene oxide/di-hexadecyl phosphate/GCE	LSV	4×10^{-4} - 1×10^{-5}	7.7×10^{-8}	[32]
Fe_3O_4 nanobeads/graphene-based molecularly imprinted polymer/GCE	DPV	5×10^{-5} - 1×10^{-5}	8.19×10^{-10}	[33]
Gold nanoparticle/ graphene/Molecularly Imprinted Polymer/GCE	DPV	3×10^{-6} - 1×10^{-6}	1×10^{-9}	[34]
Ultrasonicated exfoliated graphene in N-methyl-2-pyrrolidone/GCE	DPV	1×10^{-5} - 1.5×10^{-5}	4.9×10^{-9}	[35]
Reduced graphene oxide-platinum nanoparticles/ MIP/GCE	DPV	4×10^{-6} - 6×10^{-8}	2×10^{-9}	[36]
Reduced graphene oxide on metallic Cu (II)-meso-tetra(thien-2-yl) porphyrin/GCE	DPV	1×10^{-4} - 1×10^{-6}	5.3 nM	[37]
Cysteamine/gold nanoparticle/ fumed silica/ graphene nanoribbon/GCE	DPV	1×10^{-4} - 5×10^{-6}	7.4×10^{-9}	[38]

Aptamer- reduced graphene oxide/GCE	EIS	1.2×10^{-8} - 2.3×10^{-7}	5×10^{-15}	[39]
Anti-E1/ Polyaniline (PANI)/Graphene/SPE	EIS	3.7×10^{-13} - 7.6×10^{-10}	7.2×10^{-12}	[29]

Graphene integration (and its derivatives) has been reported to modify electrodes to improve their sensitivity for determining E2 via modification on different electrodes.

A common strategy for designing these devices involves incorporating graphene or its reduced variant onto the sensor surface via drop coating. Most graphene-based sensors mentioned in Table 4.1 offer insights from recent studies on E2 determination using graphene. Nevertheless, a limited number of studies focus on the screen-printed electrode. Most revolve around modifying glassy carbon electrodes; a handful address other estrogens besides E2. Moreover, the flexibility to customize conductive inks, substrates, and design/geometry renders SPEs exceptionally adaptable for various analytical tasks. They can be readily modified by embedding elements like enzymes, aptamers, metal nanoparticles, and conductive polymers directly into the ink before screen-printing, as showcased by Pasakon et al. and Wang et al. [40,41]. However, the synergy between graphene and screen-printed electrodes, which serve as a detection tool for E2, remains an underexplored domain, as few studies have been conducted. This chapter investigates using multifaceted graphene material [16] for E2 sensors. Notably, studies like that of Barton et al. [29] have illustrated E2 measurement using a graphene SPE modified with polyaniline, termed a polyaniline/graphene/SPE. There has been some exploration for other estrogens,

such as EE2 and E3, using graphene material-based screen-printed sensors. It is an exciting aspect of sensor design using the ‘Swiss Army’ graphene material [16] to be investigated in this study.

For instance, Santos et al. introduced screen-printed electrodes (SPE) modified with graphene, graphene quantum dots (GQDs), and molecularly imprinted polymers coated with magnetic nanoparticles (mag@MIP) for ethinylestradiol detection. The authors functionalized commercially available graphene with GQDs, synthesized from citric acid. The resulting mag@MIP-GQDs-FG-NF/SPE sensor exhibited a linear response ranging from 1 x 10^{-8} M to 2.5 x 10^{-6} M and a 2.6 x 10^{-9} M detection threshold for EE2 [42]. Zhao et al. presented a design involving a screen-printed carbon electrode (SPE) modified with reduced graphene oxide (rGO), silver nanoparticles (AgNPs), and silver nanowires (AgNWs) targeting E2 detection [43]. The RGO/AgNWs/AgNPs/SPE sensor showcased enhanced performance for the electroactive subjects under examination.

Nevertheless, the studies above entail intricate and prolonged design and fabrication processes for electrode composites [44]. Furthermore, specific synthesis methods demand extended completion times and the need to eliminate unexfoliated material [45]. When considering off-the-shelf SPEs for sensor applications, detailed specifications from manufacturers are often elusive. Contrasting the chemical synthesis of graphene, a groundbreaking method to generate graphene in a single step, known as laser scribe/induce graphene production, has recently emerged.

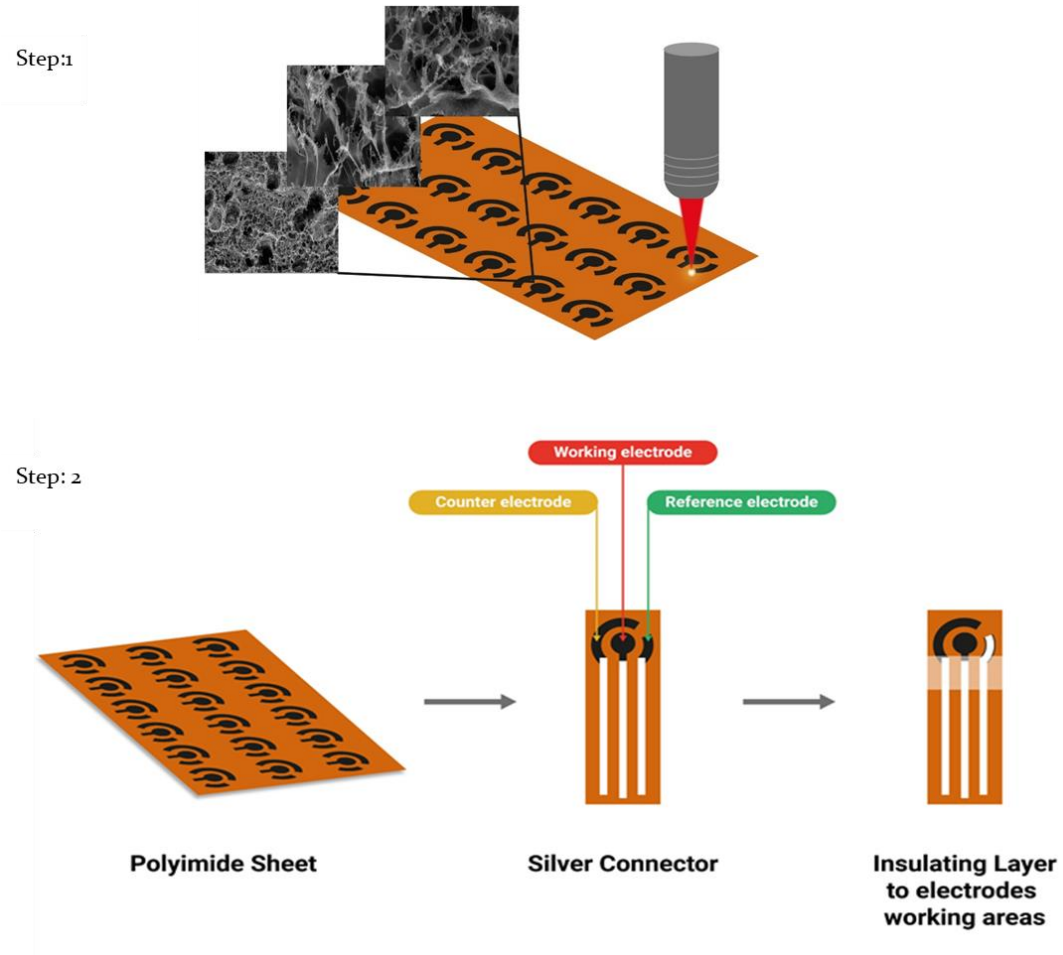

Figure 4.1. A schematic fabrication process of the laser-scribed graphene

Laser inscription or induction methods produce what is termed laser-induced graphene (LIG) or laser-scribed graphene (LSG) sensors [46]. Laser-scribed graphene is anticipated to revolutionize the next generation of disposable graphene electrochemical sensors [47]. This method involves the irradiation of a polymeric precursor, polyimide, with a laser, triggering both photochemical and thermal conversion into graphene, as shown in Figure 4.1 (step 1) and followed by screen-printing silver ink as the connectors for testing (step 2) [48,49]. This technique's utility is frequently cited in current electrochemical (bio) sensor research [50–53]. It is hailed as an efficient and direct strategy for creating a

graphene structure that amplifies the performance of electrochemical sensors [54].

Another rapid graphene synthesis approach involves the exfoliation of graphite electrodes using an electrical potential. Here, when voltage is applied, solvated ions from the electrolyte are inserted between layers of the graphite working electrode. This weakens the interlayer bonds, causing individual flakes to separate and disperse into the electrolyte [55,56]. Parvez et al. delved into the effects of various electrolytes on graphite exfoliation [56]. Meanwhile, Ambrosi et al. found that oxygenated graphene can be produced using $LiClO_4$ as an electrolyte in the electrochemical creation of graphene [57].

Electrolytic exfoliation draws attention for its efficiency, scalability, and single-step nature. However, limited studies address the application of electrolytic methods in exfoliating graphene for sensor technologies. This work also presents the utilisation of graphene-based screen-printed electrodes with electrolytic exfoliated graphene. It is an affordable and rapid method, eliminating the need for further purification or advanced facilities. This study uses amperometry to focus on graphene-ink, laser-scribed graphene, and EEFGH-modified SPE for E2 detection.

This chapter delves into the amperometric detection of E2 via direct electrochemical oxidation on graphene-based material electrodes. Specifically, it contrasts three methods: graphene-ink SPE, laser-scribed graphene, and EEFGH-modified SPE. The methods harness the acclaimed unique properties of graphene, negating any additional alterations [17,47]. Transitioning the electrochemical sensor from the laboratory to the field involves crafting an

independent electrode that leverages the merits of carbon-based nanomaterials, ready for mass production [47].

4.2 Materials

All the reagents and chemicals used were of analytical grade and used as received. In addition, 17β-Estradiol (E2), phosphate buffer tablets, sodium hydroxide (NaOH), potassium ferricyanide [$K_3Fe(CN)_6$], potassium ferrocyanide [$K_4Fe(CN)_6$], potassium chloride (KCl), and polystyrene sulfonate (PSS) were purchased from Merck (Gillingham, UK). Commercial graphite rods were employed as the precursor for the synthesis of electrolytic exfoliated graphene (EEFGH), Graphene SPEs (GHPSPE), and screen-printed electrodes were provided by Palintest Limited (Newcastle, UK). In contrast, 3D graphene foam SPEs (3D-GFSPE) were purchased from Integrated Graphene Ltd (Stirling, Scotland), consisting of a working electrode (area = 0.07 cm^2), graphite counter electrode and reference electrode. The electrodes used in this chapter have different characteristics in terms of designs and dimensions.

4.3 Methods

4.3.1 Measurements and Instrumentation

Electrochemical measurement experiments were conducted using a PalmSens Em-Stat3 Potentiostat (PalmSens BV Houten, the Netherlands) with data acquisition using PSTrace 5.8. Cyclic voltammetry (CV) and amperometry were carried out with a typical three-electrode system consisting of a working electrode (WE), a carbon counter electrode (CE) and a reference electrode (RE). Commercial Graphite Rods were employed as the precursor for graphene synthesis (EEFGH) from Findel Education Limited (UK). Graphene SPEs

(GHPSPE) were obtained from Palintest Limited (Gateshead, UK) and designed using graphene ink (Product Ink: C2171023D1; Gwent Electronic Materials Ltd, UK) and bare SPCE. In contrast, 3D graphene foam SPEs (3D-GFSPE) were purchased from Integrated Graphene (Stirling, Scotland).

Electrode performance was assessed using cyclic voltammetry. This evaluation utilized a redox probe solution comprising 5 mM equimolar $K_3Fe(CN)_6/K_4Fe(CN)_6$. The electroactive regions of these electrodes were determined using the Randles-Sevcik equation. Measurements factored in various scan rates within the redox solution, scanned over the voltage range of -0.3 to 0.6 V. For amperometric evaluations, a standard E2 solution was introduced at a +0.65 V constant potential post the electrochemical oxidation phase undertaken by CV scanning between 0 and 0.8 V in PBS (0.1M pH 7.0). All tests were executed in a 30 mL cell at ambient temperature, and each measurement was repeated thrice for three distinct electrodes.

4.3.2 Preparation of Materials

The production of graphene commonly adopted involves mechanical exfoliation or chemical vapour deposition. Nevertheless, both procedures can be challenging, from requiring specialised equipment to cleaning rooms, which will be challenging in a laboratory not specifically designed as a material science facility. Graphene can be generated by electrolysis, which involves immersing graphite electrodes into an electrolytic solution while applying a voltage difference between two graphite electrodes. This results in the oxidation of the graphite that ultimately produces graphene for a wide range of applications, making this method both uncomplicated and scalable.

4.3.2.1 Synthesis of Graphene by Electrolytic Exfoliation

The synthesis of graphene via electrochemical exfoliation was carried out as described in previous reports [40,58], with minor adjustments. Specifically, graphite rods, acting as anode and cathode, were placed in a reactor cell containing polystyrene sulfonate (PSS) as the electrolyte. A steady potential of 8 V was applied across these electrodes for 24 hours. Over time, the anode gradually eroded, turning the electrolyte a dark hue and forming sediment within the reactor. The final graphene product was then separated by centrifuging at 3,220 × g (4000 rpm).

4.3.2.2 Electrode Modification with Electrochemically Exfoliated Graphene

EEFGH was first redispersed for electrode fabrication in a mixture of deionised water and ethanol (9:1 v/v) to achieve a final concentration of 0.5 mg/mL. The suspension was then ultrasonicated for three hours to ensure optimal graphene dispersion. Subsequently, varying volumes (0.3, 0.5, 0.7, or 1.0 µL) of this dispersion were drop-cast onto the SPE working electrode and were left to air-dry at ambient temperature, yielding an electrolytic exfoliated graphene-modified SPE (EEFGHSPE).

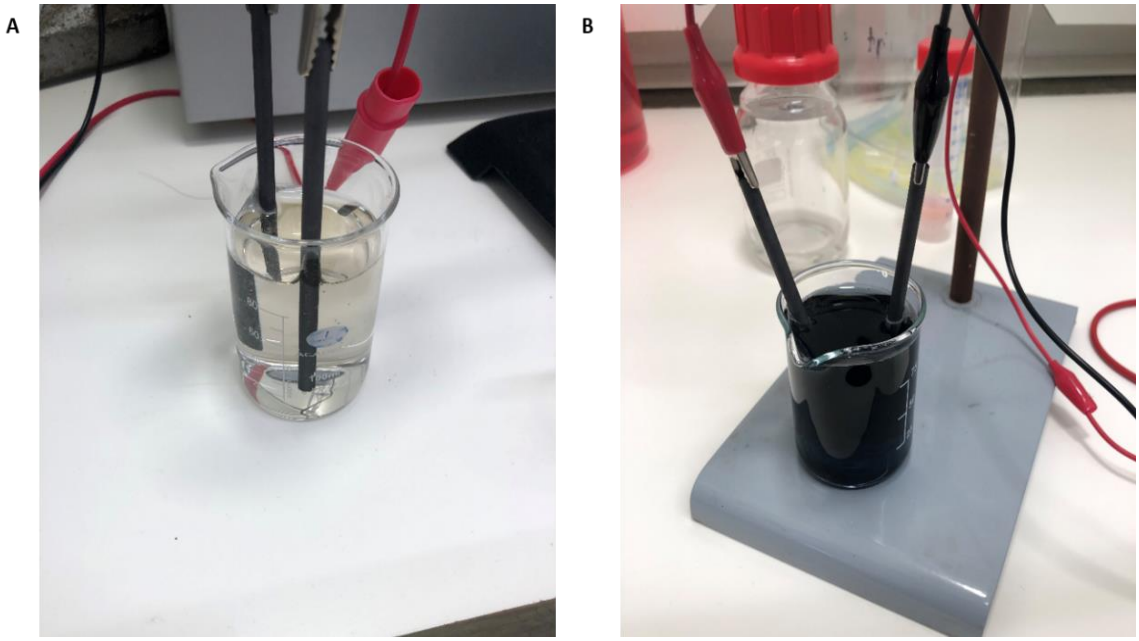

Figure 4.2 Photograph of (A) Graphite rods in PSS electrolyte at the beginning of the Electrochemical exfoliation and (B) after the Electrochemical exfoliation process

4.3.3 Characterisation of the Modified Electrode

4.3.3.1 Scanning Electron Microscopy (SEM)

The morphology of electrolytic exfoliated graphene (EEFGH), Graphene SPEs (GHPSPE), and 3D graphene foam SPEs (3D-GFSPE) were characterised using SEM measurements carried out as described in Chapter 3.

4.3.3.2 Dynamic Light Scattering (DLS)

DLS measurements for electrolytic exfoliated graphene (EEFGH) were carried out as described in Chapter 3.

4.3.3.3 Transmission Electron Microscopy

TEM measurements for electrolytic exfoliated graphene (EEFGH) were carried out as described in Chapter 3.

4.3.4 Electrochemical Characterisation.

In Chapter 3, results from cyclic voltammetry (CV) of 5 mM potassium ferricyanide at bare SPEs and CSSM/SPEs are represented in Figure 3.10 (previously in Chapter 3), have shown that the electrochemical response of $[Fe(CN)6\ ]^{3-/4-}$ redox at the electrode surface is based on surface chemical properties. Thus, the electrochemical measurements and behaviour of the various graphene-based electrodes and the modified electrodes, electrolytic exfoliated graphene (EEFGH), graphene SPEs (GHPSPE), and 3D graphene foam SPEs (3D-GFSPE) were studied by cyclic voltammetry at various scan rates in a solution of 5 mM $K_3Fe(CN)_6/K_4Fe(CN)_6$ and 0.1 M KCl as the supporting electrolyte. The cyclic voltammetry measurements were carried out in 0.1 M phosphate buffer solution pH 7.0 over a potential range of 0 V to +0.8 V at different scan rates. The amperometric measurements were conducted by inserting the various electrodes SPE in 30 mL containing 0.1 M PBS (pH 7.0) under magnetic stirring.

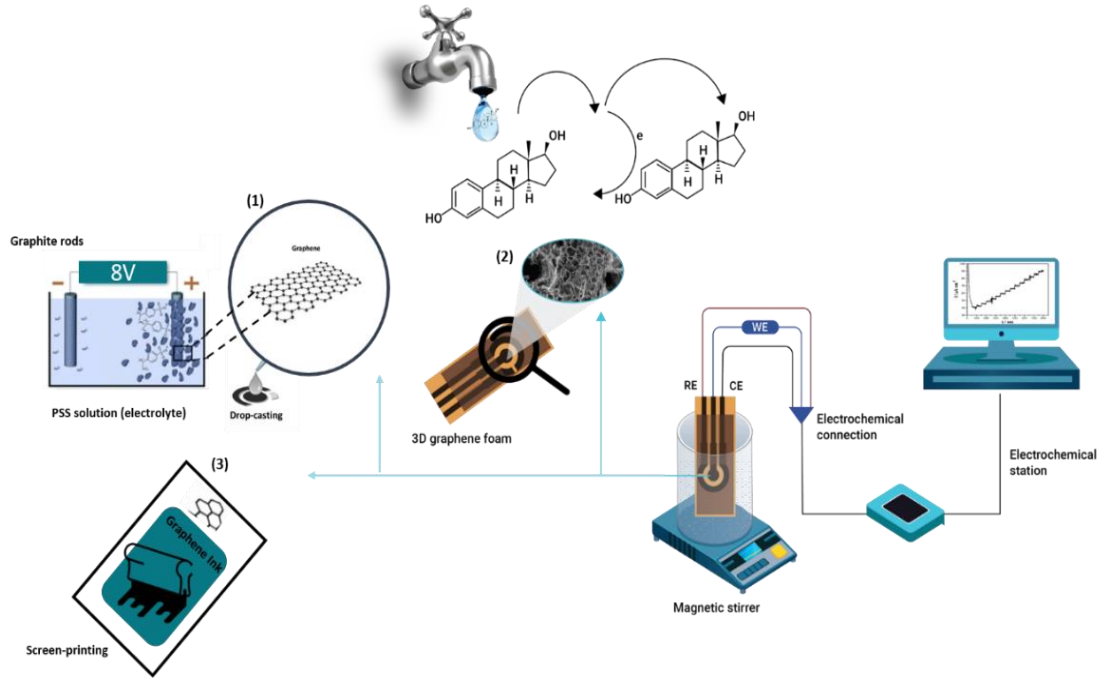

Figure 4.3 Schematic representation of the graphene-based screen-printed sensors framework. Legend: 1 electrolytically exfoliated graphene electrode; 2 Laser-scribed graphene electrode, and 3 graphene ink-based electrode.

4.4 Results and Discussion

The experimental setup for the electrochemical exfoliation of graphite was performed according to the protocol by Karuwan et al. [40,41] and illustrated in Figure 4.2. The mechanism of graphite exfoliation involves immersion of graphite rods, which are used as working and counter electrodes serving points for the intercalation of anions and cations within an electrolyte of polystyrene sulfonate. Common anions such as sulfate (SO_4^{2-}) were utilised in this study. A positive voltage (8 V) was applied to a graphite electrode; the graphite started to expand, dissociate, and move into the electrolyte solution, as shown (Figure 4.2 A and B). The applied voltage led to the oxidation of water, from which hydroxyl (OH·) and oxygen radicals (O·) are produced. Oxidation or hydroxylation by radicals

produced at edge sites and grain boundaries of the graphite opens up the graphite's structure; this allows the intercalation by anionic SO_4^{2-} [56,57]. This process leads to the release of gaseous SO_2 and anion depolarisation and causes expansion of the interlayer distance of graphite [55,59]. The voltage was kept constant for one hour to complete the exfoliation process. Furthermore, the obtained exfoliated graphitic sediments were collected by centrifugation and cleaned with deionised water.

4.4.1 Morphological Characterisation

SEM imaging is essential to reveal the surface morphology of the graphene-based electrodes. Figure 4.4 shows the SEM image of bare SPE taken at a magnification of 2500x and clearly shows the presence of binder on the surface, a common feature of SPE electrodes [60]. SEM images of the 3D-GFSPE graphene foam SPE surface at different magnifications of 280 and 25,000x are shown in Figure 4.5 and Figure 4.6, showing the formation of a porous network structure with extensive edge plane content. Furthermore, the SEM images revealed the nature of the graphene surface as a non-flaky-like structure. In addition, it can be observed that the 3D nature of the graphene foam pores was visible (Figure 4.6). Figure 4.7 shows the EDS spectrum; predominantly, C and O elements are evident, which is expected from these carbon-based materials. Figure 4.8 depicts the SEM image of the EEFGHP/SPE surface at magnifications of 1000x. Figure 4.8 of EEFGHSPE has coarse particles, which are not as prominent as those observed in the 3D-GFSPE image, confirming graphene formation. The EDS elemental analysis is shown in Figure 4.9. The EDS spectrum of the EEGHPSPE shows C, O, Ti, Si, and Cl elements. Ti, Si, and Cl

indicate the possibility of other impurities in the graphite rod composition since no further modification step in the synthesis will introduce other materials (section 4.3.3).

On top of that, the EEFGHSPE revealed a 26.84 weight % C, 71.73 weight % of O, 0.03 weight % of S, 0.05 weight % of Si, 1.14 weight % of Cl and 0.21 weight % of Ti (figure 4.9). An image of a graphene screen-printed electrode (GHSPE) is shown in Figure 4.10. with the noticeable flake-like surface. Moreover, the EDS in Figure 4.11 revealed that the spectrum for GHPSPE contains C, O, Si, and Au elements. Gold (Au) arises from the preparation step of SEM analysis.

3D-GFSPE appears to have a coarser particle grain surface than EEFGHSPE and GHPSPE. Figure 4.10 morphology looks similar to the bare SPE, likely due to the remnant binder utilised in the electrode ink formulation [60]. A binder's presence can impact an analyte's behaviour on the electrode surface, proving vital or otherwise in electroanalysis [61]. No other impurities were determinable on the SPE surface using this approach. Overall, the surface morphology of the 3D-GFSPE has a higher roughness, as seen from the SEM images, due to the non-agglomeration of graphene particles, unlike the GHPSPE fabricated with ink paste. Noteworthy, the Au was from the preparation of SEM samples; thus, its appearance on the surface is sparse. The morphology of both graphene materials is majorly different, as seen in their other electroactive surface areas.

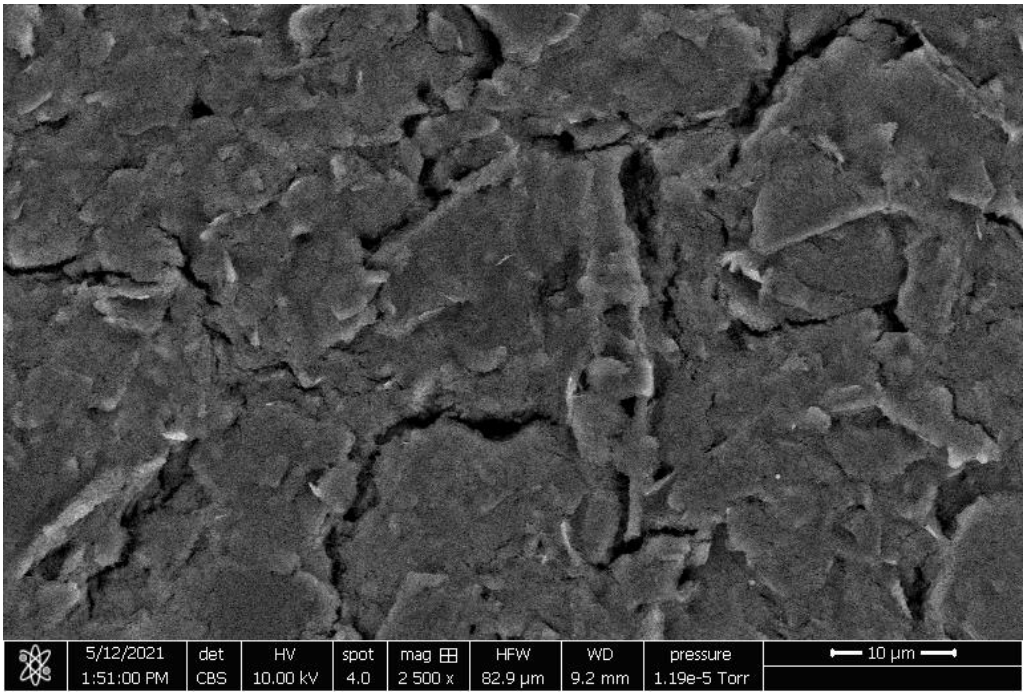

Figure 4.4. SEM image bare SPE surface at 10 kV as accelerating voltage at 2,500× magnifications.

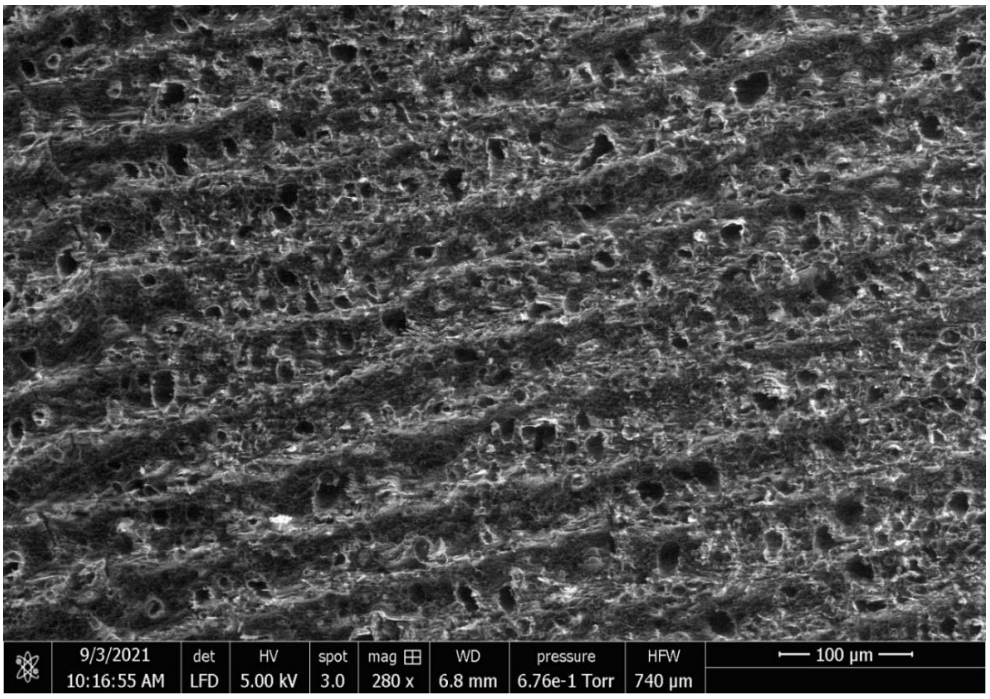

Figure 4.5 SEM images of the 3D-GFSPE surface at 10 kV as accelerating voltage at 280× magnifications.

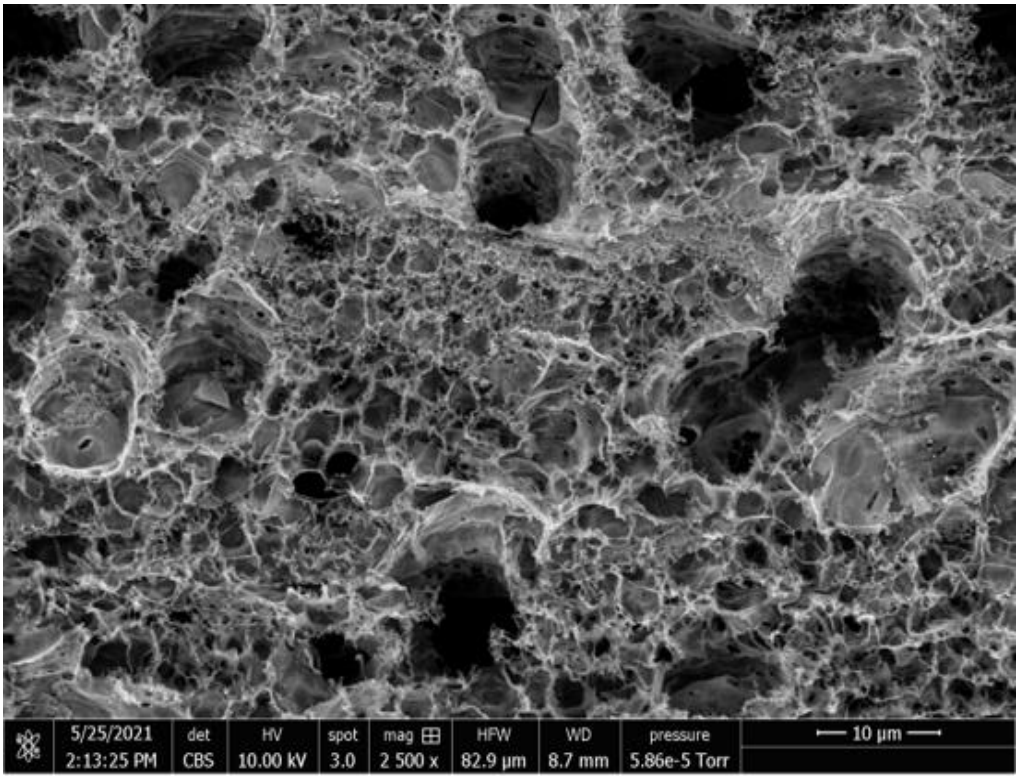

Figure 4.6. SEM images of the 3D-GFSPE surface at 10 kV as accelerating voltage at 2,500× magnifications.

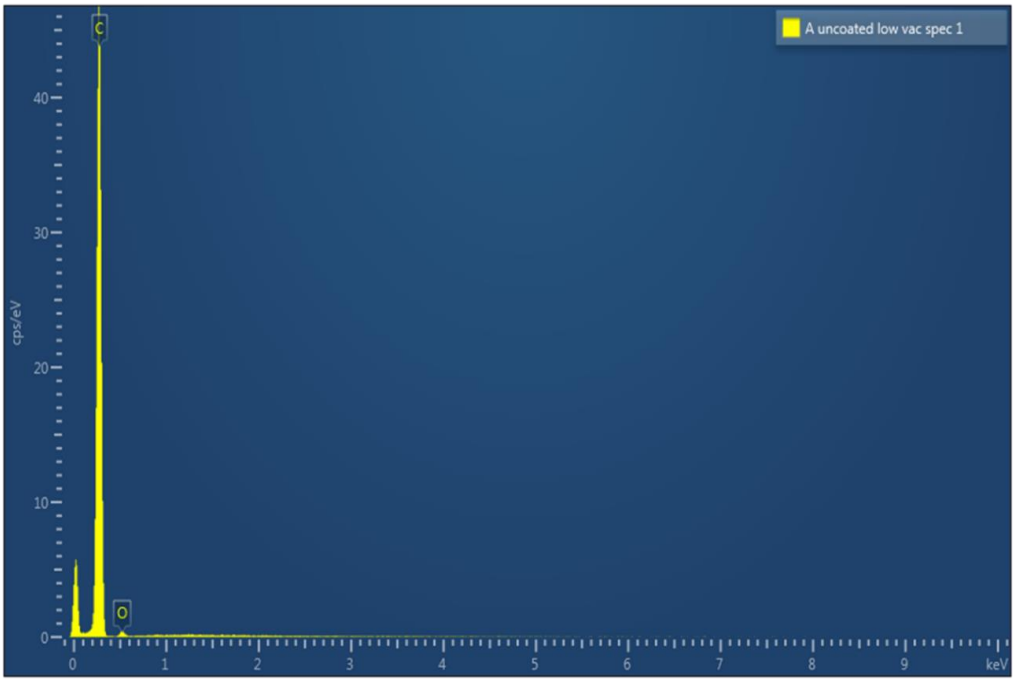

Figure 4.7. EDS spectrum of the 3D-GFSPE showing C and O elements.

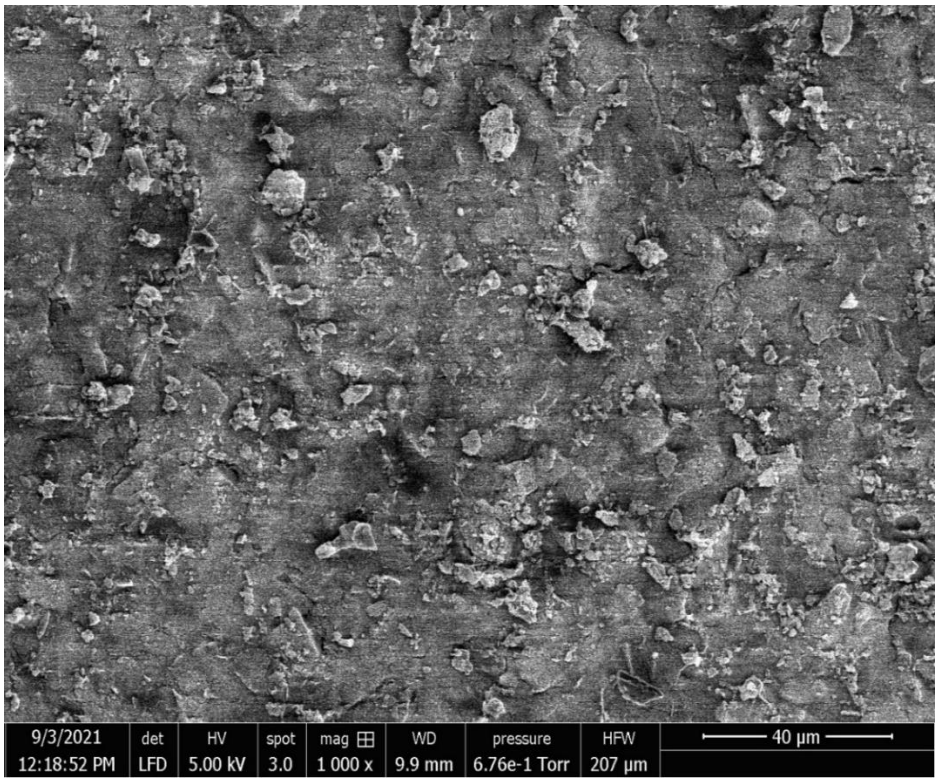

Figure 4.8. SEM images of the EEFGHP/SPE surface at 5.0 kV as accelerating voltage at magnifications of 1000x.

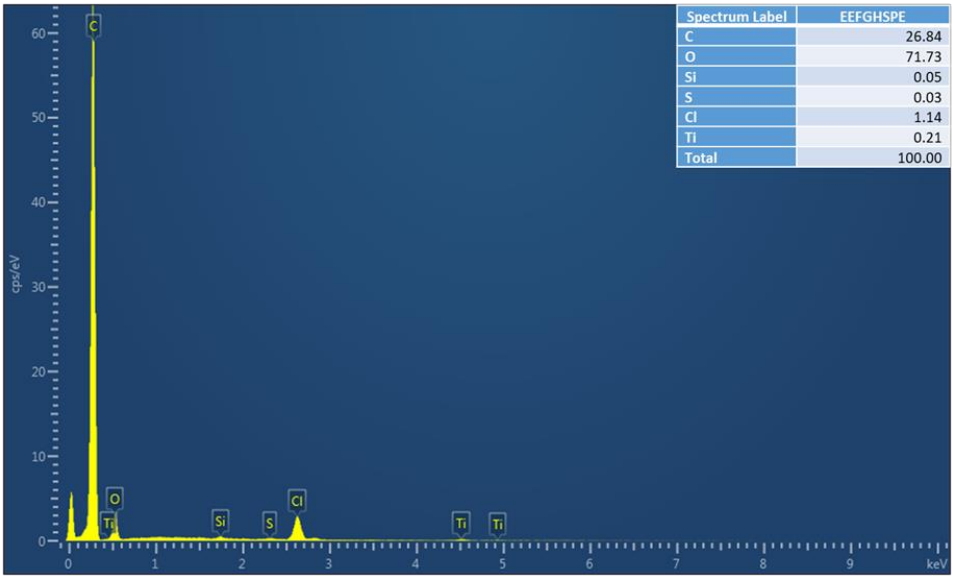

Figure 4.9. EDS spectrum of the EEGHPSPE showing C, O, Ti, Si and Cl elements.

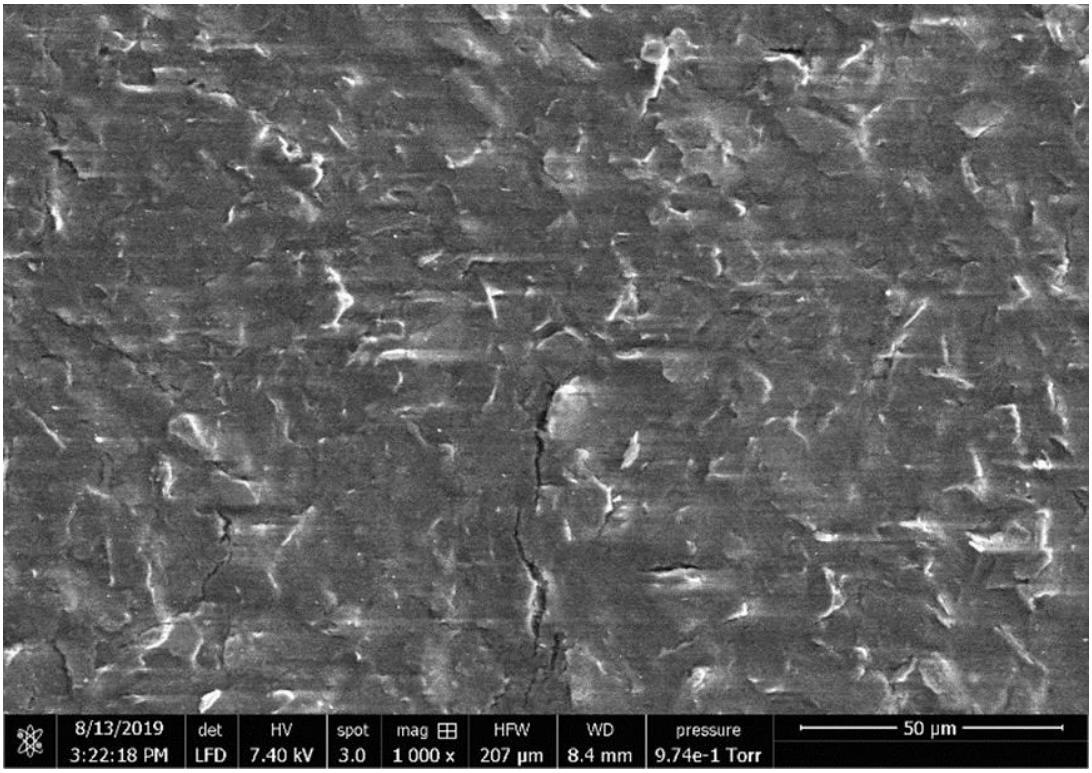

Figure 4.10. SEM images of the GHSPE surface at 7.4 kV as accelerating voltage at magnifications of 1000x.

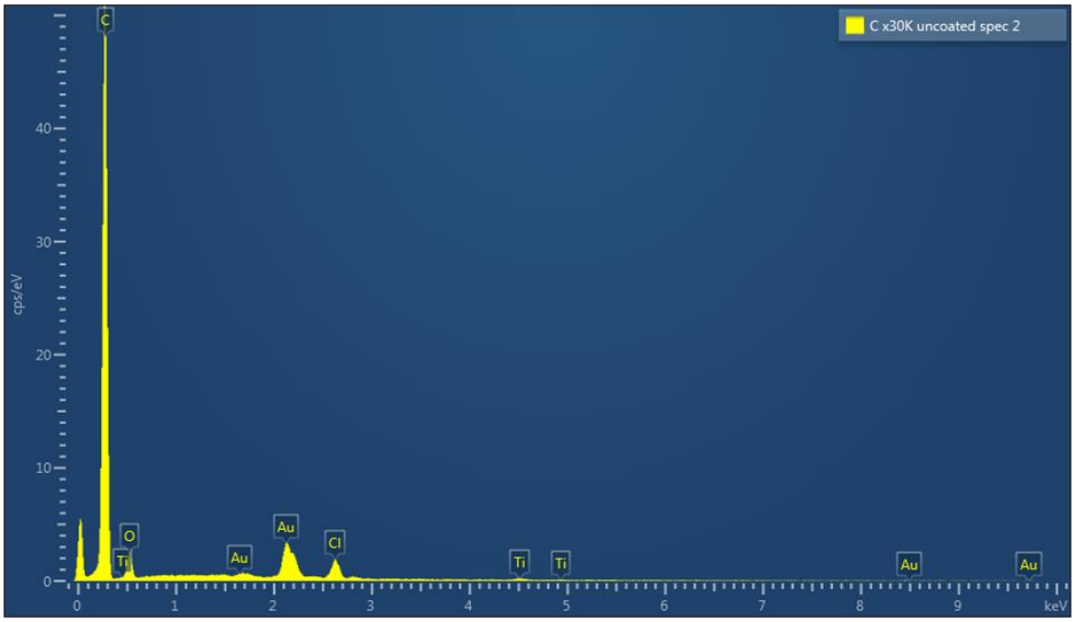

Figure 4.11. EDS spectrum of the graphene GHPSPE showing C, O, Si, Ti, and Au elements.

Dynamic light scattering was used to analyse the electrochemically exfoliated graphene prepared by applying a constant potential of 8 V, recording a particle with an average size of 398 nm. EEFGH has a polydispersity index (PdI), which measures the width molecular weight distribution of 0.77 and 917 z-average for the EEFGH (Figure 4.12A). From the result, the particles are very polydisperse with large or sedimenting particles. Also, it is impossible to observe individual graphene flakes using DLS. In contrast, Kirchner et al. reported an average size of 363 nm with a PdI = 0.25 [45], similar to our result. The TEM image indicates transparency with a dark area showing a thick stacking structure of several graphene layers (Figure 4.12B).

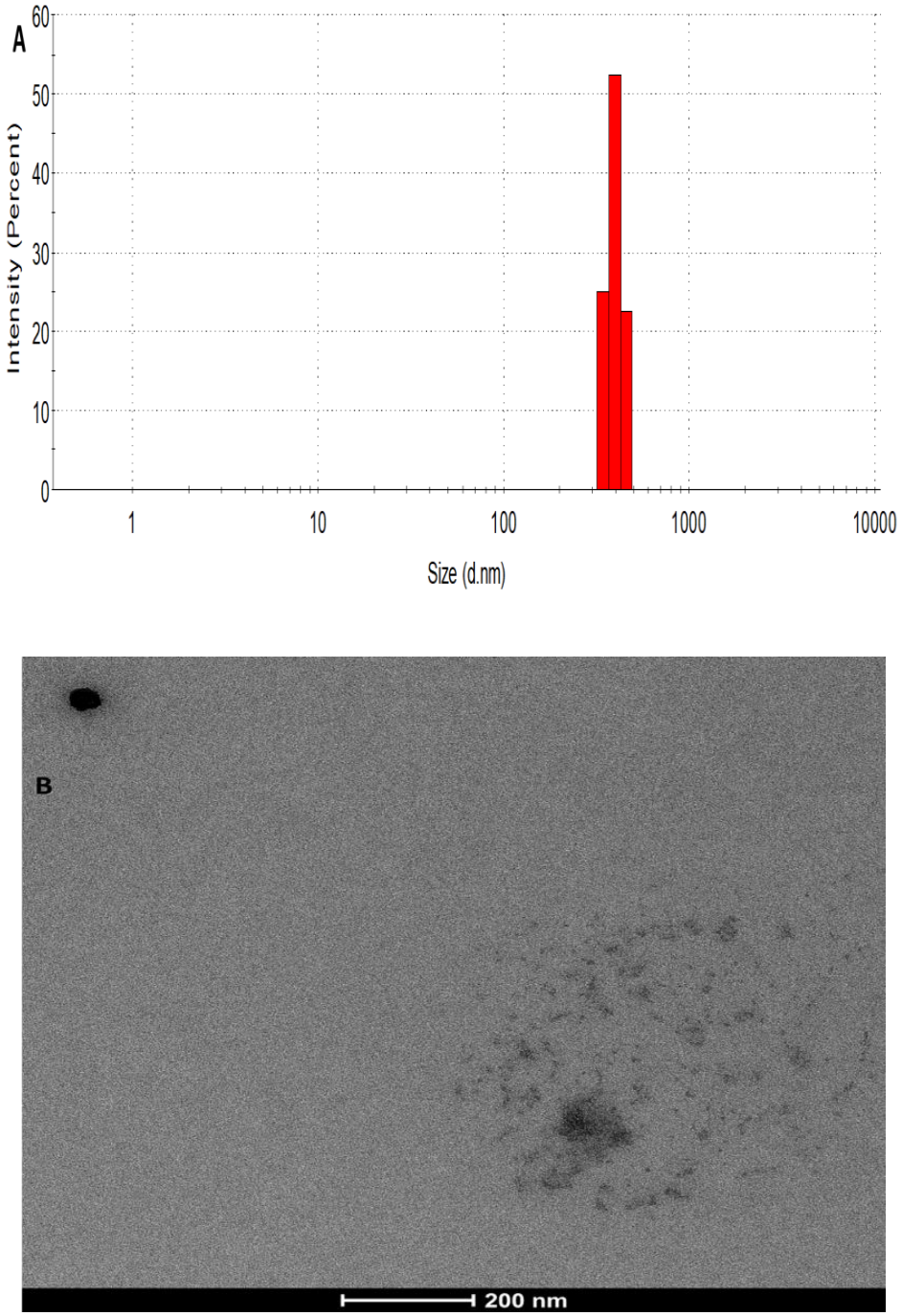

Figure 4.12. A) Intensity weighted particle size distribution for EEFGHP (red, 0.01 mg mL^{-1}) measured by dynamic light scattering of the graphene dispersions in a water-methanol mixture (9:1) v/v. B) TEM image of EEFGH.

4.4.2 Electrochemical Properties

The electroactivity of each electrode was determined from cyclic voltammetry in the presence of 5 mM potassium ferricyanide redox marker $K_3[Fe(CN)_6]$), inner-sphere redox species that is known to be sensitive to surface oxides [62] at various scan rates. The CVs revealed the behaviour of the SPE surfaces. Well-defined peaks for the oxidation and reduction of $[Fe(CN)_6]^{-3/4-}$ were obtained in Figure 4.13 at the 3D-GFSPE, Figure 4.16 GHPSPE and Figure 4.18 EEFGHSPE for a 5 mM $[Fe(CN)_6]^{-3/4-}$ solution in 0.1 M KCl. Figure 4.14 shows the plots of the peak current vs square root of scan rate ($u^{1/2}$) (25 - 250 $mV \cdot s^{-1}$) for both the anodic peak current (Ip_a) and cathodic peak current (Ip_c) of 3D-GFSPE.

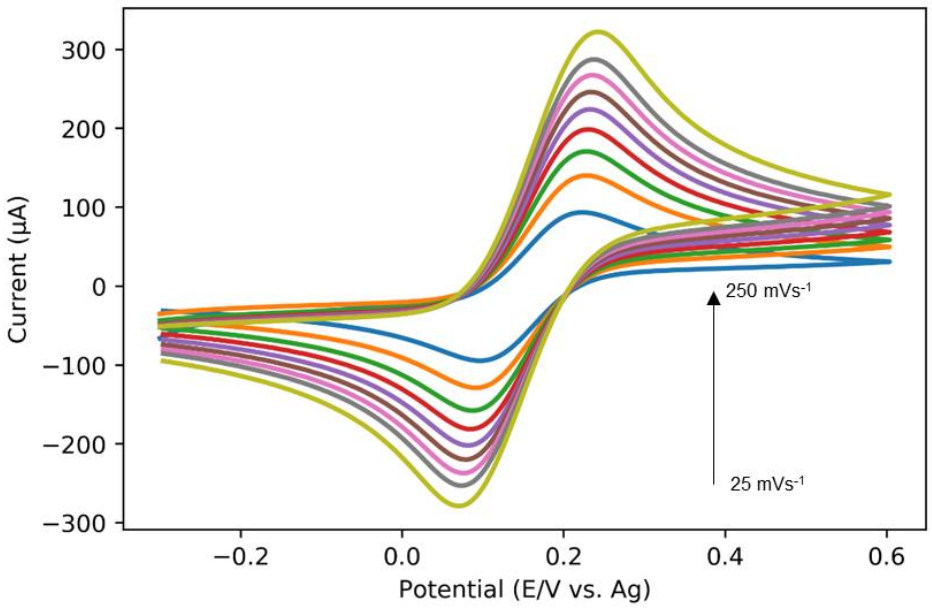

Figure 4.13. Cyclic voltammograms of the 3D-GFSPE in 5 mM $[Fe(CN)_6]^{-3/4-}$ 0.1 M KCl at potential scan rates (25 - 250 mVs^{-1}).

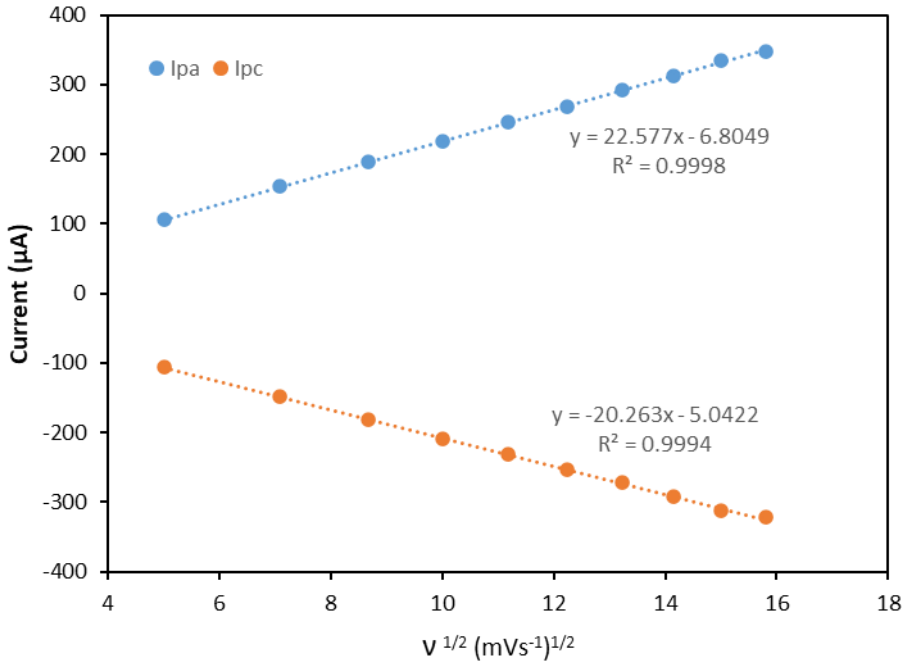

Figure 4.14. Plot of 3D-GFSPE Ipa and Ipc versus square root of scan rate ($V^{1/2}$) at potential scan rates (25 - 250 mVs^{-1}).

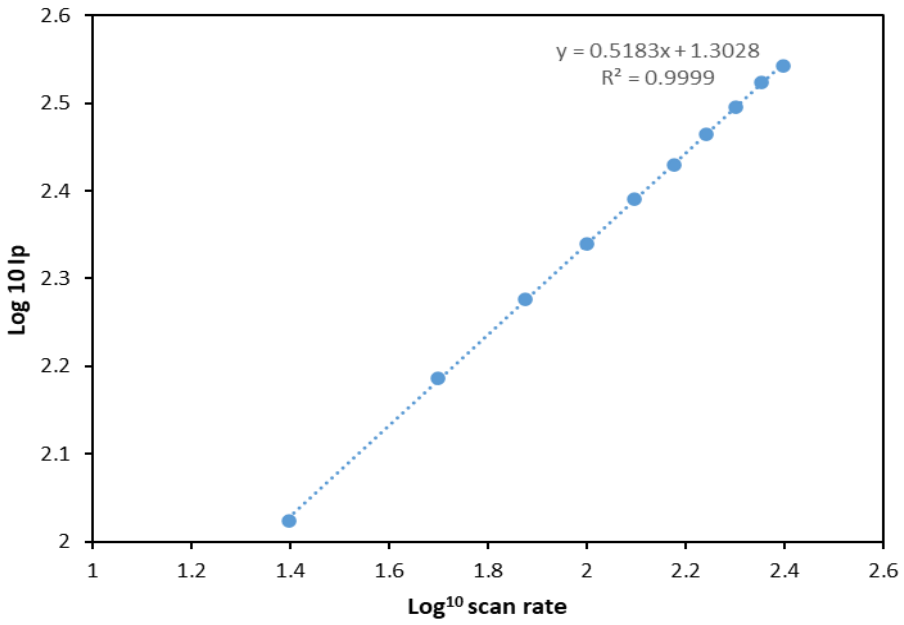

Figure 4.15 Plot of log10 of peak current vs log10 of scan rate of 3D-GFSPE.

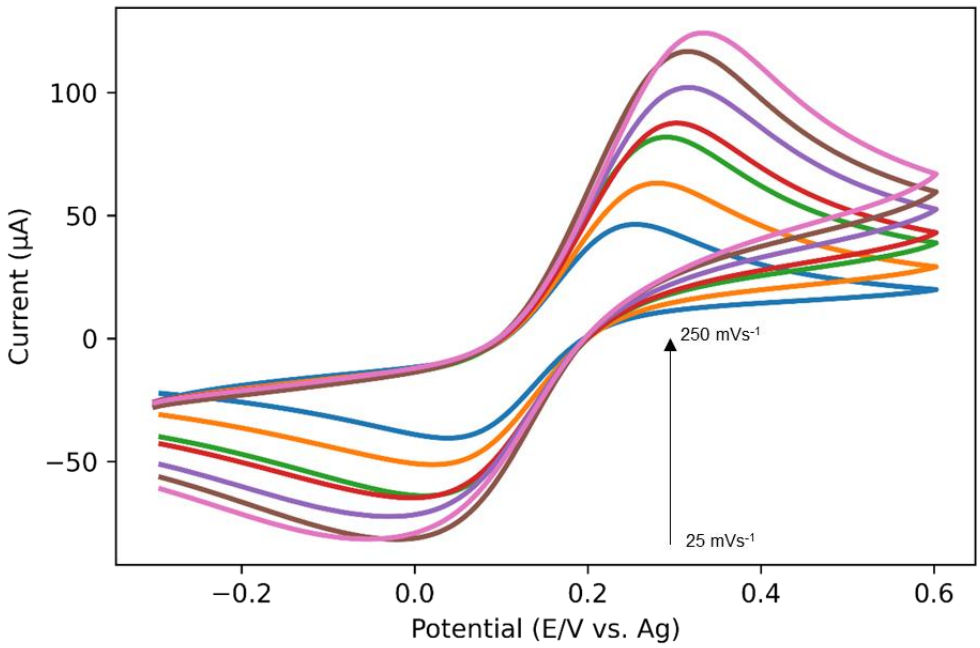

Figure 4.16. Cyclic voltammograms of the GHSPE in 5 mM $[Fe(CN)_6]^{-3/4-}$ in 0.1 M KCl at potential scan rates (25 - 250 mVs^{-1}) with poor reversibility.

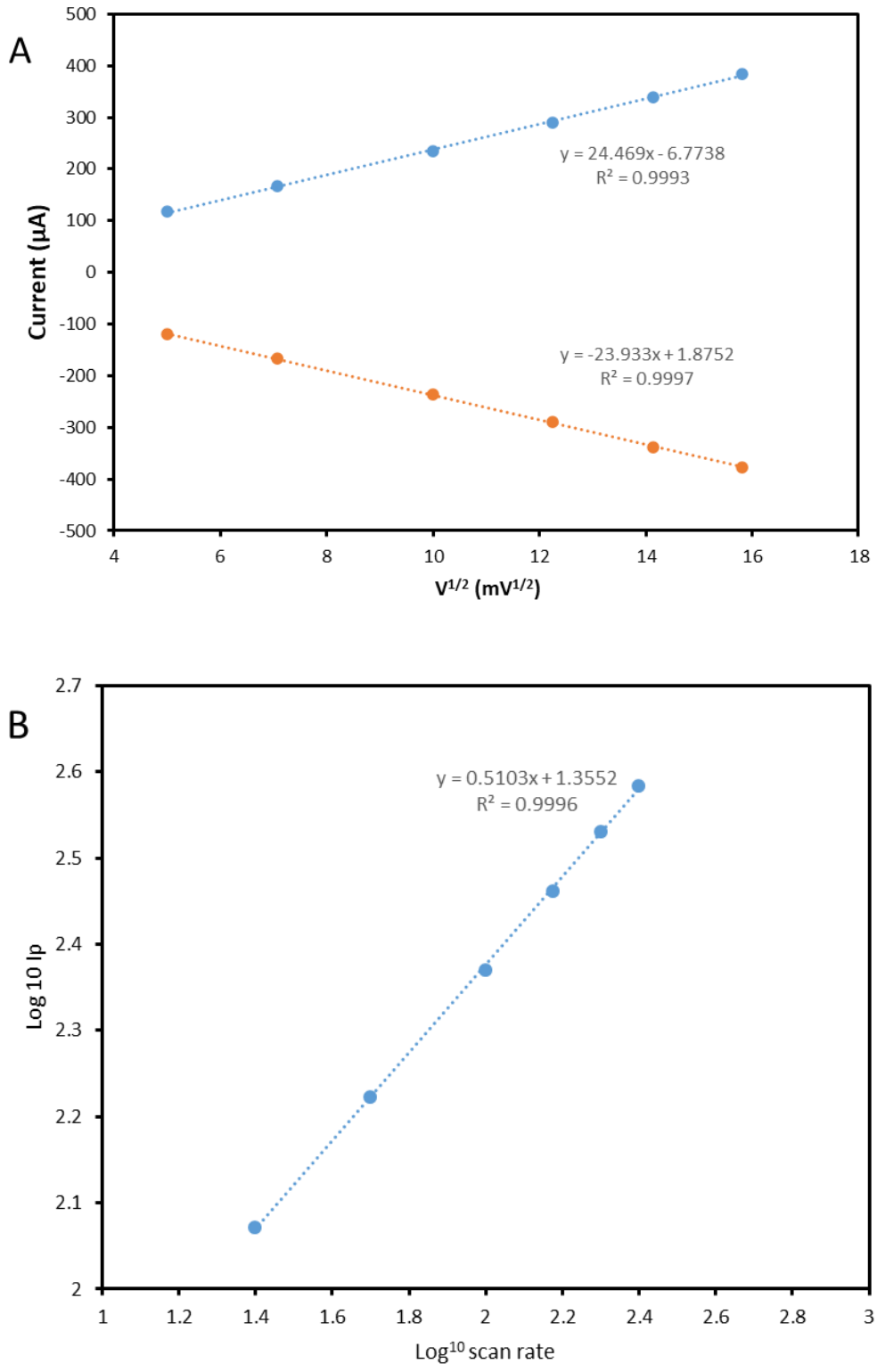

Figure 4.17. A) Cyclic voltammograms of the Plot of GHSPE Ipa and Ipc versus square root of scan rate (υ $^{1/2}$) at potential scan rates (25 - 250 mVs^{-1}). B). Plot of log10 of peak current vs log10 of scan rate.

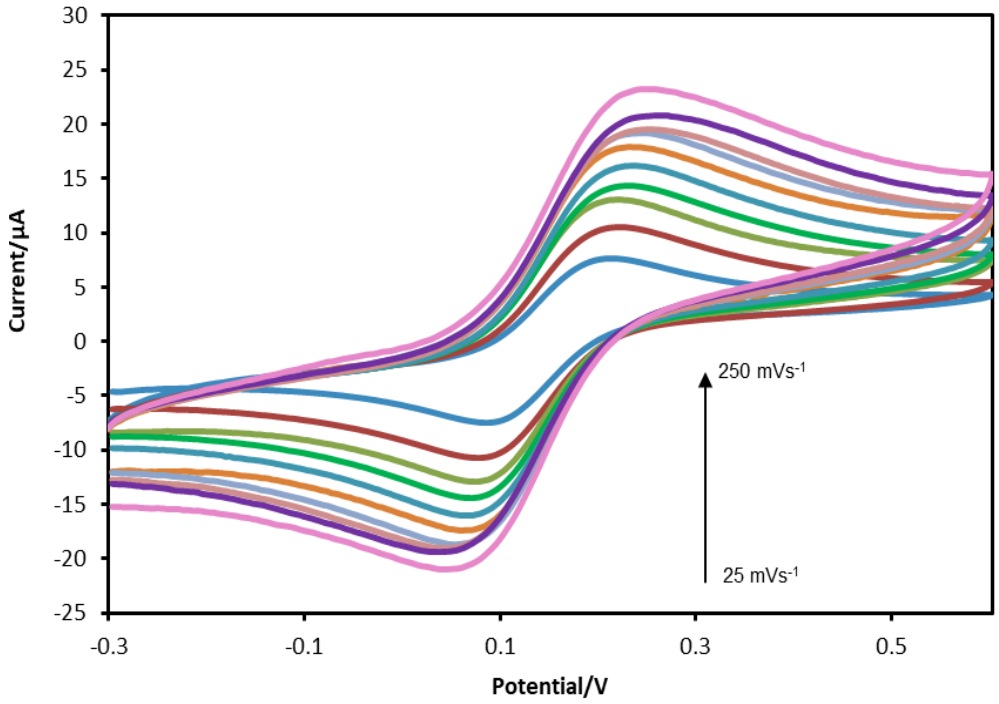

Figure 4.18. Cyclic voltammograms of the EEFGHSPE in 5 mM $[Fe(CN)_6]^{-3/4-}$ in 0.1 M KCl at potential scan rates (25 - 250 mVs^{-1}).

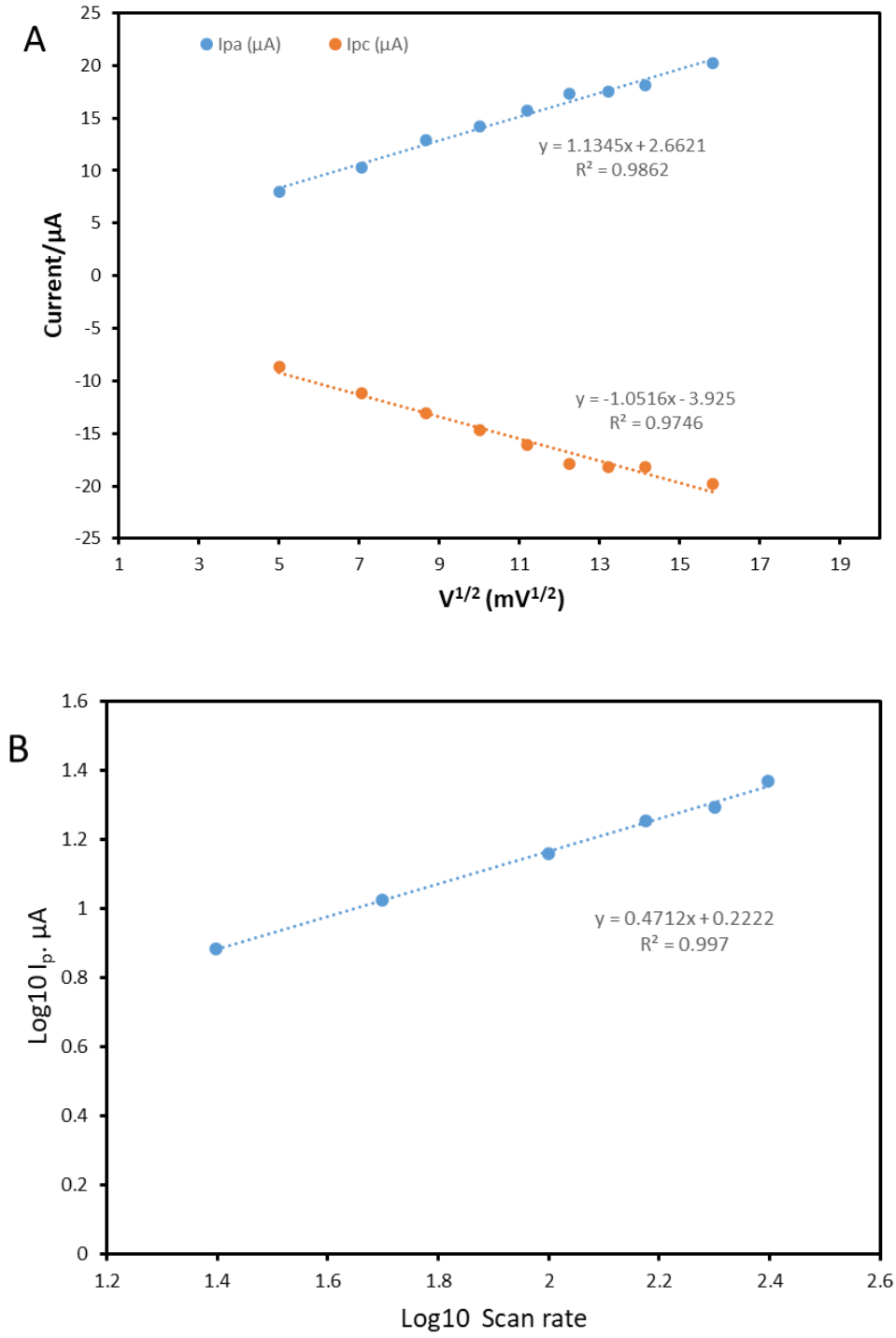

Figure 4.19 A). Plot of EEFGHSPE Ipa and Ipc versus square root of scan rate (υ $^{1/2}$) at potential scan rates (25 - 250 mVs^{-1}). B). A plot of log10 of peak current vs log10 of scan rate

The surface area of an SPE, 3D-GFSPE, GHPSPE and EEFGHSPE were evaluated by cyclic voltammetry. All plots showed a linear relationship between current magnitude and scan rate and were plotted versus the square root of the scan rate. i.e. ∆Ep increases with scan rate. This demonstrates the electrochemical processes as diffusion controlled; the observed shift of the potential peaks shifts further apart, commonly attributed to porous carbon materials where analytes move slowly to the electrode, experiencing slower target analyte diffusion rates [63]. The Randles-Sevcik equation [64] was employed to calculate the electrochemical effective area of the electrodes:

$$I_p = (2.69 \times 10^5)\, A\, D^{1/2}\, n^{3/2}\, v^{1/2}\, C \quad (1)$$

Here, I_p is the peak current; A is the electroactive area (cm^2), and n refers to the number of electrons transferred. D is the diffusion coefficient of ferricyanide redox marker ($[Fe(CN)_6]^{-3/4-}$, $D = 7.2 \times 10^{-6}\ cm^2\ s^{-1}$ [65] in 0.1 M KCl solution, C is the ferricyanide concentration (Molarity) and V is the potential scan rate (Vs^{-1}). The calculated electroactive surface area was estimated as 0.2, 0.079 and 0.0125 cm^2 for 3D-GFSPE, GHPSPE and EEFGHSPE, respectively. The CV profile peak-to-peak separation ($\Delta E_{p)}$ of 83.76 mV for 3D-GFSPE, 160 mV for EEFGH, and 308 mV for GHPSPE (298K) at 100 mVs^{-1}, which are all greater than the ideal ΔEp value of 59 mV. This compared to 371 mV for bare SPE. A high ΔE_p value of 371 mV for bare SPE has been reported for commercial screen printed electrodes, 471 mV for Euroflash™ and 416 mV Ultra™, with poor reversibility, respectively [66]. The modification of bare SPE with EEFGHP reduces the peak-to-peak separation from 336 mV to 163.76 mV. Graphene-like material Q-Graphene is reported to reduce the peak-to-peak separation by

Randviir et al. [67] on modified edge plane pyrolytic graphite (EPPG) and basal plane pyrolytic graphite (BPPG), respectively. In another report, electrochemically exfoliated graphene was prepared in 0.1 M $(NH_4)_2SO_4$ (0.1 M) at an applied potential of 10 V, exhibiting a peak-to-peak separation of 347 mV by Kirchner et al. [45]. This makes 3D-GFSPE peak-to-peak separation closer to the ideal value when compared to bare SPE, GHSPE and EEFGHSPE. The potential shift at a higher scan rate recorded for GHSPE might result from the binder on the electrode surface hindering fast electron transfer. The I_{pa} *vs* square root of the scan rate plot revealed a gradient of 20.26 μA μM^{-1} for 3D-GFSPE, 9.24 μA μM^{-1} for GHSPE and 1.098 μAμM^{-1} for EEFGHSPE. This would agree with the lower $\triangle E_p$ values recorded, indicating faster electron transfer at the 3D-GFSPE [68]. The performance of 3D-GFSPE is purely a result of its graphenic nature. It differs from the composites reported in the literature, with the vast majority being reduced graphene oxide with other materials [48,53,69]. The CV profile of 3D-GFSPE shows reversibility in the redox probe due to the uniformity of the surface and the porosity. In comparison, Figure 4.16 for GHSPE shows a greater quasi-reversible nature, resulting from a non-conductive binder at the electrode surface. Figure 4.15**,** Figure 4.17**,** and Figure 4.19 show the linearity of I_{pa} vs square root of scan rate ($\upsilon^{1/2}$), with $R^2 = 0.9994$ for 3D-GFSPE, $R^2 = 0.9746$ for EEFGHSPE and $R^2 = 0.9862$ for GHSPE. Both 3D-GFSPE, GHSPE and EEFGHSPE, respectively, showed a linear relationship between peak current and the square root of scan rate, indicating a diffusion-limited response in all cases (Figure 4.15, Figure 4.17, and Figure 4.19). The slope for each plot of $\log_{10}$ of peak current vs $\log_{10}$ of scan rate shows a slope to be 0.51 for 3D-GFSPE,

0.51 for GHSPE and 0.47 for EEFGHSPE, which close to 0.5, indicating semi-infinite diffusion.

From the results above, it can be speculated that there is an enclosure of the electroactive species within the porous structure of the graphene material in both electrodes, which affects the electrode's performance. This behaviour is typical of carbon materials [19-22]. Carbon materials' porosity enhances surface area, faster mass transfer kinetics, and electroactive sites, which can contribute to enhanced sensitivity, selectivity, and stability. Thus, the performance of sensors [19-22].

4.4.3 Electrochemical behaviour of estradiol

To compare the performance of graphene material-modified electrodes and other electrodes, the electrochemical behaviour of E2 was performed using cyclic voltammetry at various electrodes. Cyclic voltammograms of the different electrodes are presented. All the profiles in Figure 4.20 show cyclic voltammograms of E2 for the bare SPE, 3D-GFSPE, EEFGHPSPE and GHPSPE in phosphate buffer solution (PB) pH 7 for comparison. It can be observed that the electrodes have comparable potential windows, ranging from approximately 0.0 to +0.8 V (*vs* Ag/AgCl). The electrochemical behaviour of E2 at the bare SPE shows a well-defined single oxidation peak at +0.50 V, the same thing for GHPSPE and with a slight shift to + 0.52 V for EEFGHSPE with no reduction peak observed for the reverse scans for all the electrodes indicating the irreversible oxidation nature of E2 and the formation of a ketone derivative [37]. These results align with Moraes et al., as similar behaviour was observed for E2 at +0.54 V using reduced graphene oxide and Hu et al. report for liquid-phase

exfoliated graphene-modified electrode oxidation of E2 at 0.49 V [35]. Another study by Li et al. focused on nanobeads/graphene-based molecularly imprinted electrochemical sensors [33]. CV profile of E2 on bare SPE (a), EEFGHSPE (b), GHPSPE (c), and 3D-GFSPE (d) in 20 µM E2 PBS pH 7.0 at 0.1 Vs^{-1} is shown in Figure 4.20 depicting an anodic peak current of 0.23 µA, 0.28 µA, 1.30 µA and 2.28 µA, for bare SPE, EEFGHSPE, GHPSPE and 3D-GFSPE. As expected, the CV of bare electrode SPE has a lower oxidation peak current, followed by GHPSPE, EEFGHSPE, and 3D-GFSPE, which show the highest oxidation peak current. The large surface and electrochemical conductivity on graphene electrodes contribute to this.

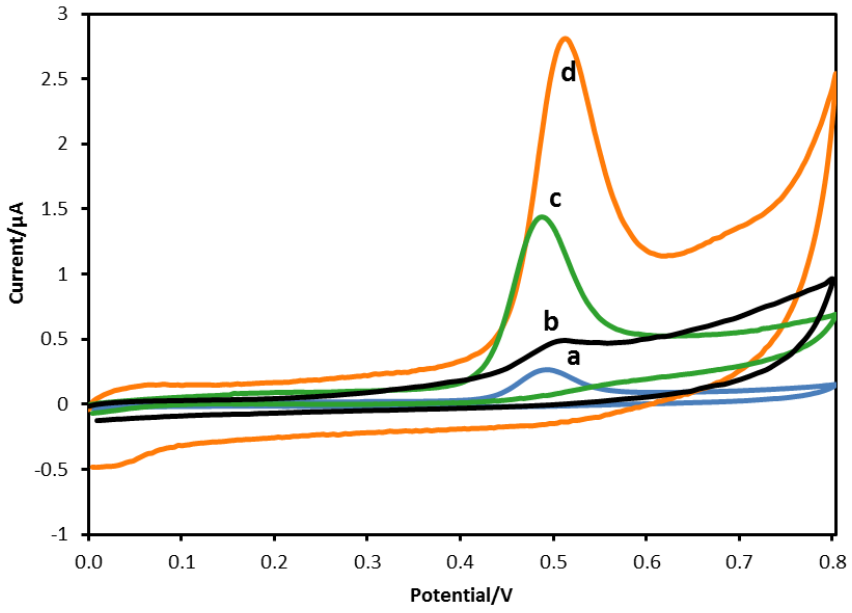

Figure 4.20. Cyclic voltammetry of E2 at Bare SPE (a), EEGHSPE (b), GHPSPE (c), 3D-GFSPE (d) in 20 µM (2 x 10^{-5} M) E2 PBS pH 7.0 at 100 mVs^{-1}.

Furthermore, CVs of the different electrochemical surfaces for the other electrodes show electrochemical activity corresponding to the electrochemical behaviour of E2 regarding carbon materials. The increase in Faradaic currents

with bare SPE after modification with EFFGHP is apparent from the CVs. Still, increased background current suggested an increased surface area with enhanced electrochemical activity compared to the bare SPE.

On the other hand, a lower background current is observed for the bare SPE 3D-GFSPE and GHPSPE compared to EFFGHSPE under the same conditions. This indicates that the 3D-GFSPE shows better performance characteristics for the oxidation of E2 than the other graphene-based EFFGHSPE and GHSPE. For GHSPE, the slow oxidation process observed for both E2 and redox solutions indicates the presence of other materials on the electrode surface, typical for SPEs, leading to the need for pre-treatment and modification of the electrode [60].

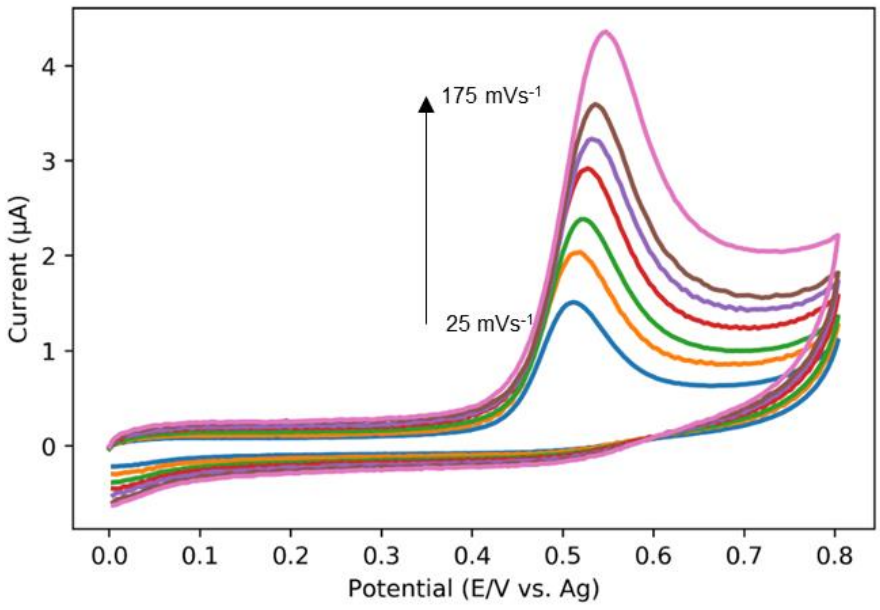

Figure 4.21. Cyclic voltammetry of 3D-GFSPE in 20 µM (2 x 10^{-5} M) E2 at scan rates of 25 - 175 mVs^{-1}.

The electrochemical behaviour of E2 at the 3D-GFSPE was investigated at various scan rates, as shown in Figure 4.23. An increased current with an

increasing scan rate was observed between 25 and 175 mV/s. A plot of the peak current versus scan rate and peak current versus square root of scan rate given in Figures 4.22A and 4.22B indicate both adsorption and diffusion processes occurring at the 3D-GFSPE surface with the equations; I_{pa} (μA) = 0.015 + 0.47 A/mVs^{-1}) (R^2 = 0.9864) and I_{pa} (μA) = 0.278 - 0.709 A/mVs^{-1}) (R^2 = 0.9976). It indicates a diffusion-controlled process. The peak-peak separation increases with increasing scan rate, indicating the irreversible nature of the electron transfer kinetics—most carbon material-modified electrodes for phenolic sensors reported diffusion-controlled processes [70,71].

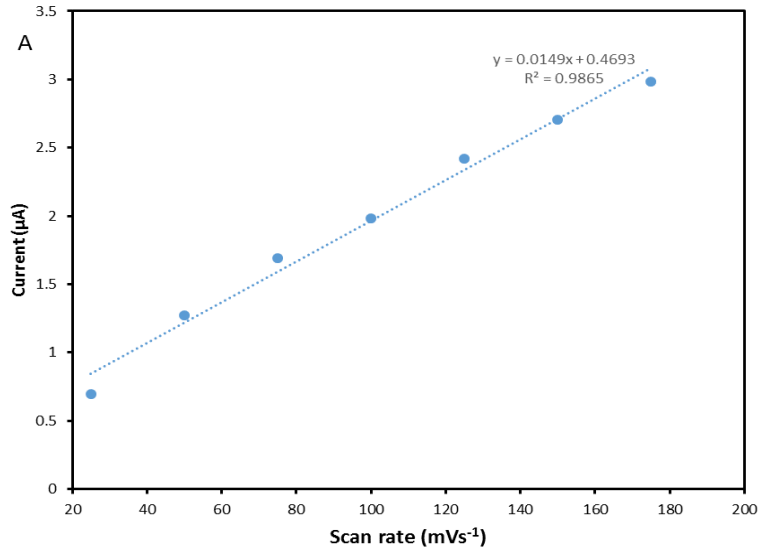

Figure 4.22. (A) Plot Ipa versus scan rate and (B) Ipa versus square root of scan rate ($V^{1/2}$).

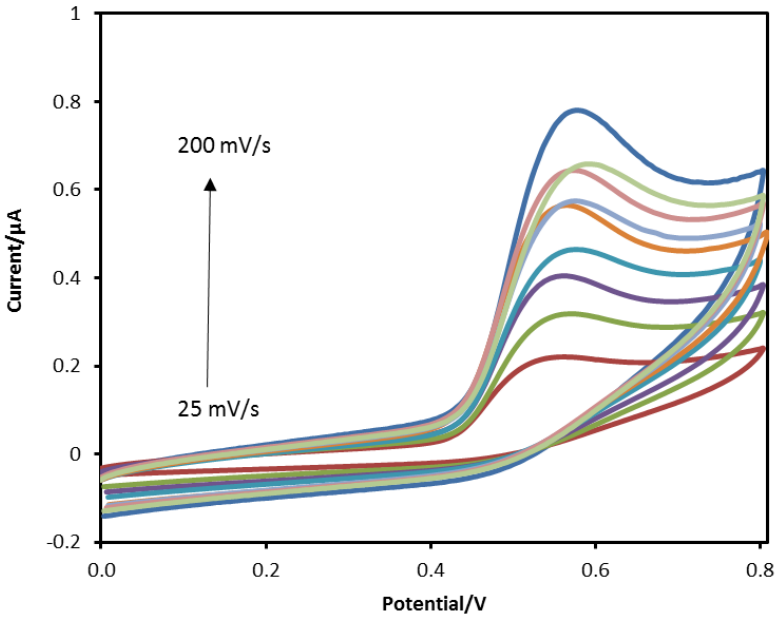

Figure 4.23. Cyclic voltammetry of GHSPE in 20 µM (2 x 10^{-5} M) E2 at scan rates (25 - 200 mVs^{-1})

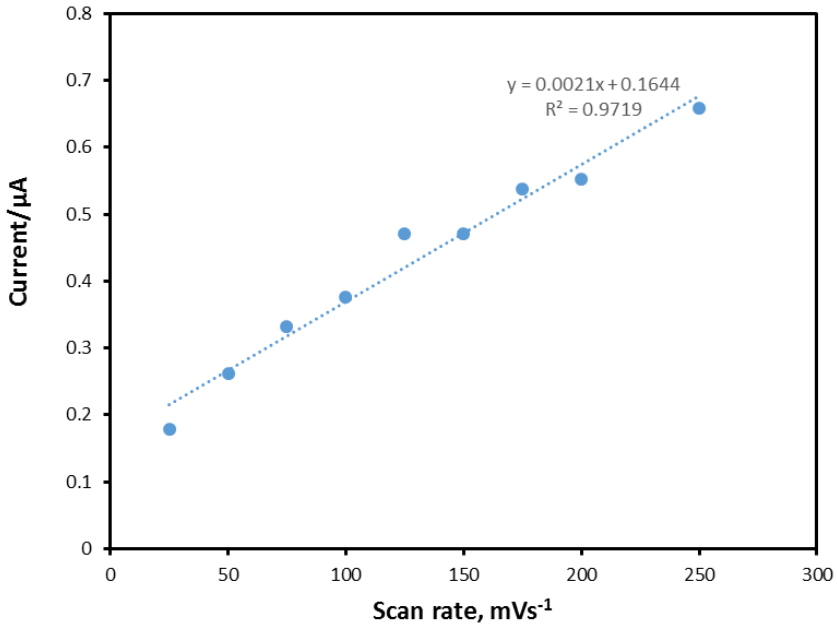

Figure 4.24. (A) Plot peak current (Ipa) versus scan rate for GHSPE.

Further information on the scan rate behaviour of GHSPE and EEFGHSPE is presented below. The effect of scan rate on the E2 oxidation at the GHPSPE was also investigated with the corresponding voltammograms shown in (Figure 4.23)

and EEFGHSPE (Figure 4.25). From the voltammograms shown in Figure 4.23, it can be observed that the Ep shifted slightly toward more positive values with an increase in scan rate over the range of 25 to 200 mV s^{-1}. A similar feature was also observed for EEFGHSPE in Figure 4.25. Figure 4.24 shows a linear relationship between peak current (Ipa) versus scan according to the equation y = 0.0021x + 0.1644, R^2 = 0.9719 for GHPSPE. The dependence of peak current versus scan rate was studied in Figure 4.26, and a linear relationship between peak current (Ipa) versus scan rate according to the equation y = 0.0011x + 0.0805 (R^2 = 0.9355) for EEFGHSPE is observed. These results suggested an adsorption-controlled mechanism for the graphene electrodes and E2.

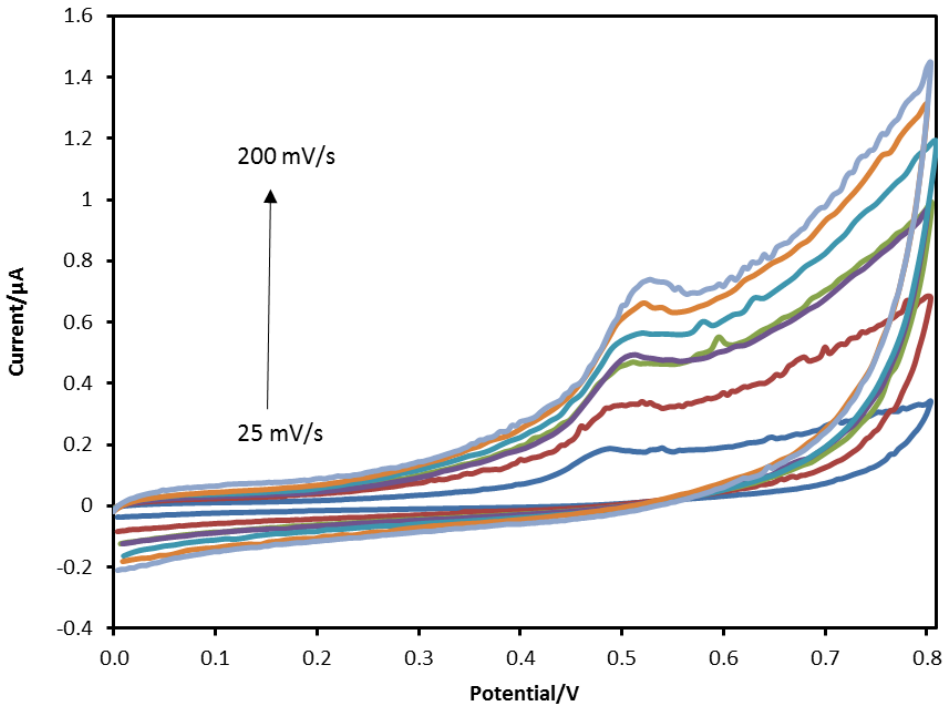

Figure 4.25. Cyclic voltammetry of EEFGHSPE in 20 µM (2 x 10^{-5} M) E2 at scan rates (25 - 200 mVs^{-1})

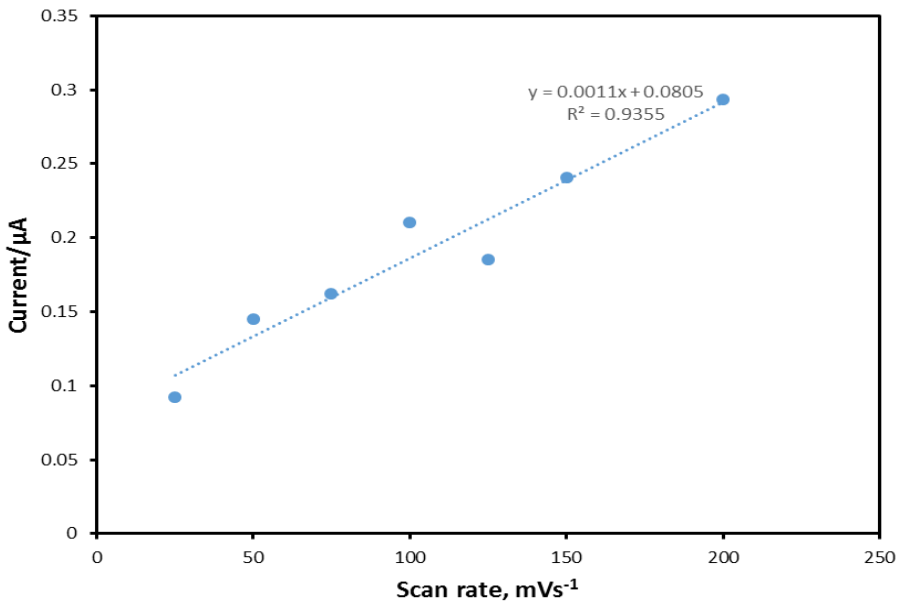

Figure 4.26. Plot Peak current (Ipa) versus scan rate for EEFGHSPE.

4.4.4 Amperometric Measurement and Calibration

Combining amperometry and screen-printed electrodes provides an attractive way to offer low-cost sensing [72]. It is widely applied in the determination of phenolic [73]. A fixed potential is applied between the working and counter electrode, which leads to the added analyte being oxidised at the electrode surface and a current being generated and monitored. From this potential, the magnitude of the current is directly proportional to concentration. Amperometry measurements were carried out in a 30 mL cell, stirring at room temperature, to determine E2. After establishing a stable baseline at 400 s, an aliquot of 50 µL of E2 (0.5 mM) was injected at regular intervals for six injections. The CV results in E2 of 20 µM (2 x 10^{-5} M) concentrations revealed peak oxidation at a voltage of approximately +0.5 V (Figure 4.20). This potential was utilised to choose the potential for subsequent amperometric measurements (Figure 4.27, 4.29 & 4.31) conducted at a working potential of +0.65 V. This choice was because during

cyclic voltammetry, the analyte moves to the electrode based on mass transport and to allow stable oxidation during amperometry experiments under stirring, various potentials were tested from 0.3 V to 0.65 V. No currents were observed for 0.3, 0.4, 0.5 V. Until currents were generated at 0.55 V and 0.65 V with +0.65 V giving a less noisy background compared to 0.55 V, and consequently, +0.65 V was chosen for further amperometric investigations.

Higher applied potentials have previously been reported for the amperometric determination of E2 in other works [74]. For example, Batista et al. [75] investigated the measurements of E2 in MeCN/0.1 M phosphate buffer (pH 6.0) at an applied potential of +0.6 V [75]. The responses for both 3D-GFSPE and GHSPE electrodes were investigated in blank solutions. No noticeable current reactions were observed at the potentials 0.3 V and 0.4 V. Figure 4.27, Figure 4.29, and Figure 4.31 depict the amperometric responses obtained for GHPSPE, 3D-GFSPE, and EEFGHSPE for consecutive additions of 50 µL of 0.5 mM E2 in PBS (pH 7.0) at an applied potential of +0.65 V at 60-second intervals with the resulting calibration plots (Figures 4.28, Figures 4.30, and Figures 4.32) of current against concentration. From Figure 4.31, the current generated at EEFGHSPE is low compared to GHPSPE and 3D-GFSPE electrodes for E2, showing that lower concentrations will be too low to be detected. However, there is noise and changes in the amperometric current. To reduce the noise observed, a moving average of window size of 5 datapoint points was used to smooth out the noise in the data, making the overall trend more apparent. While it reduces noise, smoothing can sometimes dampen the peaks, potentially affecting the analysis of peak heights or times. Thus, the method employed depends on the

research question and the data's characteristics. This is why this method has been employed to analyse all amperometric data.

Figure 4.28 shows a calibration plot obtained from the amperometric measurement. The GHPSPE shows a linear concentration range from 8.3×10^{-7} M to 2.49×10^{-6} M (0.83 - 4.98 µM) with $R^2 = 0.9922$. This linear behaviour has been observed in the literature for the electroanalysis of E2 [8]. The LOD was calculated as (3 × SD blank)/slope was 0.71 µM (n = 3), which is compared to 3D-GFSPE (Figures 4.30) and EEFGHSPE (Figures 4.32)**,** as shown in Table 4.2 and their performance. Each point represents the mean value for three measurements. The various slopes from each electrode in Table 4.2, GHPSPE, 3D-GFSPE, and EEFGHSPE are 0.0391 µA/µM, 0.0242 µA/µM, and 0.0033 µA/µM. This is similar to the report by Kirchner et al., which states that graphene-based electrode behaviour and performance solely depend on the production method [45]. Thus, the preparation method influences the performance of the sensor material due to the different intrinsic characteristics [45]. A steady increase in current response from each injection represents the behaviour of both electrodes towards the E2 concentrations. A detailed breakdown of the raw data supporting these findings can be seen in Appendix C. GHPSPE unprocessed amperometric data in Appendix C, Appendix C3 form the basis for all subsequent data processing and analysis made in Appendix C, Appendix C1. 3D graphene foam screen-printed electrodes (3D-GFSPE) performance involves analysing the raw amperometric signals before preprocessing. Appendix C depicts these raw data signals from three separate experimental trials, as shown in Figure C2.

Similar to 3D-GFSPE, the raw amperometric data for the EEFGHSPE are in Appendix C, Figure C3.

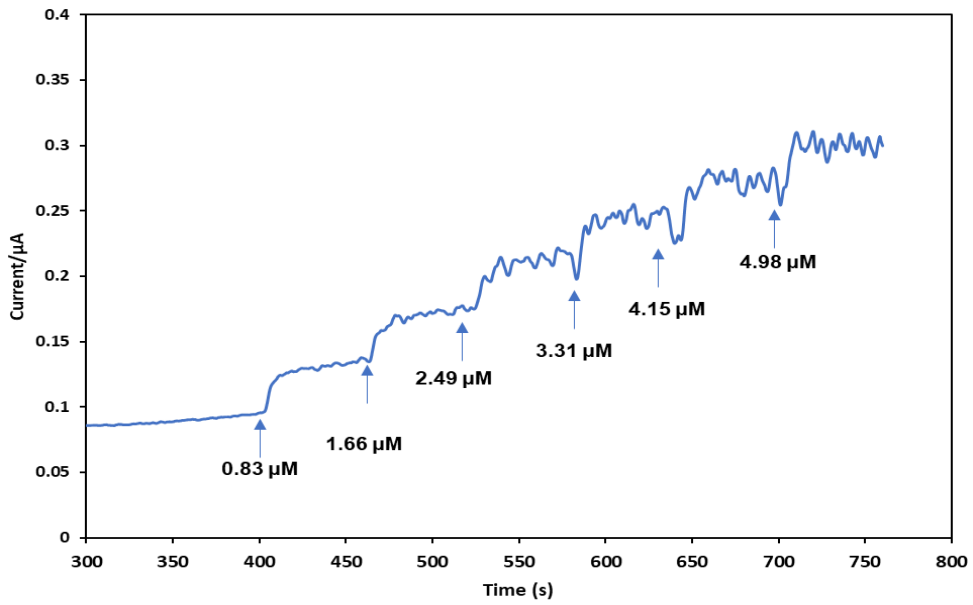

Figure 4.23. The amperometric response obtained for GHPSPE for successive addition of 50 µL of 0.5 mM E2 in PBS (pH 7.0) at an applied potential of +0.65 V vs Ag/AgCl at a 60s interval. (Arrow represent the injection point and sensor response to successive estradiol additions.

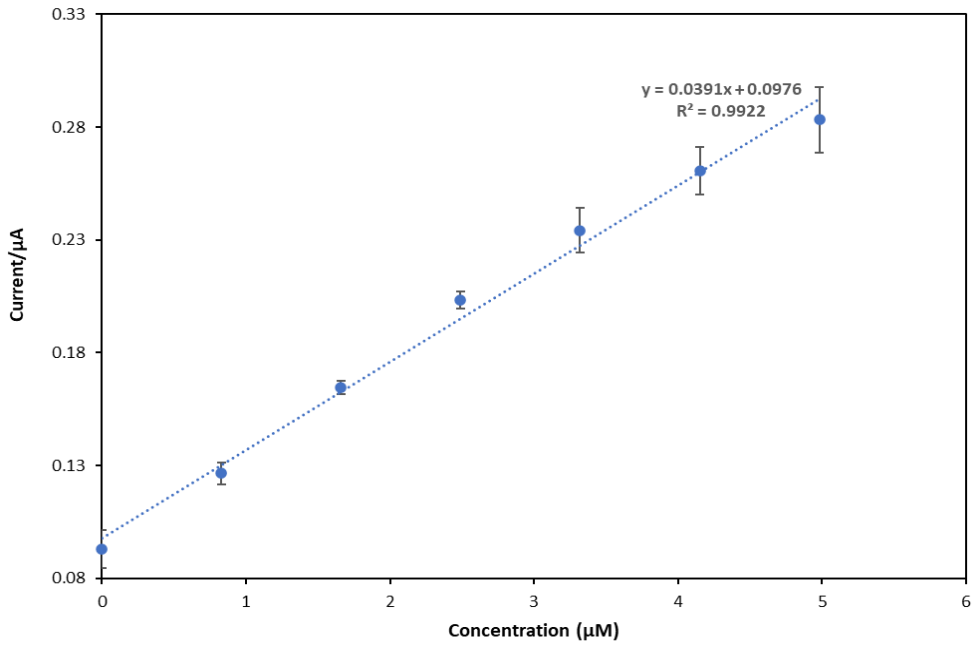

Figure 4.24. GHPSPE Calibration plot of the average of the current plateau (relative to baseline) against concentration. Error bars depict the standard deviation, representing the variability within triplicate measurements for each concentration point, n = 3.

In Figure 4.27, a steady increase in current response from each injection represents the behaviour of the electrodes (GHPSPE, 3D-GFSPE, and EEFGHSPE) towards the E2 concentrations. Furthermore, the interference in the presence of other analytes was investigated to examine the robustness of the sensor. An essential aspect of sensor design is its ability to determine the target analyte with an acceptable level of precision for an actual sample over the appropriate concentration range. Since the sensor is aimed to serve as an alternative to conventional methods, with no sample pre-treatment, we subjected the sensors to tap water samples (Bristol, UK) directly without adding a supporting electrolyte. Figure 4.35 depicts the response of the 3D-GFSPE and GHSPE electrodes in tap water with consecutive injections of E2 stock solution.

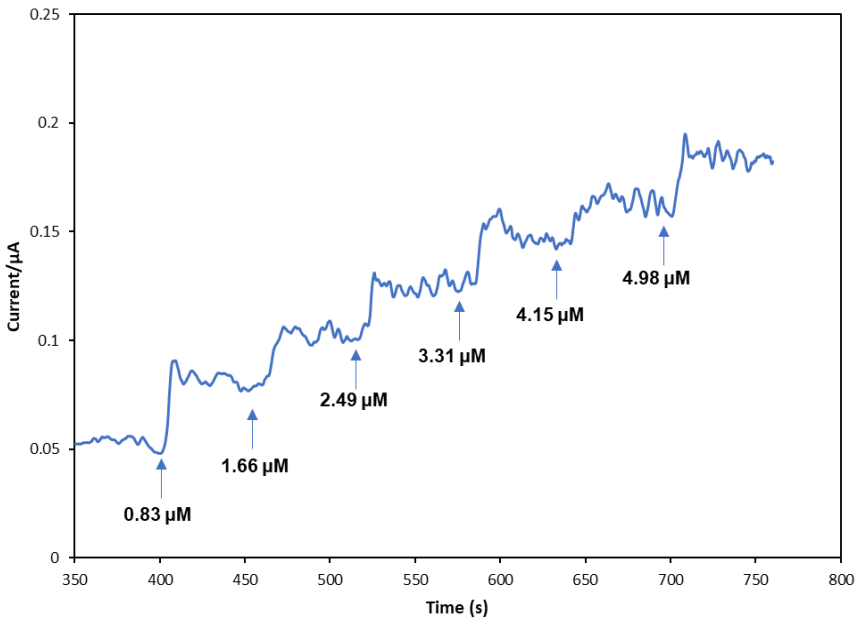

Figure 4.25. The amperometric response was obtained for 3D-GFSPE for successive addition of 50 µL of 0.5 mM E2 in PBS (pH 7.0) at an applied potential of +0.65 V vs Ag/AgCl 60s interval. (Arrow represents the injection point and sensor response to successive E2 additions).

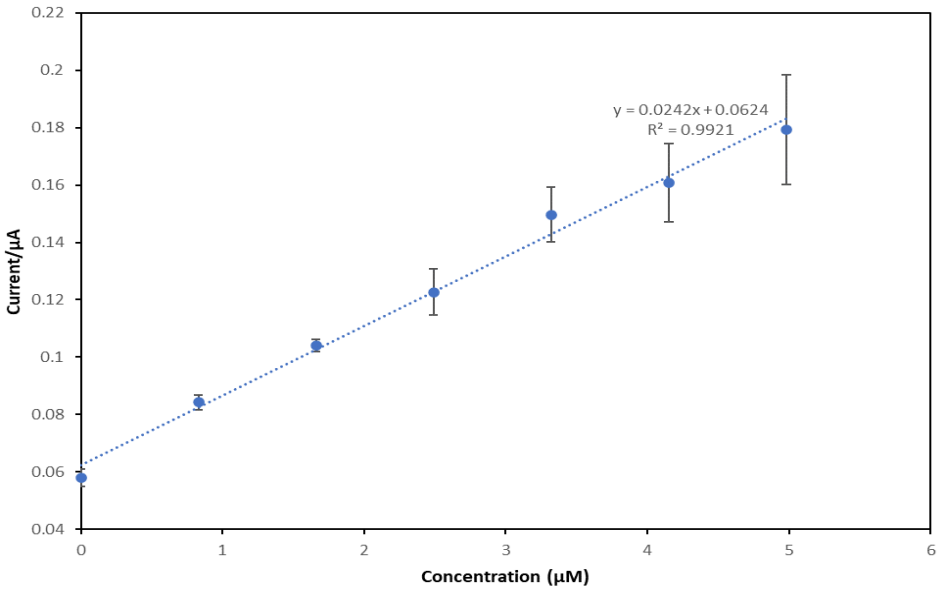

Figure 4.26. 3D-GFSPE Calibration plot of the average of the current plateau (relative to baseline) against concentration. Error bars depict the standard deviation, representing the variability within triplicate measurements for each concentration point, n = 3.

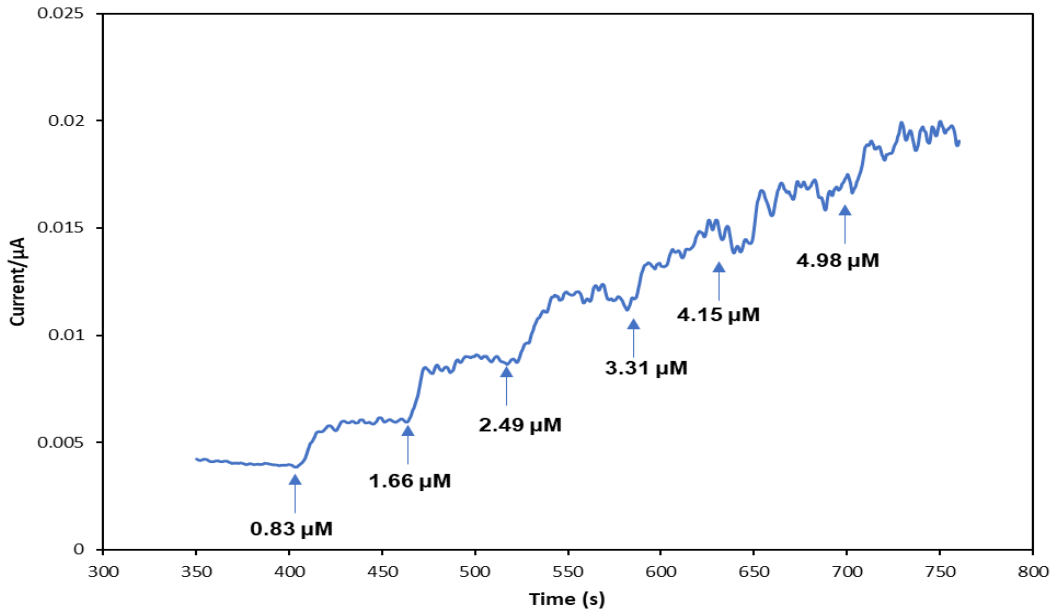

Figure 4.27. The amperometric response was obtained for EEFGHSPE for successive addition of 50 µL of 0.5 mM E2 in PBS (pH 7.0) at an applied potential of +0.65 V vs Ag/AgCl 60s interval. (Arrows represent the injection point and sensor response to successive E2 additions).

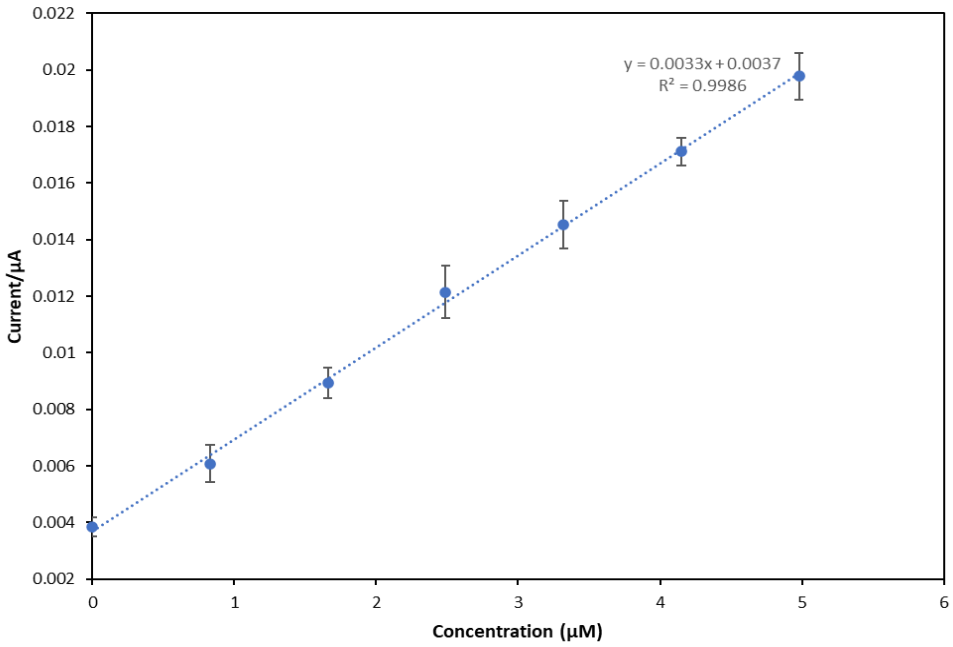

Figure 4.328. EEFGHSPE Calibration plot of average of the current plateau (relative to baseline) against concentration. Error bars depict the standard deviation, representing the variability within triplicate measurements for each concentration point, n = 3.

Table 4.2. Performance of GHSPE, 3D-GFSPE and EEFGHSPE sensors for determination of E2.

	GHSPE	3D-GFSPE	EEFGH
Working potential (V)	+0.65	+0.65	+0.65
Linear range (M)	8.3×10^{-7} - 4.98×10^{-6}	8.3×10^{-7} – 4.98×10^{-6}	8.3×10^{-7} – 4.98×10^{-6}
Reproducibility (%RSD)	4.27	6	6.54
Detection Limit (M)	7.1×10^{-7}	4.1×10^{-7}	3.3×10^{-7}
Slope	0.0391	0.0242	0.0033
Sensitivity ($\mu A \mu M^{-1} cm^{-2}$)	0.495	0.121	0.264

As an interference study, Figure 4.33 shows the amperometric response obtained for 3D-GFSPE and GHSPE for successive additions of 50 µL of 0.5 mM E2, followed by citric acid and ibuprofen in PBS (pH 7.0) at an applied potential of +0.65 V *vs* Ag/AgCl. A noticeable change in the current response was observed after the addition of each E2. In contrast, no apparent current response was observed after adding citric acid or ibuprofen. The same goes for Figure 4.34. Notably, even after adding both citric acid and ibuprofen, further additions of E2 still resulted in further increases in current, demonstrating that the sensor was unaffected by the presence of both citric acid and ibuprofen. Thus, the sensor shows both selectivity and sensitivity for E2 at an applied potential of +0.65 V *vs* Ag/AgCl, verifying the practicality of the sensors. These interferents are found in water, and the electrochemical sensor has been investigated for their presence in water as emerging pollutants due to rampant use. Citric acid has been seen as part of pharmaceutical waste, phosphate-based detergents [76], manufacturing of explosives [65], and illegal use in drug making. Ibuprofen is the third largest drug used globally, and its presence in water comes from both usage and deficient water treatment systems [77]. The non-interference of these

compounds is related to being non-phenolic; as such, they do not interfere with the oxidation of E2. Unlike structurally similar compounds (estrone, estriol, and Bisphenol A) seen in Chapter 3, which are hydrophobic and contain a hydroxy group attached to the benzene aromatic hydrocarbon, which may cause the oxidation of the benzene ring. Thus, its oxidation on the electrode surface causes an increase in the oxidation peak current of E2. The performance of GHSPE, 3D-GFSPE and EEFGHSPE sensors for determining E2 are depicted in Table 4.2. GHSPE demonstrated a sensitivity of 0.4953 μA/μM/cm², with an average %RSD of 4.27% across the concentration range investigated.

In comparison, 3D-GFSPE has a sensitivity of 0.121 μA/μM/cm², with an average %RSD of 6% and EEFGHSPE sensitivity of 0.264 μA/μM/cm², with an average %RSD of 6.54% respectively. Table 4.3 shows the comparison of recent reports on E2 sensors. ANOVA analysis was conducted to compare the %RSD of the three sensors (GHSPE, 3D-GFSPE, and EEFGHSPE) to determine if there are statistically significant differences between them. The p-value obtained from the ANOVA test was approximately 0.182, more significant than 0.05 (typically considered the threshold for statistical significance). This suggests no statistically significant differences in the %RSD values across the three sensors.

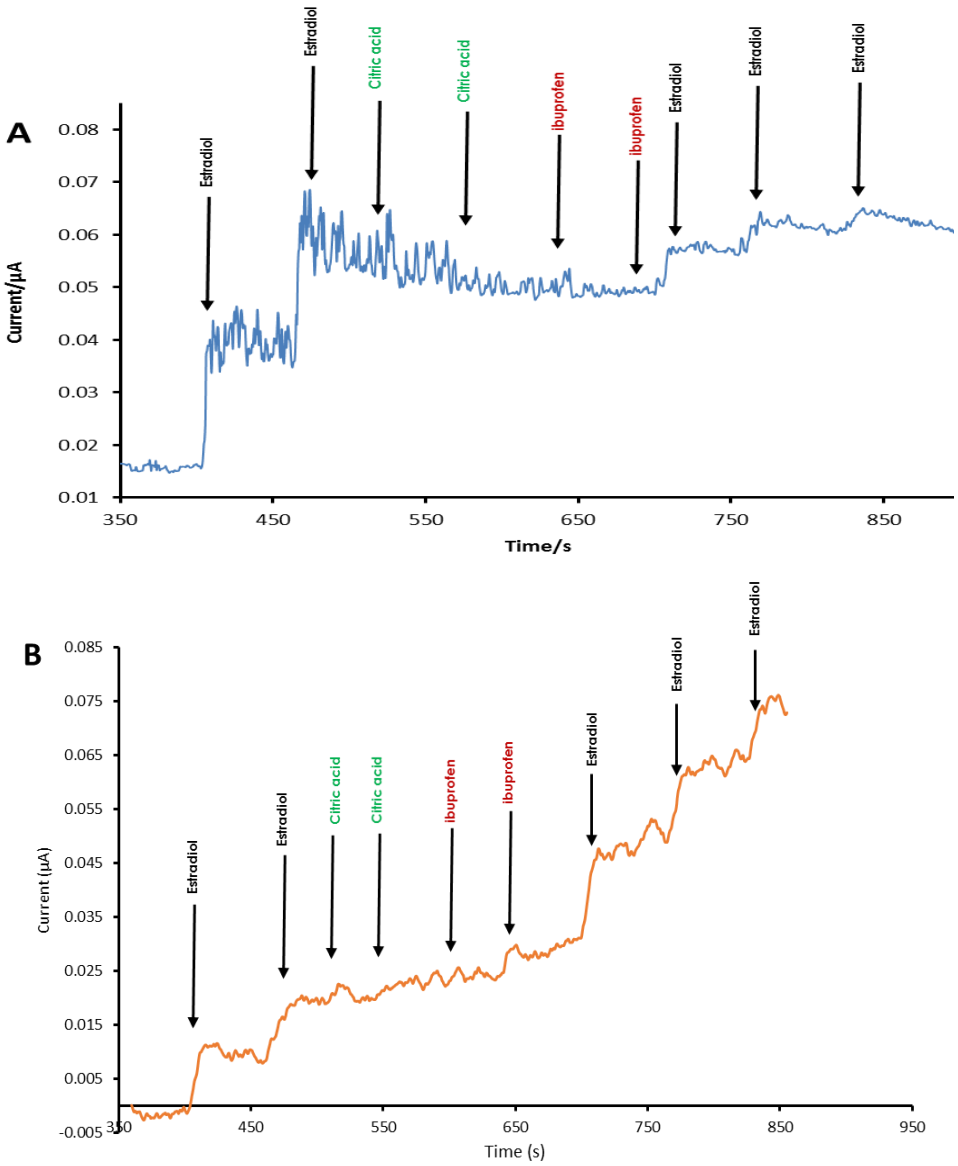

Figure 4.29 A) Amperometric response obtained for 3D-GFSPE for successive addition of 50 µL of 0.5 mM E2, citric acid and Ibuprofen in PBS (pH 7.0) at an applied potential of +0.65 V at 60 s interval. B) Amperometric response obtained for GHPSPE for successive addition of 50 µL of 0.5 mM E2, citric acid and Ibuprofen in PBS (pH 7.0) at an applied potential of +0.65 V at 60 s interval.

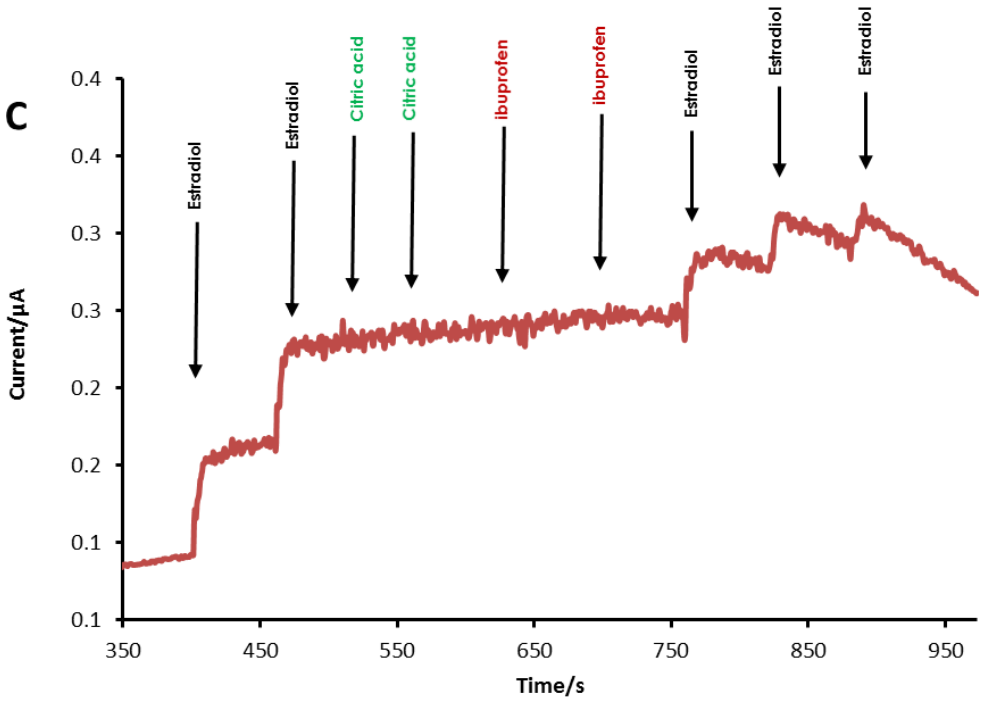

Figure 4.30. The amperometric response obtained for EEFGHPSPE for successive addition of 50 µL of 0.5 mM estradiol, citric acid, and Ibuprofen in PBS (pH 7.0) at an applied potential of +0.65 V at 60 s interval.

The results of this study can be compared with the previously reported flow injection chronoamperometric assay of Brocenshi et al., which reported a sensitivity of 10 mA mol^{-1} using a boron-doped electrode, which is lower than this work [13]. Similarly, Batista et al. reported a 12.16 mA/mol^{-1} sensitivity at an iron tetrapyridinoporphyrazine-modified carbon paste electrode [75]. Antifouling property is a requirement for a sensor as this is vital in the natural world setting and improves the sensor's sensitivity [78].

Furthermore, graphene surfaces with few oxygen groups are reported to be less prone to fouling [25]. Therefore, the graphene SPEs' response is faster than that of bare SPEs at the operating potential of +0.65 V. Another exciting feature observed at 3D-GFSPE and GHPSPE is its antifouling properties in tap water. This explains the surface sensitivities of the two materials towards the E2 analyte.

These are similar due to the properties of the graphene material, as reported in [25,79]. However, E2 is known to passivate the surface of electrodes by forming an insoluble layer that lowers the sensor's sensitivity. Consequently, it is expected that the surfaces of the GHPSPE and 3D-GFSPE will be masked with a similar passivating layer following the oxidation of E2. To confirm this, a bare SPE was subjected to the same condition as the two graphene-based electrodes, and as expected, the electrode was fouled after two injections (Appendix).

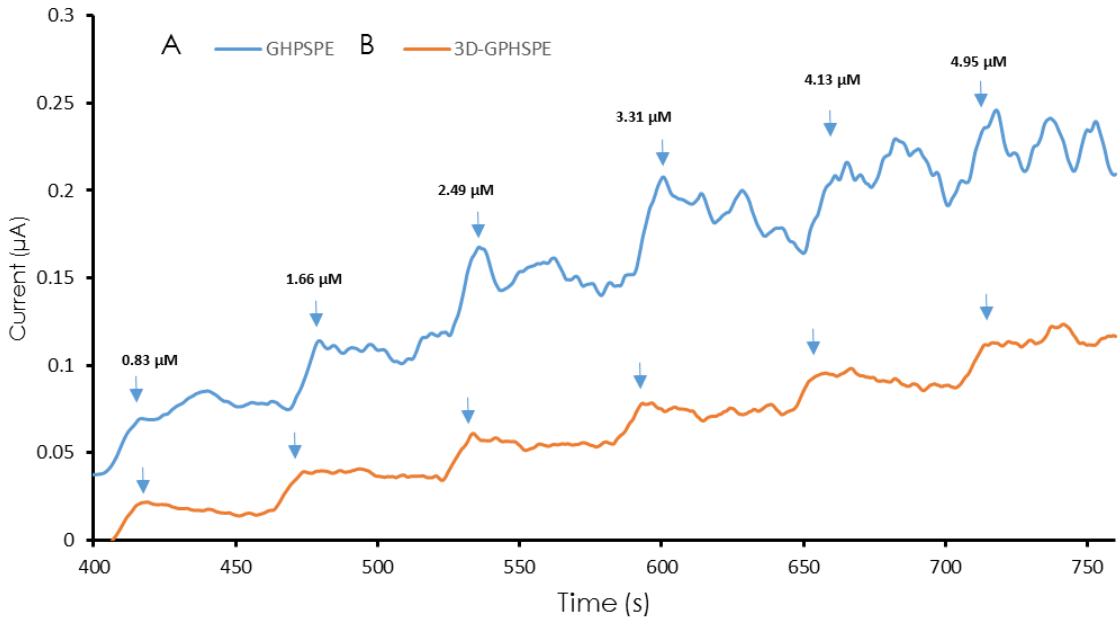

Figure 4.31 (A) Amperometric response obtained for (A) GHPSPE, (B) 3D-GHPSPE for successive addition of 50 µL of 0.5 mM E2 in a tap water sample at an applied potential of +0.65 V at 60 s interval.

Table 4.3 Some recent reports on estradiol sensors

Electrode	Technique Detection	Linear Range (M)	LOD (M)	Sample	Ref.
Glassy carbon electrode with reduced graphene oxide and di-hexadecyl phosphate	Differential pulse voltammetry	4.0×10^{-7} - 1.0×10^{-5}	7.7×10^{-8}	Urine	32]
Glassy carbon with poly(L-serine)	Square wave voltammetry	1.0×10^{-7} - 3.0×10^{-5}	2.0×10^{-8}	Serum	80]
Glassy carbon electrode with Platinum/ multi-walled carbon nanotubes MWNTs	Square wave voltammetry	5×10^{-7} - 1×10^{-6}	1.8×10^{-8}	Serum	81]
Boron-doped diamond electrode	Amperometry	1×10^{-7} – 3.0×10^{-6}	1×10^{-7}	River water	13]
Carbon paste Modified with iron tetrapyridinoporphyrazine	Amperometry	4.5×10^{-5} - 4.5×10^{-4}	1.3×10^{-8}	injection	75]
3D- graphene foam screen-printed electrode	Amperometry	8.3×10^{-7} - 4.98×10^{-6}	7.1×10^{-7}	Tap water	This work
Graphene ink screen-printed electrode	Amperometry	8.3×10^{-7} - 4.98×10^{-6}	4.1×10^{-7}	Tap water	This work
Electrolytically exfoliated graphene (EEFGH) screen-printed electrode	Amperometry	8.3×10^{-7} - 4.98×10^{-6}	3.3×10^{-7}	Tap water	This work

4.5 Conclusions

This chapter investigated the various graphene SPEs as standalone electrodes with no modifications and pre-treatment steps as a portable amperometric sensor. The electrochemical behaviour of 3D-GFSPE, EEFGHSPE and GHPSPE in the presence of E2 were investigated and compared. Surprisingly, the performance of these electrodes using a redox marker shows GHPSPE performs poorly, followed by EEFGHPSPE, which is in line with the theory of a defect-free basal-plane structure [62]. GHPSPE has increased sensitivity for E2 analysis compared to EEFGH and 3D-GFSPE, despite the redox probe showing 3D-GFSPE to have better electrochemical features. Using binders in graphene-based ink could have uncontrollable effects on electrochemical performance. The LOD was 0.71 µM (7.1×10^{-7} M) for GHPSPE, 0.33 µM (3.3×10^{-7} M) for EEFGHSPE and 0.41 µM (4.1×10^{-7} M) for 3D-GFSPE. Furthermore, the sensor was successfully applied to the tap water sample and gave an average percentage recovery for a fortification of 0.83 µM (8.3×10^{-7} M) E2 of 95 % with an associated coefficient of variance of 5.7% (n=5).

Interference studies were also performed to investigate the sensor's selectivity at +0.65 V *vs* Ag/AgCl in the presence of other analytes. From the literature, graphene is applied as a composite with additional material as an electrochemical transducer [47]. 3D-GFSPE requires further investigation, such as optimising the different laser parameters, as changing these can lead to different surface morphologies [82]. The application of graphene in sensor design is well established but generally used in conjunction with other materials to produce composites. The variation in the chemical composition resulting from different preparation methods is investigated for its impact on the resulting electrochemical

properties. It is revealed that the quality of graphene strongly depends on the preparation method [69]. No uniform deposition protocol can be adapted for graphene dispersions. The lateral dimensions of graphene flakes were examined via electron microscope and dynamic light scattering, and the results concurred with the literature. Our results highlighted the importance of choosing low-capacitive electrode materials and small electrodes if low current noise is crucial. This chapter demonstrates that further work on EEFGHPSPE is required as the graphite rod's quality cannot be proven, and information is not openly available from the supplier. The simple method of producing graphene using the electrolytic method and laser scribing offers the production of standalone disposable sensors as cost-effective disposable electrochemical sensors suited to environmental testing, which would open numerous opportunities in electroanalysis. Future experiment design should assess the sensor's specificity with other interferents beyond citric acid and ibuprofen in complex matrices, as many other pharmaceuticals and compounds from personal care products are commonly found in environmental waters.

On top of that, various concentration ranges should be explored at the same environmentally relevant concentrations. Amperometric tests could include variations in the sequence of analytes and interference beyond the procedure adopted by Istrate et al. [86] in this study. The idea behind fast sensor design and injection time of 60 seconds is welcome. However, the time should be extended to expose the sensor for a longer analysis period, e.g. several hours of exposure to interferents. Alternative techniques like electrochemical impedance spectroscopy would offer additional valuable information.

References

[1] R. Owen, S. Jobling, The hidden costs of flexible fertility, Nature. 485 (2012) 441–441. https://doi.org/10.1038/485441a.

[2] H. Pu, Z. Huang, D.W. Sun, H. Fu, Recent advances in the detection of 17β-estradiol in food matrices: A review, Crit. Rev. Food Sci. Nutr. 59 (2019) 2144–2157. https://doi.org/10.1080/10408398.2019.1611539.

[3] Q. Liu, Q. Zhou, G. Jiang, Nanomaterials for analysis and monitoring of emerging chemical pollutants, TrAC Trends Anal. Chem. 58 (2014) 10–22. https://doi.org/10.1016/J.TRAC.2014.02.014.

[4] M. Adeel, X. Song, Y. Wang, D. Francis, Y. Yang, Environmental impact of estrogens on human, animal and plant life: A critical review., Environ. Int. 99 (2017) 107–119. https://doi.org/10.1016/j.envint.2016.12.010.

[5] C. Li, Y. Wei, S. Zhang, W. Tan, Advanced methods to analyse steroid estrogens in environmental samples, Environ. Chem. Lett. (2020). https://doi.org/10.1007/s10311-019-00961-2.

[6] A.M. Musa, J. Kiely, R. Luxton, K.C. Honeychurch, Recent progress in screen-printed electrochemical sensors and biosensors for the detection of estrogens, TrAC - Trends Anal. Chem. 139 (2021) 116254. https://doi.org/10.1016/j.trac.2021.116254.

[7] J.P. Hart, A. Crew, E. Crouch, K.C. Honeychurch, R.M. Pemberton, Some Recent Designs and Developments of Screen-Printed Carbon Electrochemical Sensors/Biosensors for Biomedical, Environmental, and Industrial Analyses, Anal. Lett. 37 (2004) 789–830. https://doi.org/10.1081/AL-120030682.

[8] O.D. Renedo, M.A. Alonso-Lomillo, M.J.A. Martínez, Recent developments in the field of screen-printed electrodes and their related applications, Talanta. 73 (2007) 202–219. https://doi.org/10.1016/j.talanta.2007.03.050.

[9] D. Butler, G.G. Guilbault, Disposable amperometric immunosensor for the detection of 17-β estradiol using screen-printed electrodes, Sensors Actuators, B Chem. 113 (2006) 692–699. https://doi.org/10.1016/j.snb.2005.07.019.

[10] A.U. Alam, D. Clyne, H. Jin, N.X. Hu, M.J. Deen, Fully Integrated, Simple, and Low-Cost Electrochemical Sensor Array for in Situ Water Quality Monitoring, ACS Sensors. 5 (2020) 412–422. https://doi.org/10.1021/acssensors.9b02095.

[11] T.A. Enache, A.M. Oliveira-Brett, Phenol and para-substituted phenols electrochemical oxidation pathways, J. Electroanal. Chem. 655 (2011) 9–16. https://doi.org/10.1016/j.jelechem.2011.02.022.

[12] D. Talarico, F. Arduini, A. Constantino, M. Del Carlo, D. Compagnone, D. Moscone, G. Palleschi, Carbon black as successful screen-printed electrode modifier for phenolic compound detection, Electrochem. Commun. 60 (2015) 78–82. https://doi.org/10.1016/j.elecom.2015.08.010.

[13] R.F. Brocenschi, R.C. Rocha-Filho, B. Duran, G.M. Swain, The analysis of estrogenic compounds by flow injection analysis with amperometric detection using a boron-doped diamond electrode, Talanta. 126 (2014) 12–19. https://doi.org/10.1016/j.talanta.2014.02.047.

[14] D.H. Seo, S. Pineda, Y.C. Woo, M. Xie, A.T. Murdock, E.Y.M. Ang, Y. Jiao, M.J. Park, S. Il Lim, M. Lawn, F.F. Borghi, Z.J. Han, S. Gray, G. Millar, A. Du, H.K. Shon, T.Y. Ng, K. Ostrikov, Anti-fouling graphene-based membranes for effective water desalination, Nat. Commun. 9 (2018) 1–12. https://doi.org/10.1038/s41467-018-02871-3.

[15] S.J. Rowley-Neale, D.A.C. Brownson, G. Smith, C.E. Banks, Graphene oxide bulk-modified screen-printed electrodes provide beneficial electroanalytical sensing capabilities, Biosensors. 10 (2020) 8–10. https://doi.org/10.3390/bios10030027.

[16] A. Ferrand, M. Siaj, J.P. Claverie, Graphene, the Swiss Army Knife of

Nanomaterials Science, ACS Appl. Nano Mater. 3 (2020) 7305–7313. https://doi.org/10.1021/acsanm.0c02055.

[17] E.P. Randviir, D.A.C. Brownson, J.P. Metters, R.O. Kadara, C.E. Banks, The fabrication, characterisation and electrochemical investigation of screen-printed graphene electrodes, Phys. Chem. Chem. Phys. 16 (2014) 4598–4611. https://doi.org/10.1039/c3cp55435j.

[18] F. Liu, C. Wang, X. Sui, M.A. Riaz, M. Xu, L. Wei, Y. Chen, Synthesis of graphene materials by electrochemical exfoliation: Recent progress and future potential, Carbon Energy. 1 (2019) 173–199. https://doi.org/10.1002/cey2.14.

[19] K.S. Novoselov, V.I. Fal'Ko, L. Colombo, P.R. Gellert, M.G. Schwab, K. Kim, A roadmap for graphene, Nature. 490 (2012) 192–200. https://doi.org/10.1038/nature11458.

[20] K. S. Novoselov et al, Electric Field Effect in Atomically Thin Carbon Films, 306 (2016) 666–669.

[21] S. Cinti, F. Arduini, Graphene-based screen-printed electrochemical (bio)sensors and their applications: Efforts and criticisms, Biosens. Bioelectron. 89 (2017) 107–122. https://doi.org/10.1016/j.bios.2016.07.005.

[22] C. Mattevi, G. Eda, S. Agnoli, S. Miller, K.A. Mkhoyan, O. Celik, D. Mastrogiovanni, G. Granozzi, E. Carfunkel, M. Chhowalla, Evolution of electrical, chemical, and structural properties of transparent and conducting chemically derived graphene thin films, Adv. Funct. Mater. 19 (2009) 2577–2583. https://doi.org/10.1002/adfm.200900166.

[23] S. Shivaraman, R.A. Barton, X. Yu, J. Alden, L. Herman, M.S.V. Chandrashekhar, J. Park, P.L. McEuen, J.M. Parpia, H.G. Craighead, M.G. Spencer, Free-standing epitaxial graphene, Nano Lett. 9 (2009) 3100–3105. https://doi.org/10.1021/nl900479g.

[24] D. Nuvoli, V. Alzari, R. Sanna, S. Scognamillo, J. Alongi, G. Malucelli, A. Mariani, Synthesis and characterization of graphene-based nanocomposites with potential use for biomedical applications, J. Nanoparticle Res. 15 (2013). https://doi.org/10.1007/s11051-013-1512-x.

[25] G.P. Keeley, A. O'Neill, M. Holzinger, S. Cosnier, J.N. Coleman, G.S. Duesberg, DMF-exfoliated graphene for electrochemical NADH detection, Phys. Chem. Chem. Phys. 13 (2011) 7747–7750. https://doi.org/10.1039/c1cp20060g.

[26] J.N. Coleman, Liquid exfoliation of defect-free graphene, Acc. Chem. Res. 46 (2013) 14–22. https://doi.org/10.1021/ar300009f.

[27] A. Baradoke, I. Pastoriza-Santos, E. González-Romero, Screen-printed GPH electrode modified with Ru nanoplates and PoPD polymer film for NADH sensing: Design and characterization, Electrochim. Acta. 300 (2019) 316–323. https://doi.org/10.1016/j.electacta.2019.01.128.

[28] Y. Zhou, F. Cheng, Y. Hong, J. Huang, X. Zhang, X. Liao, Rapid and Sensitive Detection of Isoproturon Via an Electrochemical Sensor Based on Highly Water-Dispersed Carbon Hybrid Material, Food Anal. Methods. (2020). https://doi.org/10.1007/s12161-020-01707-5.

[29] H. Barton, W.M. Berbel-Filho, S. Consuegra, L. Francis, C. Tizaoui, R.S. Conlan, S.R. Teixeira, Ultrasensitive environmental assessment of xeno-estrogens in water samples using label-free graphene immunosensors, Anal. Biochem. 548 (2018) 102–108. https://doi.org/10.1016/j.ab.2018.02.027.

[30] M. Arvand, S. Hemmati, Analytical methodology for the electro-catalytic determination of estradiol and progesterone based on graphene quantum dots and poly(sulfosalicylic acid) co-modified electrode, Talanta. 174 (2017) 243–255. https://doi.org/10.1016/j.talanta.2017.05.083.

[31] G.B. Braga, A.E.F. Oliveira, A.C. Pereira, Total Determination of Estrogenic Phenolic Compounds in River Water Using a Sensor Based

on Reduced Graphene Oxide and Molecularly Imprinted Polymer, Electroanalysis. 30 (2018) 2176–2184. https://doi.org/10.1002/elan.201800238.

[32] B.C. Janegitz, F.A. Dos Santos, R.C. Faria, V. Zucolotto, Electrochemical determination of estradiol using a thin film containing reduced graphene oxide and dihexadecylphosphate, Mater. Sci. Eng. C. 37 (2014) 14–19. https://doi.org/10.1016/j.msec.2013.12.026.

[33] Y. Li, X. Zhao, P. Li, Y. Huang, J. Wang, J. Zhang, Highly sensitive Fe<inf>3</inf>O<inf>4</inf> nanobeads/graphene-based molecularly imprinted electrochemical sensor for 17β-estradiol in water, Anal. Chim. Acta. 884 (2015) 106–113. https://doi.org/10.1016/j.aca.2015.05.022.

[34] T.H. Li, D. Wang, H.Z. Lan, N. Gan, Determination of 17β-estradiol based on electropolymerized-molecularly imprinted polymer on gold nanoparticles-graphene modified electrode, 2014. https://doi.org/10.4028/www.scientific.net/AMR.881-883.93.

[35] L. Hu, Q. Cheng, D. Chen, M. Ma, K. Wu, Liquid-phase exfoliated graphene as highly-sensitive sensor for simultaneous determination of endocrine disruptors: Diethylstilbestrol and estradiol, J. Hazard. Mater. 283 (2015) 157–163. https://doi.org/10.1016/j.jhazmat.2014.08.067.

[36] T. Wen, C. Xue, Y. Li, Y. Wang, R. Wang, J. Hong, X. Zhou, H. Jiang, Reduced graphene oxide-platinum nanoparticles composites based imprinting sensor for sensitively electrochemical analysis of 17β-estradiol, J. Electroanal. Chem. 682 (2012) 121–127. https://doi.org/10.1016/j.jelechem.2012.07.015.

[37] F.C. Moraes, B. Rossi, M.C. Donatoni, K.T. de Oliveira, E.C. Pereira, Sensitive determination of 17β-estradiol in river water using a graphene based electrochemical sensor, Anal. Chim. Acta. 881 (2015) 37–43. https://doi.org/10.1016/j.aca.2015.04.043.

[38] A. Özcan, D. Topçuoğulları, Voltammetric determination of 17-β-estradiol

by cysteamine self-assembled gold nanoparticle modified fumed silica decorated graphene nanoribbon nanocomposite, Sensors Actuators, B Chem. 250 (2017) 85–90. https://doi.org/10.1016/j.snb.2017.04.131.

[39] J.A. Rather, E.A. Khudaish, P. Kannan, Graphene-amplified femtosensitive aptasensing of estradiol, an endocrine disruptor, Analyst. 143 (2018) 1835–1845. https://doi.org/10.1039/c7an02092a.

[40] C. Karuwan, A. Wisitsoraat, D. Phokharatkul, C. Sriprachuabwong, T. Lomas, D. Nacapricha, A. Tuantranont, A disposable screen printed graphene-carbon paste electrode and its application in electrochemical sensing, RSC Adv. 3 (2013) 25792–25799. https://doi.org/10.1039/c3ra44187c.

[41] P. Pasakon, J.P. Mensing, D. Phokaratkul, C. Karuwan, T. Lomas, A. Wisitsoraat, A. Tuantranont, A high-performance, disposable screen-printed carbon electrode modified with multi-walled carbon nanotubes/graphene for ultratrace level electrochemical sensors, J. Appl. Electrochem. 49 (2019) 217–227. https://doi.org/10.1007/s10800-018-1268-1.

[42] A.M. Santos, A. Wong, T.M. Prado, E.L. Fava, O. Fatibello-Filho, M.D.P.T. Sotomayor, F.C. Moraes, Voltammetric determination of ethinylestradiol using screen-printed electrode modified with functionalized graphene, graphene quantum dots and magnetic nanoparticles coated with molecularly imprinted polymers, Talanta. (2020) 121804. https://doi.org/10.1016/j.talanta.2020.121804.

[43] Q. Zhao, Y. Faraj, L.Y. Liu, W. Wang, R. Xie, Z. Liu, X.J. Ju, J. Wei, L.Y. Chu, Simultaneous determination of dopamine, uric acid and estriol in maternal urine samples based on the synergetic effect of reduced graphene oxide, silver nanowires and silver nanoparticles in their ternary 3D nanocomposite, Microchem. J. 158 (2020) 105185. https://doi.org/10.1016/j.microc.2020.105185.

[44] T. Wang, E.P. Randviir, C.E. Banks, Detection of theophylline utilising portable electrochemical sensors, Analyst. 139 (2014) 2000–2003. https://doi.org/10.1039/c4an00065j.

[45] E.M. Kirchner, T. Hirsch, Recent developments in carbon-based two-dimensional materials: synthesis and modification aspects for electrochemical sensors, Microchim. Acta. 187 (2020). https://doi.org/10.1007/s00604-020-04415-3.

[46] A.C. Marques, A.R. Cardoso, R. Martins, M.G.F. Sales, E. Fortunato, Laser-Induced Graphene-Based Platforms for Dual Biorecognition of Molecules, ACS Appl. Nano Mater. 3 (2020) 2795–2803. https://doi.org/10.1021/acsanm.0c00117.

[47] K. Griffiths, C. Dale, J. Hedley, M.D. Kowal, R.B. Kaner, N. Keegan, Laser-scribed graphene presents an opportunity to print a new generation of disposable electrochemical sensors, Nanoscale. 6 (2014) 13613–13622. https://doi.org/10.1039/c4nr04221b.

[48] F.M. Vivaldi, A. Dallinger, A. Bonini, N. Poma, L. Sembranti, D. Biagini, P. Salvo, F. Greco, F. Di Francesco, Three-Dimensional (3D) Laser-Induced Graphene: Structure, Properties, and Application to Chemical Sensing, ACS Appl. Mater. Interfaces. 13 (2021) 30245–30260. https://doi.org/10.1021/acsami.1c05614.

[49] J. Lin, Z. Peng, Y. Liu, F. Ruiz-Zepeda, R. Ye, E.L.G. Samuel, M.J. Yacaman, B.I. Yakobson, J.M. Tour, Laser-induced porous graphene films from commercial polymers, Nat. Commun. 5 (2014) 5–12. https://doi.org/10.1038/ncomms6714.

[50] A.R. Cardoso, A.C. Marques, L. Santos, A.F. Carvalho, F.M. Costa, R. Martins, M.G.F. Sales, E. Fortunato, Molecularly-imprinted chloramphenicol sensor with laser-induced graphene electrodes, Biosens. Bioelectron. 124–125 (2019) 167–175. https://doi.org/10.1016/j.bios.2018.10.015.

[51] K. Settu, Y.C. Lai, C.T. Liao, Carbon nanotube modified laser-induced graphene electrode for hydrogen peroxide sensing, Mater. Lett. 300 (2021) 130106. https://doi.org/10.1016/j.matlet.2021.130106.

[52] R.A. Olowu, O. Arotiba, S.N. Mailu, T.T. Waryo, P. Baker, E. Iwuoha, Electrochemical aptasensor for endocrine disrupting 17β-estradiol based on a Poly(3,4-ethylenedioxylthiopene)-gold nanocomposite platform, Sensors (Switzerland). (2010). https://doi.org/10.3390/s101109872.

[53] Z. Chang, B. Zhu, J.J. Liu, X. Zhu, M. Xu, J. Travas-Sejdic, Electrochemical aptasensor for 17β-estradiol using disposable laser scribed graphene electrodes, Biosens. Bioelectron. 185 (2021) 113247. https://doi.org/10.1016/j.bios.2021.113247.

[54] H. Yoon, J. Nah, H. Kim, S. Ko, M. Sharifuzzaman, S.C. Barman, X. Xuan, J. Kim, J.Y. Park, A chemically modified laser-induced porous graphene based flexible and ultrasensitive electrochemical biosensor for sweat glucose detection, Sensors Actuators, B Chem. 311 (2020) 127866. https://doi.org/10.1016/j.snb.2020.127866.

[55] Y. Yang, H. Hou, G. Zou, W. Shi, H. Shuai, J. Li, X. Ji, Electrochemical exfoliation of graphene-like two-dimensional nanomaterials, Nanoscale. 11 (2019) 16–33. https://doi.org/10.1039/c8nr08227h.

[56] K. Parvez, R. Li, S.R. Puniredd, Y. Hernandez, F. Hinkel, S. Wang, X. Feng, K. Müllen, Electrochemically exfoliated graphene as solution-processable, highly conductive electrodes for organic electronics, ACS Nano. 7 (2013) 3598–3606. https://doi.org/10.1021/nn400576v.

[57] A. Ambrosi, M. Pumera, Electrochemically Exfoliated Graphene and Graphene Oxide for Energy Storage and Electrochemistry Applications, Chem. - A Eur. J. 22 (2016) 153–159. https://doi.org/10.1002/chem.201503110.

[58] C. Karuwan, C. Sriprachuabwong, A. Wisitsoraat, D. Phokharatkul, P. Sritongkham, A. Tuantranont, Inkjet-printed graphene-poly(3,4-

ethylenedioxythiophene):poly(styrene- sulfonate) modified on screen printed carbon electrode for electrochemical sensing of salbutamol, Sensors Actuators, B Chem. 161 (2012) 549–555. https://doi.org/10.1016/j.snb.2011.10.074.

[59] S. Yang, P. Zhang, A.S. Nia, X. Feng, Emerging 2D Materials Produced via Electrochemistry, Adv. Mater. 32 (2020). https://doi.org/10.1002/adma.201907857.

[60] G. Cui, Jae Hyun Yoo, Joung Su Lee, J. Yoo, Jung Hee Uhm, Geun Sig Cha, H. Nam, Effect of pre-treatment on the surface and electrochemical properties of screen-printed carbon paste electrodes, Analyst. 126 (2001) 1399–1403. https://doi.org/10.1039/b102934g.

[61] J.P. Metters, R.O. Kadara, C.E. Banks, New directions in screen printed electroanalytical sensors: An overview of recent developments, Analyst. 136 (2011) 1067–1076. https://doi.org/10.1039/c0an00894j.

[62] R.L. McCreery, M.T. McDermott, Comment on electrochemical kinetics at ordered graphite electrodes, Anal. Chem. 84 (2012) 2602–2605. https://doi.org/10.1021/ac2031578.

[63] Q. Cao, Z. Shao, D.K. Hensley, N. V. Lavrik, B.J. Venton, Influence of Geometry on Thin Layer and Diffusion Processes at Carbon Electrodes, Langmuir. 37 (2021) 2667–2676. https://doi.org/10.1021/acs.langmuir.0c03315.

[64] A.G.M. Ferrari, C.W. Foster, P.J. Kelly, D.A.C. Brownson, C.E. Banks, Determination of the electrochemical area of screen-printed electrochemical sensing platforms, Biosensors. 8 (2018) 1–10. https://doi.org/10.3390/bios8020053.

[65] S.J. Konopka, B. McDuffie, Diffusion Coefficients of Ferri- and Ferrocyanide Ions in Aqueous Media, Using Twin-Electrode Thin-Layer Electrochemistry, Anal. Chem. 42 (1970) 1741–1746. https://doi.org/10.1021/ac50160a042.

[66] A. Morrin, A.J. Killard, M.R. Smyth, Electrochemical characterisation and home-made screen-printed carbon electrodes, Anal. Lett. 36 (2003) 2021–2039. https://doi.org/10.1081/AL-120023627.

[67] E.P. Randviir, D.A.C. Brownson, M. Gómez-Mingot, D.K. Kampouris, J. Iniesta, C.E. Banks, Electrochemistry of Q-Graphene, Nanoscale. 4 (2012) 6470–6480. https://doi.org/10.1039/c2nr31823g.

[68] X. Fan, Y. Xu, T. Sheng, D. Zhao, H. Yuan, F. Liu, X. Liu, X. Zhu, L. Zhang, J. Lu, Amperometric sensor for dopamine based on surface-graphenization pencil graphite electrode prepared by in-situ electrochemical delamination, Microchim. Acta. 186 (2019) 1–8. https://doi.org/10.1007/s00604-019-3430-9.

[69] C. Fenzl, P. Nayak, T. Hirsch, O.S. Wolfbeis, H.N. Alshareef, A.J. Baeumner, Laser-Scribed Graphene Electrodes for Aptamer-Based Biosensing, ACS Sensors. 2 (2017) 616–620. https://doi.org/10.1021/acssensors.7b00066.

[70] Y.P. Ding, W.L. Liu, Q.S. Wu, X.G. Wang, Direct simultaneous determination of dihydroxybenzene isomers at C-nanotube-modified electrodes by derivative voltammetry, J. Electroanal. Chem. 575 (2005) 275–280. https://doi.org/10.1016/j.jelechem.2004.09.020.

[71] G. Ziyatdinova, A. Gainetdinova, M. Morozov, H. Budnikov, S. Grazhulene, A. Red'kin, Voltammetric detection of synthetic water-soluble phenolic antioxidants using carbon nanotube based electrodes, J. Solid State Electrochem. 16 (2012) 127–134. https://doi.org/10.1007/s10008-011-1295-x.

[72] P. Nicholas, R. Pittson, J.P. Hart, Development of a simple, low cost chronoamperometric assay for fructose based on a commercial graphite-nanoparticle modified screen-printed carbon electrode, Food Chem. 241 (2018) 122–126. https://doi.org/10.1016/j.foodchem.2017.08.077.

[73] S. Hashemnia, S. Khayatzadeh, M. Hashemnia, Electrochemical

detection of phenolic compounds using composite film of multiwall carbon nanotube/surfactant/tyrosinase on a carbon paste electrode, J. Solid State Electrochem. 16 (2012) 473–479. https://doi.org/10.1007/s10008-011-1355-2.

[74] Y. Sun, K. Wu, S. Hu, Fabrication of a multi-wall carbon nanotubes modified glassy carbon electrode and its catalytic effect on the oxidation of estradiol, estrone and estriol, Mikrochim. Acta. 142 (2003) 49–53. https://doi.org/10.1007/s00604-003-0949-5.

[75] I. V. Batista, M.R.V. Lanza, I.L.T. Dias, S.M.C.N. Tanaka, A.A. Tanaka, M.D.P.T. Sotomayor, Electrochemical sensor highly selective for estradiol valerate determination based on a modified carbon paste with iron tetrapyridinoporphyrazine, Analyst. 133 (2008) 1692–1699. https://doi.org/10.1039/b804462g.

[76] M. Berovic, M. Legisa, Citric acid production, Biotechnol. Annu. Rev. 13 (2007) 303–343. https://doi.org/10.1016/S1387-2656(07)13011-8.

[77] S. Motoc, A. Remes, A. Pop, F. Manea, J. Schoonman, Electrochemical detection and degradation of ibuprofen from water on multi-walled carbon nanotubes-epoxy composite electrode, J. Environ. Sci. (China). 25 (2013) 838–847. https://doi.org/10.1016/S1001-0742(12)60068-0.

[78] S. Campuzano, M. Pedrero, M. Gamella, V. Serafín, P. Yáñez-Sedeño, J.M. Pingarrón, Beyond sensitive and selective electrochemical biosensors: Towards continuous, real-time, antibiofouling and calibration-free devices, Sensors (Switzerland). 20 (2020) 1–22. https://doi.org/10.3390/s20123376.

[79] B.L. Hanssen, S. Siraj, D.K.Y. Wong, Recent strategies to minimise fouling in electrochemical detection systems, Rev. Anal. Chem. 35 (2016) 1–28. https://doi.org/10.1515/revac-2015-0008.

[80] J. Song, J. Yang, X. Hu, Electrochemical determination of estradiol using a poly(l-serine) film-modified electrode, J. Appl. Electrochem. 38 (2008)

833–836. https://doi.org/10.1007/s10800-008-9520-8.

[81] X. Lin, Y. Li, A sensitive determination of estrogens with a Pt nano-clusters/multi-walled carbon nanotubes modified glassy carbon electrode, Biosens. Bioelectron. 22 (2006) 253–259. https://doi.org/10.1016/j.bios.2006.01.005.

[82] K. Muzyka, G. Xu, Laser-induced Graphene in Facts, Numbers, and Notes in View of Electroanalytical Applications: A Review, Electroanalysis. 34 (2022) 574–589. https://doi.org/10.1002/elan.202100425.

[83] A.J. Killard, S. Zhang, H. Zhao, R. John, E.I. Iwuoha, M.R. Smyth, Development of an electrochemical flow injection immunoassay (FIIA) for the real-time monitoring of biospecific interactions, Anal. Chim. Acta. 400 (1999) 109–119. https://doi.org/10.1016/S0003-2670(99)00611-X.

[84] K. Grennan, A.J. Killard, M.R. Smyth, Physical characterizations of characterisations of electrode for use in an amperometric biosensor system, Electroanalysis. 13 (2001) 745–750. https://doi.org/10.1002/1521-4109(200105)13:8/9<745::AID-ELAN745>3.0.CO;2-B.

[85] T.J. Davies, R.G. Compton, J. Electroanal. Chem. 585 (2005) 63.

[86] Istrate, O.M., Rotariu, L. and Bala, C., 2021. Amperometric L-Lactate biosensor based upon a gold nanoparticles/reduced graphene oxide/polyallylamine hydrochloride modified screen-printed graphite electrode. Chemosensors, 9(4), p.74.

Chapter 5 Gold Nanoparticle Decorated Reduced Graphene Oxide Carbon Nanotubes Composites

5.1 Introduction

The previous chapter (4) illustrated the use of graphene based SPEs for the amperometric measurement of E2. However, despite the promising results and ease of preparation of graphene by electrochemical exfoliation, these electrodes are limited in outcomes used in electroanalysis due to their small active area, demonstrating the importance of electrode geometry for enhanced sensor performance. With that in mind, gold nanoparticles (AuNPs), graphene and carbon nanotubes (CNTs) provide their features as a composite and allow fast electron transfer on the electrode. The hybrid electrode is fabricated using a green approach. The facile strategy consists of using a plant extract to synthesise AuNPs and reduce graphene oxide to graphene with the integration of CNTs. As a result, they benefit from low costs, are highly sensitive, and have been extensively used for electroanalysis. The work of Chapter 5 has been published in the journal Biosensors.

Over the past few decades, researchers have used electrochemical methods to accumulate various analytes on electrode surfaces using adsorptive stripping voltammetry as a possible replacement for traditional analytical techniques and to overcome associated drawbacks [4]. Disposable screen-printed electrodes (SPEs) have been given considerable attention among these electrochemical methods. They are a promising alternative to the common micro three-electrode setup in terms of portability, measurement speed, mass production and low cost

[5,6]. However, some of the components within the ink formulation of an SPE are non-conductive, resulting in poor conductivity and performance, ultimately affecting the sensitivity of the SPE. E2 measurements have been reported on electrode surfaces [7,8,17,18,9-16]. Electrochemical oxidation of the phenolic group within the hormones results in electrode fouling due to forming an insoluble layer on the working electrode. However, as the electrochemical oxidation of E2 is irreversible due to the presence of the phenolic group, a non-conductive layer is formed on the electrode, leading to the passivation of the electrode (fouling) [15-18].

Consequently, a low current generation is reported [19], which calls for developing new materials for SPEs with improved performance [20]. Furthermore, it is well known that sensing materials play a vital role in electrochemical sensing [21]. Carbon-based nanomaterials have been incorporated into the design of electrochemical sensors to detect many analytes [22]. CNT and graphene (Gr) are the most utilised carbon nanomaterials in SPE sensor fabrication [23]. This is due to high conductivity, sizeable electrochemical potential windows, specific surface area, and electrochemical stability. These are essential considerations for any ideal and potential materials used in electrode modification [20,24,25]. CNTs are widely employed in modifying electrodes for electrochemical measurements as they promote electron transfer reactions and enhance electrochemical reactivity [26]. Combining graphene and CNT as a composite has been extensively studied in various electrochemical sensor applications [27].

CNT and the Gr material must be dispersed in solvents and surfactants to make it suitable for electrode modification [28]. However, the abundant oxygen in graphene oxide can also serve as a dispersant of CNTs to improve the resulting composite properties. In addition, the CNTs prevent the irreversible aggregation of graphene. Thus, carefully tailoring these materials and developing hybrid composites promises to enhance the limitations of each material [29]. Graphene has been adopted in electrochemical sensor design due to its specific surface area and electronic transfer properties [30,31].

Furthermore, graphene has been reported to have few oxygen groups on its surface, which makes it less prone to fouling [32]. However, there is a setback to graphene surface area distortion due to the strong van der Waals force of attraction between the graphene layers, leading to aggregation resulting in a reduction in the availability of graphene surface area [33,34]. One way to circumvent this is doping the graphene with nanoparticles (NPs), an active research area under intensive study. Pumera et al. highlighted critical applications of graphene in sensing and bio-sensing into i) directly using graphene powder or graphene-composite as a transducer to modified electrodes for electrochemical sensing, ii) incorporating bio-recognition compounds for biosensing [35].

Gold nanoparticles (AuNPs) have been extensively used in the design of sensitive electrochemical sensors due to their high stability, biocompatibility, tuning with other sensor surfaces, ease of synthesis, good thermal and electrical conductivity, chemical stability, and good electrocatalytic properties [20,36–38]. Recently, AuNPs have been applied to EDC sensors [39,40]. An endocrine-

disrupting MIP-aptasensor was developed for Bisphenol A (BPA) detection using AuNPs as amplifiers [41]. Carbonous nanomaterials, such as carbon nanotubes and graphene, have been utilised as supports to immobilise metal nanoparticles for electrocatalytic applications [42]. The use of various materials as composites allows the synergy between each material as a means of enhancing the limitation of each material. Thus improving the electrochemical sensitivity of the sensors [43]. Currently, synthesised gold-based composites are applied to designing sensors to determine phenolics [44]. Recently, there has been development in sensing platforms based on gold-carbon composites such as AuNPs-carbon nanotubes and AuNPs-graphene hybrids for electrochemical sensors for the measurements of phenolics. These materials display various properties derive from their distinctive features, including high conductivity, facilitated electron transfer kinetics, and large surface area. Carbon-based materials such as CNTs can be easily modified with AuNPs for sensor application. Gold can be attached to CNTs, and the CNT can serve as a wire to other structures in the form of Au-S bond (self-assembly) and non-covalent links such as π-π stacking and electrostatic forces [38,45].

Several synthesis routes have been reported for AuNPs, including physical, chemical, biological, and electrochemical [38]. Among the various routes reported for synthesising NPs like AuNPs, the use of plant extracts as reducing agents (bio-reductants) for synthesising metallic nanoparticles has been extensively studied [46,47]. These remove the need for toxic, corrosive, and hazardous chemicals to the environment. For example, AuNPs have been prepared using Lemongrass (*Cymbopogon citratus*) [48], *Zingiber oicinale* [49],

Acalypha indica [50], *Abelmoschus esculentus* [51] and bay leaf extract (*Syzygium polyanthum*) [52]. Another application of plant extract as a reductant for reducing graphene oxide using a green approach has been reported with over 50 plant species [53,54] as an alternative to electrochemical reduction, thermal reduction, and photocatalytic reduction [54]. Bay leaf extract (*Syzygium polyanthum*) was chosen in this study as it has been reported to successfully synthesised AuNPs in which plant extracts mediated the reduction of Au metal ions [52] and also reported in the reduction of graphene oxide, thus allowing dual-purpose in this regards with the need for stabilising/capping agents [55]. Compared to a two-step approach, the one-step reduction was much more straightforward in obtaining the composite with high performance [55].

This chapter explores a 'green approach' for synthesising AuNPs doped on reduced graphene oxide-multiwalled CNTs (rGO/AuNP/CNT) composite material. Chapter 3 indicates that our SPE is not solvent-friendly, and modification with solvent material can affect sensor performance. Therefore, we combine gold nanoparticle synthesis with plant extract and reduction of graphene oxide with plant extract in addition to CNTs to circumvent problems such as stacking CNT and using a benign solvent in one approach to disperse the materials. As a result, this will envisage the E2 screen-printed sensor exhibiting remarkable performance, a stable electrode surface, and fast sensing. In addition, the green approach to AuNP synthesis, which has good stability and little or no toxicity, is discussed. It is soluble in a benign solvent in line with the twelve principles of green chemistry for the fabrication of electrochemical sensors [56,57].

Using gold nanoparticles (AuNPs) in electrochemical sensors significantly improves their capabilities. It has been similarly exploited due to excellent electrical conductivity and can facilitate electron transfer [40]. Nazarpour et al. (2020) demonstrated the green synthesis of reduced graphene oxide/gold nanoparticles (rGO/AuNPs) for the sensitive detection of tryptophan [58]. Fei et al. reported an impedimetric aptasensor utilising AuNP-decorated multiwalled carbon nanotube-reduced graphene oxide nanoribbon composites showing enhanced sensitivity to tryptophan [59]. Incorporating AuNPs into sensor fabrication results in an increased surface area for better analyte interaction, improved electrical conductivity for enhanced signal transduction catalytic activity, and, thus, improved sensor performance [58-61]. Thus, these studies reinforce the significance of ongoing research and development in this area using this approach. In conclusion, using AuNPs enhances the sensor's performance. AuNPs can enhance the electron transfer, sensor stability, and sensitivity characteristics of electrochemical sensors, as reported by [58-61].

5.2 Materials and Methods

5.2.1 Materials

Graphene oxide (GO), Multiwalled carbon nanotube (MWCNT), Bay leaf extract, Gold (III) chloride trihydrate $HAuCl_4$. $3H_2O$, 17β-Estradiol (E2) standard, Sodium hydroxide (NaOH), Potassium ferricyanide [$K_3Fe(CN)_6$], Potassium ferrocyanide [$K_4Fe(CN)_6$], Potassium chloride (KCl), Glacial acetic acid, Phosphoric acid, Boric acid, and Sulfuric acid (H_2SO_4), were purchased from Sigma-Aldrich (Gillingham, UK). Deionised water obtained from a Suez Water System (UK) was used to prepare reagents for solution throughout the study. An E2 (0.01 M) stock was

prepared in ethanol stored at +4^{o}C. Britton-Robinson buffer solution (B-R) was made from (0.04 M) acetic acid, boric acid (0.04 M) and phosphoric acid (0.04 M); NaOH was used for the preparation of varying pH 2-8 buffer solutions. Working standards solutions of appropriate concentrations were made by diluting the stock solution with buffer. All glassware and plastic containers were washed using isopropanol, acetone, and deionised water.

5.2.2 Instrumentation

All voltammetric measurements were carried out using a PalmSens EmStat3 Potentiostat (PalmSens BV Houten, the Netherlands) and PSTrace 5.8 software for instrument control and data acquisition during the voltammetric measurements. Screen-printed carbon electrodes (SPEs) were obtained from Palintest Limited (Gateshead, UK). They were used in a three-electrode system, including a working electrode, a carbon counter-electrode, and a silver reference electrode. The working electrode was modified in some cases. Cyclic voltammograms were initially recorded with blank buffer solutions and then in the same solutions containing E2. A starting potential of 0.0 V, an initial switching potential of 0.8 V, and an end potential of 0.0 V were utilised. Differential pulse voltammetry (DPV) was undertaken using a starting potential of 0.0 V and a final potential of 0.8 V, using a step height of 7 mV, pulse repetition time of 0.5 s, and pulse amplitude of 100 mV. The DPV parameters were selected based on previous works reported in the literature for E2 sensing [51].

5.2.3 Atomic force Microscopy (AFM)

The surface topography of the prepared material was measured by employing a Bruker-Innova Atomic Force Microscope (AFM) (UK). An Innova atomic force

microscope (Bruker, UK) was used for AFM imaging. The images were acquired in tapping mode using aluminium-coated silicon probes with a spring constant of 2.8 N/m and a resonant frequency of 75 kHz. After scanning the samples, the images were processed and analysed using Nanoscope software (Bruker, UK) with plane fitting.

5.2.4 Fourier Transform infrared spectroscopy (FTIR)

Attenuated total reflectance-Fourier transform infrared spectroscopy (ATR-FTIR) Fourier-transform infrared spectroscopy (FTIR) analyses were carried out as described in Chapter 3 using FT-IR (PerkinElmer).

5.2.5 Scanning Electron Microscopy (SEM)

SEM measurements were carried out as described in Chapter 3.

5.2.6 Ultraviolet-visible (UV-vis) spectroscopy

Ultraviolet-visible (UV-Vis) absorption spectroscopic measurements were performed using a Cary 60 Agilent Cary 60 UV-VIS spectrophotometer (Santa Clara, United States).

5.3 Preparation of Gold Nanoparticle Decorated Reduced Graphene Oxide Carbon Nanotubes Composites

Gold-nanoparticle-decorated reduced graphene/carbon nanotube composites were prepared using methods adapted from our group, with a few modifications [52]. Briefly, Bay leaf extract was prepared by grinding dried bay leaves to a powder, adding the powdered leaves to deionised water at 80 °C for 10 min, and then straining and centrifuging the resultant solution to remove plant material. The bay leaf extract was stored at 4 ^{o}C and used within four weeks. Equal volumes of the abovementioned GO suspension, bay leaf extract, and $HAuCl_4$

(10 mM) (1:1:1) v/v/ were then mixed and kept overnight for nanoparticle formation, where the light-yellow-coloured mixture changed to a wine-red colour, indicating the formation of AuNPs [53]. The decorated graphene oxide containing AuNPs was extracted by centrifugation at 4,032 × g (5000 rpm) for 15 min, washed three times in deionised water, and then suspended again in deionised water with the concentration of GO set to 0.05 mg/mL. Carbon nanotubes (0.1 mg/mL) were added to the rGO-AuNPs and then ultrasonicated for three hours to ensure complete dispersion of the rGO-AuNPs/CNT. Finally, the SPE was modified with rGO-AuNPs/CNT by drop-casting suspensions of either 0.3, 0.5, 0.7, or 1.0 µL on the working electrode of the SPE. These were then allowed to dry at room temperature. An untreated MWCNT/GO concentration dispersion was also created. As previously stated, AuNP solutions without GO or CNTs were prepared for characterisation. A graphical representation of the modification steps for the fabrication of the rGO-AuNP/CNT/SPE sensor is shown in Figure 5.1.

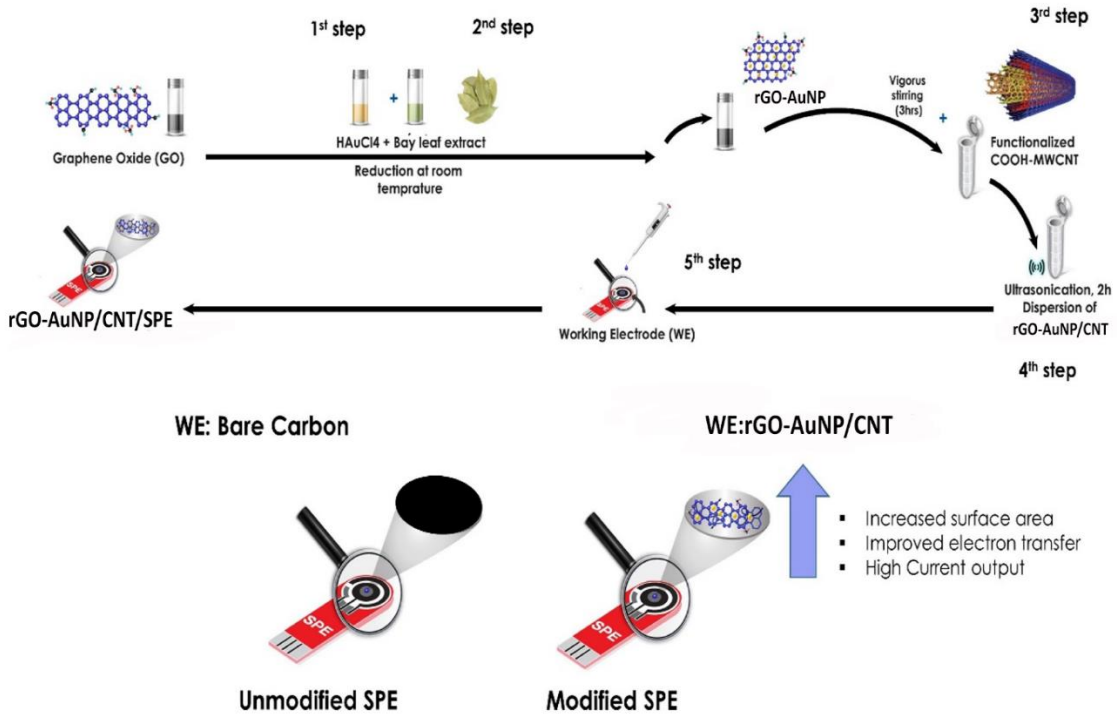

Figure 5.1 represents the rGO-AuNP/CNT modified screen-printed electrode fabrication process.

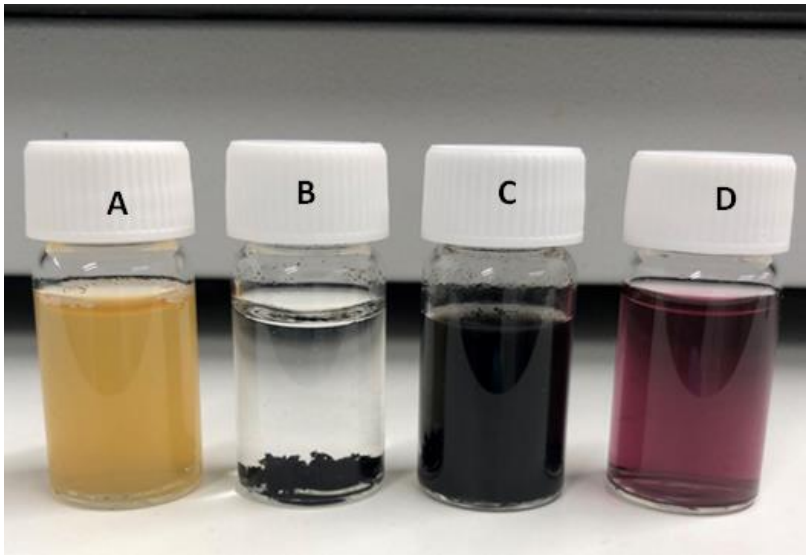

Figure 5.2 Photograph of (A) Bay leaf extract (B) carbon-nanotubes in water (C) Gold nanoparticle on graphene oxide-carbon nanotubes D) Gold nanoparticle.

5.4 Results and Discussion

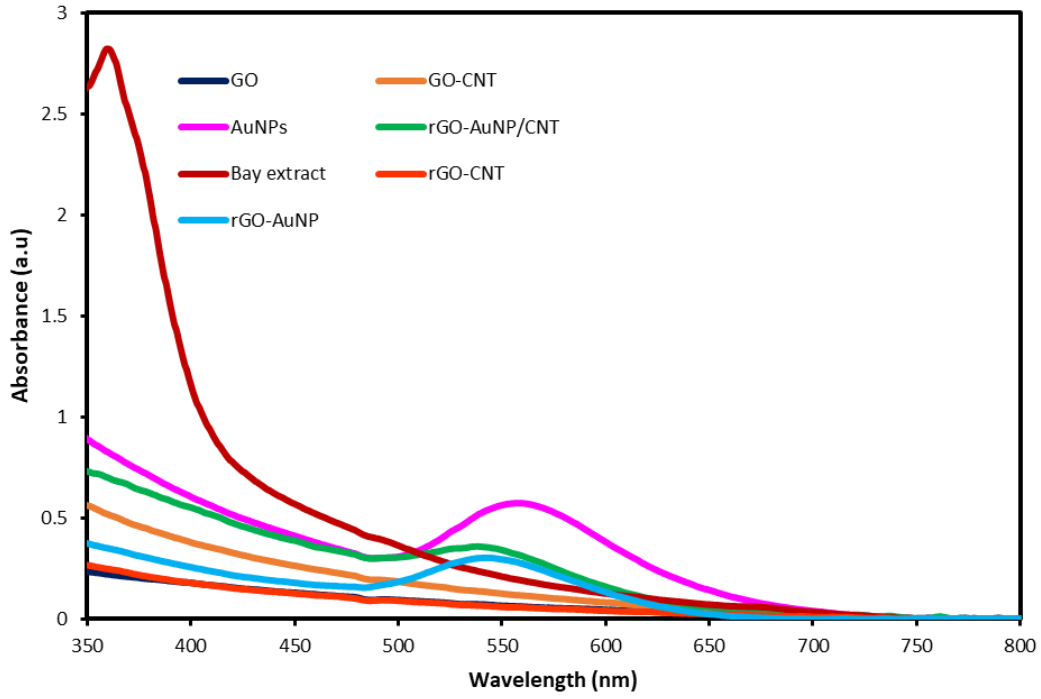

Figure 5.3: UV−vis absorbance spectra of GO, AuNPs, bay laurel extract, rGO-AuNPs, GO-CNT, rGO-CNT, and rGO-AuNPs/CNT.

Figure 5.3 shows the UV–Vis spectra of bay leaf extract, rGO-AuNPs/CNT, AuNPs, rGO-AuNP, rGO-CNT, GO/CNT, and GO. The spectrum of AuNP shows a sharp absorption peak at 560 nm, a typical absorption peak range for gold nanoparticles, evidencing the formation of the gold nanoparticles using bay leaf extract. This concurred with results in the literature, which presented an absorbance of gold nanoparticle solutions in the 500 - 550 nm range, as indicated in [52]. The absorption peaks observed here correspond to the wavelengths reported in the literature for AuNPs at 520, 522, 524, 528, and 530 nm [53]. They are consistent with the typically quoted absorption seen at 500–550 nm for AuNPs [71]. The difference in peak values (absorption) compared to the reports in the literature can be attributed to the presence of GO in the solution. No peaks were seen for GO, rGO-CNT, and bay leaf extract. Wang et al. reported the GO spectrum peak at 226 nm [59]. A shoulder at ~300 nm can be attributed to the n→π* transition of the carbonyl groups (C=O bond), like a previous report [60]. However, this study was carried out between 350 and 800 nm, which would explain why no GO peaks were recorded. These absorption peaks cannot be seen in the spectrum of rGO-AuNPs/CNT, indicating that these free carboxyl groups are committed to accommodating AuNPs. Figure 5.2. show the photograph image of (A) Bay leaf extract, (B) carbon nanotubes in water, (C) gold nanoparticle reduced/graphene oxide-carbon nanotubes, and (D) gold nanoparticles at various stages of the fabrication process.

5.4.1 Surface Characterisation

Morphological characterisation was carried out using scanning electron microscopy (SEM) to characterise the morphology of electrodes, both modified

and unmodified. SEM measurements were performed on the Bare SPE, modified GO/CNT/SPE and rGO-AuNP/CNT/SPE, and the resulting images are shown in Figures 5.4, 5.6, and 5.7. SEM images show the surface morphology of the modified electrodes with graphene oxide-carbon nanotube (GO/CNT/SPE) Figure 5.4 and gold nanoparticles (AuNP) decorated on reduced graphene oxide-carbon nanotube rGO-AuNP/CNT/SPE Figure 5.7 at magnification 25,000x. Figure 5.8 shows rGO-AuNP/CNT/SPE at 50,000x magnification. Figure 5.5 shows the energy-dispersive X-ray spectrometer (EDS) image. The remaining figures present images of SEM-EDS mappings of C, O, Cl and Au elements for the rGO-AuNP/CNT/SPE (Figure 5.9). To confirm the assembly of AuNPs, the surface composition of the rGO-AuNP/CNT composite was analysed using EDS analysis. The observed Au and C element peaks indicated AuNPs were incorporated in the composite, as shown in Figure 5.9; the main co-existent elements of rGO-AuNP/CNT are C, Cl, O and Au, indicating the successful assembly of AuNPs, unlike bare SPE, which are C, O, and Cl elements in Figure 5.5. We speculated that the Cl might stem from the SPE itself, as seen in bare SPE.

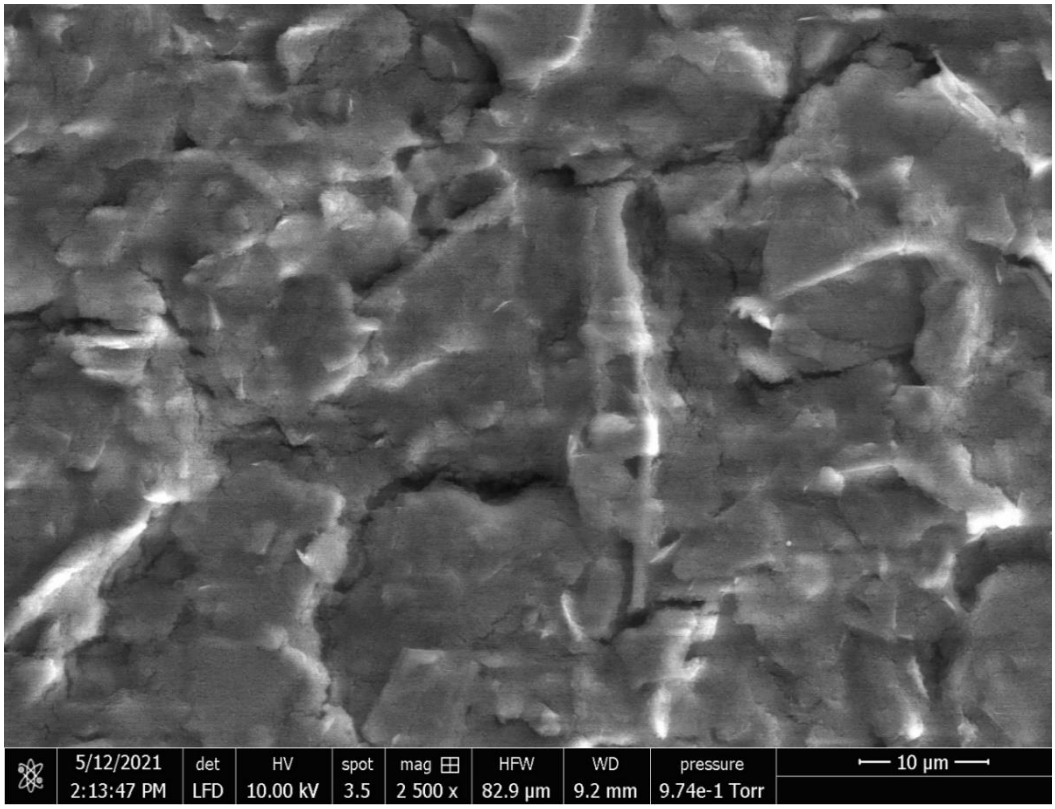

Figure 5.4 SEM image of Bare SPE at magnification 25,00x

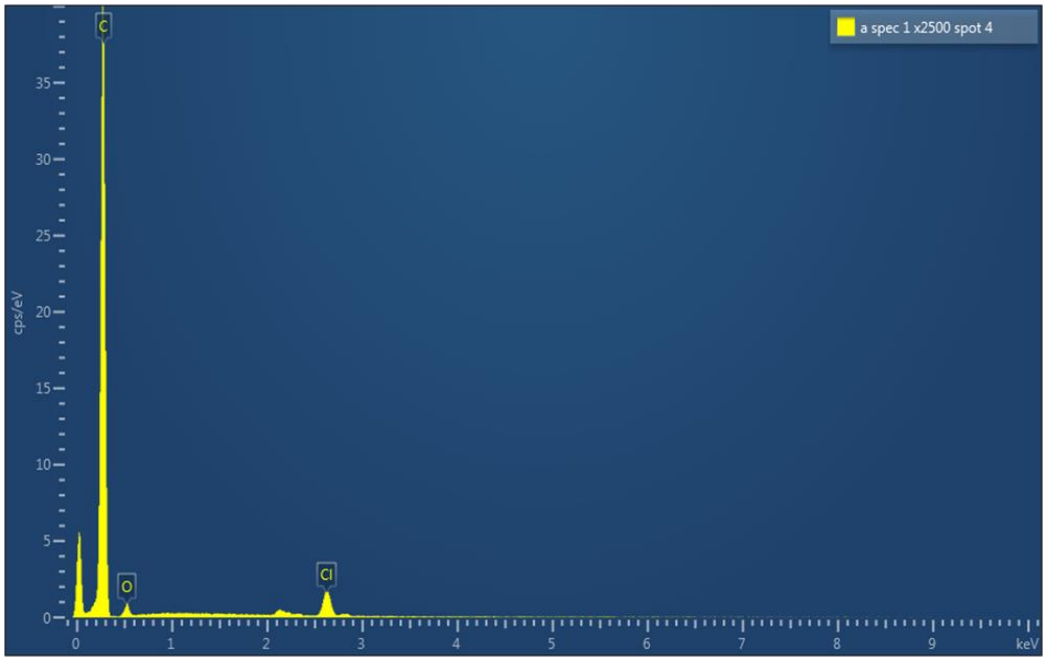

Figure 5.5 EDS image of Bare SPE shows C, O, and Cl elements.

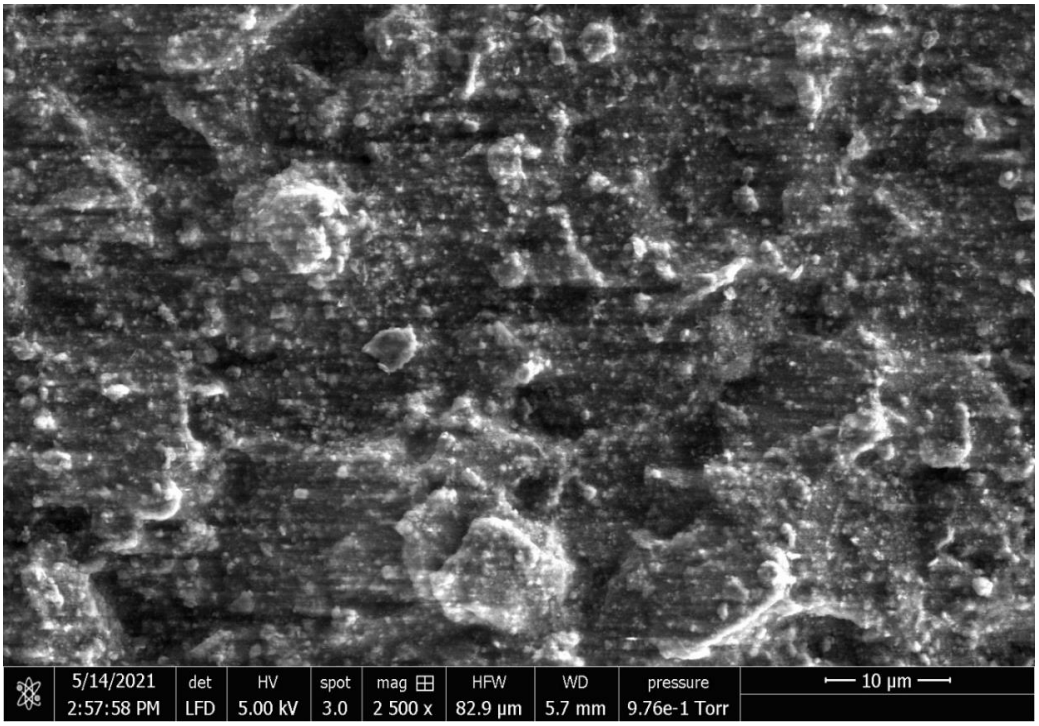

Figure 5.6. SEM image of GO/CNT/SPE

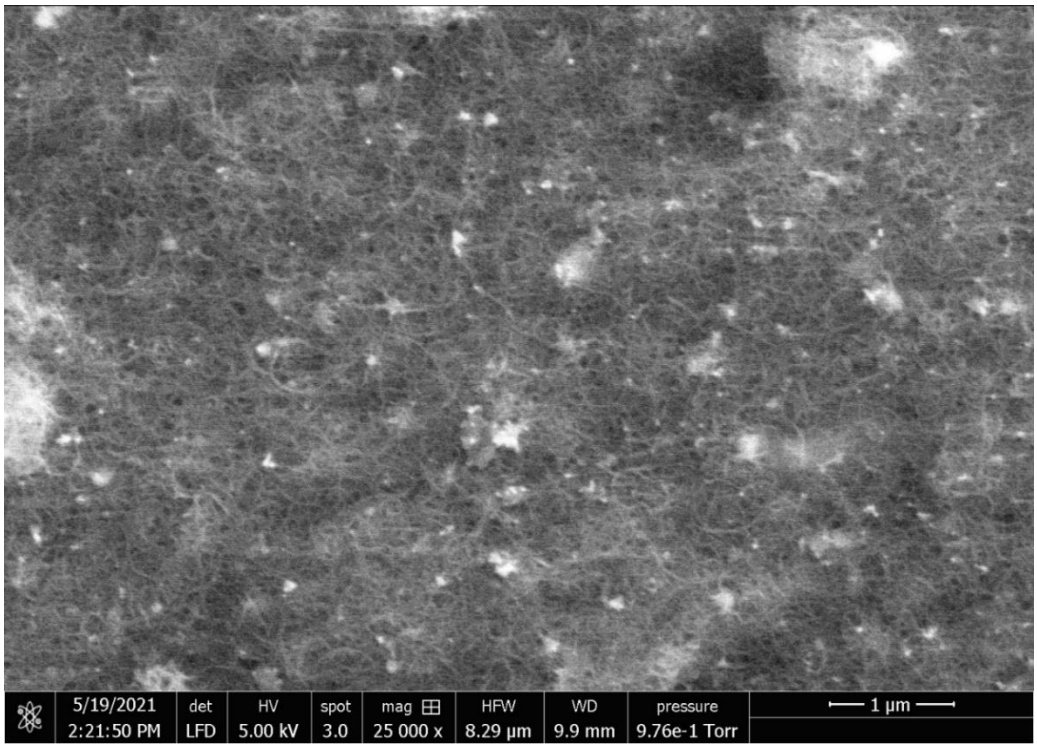

Figure 5.7. SEM image of rGO-AuNP/CNT/SPE at magnification 25,000x

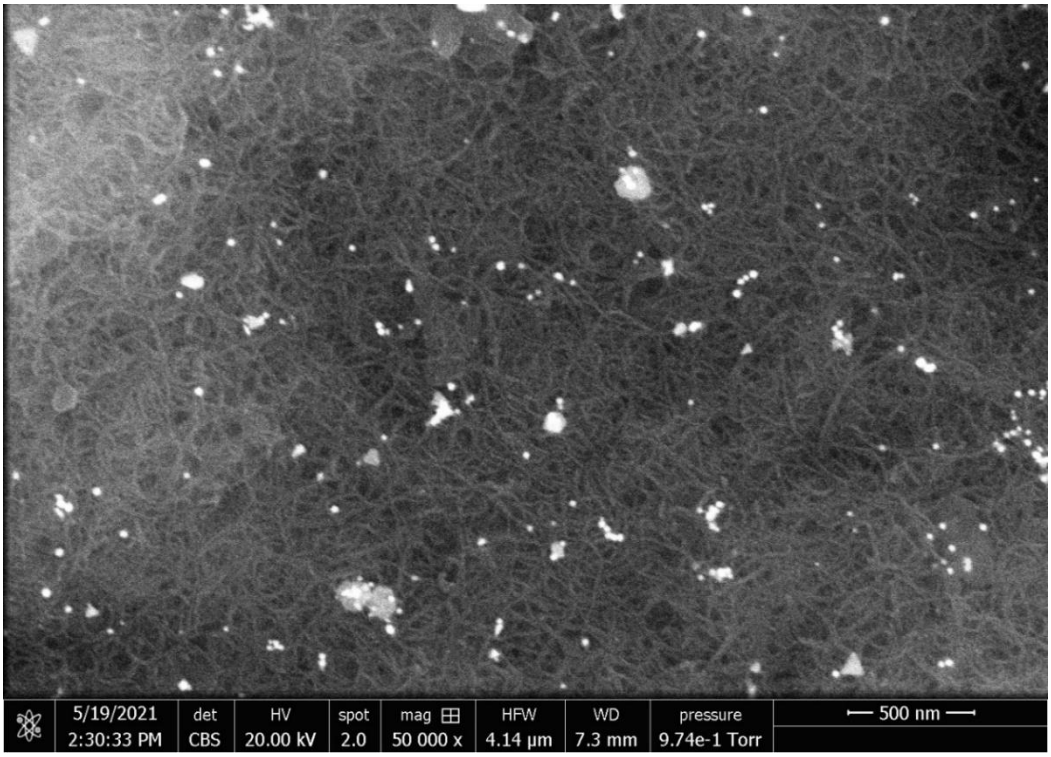

Figure 5.8. SEM image of rGO-AuNP/CNT/SPE at magnification 50,000x

Figures 5.4, 5.6, 5.7, and 5. 8 indicate a surface structure change with the different modifiers. Figure 5.4 of bare SPE shows graphitic sheet-like structures typical of SPE. According to the composition of the electrode, these structures can be assigned as graphitic carbon powder. Some SPE shows small particles dispersed throughout the surface electrodes based on the different curing temperatures suggested by Killard et al. [61,62] and the composition of the ink. These structures noticed can be assigned as graphitic graphite particles. Figure 5.4 has a coarse system, illustrating typical graphene oxide features in a non-uniform pattern from different oxidation of graphite. Figure 5.7 shows uniform meshed-like structures that observe the presence of rGO-AuNP/CNT, which covered and bridged the graphene sheet and small particles of gold nanoparticles. The figure shows the CNT interwoven mesh of nanotubes, with thin layers of space between each nanotube [63]. This can be attributed to

reducing the graphene oxide to sheet-like graphene with 'sprinkled' gold nanoparticles. The SEM image of rGO-AuNP/CNT/SPE (Figure 5.7) depicts a well-decorated graphene oxide-carbon nanotube at 25 000x magnification (Figure 5.7). Gold nanoparticles in the composites have the advantage of a) bioreduction without a hazardous reducing agent such as sodium borohydride and b) Gold particles can be attached to the surface more accessible to the rGO/CNT surface [59,64,65]. Figure 5.10 shows elemental mapping distributions of C (a), O (b), Cl (c) and (d) Au elements for the rGO-AuNP/CNT. From Figure 5.10, the homogeneous distribution of all elements was observed. Jian et al. reported similar results for the electrochemically reduced graphene oxide/gold nanoparticles [66]. EDS spectra (Figure 5.9) suggest that the composite mainly includes the elements of C, O, Au, and Cl. A similar phenomenon has been reported in the electrochemically synthesized AuNPs/single-walled carbon nanotubes hybrids [43]. The surface of GO-CNT is shown in Figure 5.6. Graphene oxide has been described to have individual sheets formed as bundles.

In contrast, reduced graphene has a flocculent flake layer [67]. However, in the presence of CNT, the nature of graphene was different, as revealed in the study [68]. GO-CNT is not comparable with rGO-AuNP/CNT material, which is smoother than GO-CNT, which appears clumped and stacked, a common feature of GO-CNT in a composite [69].

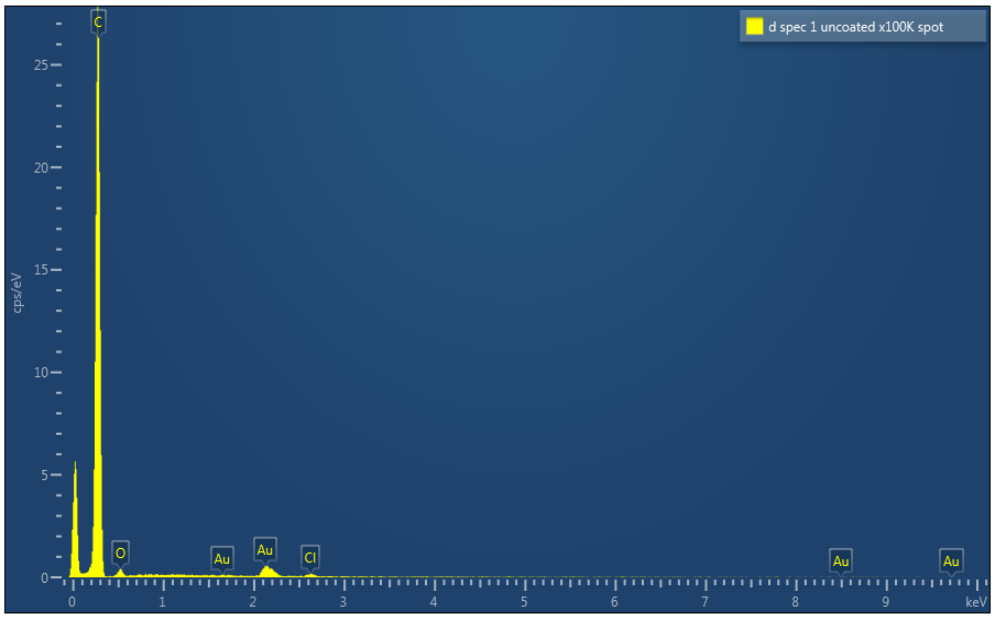

Figure 5.9. The EDS image of rGO-AuNP/CNT/SPE shows C, O, Cl, and Au elements.

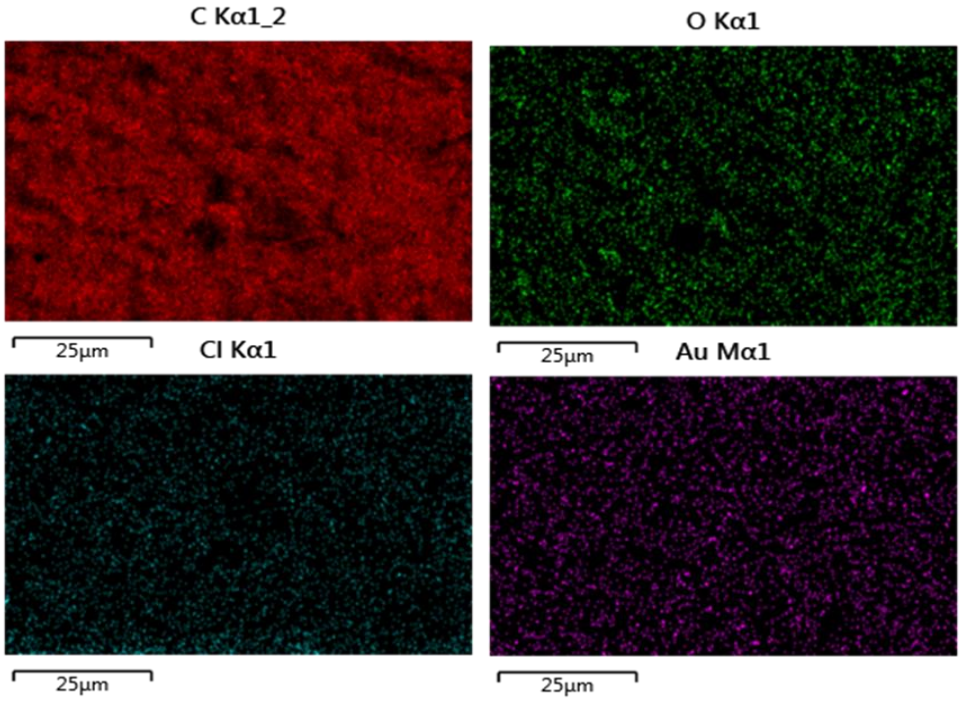

Figure 5.10 Elemental mapping of C (a), O (b), Cl (c) and (d) Au elements for the rGO-AuNP/CNT/SPE.

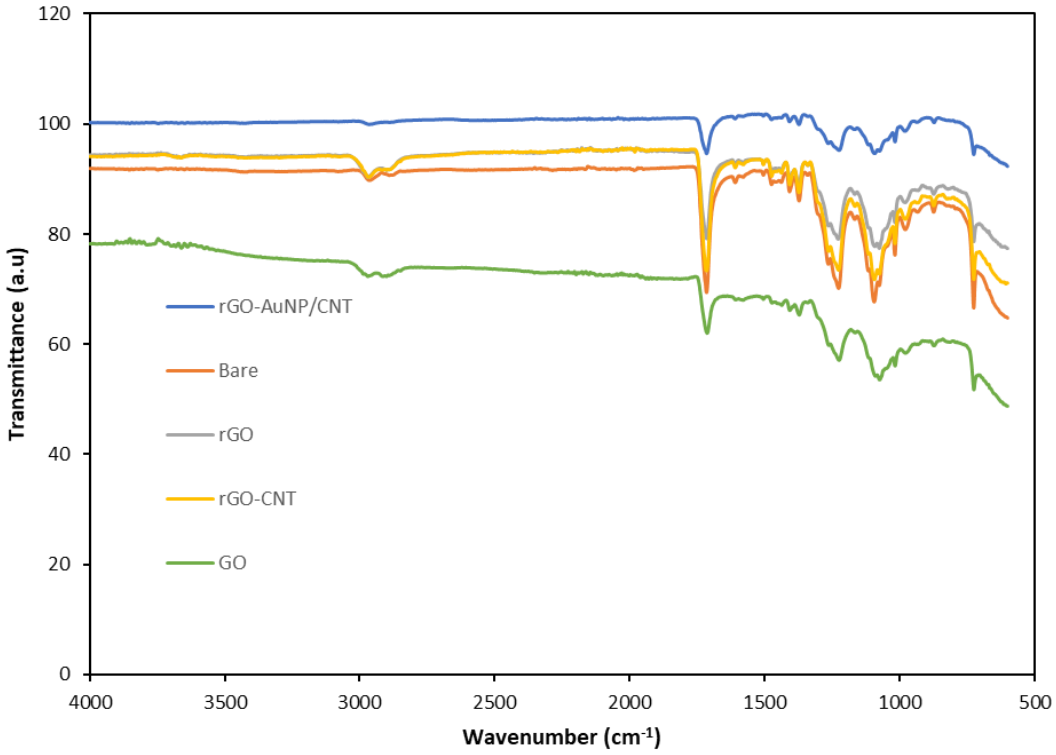

Figure 5.11: FTIR spectra of rGO-AuNPs/CNT/SPE, rGO, rGO-CNT, GO and bare SPE.

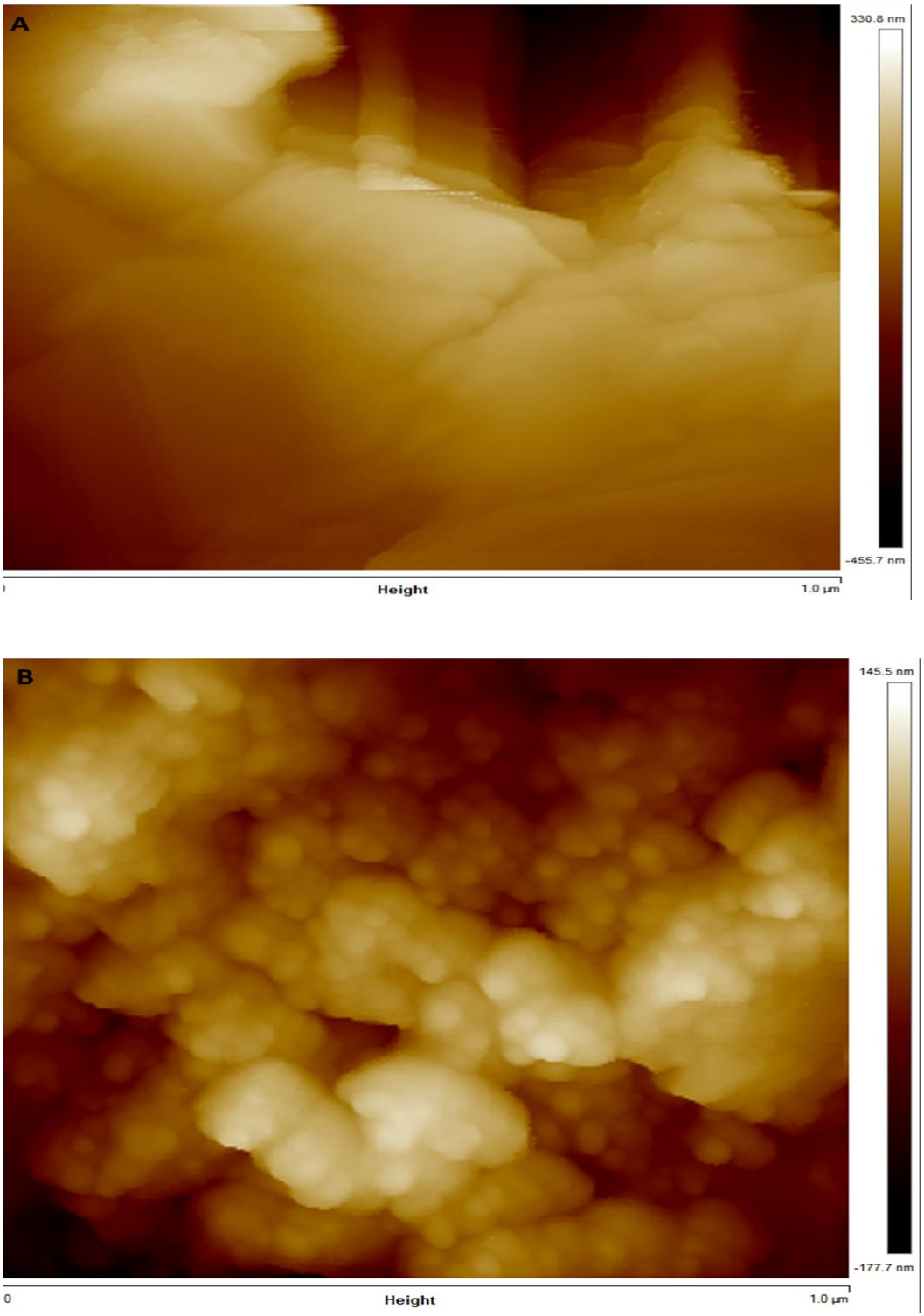

Figure 5.12: A) AFM image of rGO-AuNP/CNT/SPE B) AFM image of bare SPE.

The FTIR spectrum of the bare SPE (illustrated by the orange spectrum in Figure 5.11) demonstrates distinct peaks at 2966 cm^{-1},1714 cm^{-1}, 1227 cm^{-1}, and 1094 cm^{-1} that correspond to OH, CH_3, $COOCH_3$, and C=O functional groups, respectively. These same functional groups were identified but not well-defined as the peaks in the rGO-CNT/AuNPs (depicted by the blue spectrum in Figure 5.11), indicating that oxygen functionalities had been eliminated during reduction. A similar occurrence has been reported with plant extract-converted graphene nanosheets (PCGN) [68].

Furthermore, we examined the morphological characterisation of surface topography and roughness [68] of the rGO-AuNPs/CNT using atomic force microscopy (AFM). The respective AFM images of bare and rGO-AuNP/CNT SPEs in Figure 5.12A display morphological AFM images of the rGO-AuNP/CNT composite material, indicating a thick compacted uniform sheet [68]. The surface of the rGO-AuNP/CNT (Figure 5.12B) showed a significant increase in surface roughness compared with that of the bare SPE. Notably, the drop-casting procedure can yield agglomerations of material [68]. In Figure 5.12A, clear, rough surfaces with sharp layered steps and terraces can be observed in the topography of the carbon ink on the bare SPE. No peak-to-peak interlayer distance was measured due to the composite's lack of X-ray diffraction measurements.

5.4.2 Electrochemical Characterisation

Figure 5.13 depicts the CVs of bare SPE, rGO-CNT/SPE, GO-CNT/SPE, rGO-AuNPs/CNT/SPE, and rGO-AuNP are illustrated immersed in 0.1 M KCl containing a mixture of ferricyanide/ferrocyanide at concentrations of 5 mM [Fe

$(CN)_6]^{-3/-4}$ at 100 mVs^{-1} scan rate. According to Figure 5.13, the peak current of redox was consistent for GO-CNT, rGO-AuNP, and rGO-CNT. It remained unaffected by any discernible impact observed from rGO-AuNP/CNT. Hence, it was concluded that model electrodes in subsequent measurements would use rGO-AuNPs/CNT, GO-CNT benchmarked to bare SPE. Looking at Figure 5.13, the peak current of the redox probe was consistent for GO-CNT, rGO-AuNP, and rGO-CNT and remained unaffected compared to rGO-AuNP/CNT. Hence, it was concluded that model electrodes in subsequent measurements would use rGO-AuNPs/CNT and GO-CNT benchmarked to bare SPE.

Figure 5.14 shows CVs of rGO-AuNP/CNT/SPE at different scan rates (25-250 mVs^{-1}) with 0.1 M KCl containing 5 mM [Fe $(CN)_6]^{-3/-4}$. The plot of anodic current peak *vs* square root of scan rate and cathodic current peak vs square root of scan rate was linear over the investigated range scan rate (Figure 5.14). rGO-AuNP/CNT/SPE hybrid composite enhanced specific surface area resulted in well-defined cathodic and anodic peak currents with improved peak-to-peak separation of Δ_{Ep} 91.94 mV compared to bare SPE Δ_{Ep} 331.8 mV, indicating faster electron transfer. A report by Wang et al. recorded a close peak-to-peak separation for rGO/CNT/AuNPs-SPE of 97 mV for an electrochemical sensor for Bisphenol A [58].

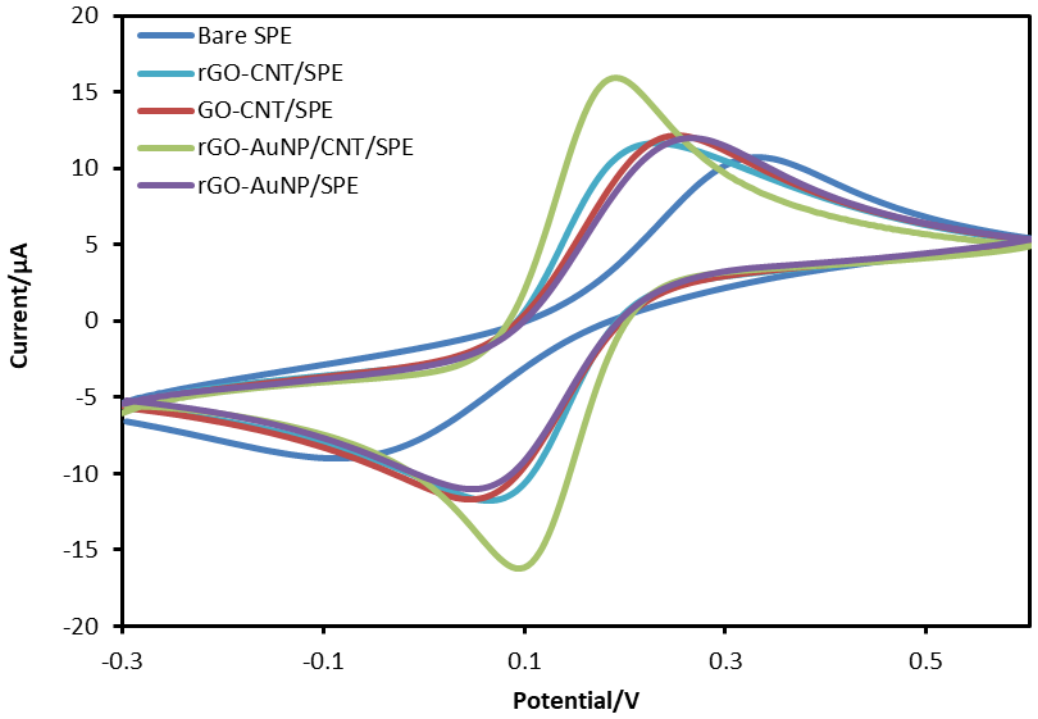

Figure 5.13 CV of bare SPE, rGO-CNT/SPE, GO-CNT/SPE, rGO-AuNPs/CNT/SPE, and rGO-AuNP immersed in 0.1 M KCl containing 5 mM $[Fe(CN)_6]^{-3/-4}$ at 100 mVs^{-1} scan rate.

Figure 5.13 shows the cyclic voltammograms of Bare SPE and rGO-AuNP/CNT/SPE electrodes in a 0.5 M H_2SO_4 solution at a scan rate of 0.05 V/s. For the Gr-AuNPs-CNT/SPE, a single reduction peak of oxide species appeared at about 0.58 V in the cyclic voltammogram, corresponding to the reduction of gold oxide species. The atomic content of the Gr-AuNPs-CNT/SPE can be deduced from the electrode surface covered by gold, just as shown in Figure 5.9 EDS. Characteristic gold oxide reduction peaks are visible at 0.55 V. This figure agrees with data in the literature [72]. The behaviour shown in this figure is characteristic of the Au surface in a clean sulfuric acid [73–76].

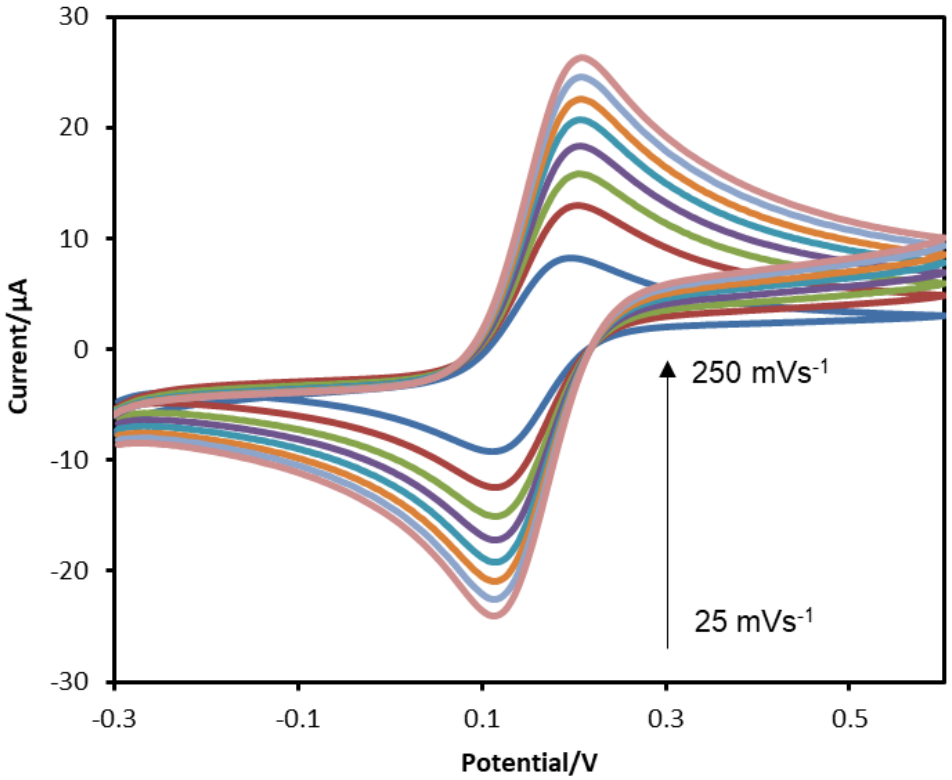

Figure 5.14 CVs of rGO-AuNP/CNT/SPE at different scan rates (25-250mVs^{-1}) 0.1 M KCl containing 5 mM $[Fe(CN)_6]^{-3/-4}$.

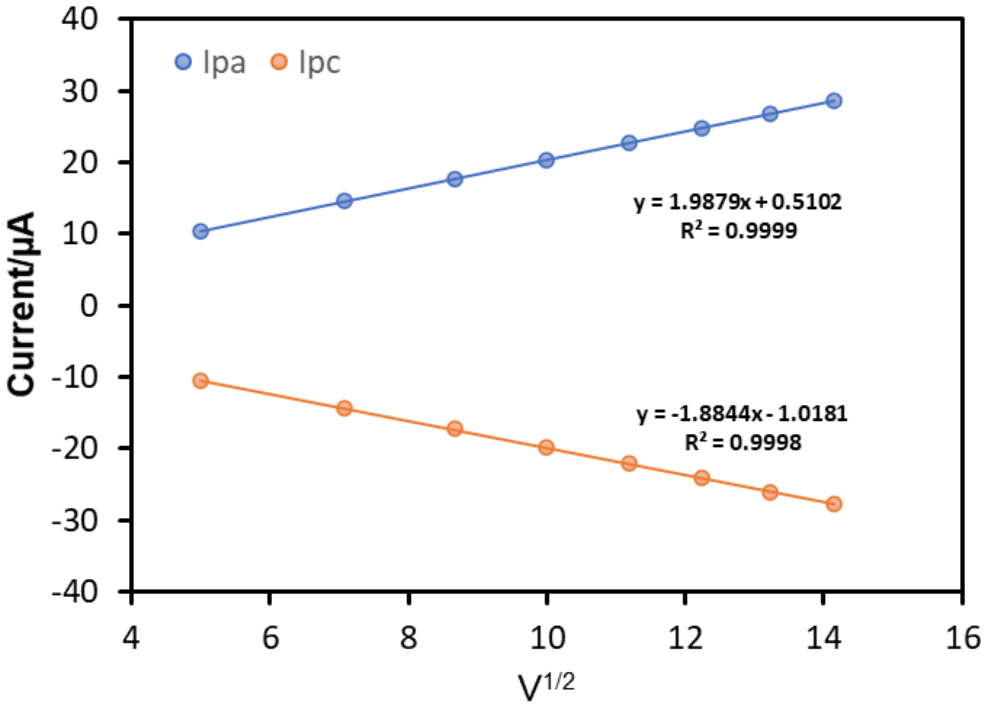

Figure 5.15 Plot anodic current peak vs square root of scan rate and cathodic current peak vs square root of scan rate.

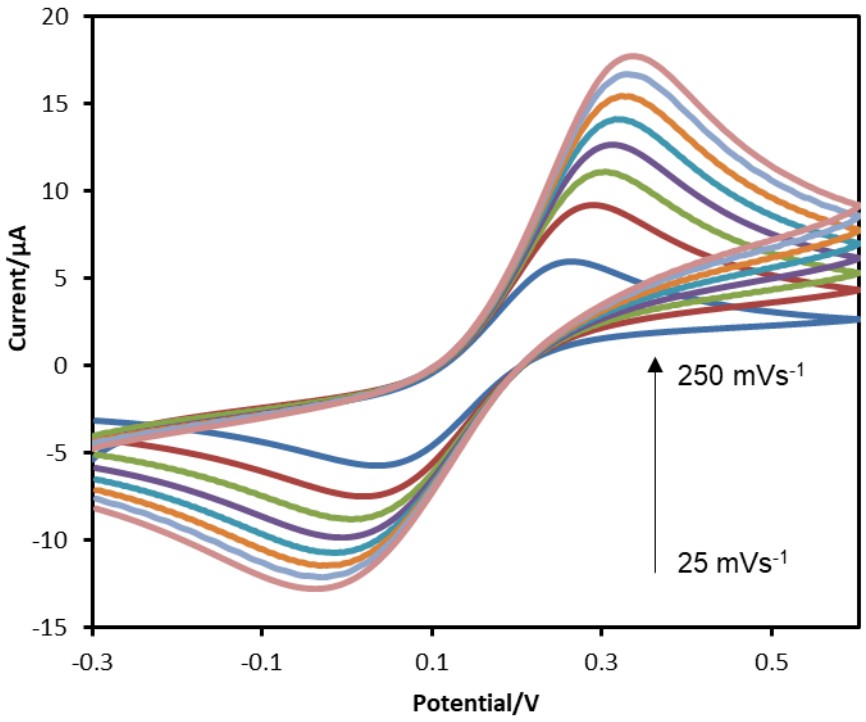

Figure 5.16 CVs of Bare SPE at different scan rates (25-250mVs^{-1}) 0.1 M KCl containing 5 mM [Fe (CN)6]$^{-3/-4}$.

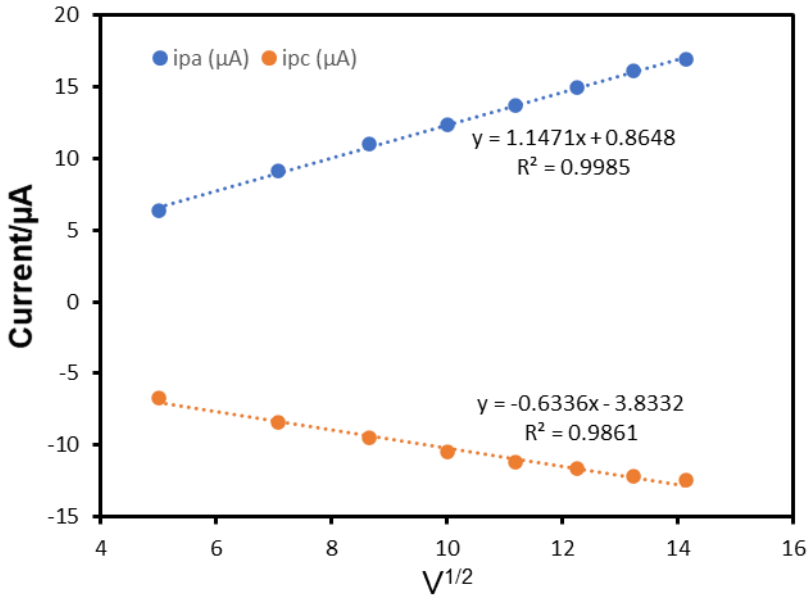

Figure 5.17 Plot anodic current peak vs square root of scan rate and cathodic current peak vs square root of scan rate

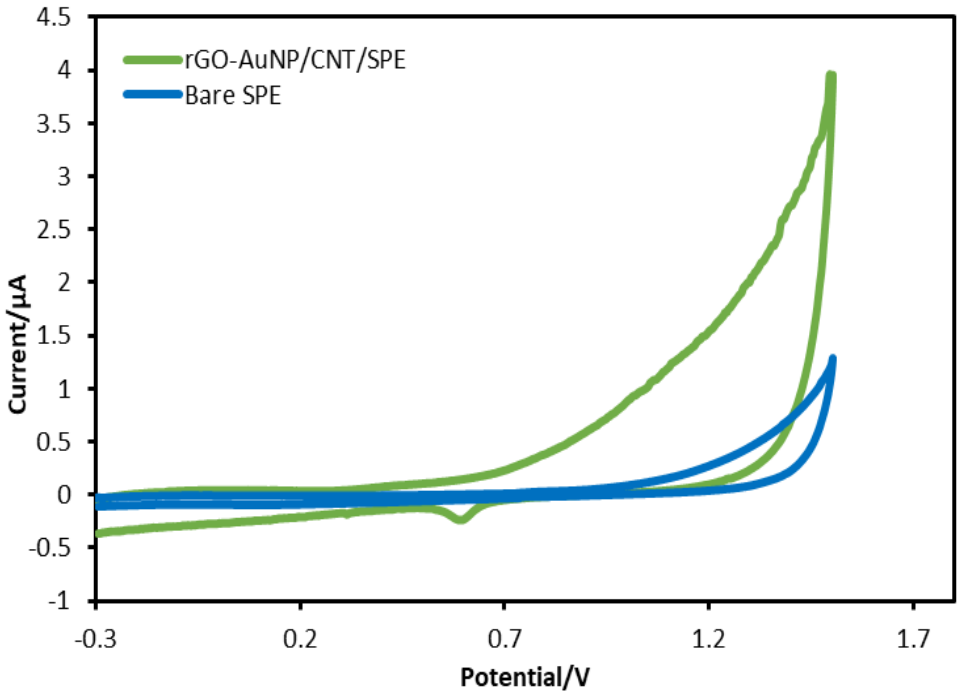

Figure 5.18. Cyclic voltammograms of bare SPE (blue) and rGO-AuNP/CNT/SPE (green) in a 0.5 M H_2SO_4 solution. Scan rate: 50 mVs^{-1}.

Next, we determined the electrochemical activity and the electrochemically active surface area of the electrode, which is essential in electrochemical sensor reportage of the electrode's electroactive area as the interface's unit area. Electrochemical processes at the electrode surface are benchmarked based on the actual surface area of electrodes [77,78]. The electrochemical active surface area of the modified electrode was measured using 5 mM potassium ferrocyanide as the redox probe. The Randles Sevcik equation describes the current for the electrochemical reaction of ferrocyanide (at a mass-transfer-limited rate) that diffuses to an electrode surface [77]. The electrochemical active surface area of rGO-AuNP/CNT was calculated using Eq. (1) for the peak current (I_p) [79]:

$$I_p = (2.69 \times 10^5)\, A D^{1/2} n^{3/2} v^{1/2} C \qquad (1)$$

Where n is the number of electrons, A the electroactive surface area of the rGO-AuNP/CNT/SPE (cm^2), and *D* is the diffusion coefficient of the redox marker ($[Fe(CN)_6]^{-3/4-}$, D= 7.2×10^{-6} cm^2 s^{-1} ([79,80]) in 0.1 M KCl, C the concentration of the redox probe in the solution (M) and v is the scan rate (V/s).

Figure 5.13 shows an increase in the peak currents of $[Fe(CN)_6]^{4-/3-}$ redox couple at the rGO-AuNP/CNT/SPE compared to bare SPE due to composite**.** These results indicate that the electron transfer rate of the redox marker increases in the presence of rGO-AuNP/CNT on SPE. The surface area value is estimated at 0.014 cm^2 for rGO-AuNP/CNT/SPE, significantly higher than the bare SPE figure of 0.009 cm^2. The electroactive surface area values of all SPEs are provided in Table 5.1, which shows that introducing modifier materials to bare SPE surfaces slightly increases the electroactive surface area. Scan rate studies used equimolar Ferri/ferrocyanide 5mM $[Fe(CN)_6]^{-3/4-}$. Both showed a linear relationship between peak current and the square root of the scan rate, indicating a diffusion-limited response in all cases. As shown in Figure 5.13, a peak-to-peak potential difference (ΔE_p) of the $[Fe(CN)_6]^{3-/4-}$ redox probe shows the changes between the bare and the surface-modified SPE. The unmodified bare SPE indicate a quasi-reversible electrochemical response for the $[Fe\ (CN)_6]^{3-/4-}$ redox couple with ΔE_p of 331.8 mV. At the same time, the modified rGO-AuNP/CNT ΔE_p value is 91.9 mV. The attributed feature of the modifier accelerates the electron transfer of the $[Fe(CN)_6]^{3-/4-}$, causing an efficient electron transfer reaction on the electrode surface [77]. In Figure 5.15, a linear relation was observed for both anodic and cathodic peak currents, suggesting that the electrochemical process results from the uniform electroactive thin layer of the

composite deposited [81]. The peak potential shift indicates slow electron transfer and a quasi-reversible reaction for the unmodified SPE. Also, the theoretically ideal equal number of electron oxidation/reduction reactions due to this shift would not be observed.

Table 5.1 Electroactive surface area vs. electrode composition.

Electrode-Design-Modifier	**Surface Area (cm^2)**
Bare SPE	0.009
GO-CNT	0.011
rGO-CNT	0.010
rGO-AuNP/CNT/SPE	0.014
rGO-AuNP	0.007

Abbreviations: Bare SPE: bare Screen-printed electrode; GO-CNT: Graphene oxide-carbon nanotubes; rGO-CNT: Reduced graphene oxide-carbon nanotube; rGO-AuNP/CNT/SPE: gold nanoparticles-Reduced graphene oxide-carbon nanotube; rGO-AuNP: gold nanoparticles-Reduced graphene oxide

5.4.3 Electro-oxidation of 17β-estradiol

The electrooxidation of E2 was investigated on the modified SPE. Figure 5.19A shows the bare, GO/CNT/SPE CVs and rGO-AuNP/CNT/SPE in 100 µM (1 x 10^{-4} M) estradiol. It was observed that the response of E2 peak current is highest for rGO-AuNP/CNT/SPE compared with the bare and the GO/CNT/SPE. A single oxidation peak current of 0.19 µA can be observed for E2 at +0.363 V over unmodified SPE, GO-CNT/SPE 0.322 µA at 0.359 V, and 0.536 µA 0.363V for rGO-AuNP/CNT/SPE surfaces respectively. This agrees with the reported literature [83]. This increase is due to the rGO-AuNP/CNT material properties providing enhanced electron transfer. This result suggests E2's excellent affinity to the rGO-AuNP/CNT hybrid composite. The modified SPEs were utilised to study the electro-oxidation of E2, as depicted in Figure 5. The CVs for the bare SPE, rGO-CNT/SPE, GO-CNT/SPE, rGO-AuNPs/CNT/SPE, and rGO-AuNP were recorded at pH 5 using a B-R buffer solution with a 20 µM concentration of E2. To achieve greater depth, an investigation was conducted into the influence of various configurations of modified SPEs on the oxidation peaks of the estradiol, as shown in Figure 5A and B. Figure 5A revealed shows varying oxidation peaks obtained, according to Figure 5A below with rGO-AuNPs/CNT had the highest, followed by GO-CNT. Also, the differential pulse voltammograms of the bare SPE, GO-CNT/SPE, and rGO-AuNPs/CNT/SPE at 20 µM E2 are depicted in Figure 5B. The results show that the E2 peak current for the bare SPE, GO/CNT/SPE, and rGO-AuNPs/CNT/SPE is elevated compared to CV. This is because differential pulse voltammetry (DPV) is a frequently used electrochemical technique due to its heightened sensitivity and specificity in detecting different analytes. This enables better differentiation between charging

and Faradaic currents [16]. The oxidation peak current recorded at +0.385 V was 1.48 µA for the bare SPE. In comparison, GO-CNT/SPE exhibited a value of 2.95 µA at 0.392 V, and rGO-AuNPs/CNT/SPE showed an even higher reading of 5.079 µA at 0.371 V.

Furthermore, cyclic voltammetry experiments were carried out to elucidate the oxidation behaviour of estradiol at the rGO-AuNP/CNT/SPE electrode in Britton-Robinson (pH 5) and scan rate studies from 25 to 150 mV s^{-1} in figure 5.20. Voltammetric measurements on SPEs were performed by placing a 100 µL drop of the corresponding solution on the working area. A baseline measurement was taken at 0.0 to +0.8 V in buffer solutions for the various electrodes before the target (estradiol) was added. After the baseline measurement, E2 was added at a concentration of 100 µM, and a CV was recorded. DPV was employed from 0.0 to 0.8 V using a step potential of 7 mV, pulse amplitude of 100 mV, scan rate at 50 mV s^{-1} and modulation time of 10 ms. Figure 5.19B shows the differential pulse voltammograms of bare, GO-CNT/SPE and RGO-AuNP/CNT/SPE in 100 µM estradiol. The observed response of E2 peak current is higher than CV for bare SPE, GO/CNT/SPE, and RGO-AuNP/CNT/SPE. A single oxidation peak current of 1.481 µA can be observed for 17β-estradiol at +0.385 V for unmodified SPE, GO-CNT/SPE 2.95 µA at 0.392 V, and 5.079 µA at 0.371 V for RGO-AuNP/CNT/SPE. The result from DPV confirms the observed behaviour of the various individuals using CV. DPV has been commonly employed in electrochemistry for sensitive detection of various analytes as appropriate time domains can be selected, and there are minimal contributions from non-Faradaic currents [16]. It is an effective and rapid electroanalytical technique with

advantages, including good discrimination against background currents and low detection and determination limits.

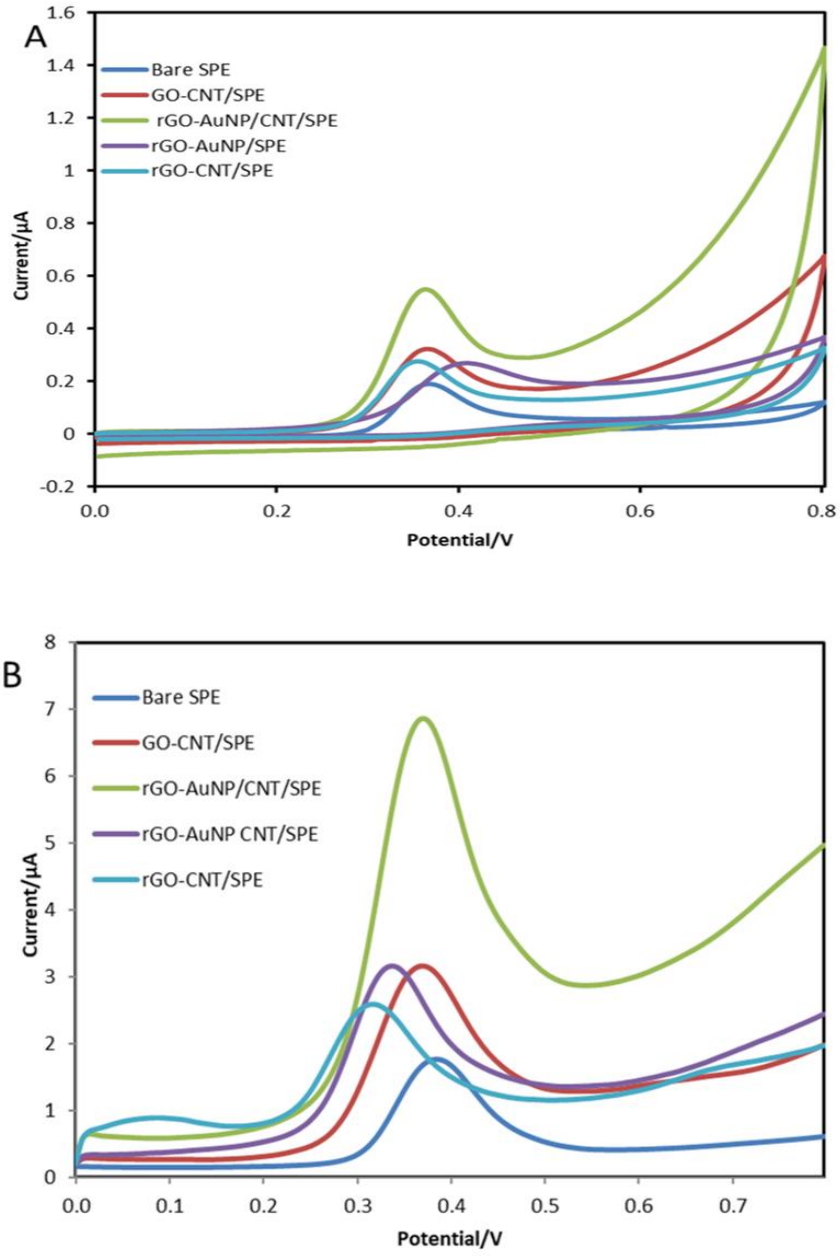

Figure 5.19 A). Cyclic voltammograms (CVs) of the bare SPE, GO-CNT/SPE, rGO-AuNPs/CNT/SPE, rGO-AuNPs/SPE, and rGO-CNT/SPE in 20 µM (2 x 10^{-5} M) E2 at 100 mVs^{-1}. (B) Differential pulse voltammograms (DPVs) of the bare SPE, GO-CNT/SPE, rGO-AuNPs/CNT/SPE, rGO-AuNPs/SPE, and rGO-CNT/SPE in 20 µM (2 x 10^{-5} M) E2 in Britton–Robinson buffer (pH 5) using a

step potential of 7 mV, pulse amplitude of 100 mV, scan rate at 50 mV s^{-1} and modulation time of 10 ms.

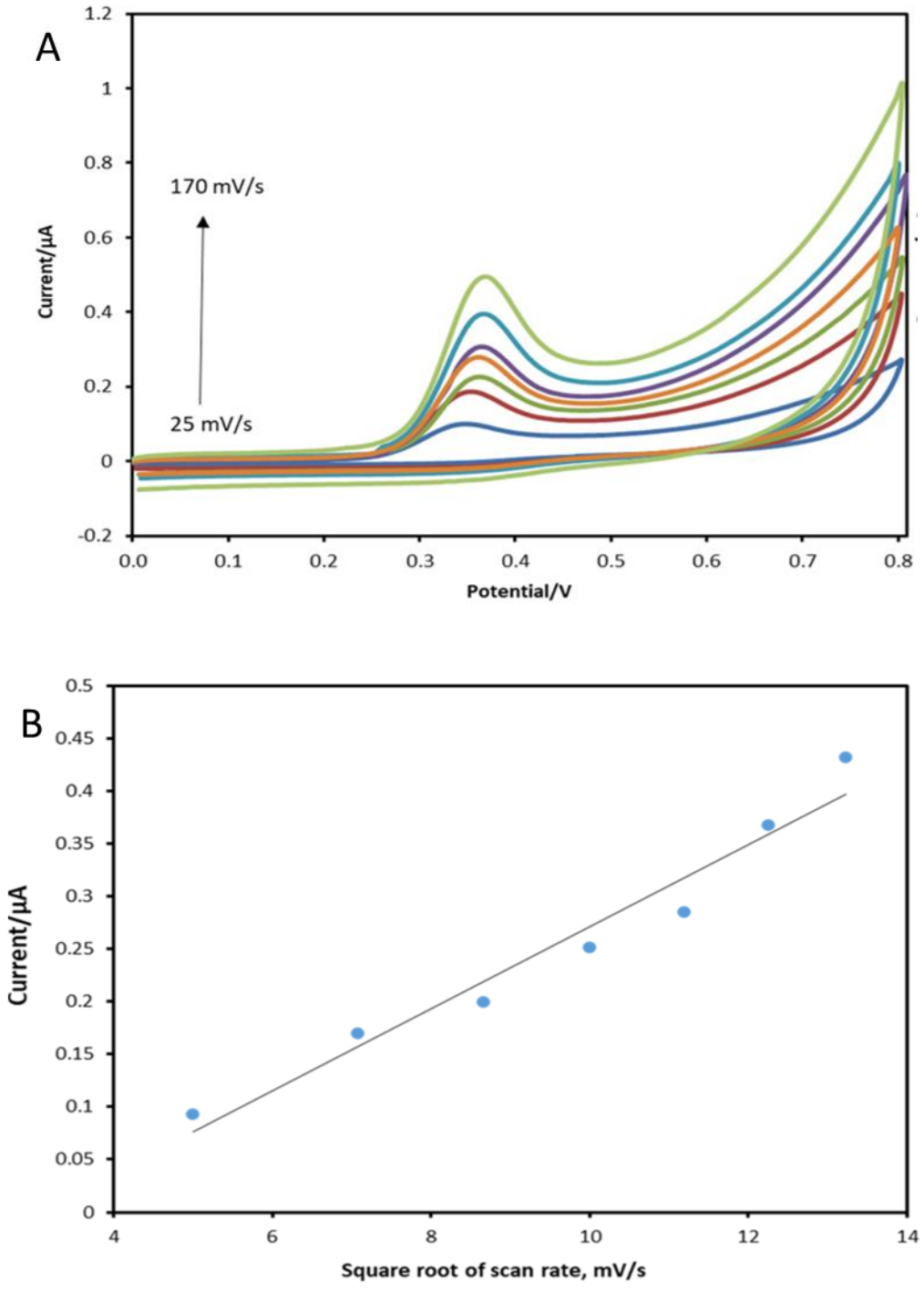

Figure 5.20. A). Cyclic voltammograms (CVs) of rGO-AuNP/CNT/SPE in 20 µM (2 x 10^{-5} M) E2 at a 25–170 mVs^{-1} scan rate. (B) Plot of current peak vs. square root of scan rate.

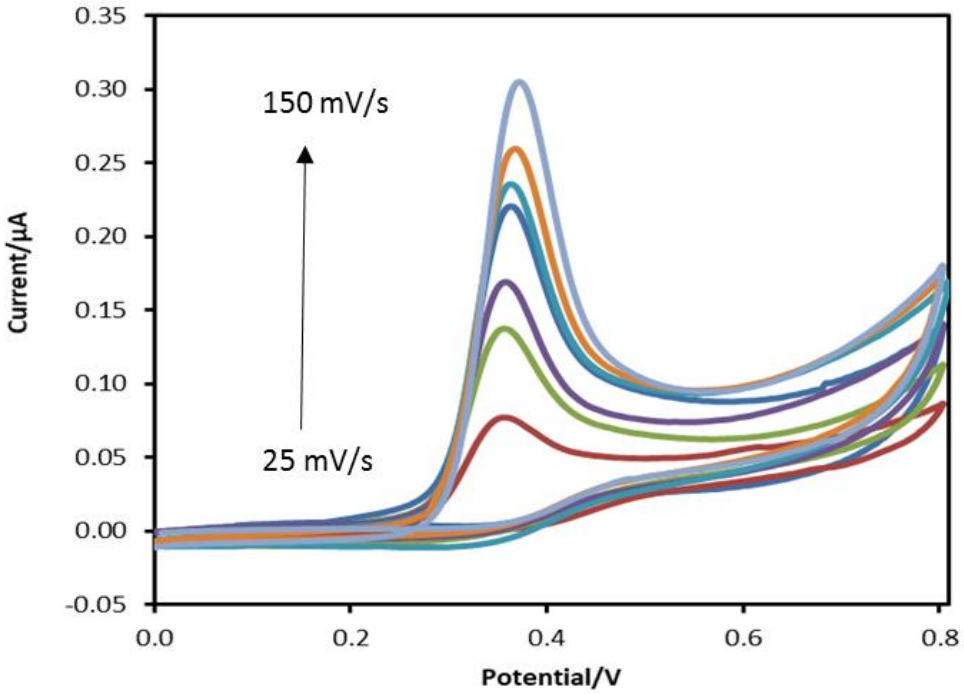

Figure 5.21. Cyclic voltammograms (CVs) of bare SPE in 20 µM (2 x 10^{-5} M) E2 at 25 -150 mVs^{-1} scan rates.

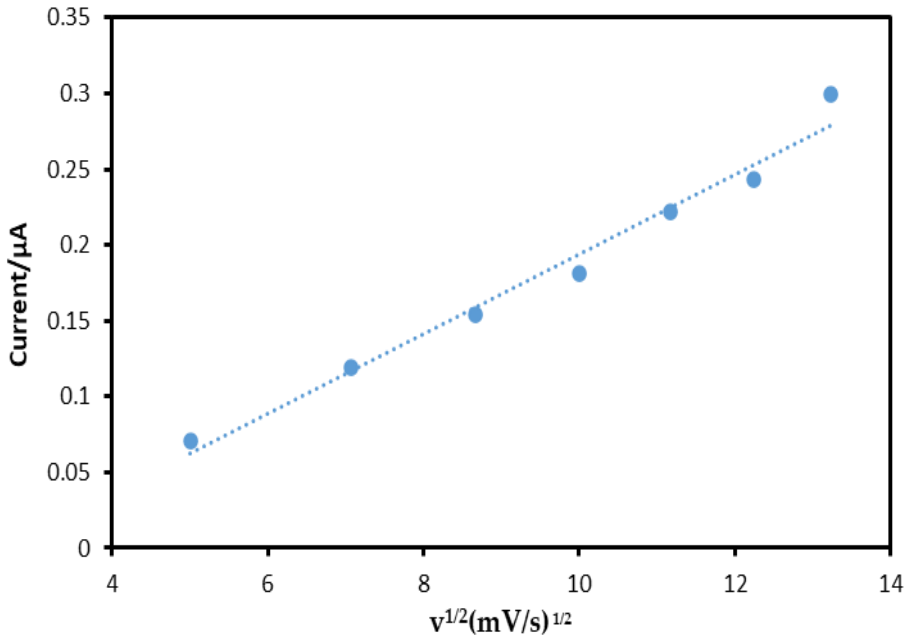

Figure 5.22. Plot of current peak vs. square root of scan rate of bare SPE.

The electrochemical response noticed was evaluated in the range of 25 - 170 mVs^{-1} in Figure 5.20, rGO-AuNP/CNT/SPE. Figure 5.20b shows the dependence of peak current on the square root of scan rate response where Ip = 0.039x - 0.1182, with a correlation coefficient $R^2 = 0.9568$. This indicates that the oxidation of E2 at rGO-AuNP/CNT/SPE is a typical diffusion-controlled reaction. For comparison, Figure 5.21 displays the response of bare SPE at various scan rates. The plot of peak current against scan rate (figure 5.22) gave a linear regression of Ip = 0.0262x - 0.0683 and had a correlation coefficient, $R^2 = 0.9783$, which indicates the adsorption-controlled process. This adsorption-controlled process is widely observed for phenolic on carbon-based modified electrodes [92].

5.4.4 Effect of pH

Figure 5.23 shows the effect of pH on the direct oxidation of E2 on the Gr/AuNP/CNT electrode. Values ranging from 2 to 7 were investigated, with RGO-AuNP/CNT having the highest peak currents (I_p) at pH 5, as shown in Figure 5.24. The plot of E_p vs pH shows good linearity (Figure 5.25). According to the following equation, the estradiol peak potential was moving toward lower values with increasing pH $Ep = -0.0552\ pH + 0.6375$, indicating a 55 mV/pH slope. The slope is close to the Nernst theoretical value of 59 mV/pH, showing a reversible electrochemical process at the modified electrode with an equal number of protons and electrons involved in the electrochemical reaction during the electro-oxidation of estradiol. Ozcan et al. chose a similar pH value for optimum estradiol determination using voltammetry [84]. Based on this information and our results, pH 5 was selected for subsequent experiments.

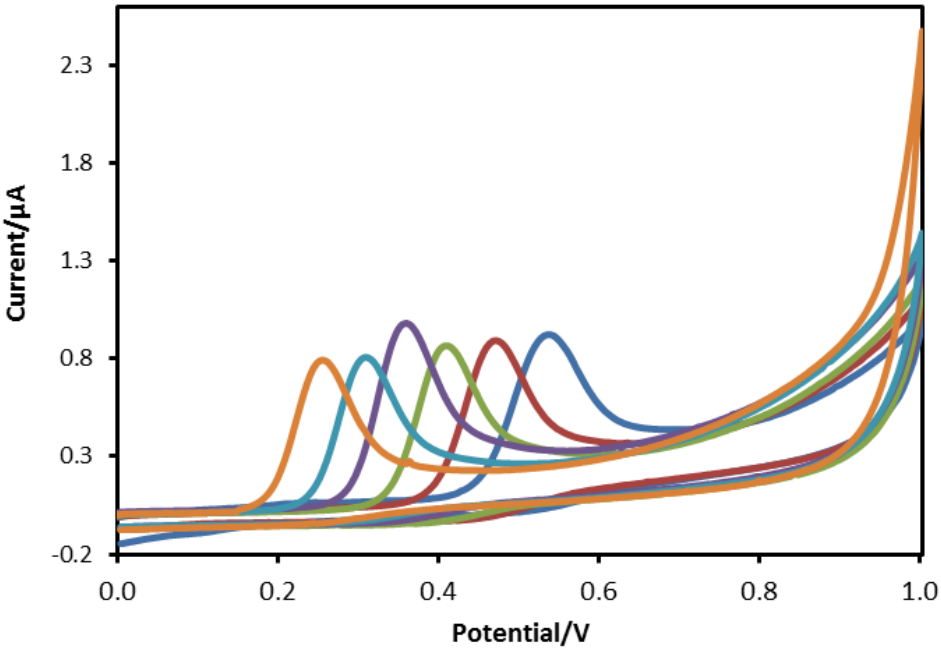

Figure 5.23. CVs of the effect of pH on the oxidation

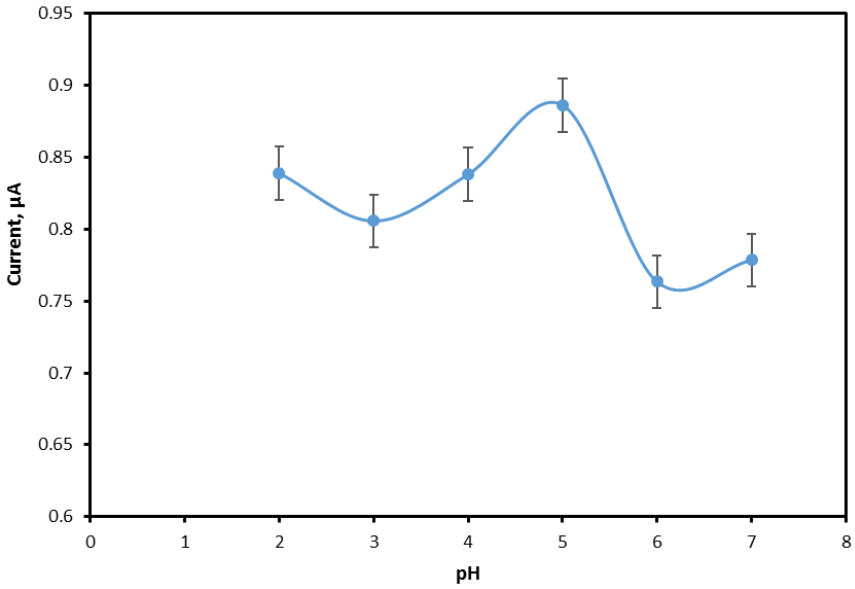

Figure 5.24. A plot of peak potential versus pH in the pH range from 2-7 for 5 µM E2 in Britton-Robison buffer solution.

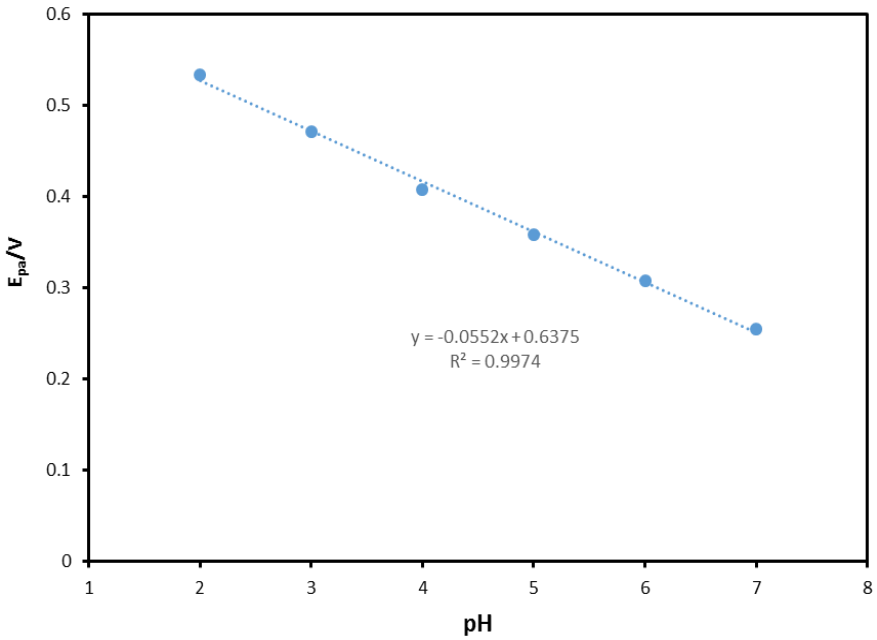

Figure 5.25. CVs of the effect of pH on the oxidation

5.4.5 Optimisation of Modifier

Figure 5.26 shows the effects of utilising different amounts of rGO-AuNP/CNT to modify the SPE regarding its resulting sensitivity. Volumes of 0.3–1.0 µL of the rGO-AuNP/CNT suspension were drop-casted onto the working electrode. Figure 5.26 shows the effects of the composites on the direct oxidation of E2 on the rGO-AuNP/CNT electrode. The highest peak current was obtained for 0.7 µL of suspension; consequently, this volume was selected to modify the SPE in further investigations. As the amount of the rGO-AuNP/CNT modifier increased, the peak current decreased. A further study that was carried out involved adding 0.7 µL of the modifier in the form of layer-by-layer modification (2x). However, the resulting current decreased using this approach due to the aggregation of the modifier particles and the stacking of various materials in the composite. Also, a single-factor ANOVA test with a p-value of less than 0.05 indicates that the

statistical difference is significant for the modifier amount. Consequently, a single 0.7 µL drop-cast was utilised for the rest of the experiments.

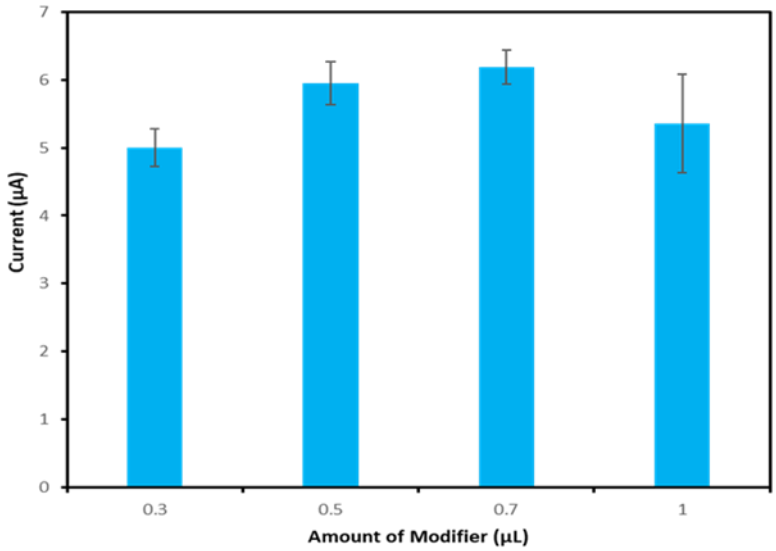

Figure 5.26. A plot of oxidation peak current peak of E2 vs the rGO-AuNP/CNT modifier amount (n=3).

5.4.6 Analytical determination of estradiol

To develop a voltammetric method for determining the E2 without a flow injection system. DPV technique was selected as it is a sensitive technique that could alleviate the effects of the background noise and provide higher current response peaks that are sharper and better defined at a lower concentration [85]. The chemometric field has been applied in electrochemistry utilising computerized methods to analyse chemical data to provide useful information from only faradaic current contributions without step and induced charging current. These methods include curve-fitting [92], Kalman filters [93], derivative techniques [94], and Fourier transform [95]. Reduction of noise in voltammetric analysis has been carried out using Fourier transform [85]. Carvalho et al. reported using a multivariate calibration method to simulate and analyse voltammetric data [85].

An algorithm developed by Górski et al. [86] is applied to resolve net faradaic current contribution. Signal-to-noise in voltammetric analysis was carried out using the Fourier transform [85] to improve signal-to-noise.

Furthermore, DPVs are effective and rapid electroanalytical techniques with well-established advantages, including good discrimination against background currents and low detection and determination limits when coupled to a data processing algorithm. DPV, as a time-based technique, allows for selective identification of analytes of interest in the presence of other interfering substances, as the difference in the electrochemical properties of different analytes is based on the applied potential and duration. Time-based nature can make it a tool for environmental pollution analysis, a case in point: heavy metals [50].

Carvalho et al. started applying a multivariate calibration method to simulate and analyse the full voltammogram to separate each peak. Thus, it explored the rGO-AuNP/CN/TSPE's analytical properties for detecting E2.

DPV was conducted to investigate the sensor's response at various concentrations between 0.05 – 1 µM (5×10^{-8} - 1×10^{-6} M). Calibration plots were obtained from the peak current against the rGO-AuNP/CNT-modified screen-printed electrode suspension concentrations. Each experiment was carried out in triplicate (n=3). The LOD, as well as the limit of quantification (LOQ), deduced using LOD = 3 s / m and LOQ = 10 s / m (s is the standard deviation of the oxidation peak currents (of the lowest detectable concentration), m is the gradient of the calibration curve). DPV was employed to determine the ability of modified rGO-AuNP/CNT/SPE to detect E2 at a lower concentration range (nM) for

enhanced detection capability. In addition, background subtraction was performed to quantify the peak current densities (Figure 5.27).

Figure 5.28 shows the sensor's linear response to E2 in the 0.05 – 1 µM (5 x 10^{-8} - 1 x 10^{-6} M) E2 analytical range. The LOD and LOQ values were 3 x 10^{-9} M and 6.6 × 10^{-7} M, respectively. The peak current versus E2 concentration plot equation correlated R^2= 0.9945 (n=3) baseline corrected. The result was compared with previously reported electrodes modified with graphene-based materials such as Gr–PANI [87], CPE/GNR-FS-Au-CA [84], RGO/CuTthP [25], and GQDs-PSSA/GO [88], with this study's results closer to Arvand et al. [88] in Table 5.2.

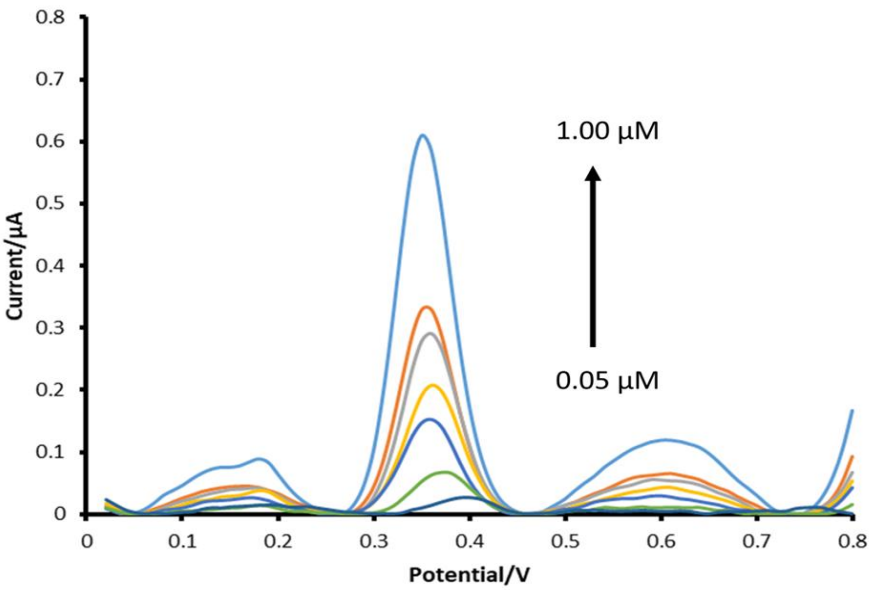

Figure 5.27. DPVs of rGO-AuNP/CNT/SPE with different concentrations of E2 0.05 – 1 µM (5 x 10^{-8} - 1 x 10^{-6} M) in B-R buffer (pH 5) with automatic baseline correction was carried out based on the report of [86].

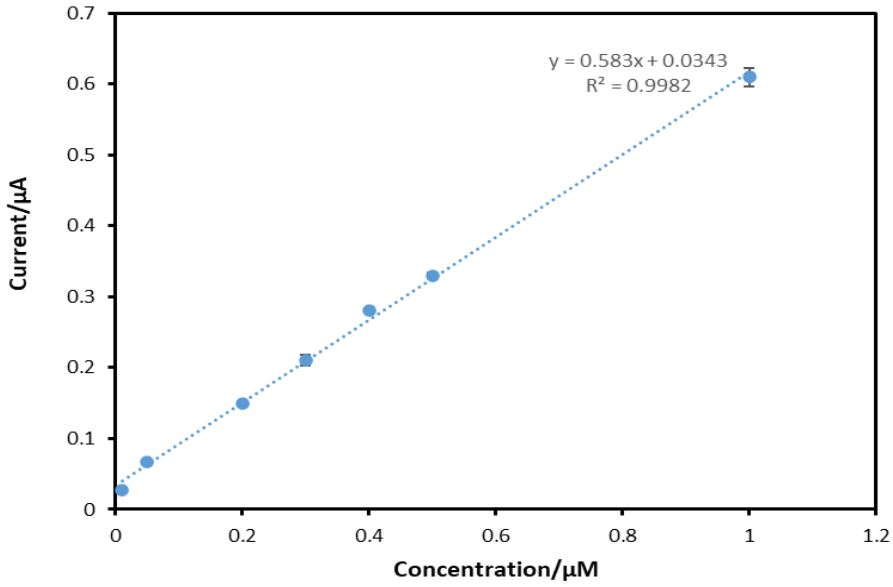

Figure 5.28. Shows the oxidation peak current plot against the E2 concentration. Error bar: standard deviation for n = 3.

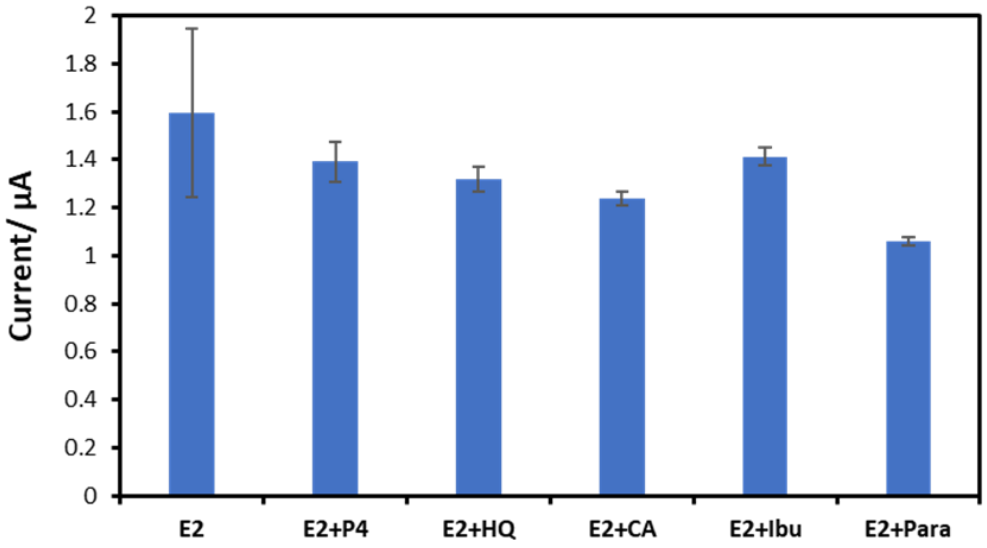

Figure 5.29. Effect of interferents that coexist in water on detecting E2. The initial concentration of target and interference molecules is at analyte: interfering was 1:10 (µM/µM).

Other supporting electrolytes were tested for the sensor's performance in various conditions. The results highlighted the electrochemical behaviour of the sensor in different supporting electrolytes, as shown in Appendix D, Figure D1.

Table 5.*2*. Different Applications of graphene-based materials for E2 electroanalysis

Electrode-Design-Modifier		Applied Technique	Sensor type	Linear Range(M)	Detection limit(M)	Ref
Glassy carbon electrode (GCE)	GR–PANI	Differential pulse voltammetry (DPV)	Immunosensor	1.47×10^{-10} - 2.57×10^{-8}	7.35×10^{-11}	[87]
Glassy carbon electrode (GCE)	RGO/CuTthP	Differential pulse voltammetry (DPV)	Electrochemical sensor	1×10^{-7} - 1×10^{-6}	5.3×10^{-9}	[25]
Carbon paste electrode	GNR-FS-Au-CA	Differential pulse voltammetry (DPV)	Electrochemical sensor	1×10^{-7} - 5×10^{-6}	7.4×10^{-9}	[84]
Glassy carbon electrode (GCE)	GQDs-PSSA/GO	Differential pulse voltammetry (DPV)	Electrochemical sensor	1×10^{-9} - 6×10^{-6}	2.3×10^{-10}	[88]
Screen-printed carbon electrode	GR/AuNP/CNT)	Differential pulse voltammetry (DPV)	Electrochemical sensor	5×10^{-8} - 1×10^{-6}	3×10^{-9}	This work

* Graphene-polyaniline (GR–PANI),

* Reduced graphene oxide and a metal complex porphyrin (RGO/CuTthP),

* Cysteamine self-assembled gold nanoparticle modified silica decorated graphene nanoribbon (GNR-FS-Au-CA),

* Graphene quantum dots and poly (sulfosalicylic acid) (GQDs-PSSA/GO),

* Gold nanoparticles (AuNP) doped on graphene oxide - multiwalled carbon nanotube (RGO-AuNP/CNT).

5.4.7 Reproducibility and interference studies

Stability and reproducibility studies were carried out to test the performance of the modified electrodes. In addition, reproducibility studies were carried out to perform the Gr-AuNP-CNT/SPCE modified electrode using DPV measurements (n = 5) in the B-R Buffer. It revealed that the 5 x 10-6 M E2 fabricated sensor shows good reproducibility with a coefficient of variance of 5.28%. To assess the influence of interferents, hydroquinone, dopamine, paracetamol, ibuprofen, and bisphenol A were investigated as they are present in the water environment. The estradiol concentration was kept at 5 x 10^{-6} M.

In comparison, the interferent concentration was 5 x 10^{-5} M, presented in Figure 5.29, demonstrating that these substances did not influence the oxidation of E2 on the fabricated sensor. No significant interference was observed for paracetamol and hydroquinone, similar to the report of Raymundo et al. in which estradiol, hydroquinone, and paracetamol were simultaneously detected on a bare electrochemically pre-treated screen-printed carbon electrode [89]. Figure 5.29 shows the effect of interferents on the detection of estradiol in water. Experiments were performed by adding the E2-interferent ratio of 1:10. It was found that natural steroid estrogens, such as estrone, E2, and estriol, as well as synthetic estrogens like 17 α-ethinylestradiol, were commonly present in WWTP effluent. These estrogen levels ranged from pg/L to µg/L, indicating significant disruption of endocrine activity within the water.

Also, there was no interference by dopamine or ibuprofen. Conversely, it was observed that Bisphenol A significantly influenced the oxidation peak current of estradiol as it had a broad high peak, resulting in a peak current signal change of

more than 50%, in contrast to less than 10% for the other interferents studied. The closed peak potential at about 0.5 V was observed and overlapped with the oxidation peak of E2. This is attributed to the similar chemical structure and physicochemical properties, especially for the acid-based dissociation constant (pKa) [91].

5.4.8 Analysis of E2 in Water Sample

To ascertain the sensor's analytical applicability for water testing, water samples from the drinking water were spiked with E2 and tested. Samples (30 mL) were spiked with E2 at 0.5 and 0.9 µM with no dilution with buffer. Table 5.3 shows the recovery studies of the sensor.

Table 5.*3*. Determination for E2 in water samples using rGO/AuNP/CNT/SPE sensor.

Added (µM)	**Found (**µM|)	**RSD**	**Recoveries (%)**
0.5	0.46	2.7	92
0.5	0.45	2.5	90
0.9	0.96	3.2	106
0.9	0.92	2.8	102

5.5 Conclusions

This chapter demonstrated a direct measurement of estradiol in water samples with no preparation or pre-treatment. This has established the applicability of the screen-printed electrode as a portable platform. A five-step method for synthesising hybrid composites has been developed by reducing gold nanoparticles via a graphene oxide suspension with bay leaf extract at room temperature. Combined with carbon nanotubes, it gave Gr/AuNP/CNT hybrid material. The overall strategy for the green synthesis of gold nanoparticles has been developed using a solvent-free method. In addition, the doped graphene oxide serves as a dispersant for carbon nanotubes with no harsh solvent. Combining gold nanoparticle-doped graphene oxide and carbon nanotubes improves the sensor's performance, showing superior electrochemical characteristics compared with other graphene-based sensors for estradiol detection reported in the literature. In addition to reproducibility (coefficient of variance of 2.58%), with a LOD of 3.4×10^{-9} M of the sensor. Finally, recoveries of 92% for analysis of water samples were reported.

References

[1] V. Geissen, H. Mol, E. Klumpp, G. Umlauf, M. Nadal, M. van der Ploeg, S.E.A.T.M. van de Zee, C.J. Ritsema, Emerging pollutants in the environment: A challenge for water resource management, Int. Soil Water Conserv. Res. 3 (2015) 57–65. https://doi.org/10.1016/J.ISWCR.2015.03.002.

[2] Z. hua Liu, Z. Dang, H. Yin, Y. Liu, Making waves: Improving removal performance of conventional wastewater treatment plants on endocrine disrupting compounds (EDCs): their conjugates matter, Water Res. 188 (2021) 116469. https://doi.org/10.1016/j.watres.2020.116469.

[3] A. Pillon, A.M. Boussioux, A. Escande, S. Aït-Aïssa, E. Gomez, H. Fenet, M. Ruff, D. Moras, F. Vignon, M.J. Duchesne, C. Casellas, J.C. Nicolas, P. Balaguer, Binding of estrogenic compounds to recombinant estrogen receptor-α: Application to environmental analysis, Environ. Health Perspect. 113 (2005) 278–284. https://doi.org/10.1289/ehp.7522.

[4] M.H. Lee, J.L. Thomas, W.C. Liu, Z.X. Zhang, B. Da Liu, C.H. Yang, H.Y. Lin, A multichannel system integrating molecularly imprinted conductive polymers for ultrasensitive voltammetric determination of four steroid hormones in urine, Microchim. Acta. 186 (2019). https://doi.org/10.1007/s00604-019-3797-7.

[5] K.C. Honeychurch, M. Piano, Electrochemical (bio) sensors for environmental and food analyses, Biosensors. 8 (2018) 2–4. https://doi.org/10.3390/bios8030057.

[6] J. Barton, M.B.G. García, D.H. Santos, P. Fanjul-Bolado, A. Ribotti, M. McCaul, D. Diamond, P. Magni, Screen-printed electrodes for environmental monitoring of heavy metal ions: a review, Microchim. Acta. 183 (2016) 503–517. https://doi.org/10.1007/s00604-015-1651-0.

[7] S. Hu, K. Wu, H. Yi, D. Cui, Voltammetric behavior and determination of estrogens at Nafion-modified glassy carbon electrode in the presence of

cetyltrimethylammonium bromide, Anal. Chim. Acta. 464 (2002) 209–216. https://doi.org/10.1016/S0003-2670(02)00496-8.

[8] F. Moreira, E.R. Santana, A. Spinelli, Ionic liquid-supported magnetite nanoparticles as electrode modifier materials for estrogens sensing, Sci. Rep. 10 (2020) 1–11. https://doi.org/10.1038/s41598-020-58931-6.

[9] A. Pavinatto, L.A. Mercante, C.S. Leandro, L.H.C. Mattoso, D.S. Correa, Layer-by-Layer assembled films of chitosan and multi-walled carbon nanotubes for the electrochemical detection of 17α-ethinylestradiol, J. Electroanal. Chem. 755 (2015) 215–220. https://doi.org/10.1016/J.JELECHEM.2015.08.002.

[10] S. Barreca, M. Busetto, L. Colzani, L. Clerici, D. Daverio, P. Dellavedova, S. Balzamo, E. Calabretta, V. Ubaldi, Determination of estrogenic endocrine disruptors in water at sub-ng L −1 levels in compliance with Decision 2015/495/EU using offline-online solid phase extraction concentration coupled with high performance liquid chromatography-tandem mass spectrometry, Microchem. J. 147 (2019) 1186–1191. https://doi.org/10.1016/j.microc.2019.04.030.

[11] L. Barreiros, J.F. Queiroz, L.M. Magalhães, A.M.T. Silva, M.A. Segundo, Analysis of 17-β-estradiol and 17-α-ethinylestradiol in biological and environmental matrices - A review, Microchem. J. 126 (2016) 243–262. https://doi.org/10.1016/j.microc.2015.12.003.

[12] A.C. Pereira, G.B. Braga, A.E.F. Oliveira, R.C. Silva, K.B. Borges, Synthesis and characterization of molecularly imprinted polymer for ethinylestradiol, Chem. Pap. 73 (2019) 141–149. https://doi.org/10.1007/s11696-018-0557-9.

[13] G. Zhang, T. Li, J. Zhang, A. Chen, A simple FRET-based turn-on fluorescent aptasensor for 17B-estradiol determination in environmental water, urine and milk samples, Sensors Actuators, B Chem. 273 (2018) 1648–1653. https://doi.org/10.1016/j.snb.2018.07.066.

[14] X. Liu, K. Deng, H. Wang, C. Li, S. Zhang, H. Huang, Aptamer based ratiometric electrochemical sensing of 17β-estradiol using an electrode modified with gold nanoparticles, thionine, and multiwalled carbon nanotubes, Microchim. Acta. 186 (2019). https://doi.org/10.1007/s00604-019-3465-y.

[15] A. Wong, A.M. Santos, F.H. Cincotto, F.C. Moraes, O. Fatibello-Filho, M.D.P.T. Sotomayor, A new electrochemical platform based on low cost nanomaterials for sensitive detection of the amoxicillin antibiotic in different matrices, Talanta. 206 (2020) 120252. https://doi.org/10.1016/j.talanta.2019.120252.

[16] A.M. Santos, A. Wong, T.M. Prado, E.L. Fava, O. Fatibello-Filho, M.D.P.T. Sotomayor, F.C. Moraes, Voltammetric determination of ethinylestradiol using screen-printed electrode modified with functionalized graphene, graphene quantum dots and magnetic nanoparticles coated with molecularly imprinted polymers, Talanta. (2020) 121804. https://doi.org/10.1016/j.talanta.2020.121804.

[17] D. Sun, Q. Deng, J. Long, Highly sensitive electrochemical sensor for estradiol based on the signal amplification strategy of Cu-BDC frameworks, J. Solid State Electrochem. 22 (2018) 487–493. https://doi.org/10.1007/s10008-017-3778-x.

[18] L. Ji, Y. Wang, K. Wu, W. Zhang, Simultaneous determination of environmental estrogens: Diethylstilbestrol and estradiol using Cu-BTC frameworks-sensitized electrode, Talanta. 159 (2016) 215–221. https://doi.org/10.1016/j.talanta.2016.06.030.

[19] J. Song, J. Yang, X. Hu, Electrochemical determination of estradiol using a poly(l-serine) film-modified electrode, J. Appl. Electrochem. 38 (2008) 833–836. https://doi.org/10.1007/s10800-008-9520-8.

[20] X. Liu, Y. Yao, Y. Ying, J. Ping, Recent advances in nanomaterial-enabled screen-printed electrochemical sensors for heavy metal

detection, TrAC - Trends Anal. Chem. 115 (2019) 187–202. https://doi.org/10.1016/j.trac.2019.03.021.

[21] A. Vasilescu, P. Fanjul-Bolado, A.M. Titoiu, R. Porumb, P. Epure, Progress in electrochemical (bio)sensors for monitoring wine production, Chemosensors. 7 (2019). https://doi.org/10.3390/chemosensors7040066.

[22] S. Radhakrishnan, J. Mathiyarasu, Graphene-carbon nanotubes modified electrochemical sensors, Elsevier Inc., 2018. https://doi.org/10.1016/B978-0-12-815394-9.00008-X.

[23] S. Cinti, F. Arduini, M. Carbone, L. Sansone, I. Cacciotti, D. Moscone, G. Palleschi, Screen-Printed Electrodes Modified with Carbon Nanomaterials: A Comparison among Carbon Black, Carbon Nanotubes and Graphene, Electroanalysis. 27 (2015) 2230–2238. https://doi.org/10.1002/elan.201500168.

[24] S. Iijima, T. Ichihashi, Single-shell carbon nanotubes of 1-nm diameter, Nature. 363 (1993) 603–605. https://doi.org/10.1038/363603a0.

[25] F.C. Moraes, B. Rossi, M.C. Donatoni, K.T. de Oliveira, E.C. Pereira, Sensitive determination of 17β-estradiol in river water using a graphene based electrochemical sensor, Anal. Chim. Acta. 881 (2015) 37–43. https://doi.org/10.1016/j.aca.2015.04.043.

[26] C.B. Jacobs, M.J. Peairs, B.J. Venton, Review: Carbon nanotube based electrochemical sensors for biomolecules, Anal. Chim. Acta. 662 (2010) 105–127. https://doi.org/10.1016/j.aca.2010.01.009.

[27] C. Nanotube, C.N.T. Biosensors, D.C. Ferrier, K.C. Honeychurch, Carbon Nanotube (CNT)-Based Biosensors, (2021) 1–33.

[28] W. Grosse, J. Champavert, S. Gambhir, G.G. Wallace, S.E. Moulton, Aqueous dispersions of reduced graphene oxide and multi wall carbon nanotubes for enhanced glucose oxidase bioelectrode performance, Carbon N. Y. 61 (2013) 467–475.

https://doi.org/10.1016/j.carbon.2013.05.029.

[29] C. Zhang, L. Ren, X. Wang, T. Liu, Graphene oxide-assisted dispersion of pristine multiwalled carbon nanotubes in aqueous media, J. Phys. Chem. C. 114 (2010) 11435–11440. https://doi.org/10.1021/jp103745g.

[30] P. Avouris, C. Dimitrakopoulos, Graphene: Synthesis and applications, Mater. Today. 15 (2012) 86–97. https://doi.org/10.1016/S1369-7021(12)70044-5.

[31] M. Velický, D.F. Bradley, A.J. Cooper, E.W. Hill, I.A. Kinloch, A. Mishchenko, K.S. Novoselov, H. V. Patten, P.S. Toth, A.T. Valota, S.D. Worrall, R.A.W. Dryfe, Electron transfer kinetics on mono- and multilayer graphene, ACS Nano. 8 (2014) 10089–10100. https://doi.org/10.1021/nn504298r.

[32] G.P. Keeley, A. O'Neill, M. Holzinger, S. Cosnier, J.N. Coleman, G.S. Duesberg, DMF-exfoliated graphene for electrochemical NADH detection, Phys. Chem. Chem. Phys. 13 (2011) 7747–7750. https://doi.org/10.1039/c1cp20060g.

[33] M.J. Allen, V.C. Tung, R.B. Kaner, Honeycomb carbon: A review of graphene, Chem. Rev. 110 (2010) 132–145. https://doi.org/10.1021/cr900070d.

[34] M.D. Verma, K.R. Ranjan, D.M. Das Mukherjee, D.P.R. Solanki, Bioinspired Synthesis of Hematite Nanoparticles-Reduced Graphene Oxide Composite for Application in Bpa Detection: A New In-Sight, SSRN Electron. J. (2022) 1–30. https://doi.org/10.2139/ssrn.4134082.

[35] A. Ambrosi, M. Pumera, Electrochemically Exfoliated Graphene and Graphene Oxide for Energy Storage and Electrochemistry Applications, Chem. - A Eur. J. 22 (2016) 153–159. https://doi.org/10.1002/chem.201503110.

[36] T.N.L. Truong, P. Van Toan, N.Q. Hao, Using AuNPs-modified screen-

printed electrode in the development of molecularly imprinted polymer for artificial bioreceptor fabrication to improve biosensor sensitivity for 17 β - estradiol detection, Adv. Nat. Sci. Nanosci. Nanotechnol. 10 (2019) 015015. https://doi.org/10.1088/2043-6254/ab0d1b.

[37] D. Zhang, W. Zhang, J. Ye, S. Zhan, B. Xia, J. Lv, H. Xu, G. Du, L. Wang, A label-free colorimetric biosensor for 17β-estradiol detection using nanoparticles assembled by aptamer and cationic polymer, Aust. J. Chem. 69 (2016) 12–19. https://doi.org/10.1071/CH14735.

[38] T. Xiao, J. Huang, D. Wang, T. Meng, X. Yang, Au and Au-Based nanomaterials: Synthesis and recent progress in electrochemical sensor applications, Talanta. 206 (2020) 120210. https://doi.org/10.1016/j.talanta.2019.120210.

[39] N. Yildirim, F. Long, C. Gao, M. He, H.C. Shi, A.Z. Gu, Aptamer-based optical biosensor for rapid and sensitive detection of 17β-estradiol in water samples, Environ. Sci. Technol. 46 (2012) 3288–3294. https://doi.org/10.1021/es203624w.

[40] Z. Altintas, A. Guerreiro, S.A. Piletsky, I.E. Tothill, NanoMIP based optical sensor for pharmaceuticals monitoring, Sensors Actuators, B Chem. 213 (2015) 305–313. https://doi.org/10.1016/j.snb.2015.02.043.

[41] A.A. Ensafi, M. Amini, B. Rezaei, Molecularly imprinted electrochemical aptasensor for the attomolar detection of bisphenol A, Microchim. Acta. 185 (2018) 265. https://doi.org/10.1007/s00604-018-2810-x.

[42] W.-R. Zhao, T.-F. Kang, L.-P. Lu, F.-X. Shen, S.-Y. Cheng, A novel electrochemical sensor based on gold nanoparticles and molecularly imprinted polymer with binary functional monomers for sensitive detection of bisphenol A, J. Electroanal. Chem. 786 (2017) 102–111. https://doi.org/10.1016/J.JELECHEM.2017.01.003.

[43] Q. Gao, N. Liu, Z. Ma, Prussian blue-gold nanoparticles-ionic liquid functionalized reduced graphene oxide nanocomposite as label for

ultrasensitive electrochemical immunoassay of alpha-fetoprotein, Anal. Chim. Acta. 829 (2014) 15–21. https://doi.org/10.1016/j.aca.2014.04.045.

[44] R. Petrucci, M. Bortolami, P. Di Matteo, A. Curulli, Gold Nanomaterials-Based Electrochemical Sensors and Biosensors for Phenolic Antioxidants Detection: Recent Advances, Nanomaterials. 12 (2022). https://doi.org/10.3390/nano12060959.

[45] M. Yaseen, M. Humayun, A. Khan, M. Usman, H. Ullah, A.A. Tahir, H. Ullah, Preparation, functionalization, modification, and applications of nanostructured gold: A critical review, Energies. 14 (2021) 1–83. https://doi.org/10.3390/en14051278.

[46] S. Ahmed, Annu, S.A. Chaudhry, S. Ikram, A review on biogenic synthesis of ZnO nanoparticles using plant extracts and microbes: A prospect towards green chemistry, J. Photochem. Photobiol. B Biol. 166 (2017) 272–284. https://doi.org/10.1016/j.jphotobiol.2016.12.011.

[47] P.D. Shankar, S. Shobana, I. Karuppusamy, A. Pugazhendhi, V.S. Ramkumar, S. Arvindnarayan, G. Kumar, A review on the biosynthesis of metallic nanoparticles (gold and silver) using bio-components of microalgae: Formation mechanism and applications, Enzyme Microb. Technol. 95 (2016) 28–44. https://doi.org/10.1016/j.enzmictec.2016.10.015.

[48] K. Murugan, G. Benelli, C. Panneerselvam, J. Subramaniam, T. Jeyalalitha, D. Dinesh, M. Nicoletti, J.S. Hwang, U. Suresh, P. Madhiyazhagan, Cymbopogon citratus-synthesized gold nanoparticles boost the predation efficiency of copepod Mesocyclops aspericornis against malaria and dengue mosquitoes, Exp. Parasitol. 153 (2015) 129–138. https://doi.org/10.1016/j.exppara.2015.03.017.

[49] C. Singh, V. Sharma, P.K. Naik, V. Khandelwal, H. Singh, A green biogenic approach for synthesis of gold and silver nanoparticles using zingiber officinale, Dig. J. Nanomater. Biostructures. 6 (2011) 535–542.

[50] C. Krishnaraj, P. Muthukumaran, R. Ramachandran, M.D. Balakumaran, P.T. Kalaichelvan, Acalypha indica Linn: Biogenic synthesis of silver and gold nanoparticles and their cytotoxic effects against MDA-MB-231, human breast cancer cells, Biotechnol. Reports. 4 (2014) 42–49. https://doi.org/10.1016/j.btre.2014.08.002.

[51] C. Jayaseelan, R. Ramkumar, A.A. Rahuman, P. Perumal, Green synthesis of gold nanoparticles using seed aqueous extract of Abelmoschus esculentus and its antifungal activity, Ind. Crops Prod. 45 (2013) 423–429. https://doi.org/10.1016/j.indcrop.2012.12.019.

[52] J. Akta, K. Indonesia, S. Firdausiah, T. Hidayat, M. Alfliadhi, Synthesis and Characterization of Gold Nanoparticles using the Bioreductor Bay Leaf (Syzygium polyanthum), Indones. Chim. Acta. 13 (2020) 0–4. https://doi.org/https://doi.org/10.20956/ica.v13i2.11798.

[53] Z. Ismail, Green reduction of graphene oxide by plant extracts: A short review, Ceram. Int. 45 (2019) 23857–23868. https://doi.org/10.1016/j.ceramint.2019.08.114.

[54] M.T.H. Aunkor, I.M. Mahbubul, R. Saidur, H.S.C. Metselaar, The green reduction of graphene oxide, RSC Adv. 6 (2016) 27807–27825. https://doi.org/10.1039/c6ra03189g.

[55] M. Shanmugam, K. Kim, Electrodeposited gold dendrites at reduced graphene oxide as an electrocatalyst for nitrite and glucose oxidation, J. Electroanal. Chem. 776 (2016) 82–92. https://doi.org/10.1016/j.jelechem.2016.06.009.

[56] S. Nazarpour, R. Hajian, M.H. Sabzvari, A novel nanocomposite electrochemical sensor based on green synthesis of reduced graphene oxide/gold nanoparticles modified screen printed electrode for determination of tryptophan using response surface methodology approach, Microchem. J. 154 (2020) 104634. https://doi.org/10.1016/j.microc.2020.104634.

[57] R. Viveiros, S. Rebocho, T. Casimiro, Green Strategies for Molecularly Imprinted Polymer Development, Polymers (Basel). 10 (2018) 306. https://doi.org/10.3390/polym10030306.

[58] Nazarpour, S., Hajian, R. and Sabzvari, M.H., 2020. A novel nanocomposite electrochemical sensor based on green synthesis of reduced graphene oxide/gold nanoparticles modified screen printed electrode for determination of tryptophan using response surface methodology approach. Microchemical Journal, 154, p.104634.

[59] Fei, A., Liu, Q., Huan, J., Qian, J., Dong, X., Qiu, B., Mao, H. and Wang, K., 2015. Label-free impedimetric aptasensor for detecting femtomole level acetamiprid using gold nanoparticles decorated multiwalled carbon nanotube-reduced graphene oxide nanoribbon composites. Biosensors and Bioelectronics, 70, pp.122-129.

[60] Yu, A., Liang, Z., Cho, J. and Caruso, F., 2003. Nanostructured electrochemical sensor based on dense gold nanoparticle films. Nano letters, 3(9), pp.1203-1207.

[61] Jin, W. and Maduraiveeran, G., 2017. Electrochemical detection of chemical pollutants based on gold nanomaterials. Trends in environmental analytical chemistry, 14, pp.28-36.

[62] A. Morrin, A.J. Killard, M.R. Smyth, Electrochemical characterization of commercial and home-made screen-printed carbon electrodes, Anal. Lett. 36 (2003) 2021–2039. https://doi.org/10.1081/AL-120023627.

[63] T.W.B. Lo, L. Aldous, R.G. Compton, The use of nano-carbon as an alternative to multi-walled carbon nanotubes in modified electrodes for adsorptive stripping voltammetry, Sensors Actuators, B Chem. 162 (2012) 361–368. https://doi.org/10.1016/j.snb.2011.12.104.

[64] J. Yang, J.R. Strickler, S. Gunasekaran, Indium tin oxide-coated glass modified with reduced graphene oxide sheets and gold nanoparticles as disposable working electrodes for dopamine sensing in meat samples,

Nanoscale. 4 (2012) 4594–4602. https://doi.org/10.1039/c2nr30618b.

[65] G. Goncalves, P.A.A.P. Marques, C.M. Granadeiro, H.I.S. Nogueira, M.K. Singh, J. Grácio, Surface modification of graphene nanosheets with gold nanoparticles: The role of oxygen moieties at graphene surface on gold nucleation and growth, Chem. Mater. 21 (2009) 4796–4802. https://doi.org/10.1021/cm901052s.

[66] J.M. Jian, L. Fu, J. Ji, L. Lin, X. Guo, T.L. Ren, Electrochemically reduced graphene oxide/gold nanoparticles composite modified screen-printed carbon electrode for effective electrocatalytic analysis of nitrite in foods, Sensors Actuators, B Chem. 262 (2018) 125–136. https://doi.org/10.1016/j.snb.2018.01.164.

[67] R.M. Dominic, P. Punniyakotti, B. Balan, S. Angaiah, Green synthesis of reduced graphene oxide using Plectranthus amboinicus leaf extract and its supercapacitive performance, Bull. Mater. Sci. 45 (2022).

[68] D. Mhamane, W. Ramadan, M. Fawzy, A. Rana, M. Dubey, C. Rode, B. Lefez, B. Hannoyer, S. Ogale, From graphite oxide to highly water dispersible functionalized graphene by single step plant extract-induced deoxygenation, Green Chem. 13 (2011) 1990–1996.

[69] L.M. Garry, The Electrochemical Characterisation of Carbon-based Nanomaterials and their Application in the Detection of Heavy Metal Ions, (2013) 262.

[70] Y.Q. He, S.P. Liu, L. Kong, Z.F. Liu, A study on the sizes and concentrations of gold nanoparticles by spectra of absorption, resonance Rayleigh scattering and resonance non-linear scattering, Spectrochim. Acta - Part A Mol. Biomol. Spectrosc. 61 (2005) 2861–2866.

[71] M.. J.E.. and Rohiman, A.; Amran B.; Bachri, I. Irman, Sintesis, Karakterisasi, dan Aplikasi Gold Nanoparticles (AuNPs) pada Penumbuhan Silicon Nanowires (SiNWs), Res. Dev. Nanotechnol. Indones. 1 (2014) 74–82.

[72] D.G. Trikkaliotis, A.K. Christoforidis, A.C. Mitropoulos, G.Z. Kyzas, Graphene oxide synthesis, properties and characterization techniques: A comprehensive review, ChemEngineering. 5 (2021). https://doi.org/10.3390/chemengineering5030064.

[73] K. Dawson, J. Strutwolf, D. Arrigan, A. Quinn, A.J. O'Riordan, Nanofabrication of Robust Nanoelectrodes for Electrochemical Applications, ECS Meet. Abstr. MA2010-01 (2010) 1842–1842. https://doi.org/10.1149/ma2010-01/42/1842.

[74] N. Hassan, R. Holze, A comparative electrochemical study of electrosorbed 2- and 4-mercaptopyridines and their application as corrosion inhibitors at C60 steel, J. Chem. Sci. 121 (2009) 693–701. https://doi.org/10.1007/s12039-009-0083-y.

[75] A. Wahl, K. Dawson, N. Sassiat, A.J. Quinn, A. O'Riordan, Nanomolar trace metal analysis of copper at gold microband arrays, J. Phys. Conf. Ser. 307 (2011) 1–7. https://doi.org/10.1088/1742-6596/307/1/012061.

[76] A. Zuzuarregui, S. Arana, E. Pérez-Lorenzo, S. Sánchez-Gómez, G. Martínez De Tejada, M. Mujika, Novel fully-integrated biosensor for endotoxin detection via polymyxin B immobilization onto gold electrodes, J. Sensors Sens. Syst. 2 (2013) 157–164. https://doi.org/10.5194/jsss-2-157-2013.

[77] L.R. de Astudillo, L. Rivera, R. Brito-Gómez, R.J. Tremont, Electrochemical study of 1,4-benzoquinone on gold surface modified, J. Electroanal. Chem. 640 (2010) 56–60. https://doi.org/10.1016/j.jelechem.2010.01.005.

[78] A.G.M. Ferrari, C.W. Foster, P.J. Kelly, D.A.C. Brownson, C.E. Banks, Determination of the electrochemical area of screen-printed electrochemical sensing platforms, Biosensors. 8 (2018) 1–10. https://doi.org/10.3390/bios8020053.

[79] S. Trasatti, O.A. Petrii, International Union of Pure and Applied Chemistry

Physical Chemistry Division Commission on Electrochemistry: Real Surface Area Measurements in Electrochemistry, Pure Appl. Chem. 63 (1991) 711–734. https://doi.org/10.1351/pac199163050711.

[80] M.J. Rodríguez Presa, L.M. Gassa, O. Azzaroni, C.A. Gervasi, Estimating diffusion coefficients of probe molecules into polyelectrolyte brushes by electrochemical impedance spectroscopy, Anal. Chem. 81 (2009) 7936–7943. https://doi.org/10.1021/ac9009808.

[81] S.J. Konopka, B. McDuffie, Diffusion Coefficients of Ferri- and Ferrocyanide Ions in Aqueous Media, Using Twin-Electrode Thin-Layer Electrochemistry, Anal. Chem. 42 (1970) 1741–1746. https://doi.org/10.1021/ac50160a042.

[82] W.S. Cardoso, V.L.N. Dias, W.M. Costa, I. De Araujo Rodrigues, E.P. Marques, A.G. Sousa, J. Boaventura, C.W.B. Bezerra, C. Song, H. Liu, J. Zhang, A.L.B. Marques, Nickel-dimethylglyoxime complex modified graphite and carbon paste electrodes: Preparation and catalytic activity towards methanol/ethanol oxidation, J. Appl. Electrochem. 39 (2009) 55–64. https://doi.org/10.1007/s10800-008-9636-x.

[83] J. Smajdor, R. Piech, M. Ławrywianiec, B. Paczosa-Bator, Glassy carbon electrode modified with carbon black for sensitive estradiol determination by means of voltammetry and flow injection analysis with amperometric detection, Anal. Biochem. 544 (2018) 7–12. https://doi.org/10.1016/j.ab.2017.12.025.

[84] A. Özcan, D. Topçuoğulları, Voltammetric determination of 17-β-estradiol by cysteamine self-assembled gold nanoparticle modified fumed silica decorated graphene nanoribbon nanocomposite, Sensors Actuators, B Chem. 250 (2017) 85–90. https://doi.org/10.1016/j.snb.2017.04.131.

[85] R.M. De Carvalho, C. Mello, L.T. Kubota, Simultaneous determination of phenol isomers in binary mixtures by differential pulse voltammetry using carbon fibre electrode and neural network with pruning as a multivariate

calibration tool, Anal. Chim. Acta. 420 (2000) 109–121.

[86] Ł. Górski, F. Ciepiela, M. Jakubowska, Automatic baseline correction in voltammetry, Electrochim. Acta. 136 (2014) 195–203. https://doi.org/10.1016/j.electacta.2014.05.076.

[87] J. Li, S. Liu, J. Yu, W. Lian, M. Cui, W. Xu, J. Huang, Electrochemical immunosensor based on graphene-polyaniline composites and carboxylated graphene oxide for estradiol detection, Sensors Actuators, B Chem. 188 (2013) 99–105. https://doi.org/10.1016/j.snb.2013.06.082.

[88] M. Arvand, S. Hemmati, Analytical methodology for the electro-catalytic determination of estradiol and progesterone based on graphene quantum dots and poly(sulfosalicylic acid) co-modified electrode, Talanta. 174 (2017) 243–255. https://doi.org/10.1016/j.talanta.2017.05.083.

[89] P.A. Raymundo-Pereira, N.O. Gomes, S.A.S. Machado, O.N. Oliveira, Simultaneous, ultrasensitive detection of hydroquinone, paracetamol and estradiol for quality control of tap water with a simple electrochemical method, J. Electroanal. Chem. 848 (2019) 113319. https://doi.org/10.1016/j.jelechem.2019.113319

[90] Davies, T.J. Davies, Compton, R.G., 2005. The cyclic and linear sweep voltammetry of regular and random arrays of microdisc electrodes: Theory. Journal of Electroanalytical Chemistry, 585(1), pp.63-82.

[91]. Ahmed, M.B., Zhou, J.L., Ngo, H.H., Johir, M.A.H., Sun, L., Asadullah, M. and Belhaj, D., 2018. Sorption of hydrophobic organic contaminants on functionalized biochar: Protagonist role of π-π electron-donor-acceptor interactions and hydrogen bonds. Journal of Hazardous Materials, 360, pp.270-278.

Chapter 6 Imparting selectivity with a molecularly imprinted polymer platform

6.1 Introduction

Electroanalytical methods facilitate the determination of environmental pollutants. Electrochemical sensors, like conventional analytical equipment such as LC-MS and HPLC, are intended to identify analytes selectively. However, most disposable sensors suffer from low selectivity, necessitating the addition of a material that can selectively identify target analytes [1]. This prompted exploring materials boasting enhanced selectivity [2-4].

Molecularly imprinted technology produces molecularly imprinted polymers (MIPs) created through a polymerization reaction between a functional monomer and a template. Post-extraction, imprinting cavities remain [5]. MIPs, a result of the molecular imprinting process, exhibit higher affinity to their target template [6]. Their affinity, selectivity, and resilience in harsh environments render them suitable for environmental monitoring [7]. In the conventional MIP synthesis, multiple porogenic solvents dissolve polymerization reagents to prevent insolubility issues. Figure 6.1 illustrates commonly used porogenic solvents in molecular imprinting technology (MIT).

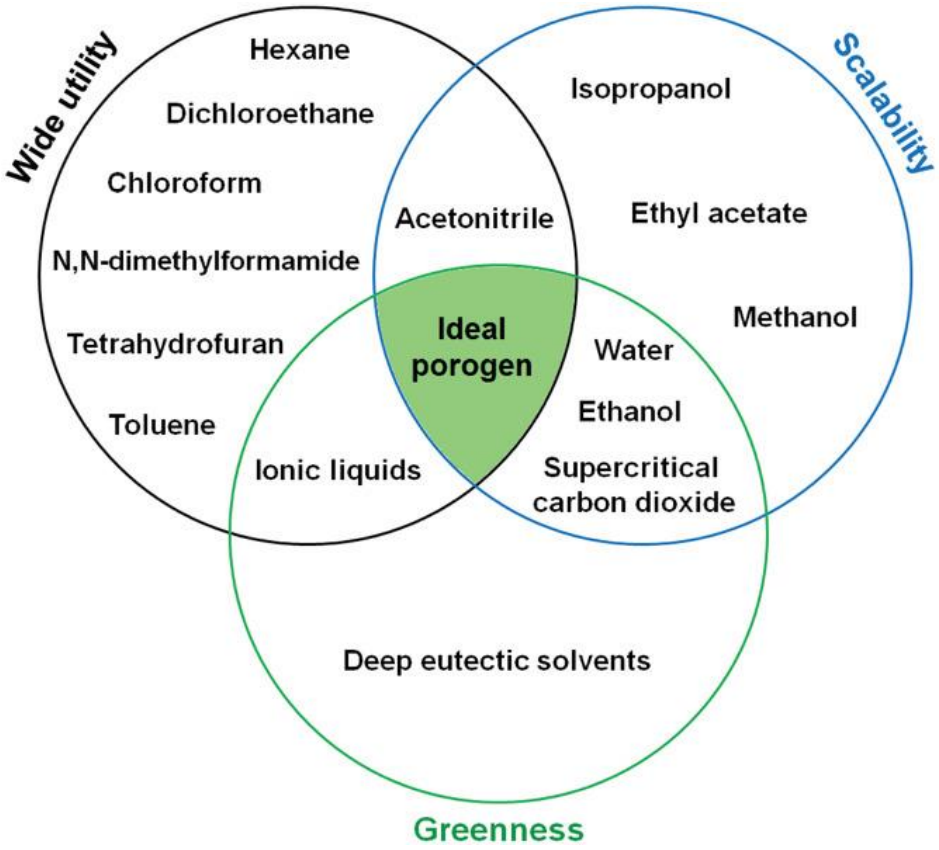

Figure 6.1 Venn diagram of common porogens/solvents in Molecular imprinting technology (MIT). Adapted from ref [3] with permission from Wiley.

On the other hand, deep eutectic solvents (DES) are designer green solvents that can serve as alternatives to harsh solvents for various applications in the chemical science fields [8]. Their biocompatibility, biodegradability, and simplicity in preparation fulfil green chemistry prerequisites [3,8,9]. Merging MIPs, DES, and disposable screen-printed sensors paves the way for platforms that can sensitively and selectively gauge analytes through electrochemical oxidation [10].

Futra et al. [11] detailed utilising molecularly imprinted polymeric microspheres combined with gold nanoparticle-grafted multi-walled carbon nanotubes to detect

E2 using SPEs. Differential pulse voltammetry (DPV) assessed the MIP sensor's performance. Lee et al. [12] introduced a multichannel electroanalytical system employing in situ electropolymerized MIP screen-printed gold electrodes. This electroanalytical system was able to detect E2 and other analytes. The MIP-modified SPE gave a LOD of 3.30 x 10^{-8} M for E2 in the concentration range of 2.20 x 10^{-8} - 3.67 x 10^{-3} M [12]. To make good candidates for aiding MIP-template interaction, DES is made from hydrogen acceptors with hydrogen donor bonds [13,14]. Furthermore, DES can function as a solvent and binder when pairing MIP with other nanomaterials [13,15]. The DES role in molecularly imprinted technology is evolving. Initial works emphasized modifying SPE with DES for an E2 sensor [17], while recent endeavours, like those by Liu et al., incorporated choline chloride in MIP synthesis [13]. Fu et al. showcased DES combined with caffeic acid, which acted as a monomer and template for polyphenol recognition [14].

6.1.1 Integrating MIP with a Sensor Transducer

MIPs are incorporated into sensor designs, aligning with various transduction types, including surface plasmon resonance (SPR), surface acoustic wave (SAW), voltammetry, impedance spectroscopy, and optical spectroscopy [12-14]. Among these, the gate effect, particularly for non-reactive analytes, dominates as the prevalent electrochemical signal transduction method in MIP sensors [18]. This facilitates measurements using cyclic voltammetry [19], differential pulse voltammetry (DPV) [20], and electrochemical impedance spectroscopy (EIS) [21,22]. The gate effect is the most common and widely used electrochemical transduction method in MIP sensors for electroanalysis, which stems from

facilitating electrode access during a redox marker's faradaic process when filling MIP's molecularly imprinted cavities with target analytes. Comparing current responses between synthesized imprinted and non-imprinted polymers establishes the foundation of sensor detection [19,23]. This involves adsorption, absorption, diffusion, transport, and transfer [23].

6.1.2 Imprinting Techniques

Numerous polymerizations have been documented for molecularly imprinted polymer preparation [24]. These include suspension polymerization, precipitation polymerization, bulk polymerization, surface polymerization, thermal polymerization, and electropolymerization, contingent on the analyte's nature and intended application [5,25-29]. Surface imprinting approaches allow the polymerization mixture to form a uniform binding site without aggregating the template within the polymer matrix. This is achieved by contact with the outer surface, hence the ability to exit the imprinted matrix, thus generating surfaces with a high density of rebinding sites [24].

Bulk imprinting involves adding the template directly to the monomer for polymerisation. This ensures that the active sites are not only on the surface of the sensing material but also evenly distributed within the whole matrix, hence the term bulk imprinting. This provides enough active sites on the sensitive layer that can only be accessed via diffusion pathways within the polymeric matrix, increasing the sensor response time in some cases (depending on the layer height). According to their application and polymerisation method, MIPs come in various physical forms, including porous microsphere, nanosphere, nanowire, thin film, and composite [5].

Electropolymerisation has proven to be a good technique for preparing MIP sensors, overcoming some inherent setbacks associated with other imprinting methods [31–33]. It allows a film deposition on the electrode surface with controlled thickness [31, 34–36]. The cyclic voltammetric technique allows for depositing a thin, uniform film layer with a good attachment to the transducer surface, with only the monomer and the template molecule giving films between 10 and 50 nm in thickness [31]. The film thickness controls how fast ions are transported. Eventually, it affects the produced MIP's equilibrium time, affinity, and selectivity [37]. Electropolymerisation can remove the complicated and time-consuming procedures for sensor fabrication [38].

Molecularly imprinted polymer sensors reported for such requirements consist predominantly of aromatic rings with different functional groups. Amines are the most reported functional groups due to their interactions via hydrogen bonding. The reported work includes polyaminophenol [39], polyaniline and its derivative poly(o-phenylenediamine) (POPD) [40], and methacrylic acid (MAA) [41].

MAA is a good choice for polymerization as it has small molecules, resulting in low non-specific interaction sites. It is easy to prepare and cost-effective [76].

Previous studies have utilized the monomer MAA MIP-sensors for E2 [11,42, 43]. The choice of MAA as the functional monomer was specifically made for E2 imprinting and has demonstrated success in various studies [11,42–44]. Following Alizadeh et al.'s protocol, MAA was considered the optimal choice for testing due to its frequent usage and extensive investigation as a functional monomer. Additionally, Schillinger et al.'s computational models for monomers exhibited the highest template-rebinding capacity and selectivity in the molecular imprinting of E2 [42].

6.1.3 Surface Polymerisation

Surface imprinting is utilized when there is inadequate generation of appropriate sites, excessive thickness of the resulting MIP, challenges in template removal, and hindered diffusion into deep cavities due to steric effects. Surface imprinting addresses these limitations by locating the imprinting sites on the surface of the MIP. This enables the complete removal of the template molecule, facilitates rapid mass transfer, and improves binding kinetics, thereby enhancing the capacity of the MIP [48].

6.1.4 Thermal Polymerisation

Thermal polymerization is conducted by subjecting the polymerization mixture to heat at 80-160°C [49]. The polymerization solution comprises a suitable crosslinker, initiator, monomer, and template ratio. Since heat is involved in the process, the initiator is typically used in trace amounts as it is sufficient for the polymerization [49]. Therefore, thermal polymerization refers to the process in which the monomer undergoes polymerization solely through the application of heat [42, 50]. Figure 6.2 illustrates the structural formulas of the ingredients in the polymerization mixture used for MIP synthesis.

However, the MIPs have been reported to be poorly compatible with transducers as they limit mass transfer and rebinding kinetics in MIP sensor applications [30]. MIPs have been developed using alternative materials [79] to improve the conductivity of functional monomers. Various materials have been employed to enhance the detection efficiency of MIPs for analytes. One effective approach, as reported, involves combining MIPs with Fe_3O_4/Graphene Oxide (GO) [45]. MIPs offer recognition sites with hydrophilic, hydrophobic, ionic, and acid-base

properties, enabling molecular moulding [46-47]. Alizadeh et al. successfully combined molecularly imprinted polymers and carbon paste to develop a voltammetric sensor to determine 2,4,6-trinitrotoluene (TNT) and para-nitrophenol [51, 52]. The study used a cost-effective and straightforward method of mixing methacrylic acid (MAA), which prepared a MIP chloroform template with EGDMA and AIBN in a reaction cell. The resulting MIP or non-imprinted Polymer (NIP) powder was used to fabricate the sensor (MIP-CP or NIP-CP). The addition of carbon paste was intended to enhance the sensor response and selectivity of the MIP by facilitating electron transfer [52].

Mostafiz et al. provided an excellent review of the approach for developing molecularly imprinted polymer-carbon paste electrode (MIP-CPE)-based sensors for detecting organic and inorganic environmental pollutants [53]. In another study, Alizadeh et al. reported the detection of Bi^{3+} ions in various samples using ion-imprinted polymers (IIP)/MWNTs-modified carbon paste electrodes. They used itaconic acid and EGDMA as the functional monomer and crosslinker to synthesize the imprinted nanoparticles for Bi^{3+} ions. The electrochemical sensor showed a linear range of 0.2-2 µM with a LOD of 8.9 nM [54]. The Alizadeh group has further incorporated MIP with carbon paste as an easy and effective way of fabricating sensors. This is an important protocol in electrochemical sensor design and fabrication [55].

This chapter explores MIP and carbon paste electrodes as disposable, selective tools for measuring E2 using amperometry as the transduction technique. Incorporating electroactive carbon paste in the MIP protocol will provide electrical conductivity [78], addressing the insulation-related lack of electrochemical signal

observed in MAA [77]. MIP involves creating specific cavities within a polymer matrix that can selectively bind with a targeted molecule or template. This binding occurs due to the cavities' size, shape, and functional groups, which match the templates. These MIPs have conventionally been used for their binding capacity in various applications [1]. Recently, researchers have expanded their use to design electrochemical sensors with composite structures to improve their performance. Therefore, nanocomposites that integrate with MIPs are expected to enhance the electrochemical sensor signals [2].

6.2 Materials and Methods

6.2.1 Materials

17β-estradiol (E2), choline chloride, ethylene glycol, initiator of 2,2′-Azobis (2-methylpropionitrile) (AIBN), methacrylic acid (MAA), N, N′-Methylenebisacrylamide (BIS-acrylamide), acrylamide and crosslinker ethylene glycolmethacrylate (EGDMA), ethanol, acetone, and acetonitrile were purchased from Merck (Gillingham, UK).

6.2.2 Methods

6.2.2.1 Fourier Transform infrared spectroscopy (FT-IR)

FTIR analyses were carried out as described in Chapter 3.

6.2.2.2 Scanning Electron Microscopy (SEM)

SEM measurements were carried out as described in Chapter 3.

6.2.2.3 Dynamic Light Scattering (DLS)

DLS measurements were carried out on the synthesised MIP to verify the size described in Chapter 3.

6.2.2.4 Transmission Electron Microscopy

TEM measurements were carried out as described in Chapter 3.

6.2.2.5 Raman spectroscopy

The Raman spectra were recorded on a Horiba LabRam HR Evolution Raman spectrometer with a Coherent Innova 300 Argon laser with a 514.5 nm laser excitation. Raman spectroscopy was carried out using a 532 nm (2.33 eV) and 633 nm (1.96 eV) laser excitation (Horiba, USA).

6.2.3 Preparation of Deep Eutectic solvent (DES)

The procedure employed by Prathish et al. [58,59] was followed for DES synthesis. First, the deep eutectic solvents were obtained by mixing quaternary choline chloride with ethylene glycol in a 1:2 molar ratio and heating to 60 °C until a homogeneous solution was obtained. The mixture was then allowed to cool to room temperature for further use.

6.2.4 Preparation of 17β-estradiol MIP sensor

Synthesis of the estradiol MIP was carried out using the procedures and ratios from previously published literature with a few modifications [11, 42-44]. A test tube containing 150 mg E2, 340 µL methacrylic acid monomer (MAA), 3800 µL ethylene glycolmethacrylate (EGDMA) crosslinker, 80 mg of 2,2′-Azobis(2-methylpropionitrile) (AIBN) initiator, and 6 mL of acetonitrile solvent was sonicated to give a completely dissolved clear homogeneous solution. The tube

was sealed and placed in an oven at 70 ^{o}C overnight. After polymerisation, the synthesised MIP was crushed into a fine powder using a mortar and pestle. Next, E2 template removal was carried out by rigorously washing three times in methanol acetic acid (7:3 v/v). This was followed by centrifugation in ethanol three times to remove any remaining reagent in the MIP. The non-imprinted polymer was synthesised as above, except for the template addition. Then, the template-free MIP particles were collected using centrifugation at 4,032 × g (5000 rpm) for 30 minutes and dried in an oven at 70 ^{o}C. The fabricated MIPs were transferred into a glass vial for further analysis after the polymer was crushed and ground using a mortar, pestle, and a 38 µm sieve. Figure 6.2 shows the photograph image of synthesised MIP and NIP.

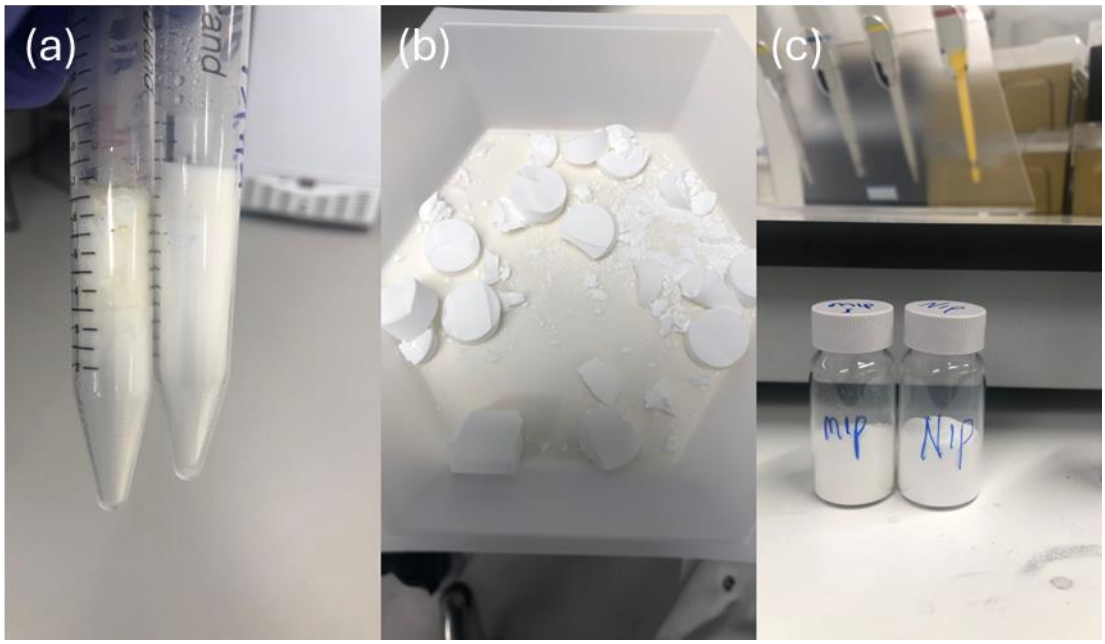

Figure 6.2 Photograph image of synthesised MIP & NIP (a and b) before template removal, (c) final synthesised MIP and NIP powder after template removal and grounded.

Adhesive and other films were used to fabricate the disposable DES-MIP-CP sensor and design the printed sensor's stencils, as seen in steps 1-2. A PET film of 100 microns was used as a stencil and substrate to construct the sensor. AutoCAD 2021 was employed to prepare the electrode dimensions. While Norland VS-540 print & cut printer was used to cut, the film desired the pattern shape and size of the electrode, making it a shadow mask. Step 3 involved mixing the various components, and the resulting mixture was named a carbon composite paste ink, which was then used as a screen-printable disposable carbon paste. Step 4 involves placing the cut film with the desired shape over another film, and the ink paste is placed on the top and spread across the shadow mask using a squeegee. The shadow mask was then removed afterwards and allowed to dry. Figure 6.4 shows the procedure for fabricating a molecularly imprinted polymer sensor. DES-MIP-CP and DES-NIP-CP disposable sensors were prepared by mixing carbon paste and DES solvent and synthesizing MIP or NIP in various ratios (66:27:7 wt.%).

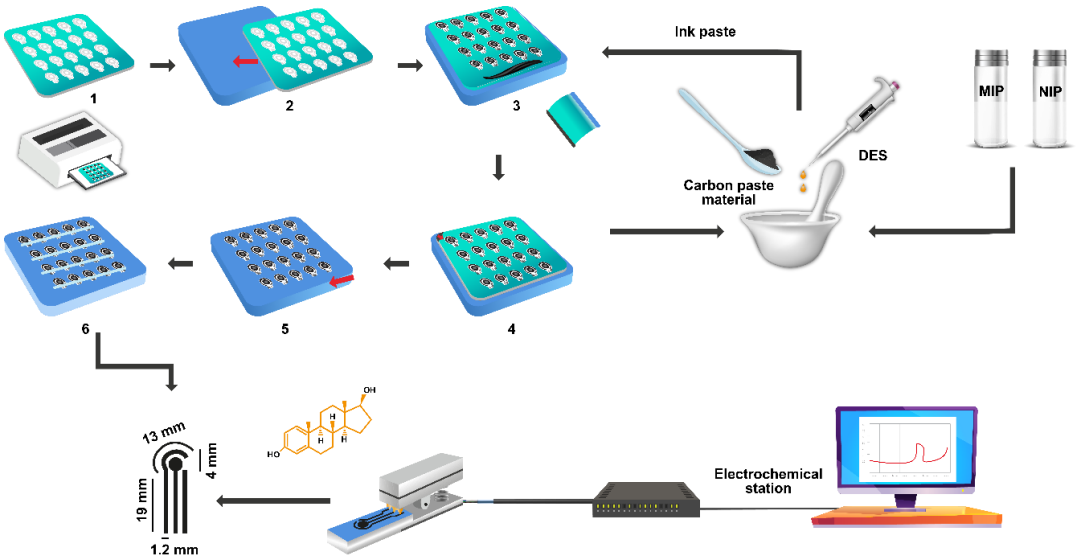

Figure 6.3 Schematic representation of the MIP & NIP sensor fabrication process. The sequence of steps includes (1) printing of the electrode pattern (stencil) set up for sensor screen printing, (2) attaching the stencil to PET, (3)spreading ink paste containing MIP or NIP with squeegee, (4) the mask is completed covered by ink paste, (5) printed sensor after removing the mask, (6) printed fabricated sensor ready for testing using potentiostat setup typically linked to a computer that generates a readout.

6.3 Results and Discussion

6.3.1 Characterization of the E2-MIP

The synthesised MIP particles were characterised using various techniques. Figure 6.4 and Figure 6.5 depict the size distribution of the particles, with an average of 543 nm for MIP (Pdi: 0.49) and 667 nm for NIP. MIP particle size measurements from the DLS technique show a hydrodynamic diameter and polydispersity index (PDI) between 0.1 and 0.4, indicating polydisperse particles. The particle size readings and PDI for MIP and NIP are comparable, indicating reproducibility. Overall, the results indicate a large particle for both NIP and MIP.

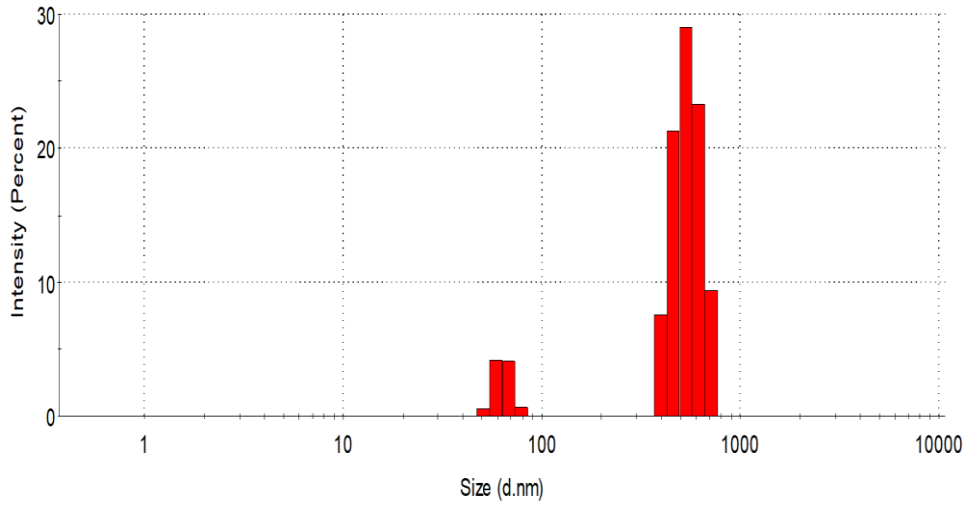

Figure 6.4. Bimodal intensity-weighted particle size distribution from DLS measurements of a Molecularly Imprinted Polymer (MIP), showing two dominant particle populations around 10 nanometers and 1000 nanometers.

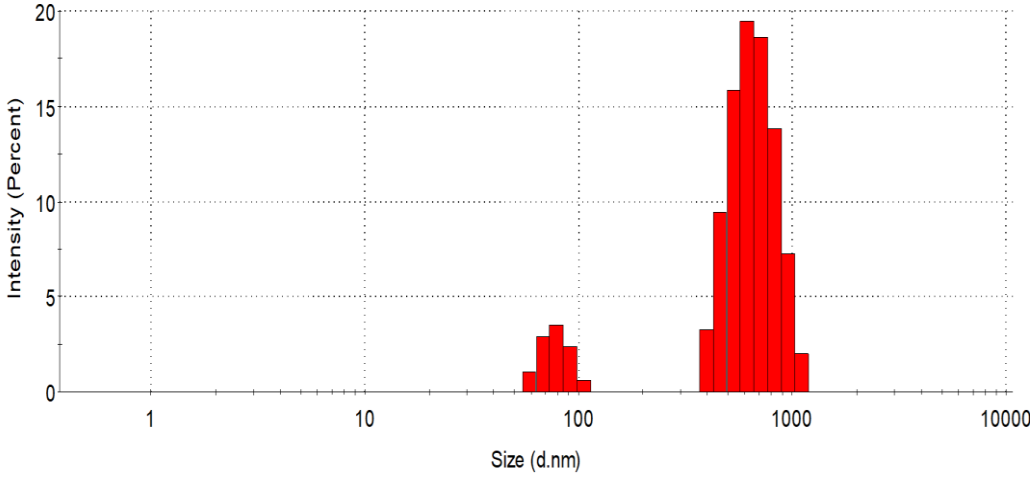

Figure 6.5: Intensity weighted particle size distribution for NIP measured by dynamic light scattering Figure 6.4. Bimodal intensity-weighted particle size distribution from DLS analysis, with significant particle populations centred around 100 nanometers and just above 1000 nanometers, indicating two distinct size regimes within the sample.

Further examination observed from the DLS results by using TEM analysis for the size and shape of the synthesised MIP in Figure 6.6 and NIP TEM results (Figure 6.7) confirmed that the synthesised imprinted polymers were less than 500 nm in size and irregularly spherical (Figure 6.6). Both TEM analyses show that the two measurements are comparable, considering experimental error and that DLS commonly overestimates size because the solvent present increases the hydrodynamic diameter.

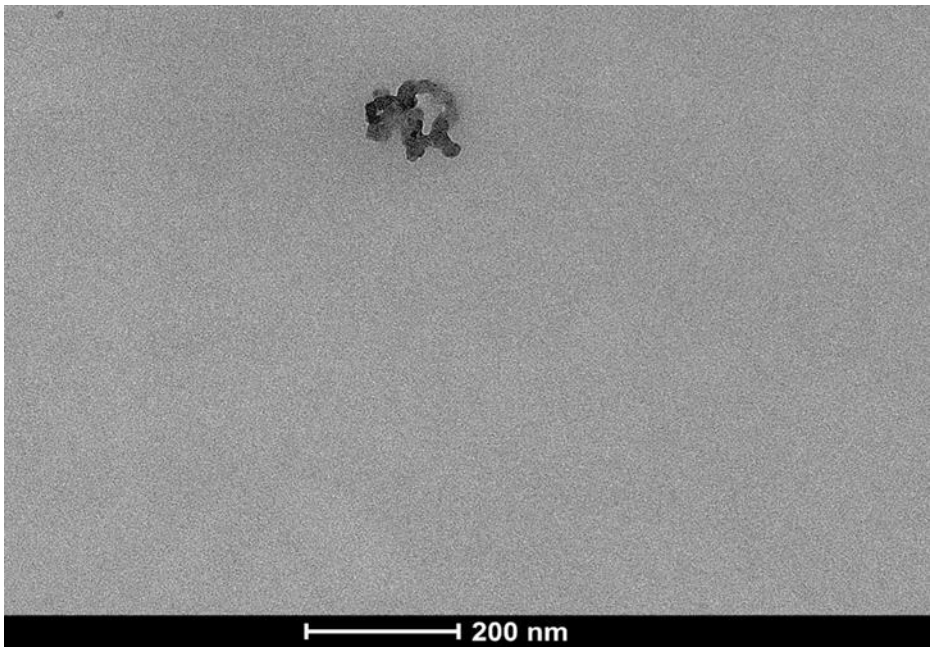

Figure 6.6 Transmission electron microscopy (TEM) image of MIP at 30 000× magnification at 120 kV.

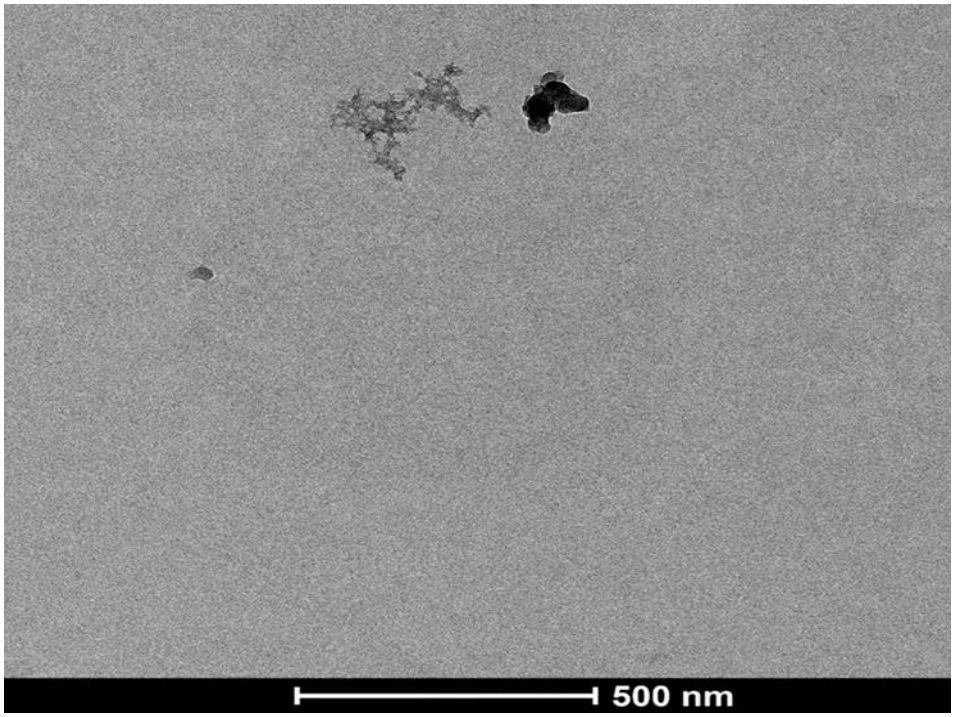

Figure 6.7 Transmission electron microscopy (TEM) image of NIP at 30 000× magnification at 120 kV.

Figure 6.8 A&C shows that both SEM images of MIP and NIP surfaces look similar. This is obvious as the graphite powder used has the same particle size and porosity (A&C) at 500 µm. Figure 6.8 B&D both reveal similar morphology and rough surfaces with irregular shapes.

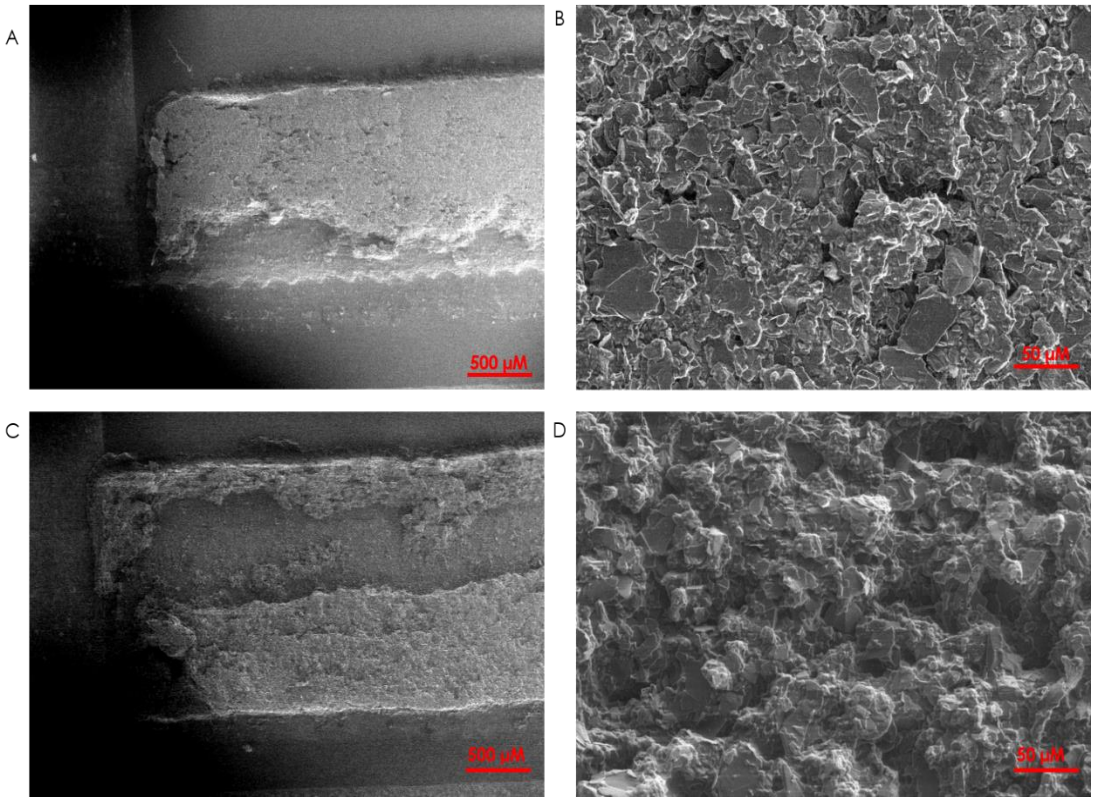

Figure 6.8 SEM images of (A) molecularly imprinted polymer (E-2 MIP) at 500 µM and (B) 50 µm; non-molecularly imprinted polymer (NIP) (C) 50 µm MIP (D) 50 µm NIP

Fourier Transform Infrared (FTIR) analysis elucidates the composition of DES formation and MIP/NIP fabricated sensors. Looking at Figure 6.9A, the peak at 3300 cm^{-1} bands corresponds to O-H stretching of the OH functional group, A typical characteristic of the DES ChCl: EG [65]. The 2932 cm^{-1} and 2878 cm^{-1} bands are characteristic of C-H stretching for SP^3 hybridized bends. Others include bands, such as C=C aromatic benzene ring at 1641 cm^{-1}, 1416 cm^{-1} for CH_2 bending attributed to an alkyl group and 1204 cm^{-1} C-O stretching, 1037 cm^{-1} C-C-O asymmetric stretching. C-C-O symmetric stretching at 863 cm^{-1} [65–67].

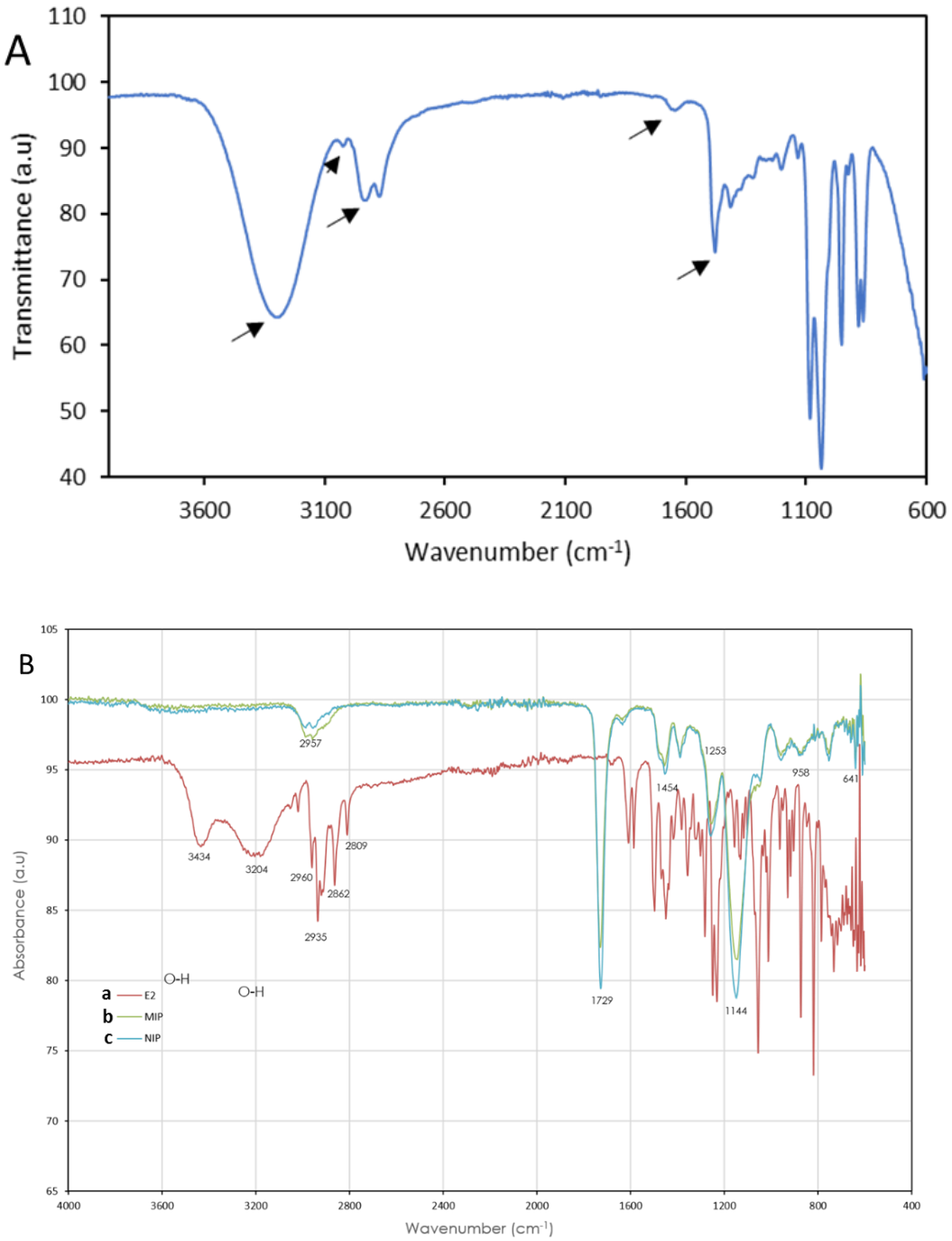

Figure 6.9 A) FT-IR spectra of Deep Eutectic Solvent. B) FTIR spectra of (a) estradiol, (b) molecularly imprinted polymer, and (c) non-molecularly imprinted polymer (NIP).

Figure 6.9B shows the E2 MIP and NIP FTIR analysis. The FTIR spectra of polymerised functional monomer showed peaks at 2957 cm^{-1} corresponding to the C–H stretching vibration in both MIP and NIP. The peak at 1729 cm^{-1} was

due to the C=C group. C–O corresponded to a peak at 1148 cm^{-1} (MIP) and 1144 cm^{-1} (NIP) because of the polymerisation between the crosslinkers and monomers. FTIR spectra confirm the successful removal of the template and the polymerisation of the monomer. This suggests the polymer particles are free of E2, ensuring the successful removal of the template using methanol: acetic acid. The E2 spectrum indicates a pronounced band at around 3434 cm^{-1} and a peak at 3204 cm^{-1}. These bands are attributed to the OH group and aromatic E2 ring that was not seen in either NIP or MIP-template-free. A similar suggestion was reported by Yang et al. [68].

The overlapped peaks at 2957 cm^{-1} for MIP and NIP correspond to the stretch vibration of the -COOH group since MIP and NIP have no E2 within the polymer matrix, confirming the successful extraction process. Thus, the polymer network formation around the template and removal was achieved. Raman spectroscopy was employed to probe further, as shown in Figures 6.10 and 6.11. Raman spectra were taken with 532 nm (green) excitation, 5% power X100 lens, 2x20 seconds, hole - 100 µm. Images were taken using View Sharp for a better-quality image of the region from which spectra were taken and recorded before and after– no apparent laser damage was observed. In duplicate spectra, no significant change in shape or intensity was observed, indicating no laser degradation by the samples (MIP and NIP) of Figure 6.10 (A&B). Other spectra were also taken at several points on the sample, which did not show significant differences between the samples of MIP and NIP (figure 6.10). The peaks observed for MIP at 1354 and 1582 cm^{-1} and NIP look similar at 1348 and 1582 cm^{-1}, corresponding to the D and G bands. The G and D peaks are two significant

features in carbonaceous material's Raman spectra and usually lie between 1560 and 1360 cm^{-1} [69]. The G band is traditionally considered the fingerprint of graphitic materials, which arises from the longitudinal optical and transverse optical lattice vibrations of graphite and graphite-based materials characteristic of sp^2-hybridized C-C bonds [70,71]. As the D band signifies the amount of disorder in a carbon-based material, looking at the (MIP and NIP) in Figure 6.10 at 1354, 1348 cm^{-1} indicates that the is Raman-active with no extraneous materials, as seen in the photographs in Figure 6.10 (A&B). Therefore, MIP and NIP in both fabricated sensors do not alter the carbon paste composition.

Figure 6.11AB illustrates the Raman spectrum of E2 and MIP. Many peaks in the E2 spectrum do not overlap with any in the MIP spectrum. As an example, the peak is at 730 cm^{-1}. This suggests that the MIP is template-free after template extraction. Figure 6.12 compares MIP and NIP. There is no immediate difference between the MIP and NIP spectra.

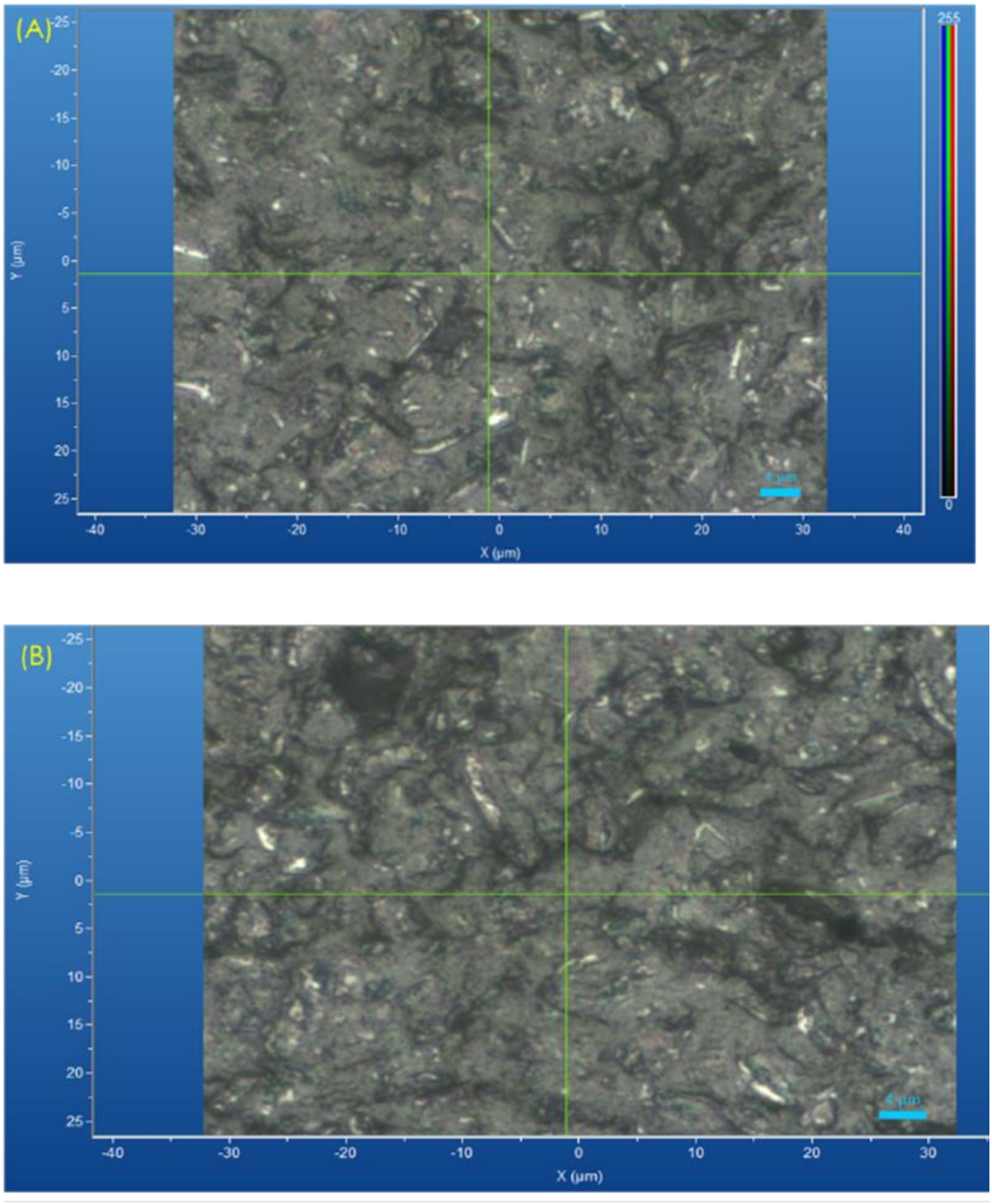

Figure 6.10 (A) Raman photograph of MIP (B) Raman photograph of NIP (C) Raman spectra of MIP(D) Raman spectra of NIP taken at 300-4000 Raman shift wave number.

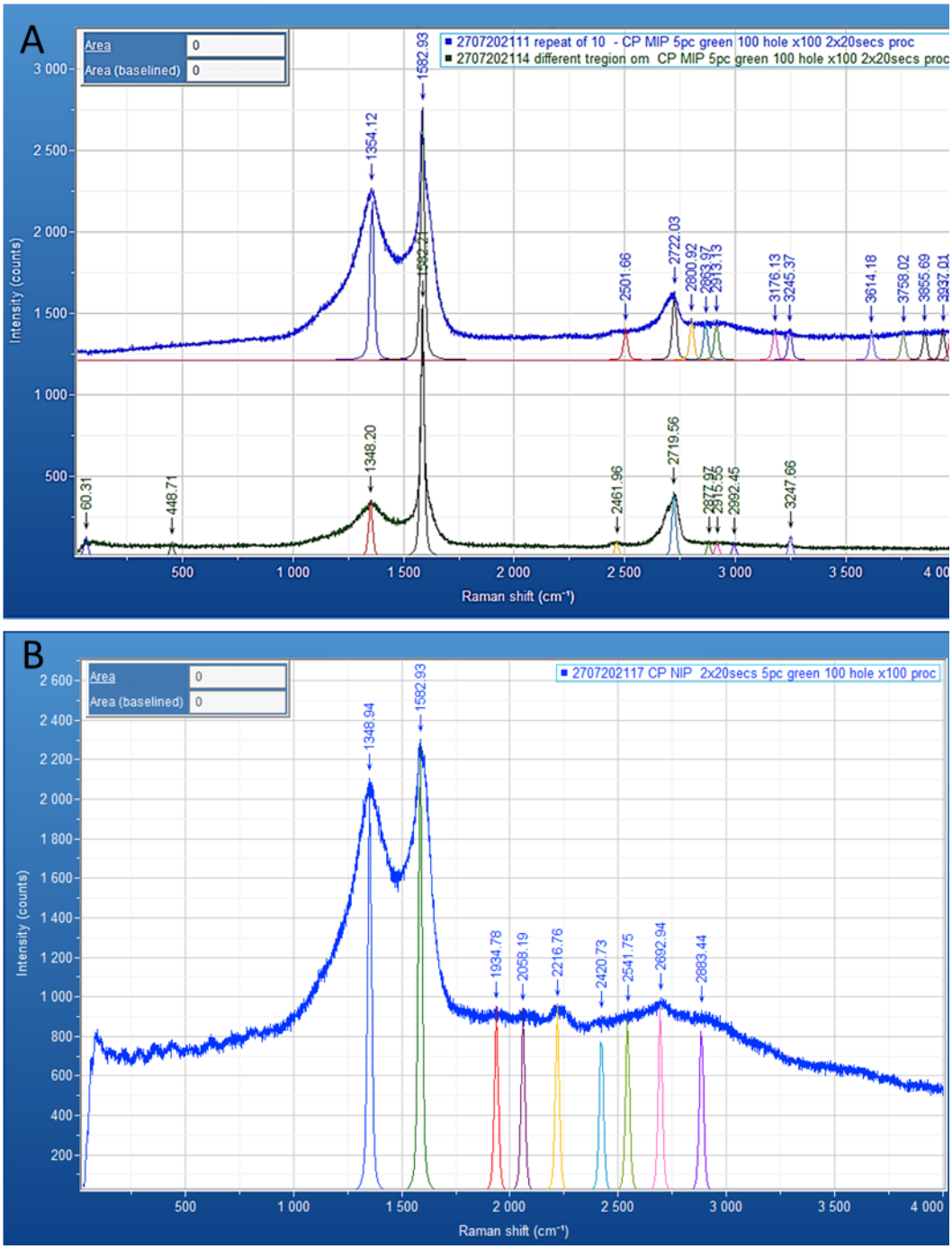

Figure 6.11 (A) Raman spectra of MIP(B) Raman spectra of NIP taken at 300-4000 Raman shift wave number.

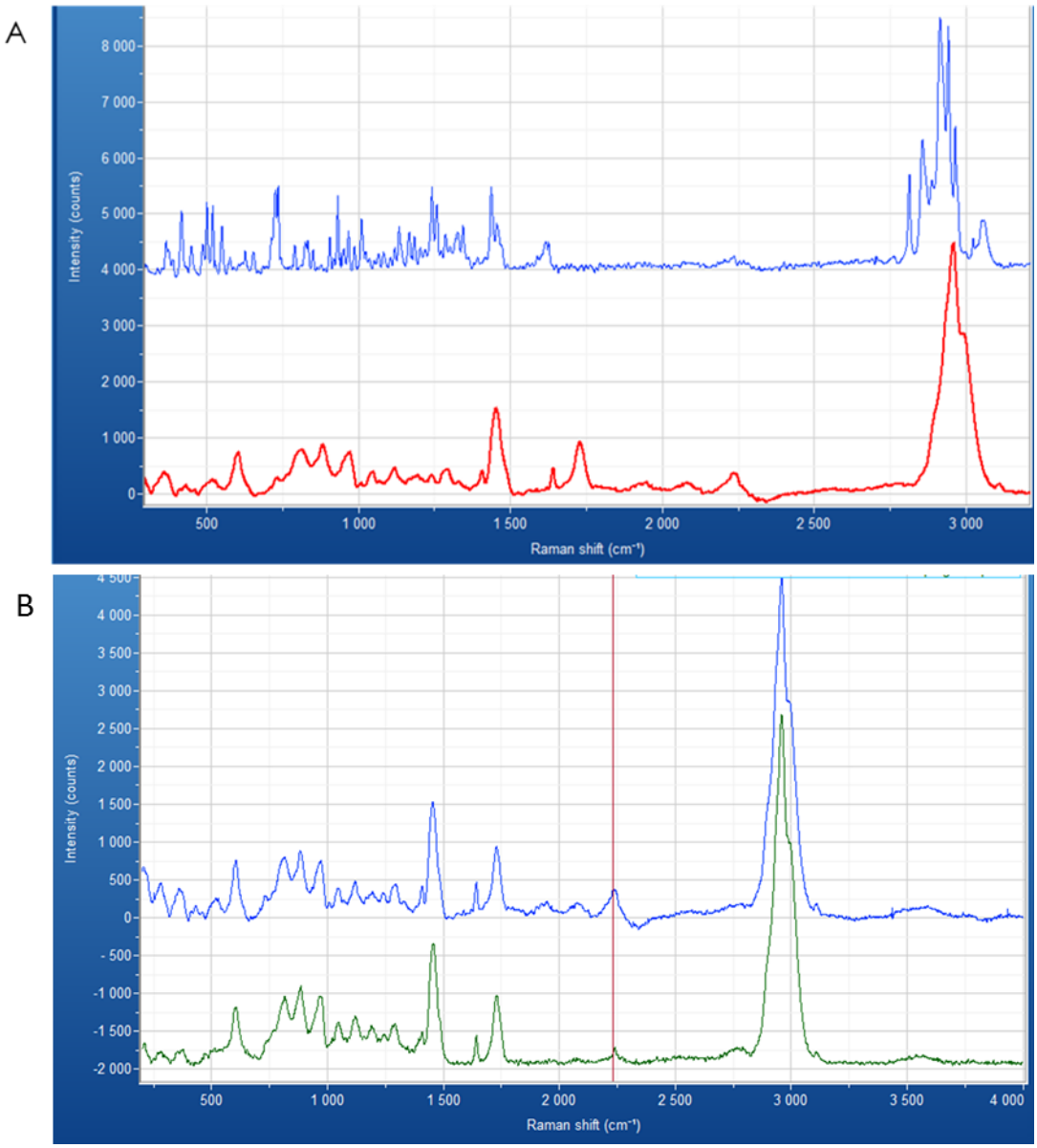

Figure 6.12 Raman spectra of (A) E2 and MIP spectra with peak positions and (B) overlapped MIP and NIP spectra.

6.3.2 Application of E2-imprinted polymers

The main analytical performance of the E2 MIP sensor was evaluated by amperometry. Figure 6.13 depicts the differential pulse voltammetry response of the various electrodes. The electrooxidation of E2 occurring at different electrodes was carried out at 0.46 V with a step potential of 10 mV, pulse amplitude of 100 mV, pulse time and a scan rate of 50 mV s^{-1}. Single oxidation was observed in all the electrodes, recording an oxidation current of 2.37 µA for CP, 2.28 µA for DES-MIP-CP and 1.32 µA for DES-NIP-CP, at the potential range of 0.2 V to 0.8 V. The results demonstrated recognition of the MIP sensor towards E2 as the cavities allow access to the electrode. This is confirmed by the polymer-free CP having a peak current of 2.37 µA as it contains only carbon paste, which is sensitive to E2, as reported by Song et al. [73]. Adding the MIP (DES-MIP-CP) lowers the signal to 2.28 µA. Gholivand et al. reported a MIP sensor using methacrylic acid (MAA) as a functional monomer. The MIP was integrated into the CP electrode to detect and distinguish the presence of piroxicam when the electrode underwent oxidation [80].

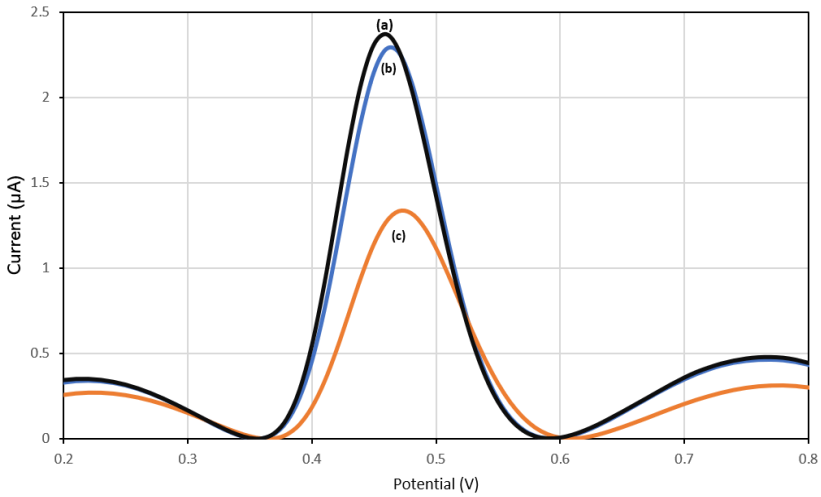

Figure 6.13 Differential pulse voltammetry responses of (a) DES-MIP-CP, (b) CP and (c) DES-NIP-CP in 5.0 x 10^{-5} M E2 in PBS pH 7.

Figure 6.13 demonstrates the ability of the E2 to bind to the MIP and that the MIP cavities are specific to it. On the other hand, DES-NIP-CP has an oxidation current of 1.32 µA, implying the hindrance to the oxidation of E2 at the electrode surface because no cavities were created that are specific to E2. The current here is from the CP itself. The results show that the MIP sensor has a signal of 2.28 µA and 1.32 µA compared to the NIP. This suggests that the NIP has a lower affinity towards E2 and confirms that the artificial cavities created in the MIP impart selectivity.

6.3.2.1 Detection of E2 Using the Amperometry Sensor

The purpose of using molecularly imprinted polymers is to be selective to the analyte of interest on the sensor. Figure 6.14a shows the amperogram oxidation current signal generated at the DES-MIP-CP electrode upon injection of E2 into the buffer solution. The E2 concentration increases on the MIP or NIP electrode surface with each injection for five consecutive additions. Figure 6.14b illustrates the current generated for various concentrations of E2 injected and

corresponding calibration curves. From Figure 6.15, a linear relationship between current and is obtained for the NIP.

On the other hand, the DES-MIP-CP has an affinity towards E2, allowing access toward the MIP surface and oxidising at the applied potential. The signal shown in Figures 6.14A and 6.14B indicates a better signal for MIP than NIP. The amperometric response of the DES-MIP-CP after successive additions of E2 was further evaluated under optimised experimental conditions for the analytical response curve (n=3), shown in Figure 6.14B. Each point represents the mean value for three measurements. The concentration ranges from 0.83 – 2.49 µM (8.3×10^{-7} to 2.49×10^{-6} M).

The slopes recorded were 0.0266 µA/µM for DES-MIP-CP y = 0.0266x + 0.0077 R^2 = 0.9962, with LOD approximately 1.13×10^{-7} M (0.113 µM). In contrast, the linear range is (2.49 - 4.98 µM) 2.49×10^{-6} - 4.98×10^{-6} M, y = 0.0073x + 0.0569 R^2 = 0.855, LOD 5.645 µM (5.645×10^{-6} M). For DES-NIP-CP, there was a linear relationship as shown in Figure 6.15B with equation y = 0.0183x + 0.0141, R^2 = 0.9978 and sensitivity and LOD of 0.25 µM (2.5×10^{-7} M), y = 0.0183x + 0.0141 R^2 = 0.9978, respectively in Figure 6.15b. The results have shown that the current density response of the DES-MIP-CP was higher than that of the DES-NIP-CP, implying that E2 imprinted sites formation of DES-MIP-CP. Figure 6.16 shows the current arising from the graphite component of the SPE only, as it is electroactive on its own. The LOD was calculated around 0.01 µM (1.3×10^{-8} M) at a signal-to-ratio (n=3). Before data preprocessing, the DES-MIP-CP raw amperometric data are displayed in Appendix E, Figure E1.

Similarly, the raw amperometric data for the non-imprinted polymer-based carbon paste electrode (DES-NIP-CP) is presented in Appendix E, Figure E2.

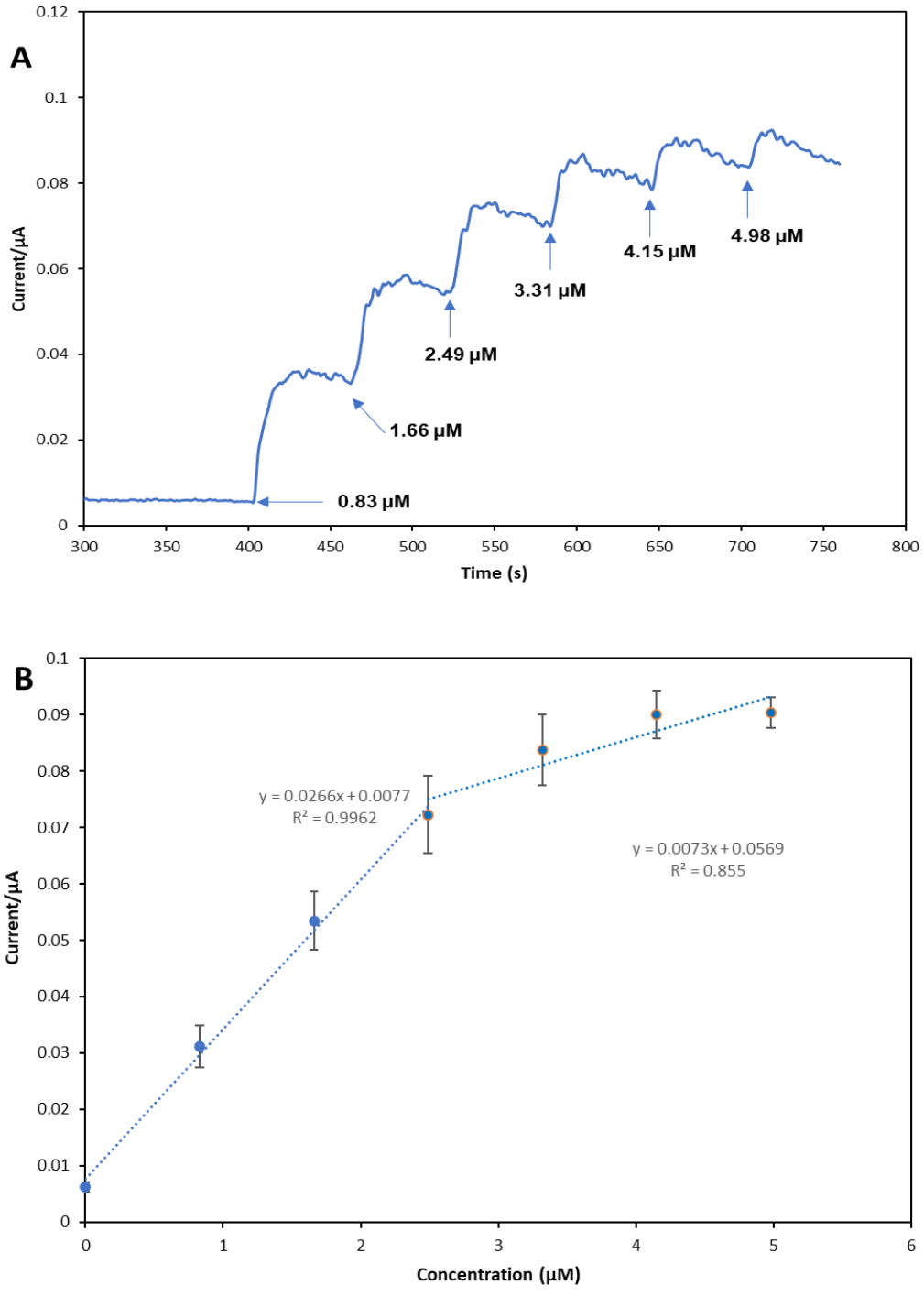

Figure 6.14 (a) The amperometric response obtained for DES-MIP-CP for successive addition of 5 of 0.5 mM E2 in PBS (pH 7.0) at an applied potential of +0.65 V vs Ag/AgCl at 60 s interval (Blue arrow represent the injection

point and sensor response to successive E2 additions) (b) Calibration plot of average of the current plateau (relative to baseline) against concentration. (E = +) 0.65 V, PBS 0.1 M pH = 7, n = 3)

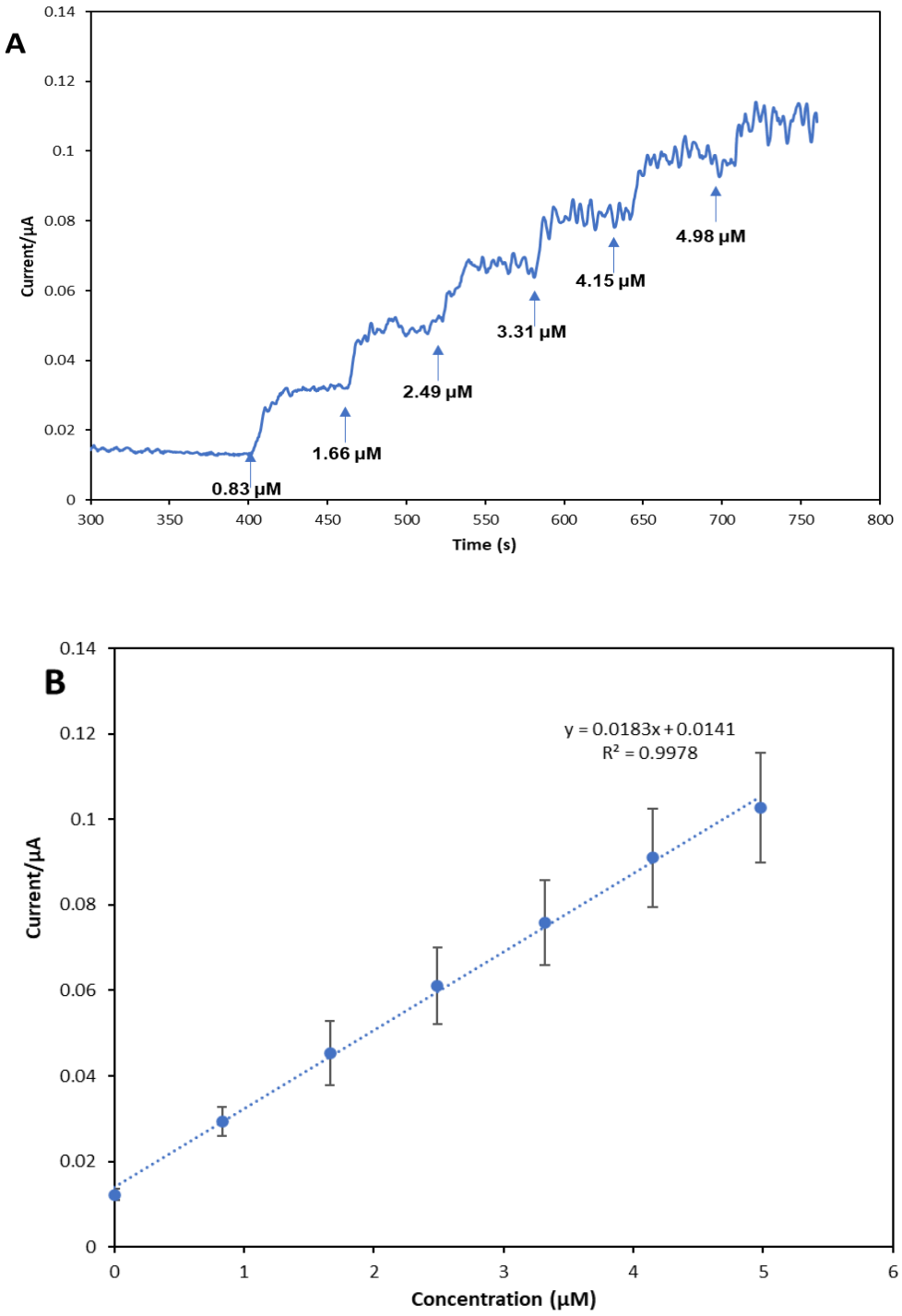

Figure 6.15 (a) The amperometric response obtained for DES-NIP-CP for successive addition of 50 µL of 0.5 mM E2 in PBS (pH 7.0) at an applied

potential of +0.65 V vs Ag/AgCl at 60 s interval (Blue arrow represent the injection point and sensor response to successive E2 additions) (b) Calibration plot of average of the current plateau (relative to baseline) against concentration. E = +0.65 V, PBS 0.1 M pH = 7, n = 3)

Figure 6.15 shows the amperogram oxidation current generated at the DES-CP electrode upon injection of E2 into the buffer solution. The current gradually decreases with more injections. This behaviour was attributed to the electrode fouling produced by forming an insulating layer from E2 oxidation that blocks the electrode surface. Therefore, it lowers the current generation. In addition, a significant difference was observed in the amperogram with and without MIP. The result is much the same for the MIP and NIP, meaning the addition of MIP/NIP does affect the oxidation of E2. The imprinted polymers were made conductive due to the added carbon paste transduction. Thus, the response is from the carbon paste, and the dose-response is noticed. Therefore, E2 selectivity could not be determined. The above results suggested that adding different amounts of MIP/NIP does not affect the carbon paste.

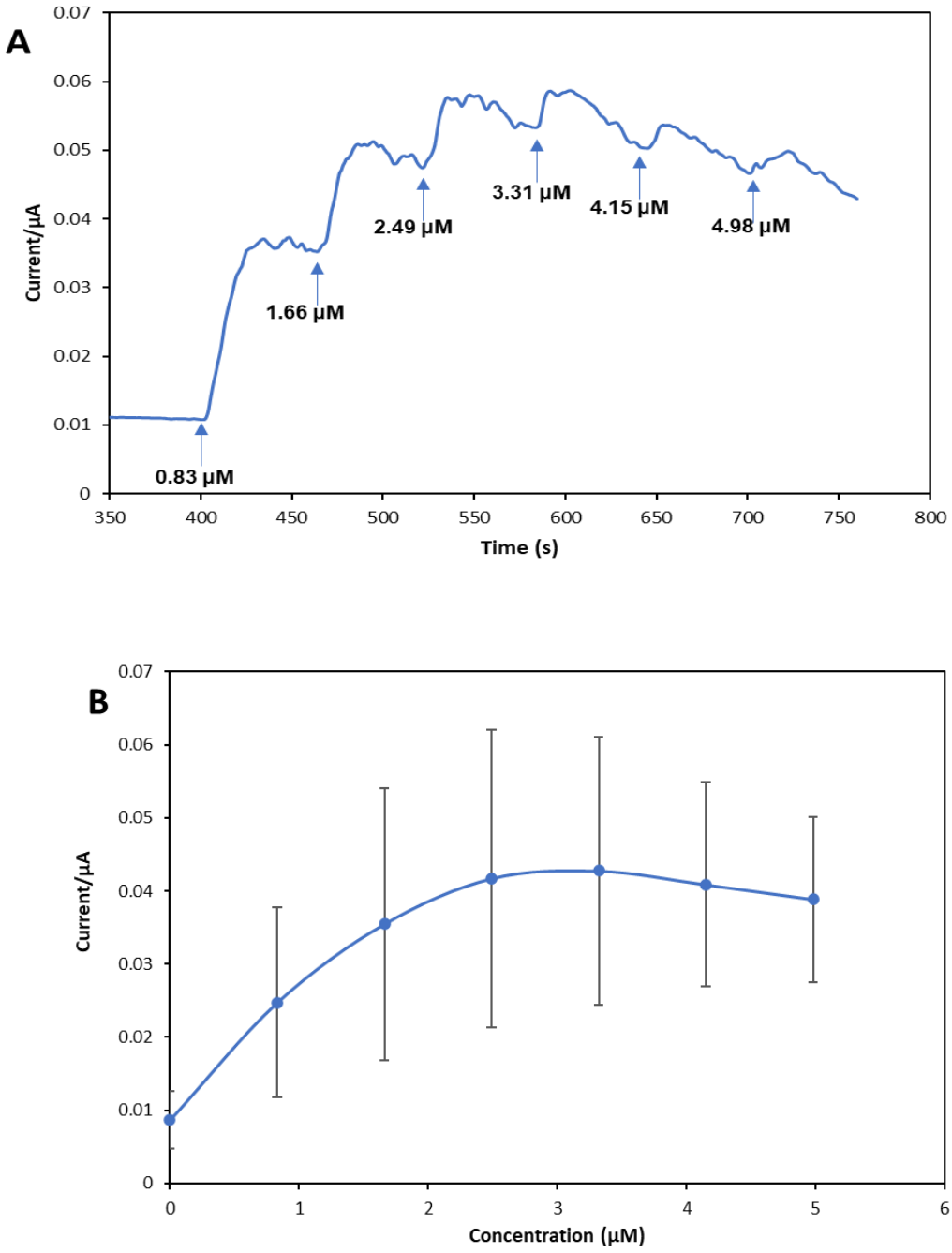

Figure 6.16 (a) The amperometric response obtained for DES-CP for successive addition of 50 µL of 0.5 mM E2 in PBS (pH 7.0) at an applied potential of +0.65 V vs Ag/AgCl at 60 s interval Blue arrow represent the injection point and sensor response to successive E2 additions) (b) Calibration plot of average of the current plateau (relative to baseline) against concentration. (E = + 0.65 V, PBS 0.1 M pH = 7, n = 3)

6.3.2.2 Tap water sample analysis.

Tap water samples were further evaluated under optimised experimental conditions. Figure 6.17 shows the amperometric response of E2 at an applied potential of 0.65 V. As illustrated, and the oxidation current increased steeply upon adding E2. It reached a steady-state current with an average response time of 60 seconds. Citric acid and ibuprofen were used as interferent analytes to examine the selectivity of the DES-MIP-CP sensor.

Figure 6.18 shows that neither interferent shows any oxidation current at the applied potential +0.65 V. However, a change in the oxidation current was noticed when E2 was injected, indicating that the sensor was unaffected by the presence of both citric acid and ibuprofen. This sensor exhibited good sensitivity and selectivity for E2 analysis at the applied potential of +0.65 V. Triplicate measurements were performed to study the sensor's reproducibility response. Figure 6.18 shows the response of the DES-MIP-CP sensor. The observed feature here is not due to the properties of the MIP but instead to the conductivity of the graphite electrode. Figure 6.16 shows the amperometric response of E2 on the DES-NIP-CP in PBS at an applied voltage of +0.65 V. As illustrated, the oxidation current increased steeply upon the addition of E2. It reached a steady-state current within an average response time of 60 seconds. Figure 6.19 shows an apparent increase in current across all three sensors with the increment in E2 additions. The fresh sensors show consistent peak currents, indicating that further study is needed to ascertain the uniform performance.

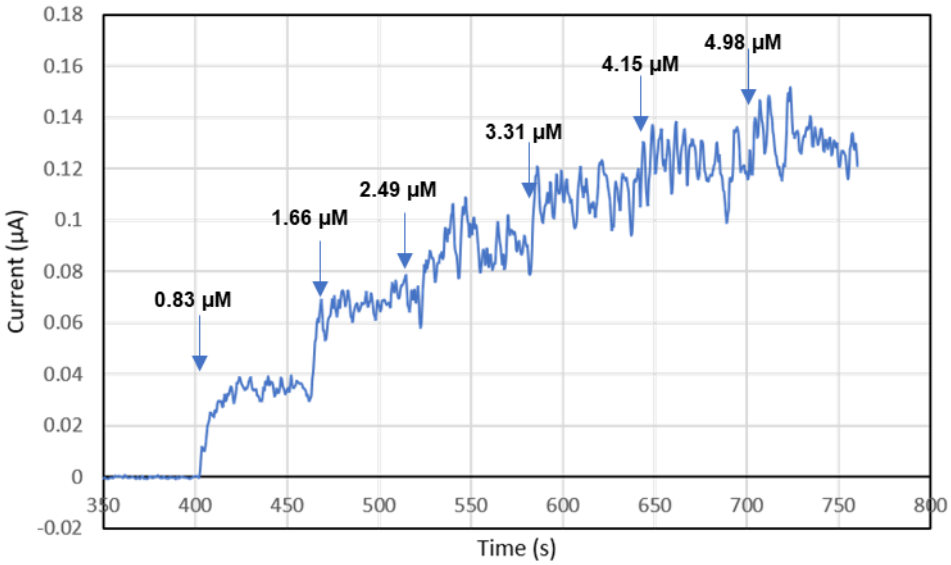

Figure 6.17 (a) The amperometric response obtained for DES-MIP-CP for successive addition of 50 µL of 0.5 mM E2 in Tap Water at an applied potential of +0.65 V vs Ag/AgCl at 60 s interval (b) Calibration plot of average of the current plateau (relative to baseline) against concentration.

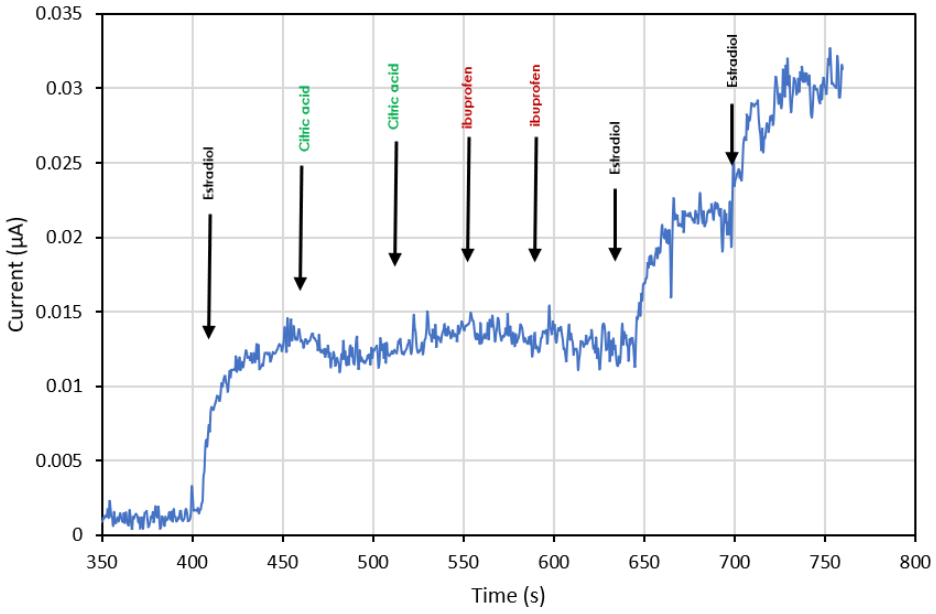

Figure 6.18 The amperometric response obtained for DES-MIP-CP for successive addition of 50 µL of 0.5 mM interferents at an applied potential of +0.65 V vs Ag/AgCl at 60 s interval.

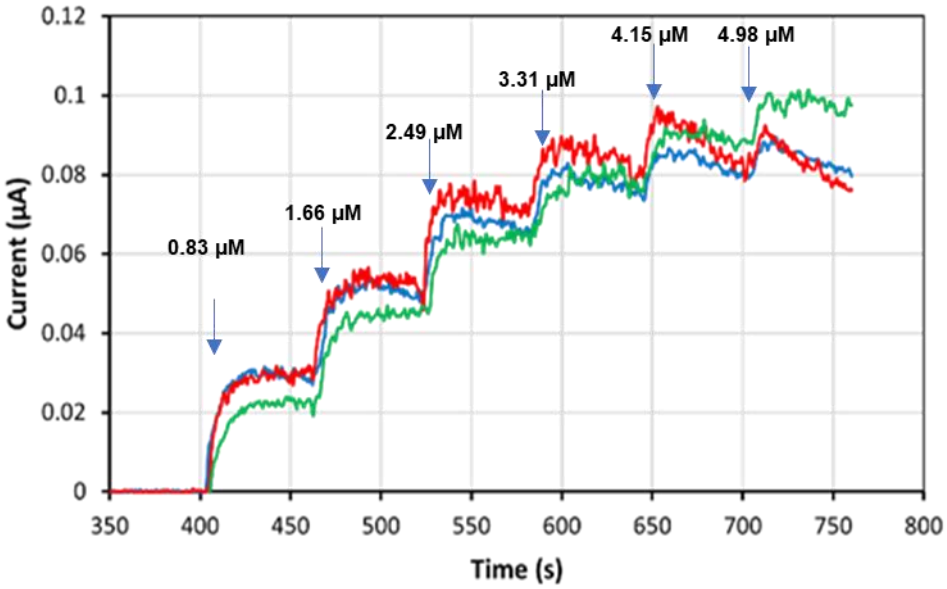

Figure 6.19 Amperometric response obtained for three freshly prepared (3) DES-MIP-CP sensors for E2.

6.4 Conclusions

This chapter describes an investigation of Molecularly Imprinted Polymers (MIPs) fabricated using carbon paste. Modifications to screen-printed paste and MIP materials were envisaged to enhance selectivity. However, experimental results reveal that the developed E2-MIP sensor using printed carbon paste did not exhibit successful performance, as both the imprinted, non-imprinted and bare carbon paste showed E2 oxidation with a similar response. This limitation needs to be addressed and expanded in future research. Despite current challenges, this type of sensor holds significant potential for fulfilling the need for a fast, inexpensive, and easy-to-use E2 detection method in environmental applications.

Further improvements and optimizations are necessary to enhance the selectivity and reliability of the MIP sensor, paving the way for its successful implementation in the environmental monitoring of E2. Nevertheless, in this case, the purpose of the work was to obtain proof of concept regarding the integration of a molecular imprinting material in carbon paste that might provide insight into the possible screen-printing electrodes. The findings have illustrated that applying MIP for selectivity in E2 analysis requires additional selectivity and sensitivity improvements. Future work should investigate the use of other novel polymers. The fabrication of sensors using carbon paste and deep eutectic solvent displays potential for further exploration.

References

[1] A. Escarpa, Food electroanalysis: Sense and simplicity, Chem. Rec. 12 (2012) 72–91. https://doi.org/10.1002/tcr.201100033.

[2] S. Campuzano, M. Pedrero, M. Gamella, V. Serafín, P. Yáñez-Sedeño, J.M. Pingarrón, Beyond sensitive and selective electrochemical biosensors: Towards continuous, real-time, antibiofouling and calibration-free devices, Sensors (Switzerland). 20 (2020) 1–22. https://doi.org/10.3390/s20123376.

[3] M. Arabi, A. Ostovan, J. Li, X. Wang, Z. Zhang, J. Choo, L. Chen, Molecular Imprinting: Green Perspectives and Strategies, Adv. Mater. 33 (2021). https://doi.org/10.1002/adma.202100543.

[4] R. Viveiros, S. Rebocho, T. Casimiro, Green strategies for molecularly imprinted polymer development, Polymers (Basel). 10 (2018). https://doi.org/10.3390/polym10030306.

[5] M.F. Frasco, L.A.A.N.A. Truta, M.G.F. Sales, F.T.C. Moreira, Imprinting technology in electrochemical biomimetic sensors, Sensors (Switzerland). 17 (2017). https://doi.org/10.3390/s17030523.

[6] B. Adhikari, S. Majumdar, Polymers in sensor applications, Prog. Polym. Sci. 29 (2004) 699–766. https://doi.org/10.1016/j.progpolymsci.2004.03.002.

[7] A. Henderson, M. V. Sullivan, R.A. Hand, N.W. Turner, Detection of selective androgen receptor modulators (SARMs) in serum using a

molecularly imprinted nanoparticle surface plasmon resonance sensor, J. Mater. Chem. B. (2022) 6792–6799. https://doi.org/10.1039/d2tb00270a.

[8] R. Viveiros, S. Rebocho, T. Casimiro, Green Strategies for Molecularly Imprinted Polymer Development, Polymers (Basel). 10 (2018) 306. https://doi.org/10.3390/polym10030306.

[9] A. Paiva, R. Craveiro, I. Aroso, M. Martins, R.L. Reis, A.R.C. Duarte, Natural Deep Eutectic Solvents – Solvents for the 21st Century, ACS Sustain. Chem. Eng. 2 (2014) 1063–1071. https://doi.org/10.1021/sc500096j.

[10] C.M.A. Brett, Deep eutectic solvents and applications in electrochemical sensing, Curr. Opin. Electrochem. 10 (2018) 143–148. https://doi.org/10.1016/j.coelec.2018.05.016.

[11] D. Futra, L.Y. Heng, M.Z. Jaapar, A. Ulianas, K. Saeedfar, T.L. Ling, A novel electrochemical sensor for 17β-estradiol from molecularly imprinted polymeric microspheres and multi-walled carbon nanotubes grafted with gold nanoparticles, Anal. Methods. (2016). https://doi.org/10.1039/C5AY02796A.

[12] M.H. Lee, J.L. Thomas, W.C. Liu, Z.X. Zhang, B. Da Liu, C.H. Yang, H.Y. Lin, A multichannel system integrating molecularly imprinted conductive polymers for ultrasensitive voltammetric determination of four steroid hormones in urine, Microchim. Acta. 186 (2019). https://doi.org/10.1007/s00604-019-3797-7.

[13] Y. Liu, Y. Wang, Q. Dai, Y. Zhou, Magnetic deep eutectic solvents

molecularly imprinted polymers for the selective recognition and separation of protein, Anal. Chim. Acta. 936 (2016) 168–178. https://doi.org/10.1016/j.aca.2016.07.003.

[14] N. Fu, L. Li, X. Liu, N. Fu, C. Zhang, L. Hu, D. Li, B. Tang, T. Zhu, Specific recognition of polyphenols by molecularly imprinted polymers based on a ternary deep eutectic solvent, J. Chromatogr. A. 1530 (2017) 23–34. https://doi.org/10.1016/j.chroma.2017.11.011.

[15] Y. Dai, J. van Spronsen, G.-J. Witkamp, R. Verpoorte, Y.H. Choi, Natural deep eutectic solvents as new potential media for green technology, Anal. Chim. Acta. 766 (2013) 61–68. https://doi.org/10.1016/j.aca.2012.12.019.

[16] P.K. Kalambate, Z. Rao, Dhanjai, J. Wu, Y. Shen, R. Boddula, Y. Huang, Electrochemical (bio) sensors go green, Biosens. Bioelectron. 163 (2020) 112270. https://doi.org/10.1016/j.bios.2020.112270.

[17] C.G. Neves, A.L. Montiel, F.E.B. Junior, G.C. Paveglio, W.R.P. Barros, Application of a Screen-Printed Carbon Electrode Modified with Printex 6L and Deep Eutectic Solvent for Detection and Quantification of 17β-estradiol, J. Electrochem. Soc. 169 (2022) 057501. https://doi.org/10.1149/1945-7111/ac68a3.

[18] P.S. Sharma, A. Garcia-Cruz, M. Cieplak, K.R. Noworyta, W. Kutner, ‘Gate effect’ in molecularly imprinted polymers: the current state of understanding, Curr. Opin. Electrochem. 16 (2019) 50–56. https://doi.org/10.1016/j.coelec.2019.04.020.

[19] Y. Yoshimi, R. Ohdaira, C. Iiyama, K. Sakai, `Gate effect’ of thin layer of

molecularly-imprinted poly(methacrylic acid-co-ethyleneglycol dimethacrylate), Sensors Actuators, B Chem. 73 (2001) 49–53. https://doi.org/10.1016/S0925-4005(00)00671-7.

[20] J.G. Pacheco, P. Rebelo, M. Freitas, H.P.A. Nouws, C. Delerue-Matos, Breast cancer biomarker (HER2-ECD) detection using a molecularly imprinted electrochemical sensor, Sensors Actuators, B Chem. 273 (2018) 1008–1014. https://doi.org/10.1016/j.snb.2018.06.113.

[21] A.R. Cardoso, A.C. Marques, L. Santos, A.F. Carvalho, F.M. Costa, R. Martins, M.G.F. Sales, E. Fortunato, Molecularly-imprinted chloramphenicol sensor with laser-induced graphene electrodes, Biosens. Bioelectron. 124–125 (2019) 167–175. https://doi.org/10.1016/j.bios.2018.10.015.

[22] A. Zamora-Gálvez, A. Ait-Lahcen, L.A. Mercante, E. Morales-Narváez, A. Amine, A. Merkoçi, Molecularly Imprinted Polymer-Decorated Magnetite Nanoparticles for Selective Sulfonamide Detection, Anal. Chem. 88 (2016) 3578–3584. https://doi.org/10.1021/acs.analchem.5b04092.

[23] S.A. Piletsky, T.L. Panasyuk, E. V. Piletskaya, I.A. Nicholls, M. Ulbricht, Receptor and transport properties of imprinted polymer membranes - A review, J. Memb. Sci. 157 (1999) 263–278. https://doi.org/10.1016/S0376-7388(99)00007-1.

[24] G. Cabral-Miranda, M. Gidlund, M.G.F. Sales, Backside-surface imprinting as a new strategy to generate specific plastic antibody materials, J. Mater. Chem. B. 2 (2014) 3087–3095.

https://doi.org/10.1039/c3tb21740j.

[25] O.S. Ahmad, T.S. Bedwell, C. Esen, A. Garcia-Cruz, S.A. Piletsky, Molecularly Imprinted Polymers in Electrochemical and Optical Sensors, Trends Biotechnol. 37 (2019) 294–309. https://doi.org/10.1016/J.TIBTECH.2018.08.009.

[26] C. Zhong, B. Yang, X. Jiang, J. Li, Current Progress of Nanomaterials in Molecularly Imprinted Electrochemical Sensing., Crit. Rev. Anal. Chem. 48 (2018) 15–32. https://doi.org/10.1080/10408347.2017.1360762.

[27] C. Malitesta, E. Mazzotta, R.A. Picca, A. Poma, I. Chianella, S.A. Piletsky, MIP sensors - The electrochemical approach, Anal. Bioanal. Chem. 402 (2012) 1827–1846. https://doi.org/10.1007/s00216-011-5405-5.

[28] S. Piletsky, S. Piletsky, I. Chianella, MIP-based Sensors, Mol. Imprinted Sensors. (2012) 339–354. https://doi.org/10.1016/B978-0-444-56331-6.00014-1.

[29] M.M. Titirici, B. Sellergren, Thin molecularly imprinted polymer films via reversible addition-fragmentation chain transfer polymerization., Chem. Mater. Pp. 18 (2006) 1773–1779.

[30] K. Haupt, Molecularly imprinted polymers in analytical chemistry, Analyst. 126 (2001) 747–756. https://doi.org/10.1039/b102799a.

[31] D. Antuña-Jiménez, G. Díaz-Díaz, M.C. Blanco-López, M.J. Lobo-Castañón, A.J. Miranda-Ordieres, P. Tuñón-Blanco, Molecularly Imprinted

Electrochemical Sensors: Past, Present, and Future, 2012. https://doi.org/10.1016/B978-0-444-56331-6.00001-3.

[32] G. Díaz-Díaz, D. Antuña-Jiménez, M. Carmen Blanco-López, M. Jesús Lobo-Castañón, A.J. Miranda-Ordieres, P. Tuñón-Blanco, New materials for analytical biomimetic assays based on affinity and catalytic receptors prepared by molecular imprinting, TrAC - Trends Anal. Chem. (2012). https://doi.org/10.1016/j.trac.2011.09.011.

[33] M. Zayats, M. Kanwar, M. Ostermeier, P.C. Searson, Molecular imprinting of maltose binding protein: Tuning protein recognition at the molecular level., Macromol. Pp. 44 (2011) 3966–3972.

[34] X. Zhang, A. Yarman, J. Erdossy, S. Katz, I. Zebger, K.J. Jetzschmann, Z. Altintas, U. Wollenberger, R.E. Gyurcsányi, F.W. Scheller, Electrosynthesized MIPs for transferrin: Plastibodies or nano-filters?, Biosens. Bioelectron. 105 (2018) 29–35. https://doi.org/10.1016/j.bios.2018.01.011.

[35] J. Erdo(double acute)ssy, V. Horváth, A. Yarman, F.W. Scheller, R.E. Gyurcsányi, Electrosynthesized molecularly imprinted polymers for protein recognition, TrAC - Trends Anal. Chem. 79 (2016) 179–190. https://doi.org/10.1016/j.trac.2015.12.018.

[36] M. Menger, A. Yarman, J. Erdossy, H.B. Yildiz, R.E. Gyurcsányi, F.W. Scheller, MIPs and aptamers for recognition of proteins in biomimetic sensing, Biosensors. 6 (2016). https://doi.org/10.3390/bios6030035.

[37] D. Hall, Molecularly Imprinted Membranes: Past, Present, and Future,

Stud. Socjol. 3 (2016) 79–99.
https://doi.org/10.1021/acs.chemrev.6b00098.

[38] S. Wu, W. Tan, H. Xu, Protein molecularly imprinted polyacrylamide membrane: for hemoglobin sensing., Analyst. 135 (2010) 2523–2527. https://doi.org/10.1039/c0an00191k.

[39] J. Li, J. Zhao, X. Wei, A sensitive and selective sensor for dopamine determination based on a molecularly imprinted electropolymer of o-aminophenol, Sensors Actuators B Chem. 140 (2009) 663–669. https://doi.org/10.1016/j.snb.2009.04.067.

[40] P.S. Sharma, A. Pietrzyk-Le, F. D'Souza, W. Kutner, Electrochemically synthesized polymers in molecular imprinting for chemical sensing., Anal. Bioanal. Chem. 402 (2012) 3177–3204. https://doi.org/10.1007/s00216-011-5696-6.

[41] E. Schillinger, M. Möder, G.D. Olsson, I.A. Nicholls, B. Sellergren, An artificial estrogen receptor through combinatorial imprinting, Chem. - A Eur. J. 18 (2012) 14773–14783. https://doi.org/10.1002/chem.201201428.

[42] G.D. Olsson, B.C.G. Karlsson, E. Schillinger, B. Sellergren, I.A. Nicholls, Theoretical studies of 17-β-estradiol-imprinted prepolymerization mixtures: Insights concerning the roles of cross-linking and functional monomers in template complexation and polymerization, Ind. Eng. Chem. Res. 52 (2013) 13965–13970. https://doi.org/10.1021/ie401115f.

[43] G.L. Marques, L.R. Rocha, M.C. Prete, F.A. Gorla, D. Moscardi dos Santos, M.G. Segatelli, C.R. Teixeira Tarley, Development of

Electrochemical Platform Based on Molecularly Imprinted Poly(methacrylic acid) Grafted on Iniferter-modified Carbon Nanotubes for 17β-Estradiol Determination in Water Samples, Electroanalysis. 33 (2021) 568–578. https://doi.org/10.1002/elan.202060270.

[44] B.S. (Ed.), Molecularly Imprinted Polymers: Man-Made Mimics of Antibodies and Their Application in Analytical Chemistry: Techniques and Instrumentation in Analytical Chemistry, Elsevier Science, Amsterdam, 2001.

[45] J. Guo, Y. Wang, Y. Liu, C. Zhang, Y. Zhou, Magnetic-graphene based molecularly imprinted polymer nanocomposite for the recognition of bovine hemoglobin, Talanta. 144 (2015) 411–419. https://doi.org/10.1016/j.talanta.2015.06.057.

[46] C. Malitesta, F. Palmisano, L. Torsi, P.G. Zambonin, Glucose Fast-Response Amperometric Sensor Based on Glucose Oxidase Immobilized in an Electropolymerized Poly(o-phenylenediamine) Film, Anal. Chem. 62 (1990) 2735–2740. https://doi.org/10.1021/ac00223a016.

[47] W. Liu, Y. Ma, G. Sun, S. Wang, J. Deng, H. Wei, Molecularly imprinted polymers on graphene oxide surface for EIS sensing of testosterone, Biosens. Bioelectron. 92 (2017) 305–312. https://doi.org/10.1016/j.bios.2016.11.007.

[48] J. Zhang, L. Wang, Y. Han, Preparation of 17β-estradiol surface molecularly imprinted polymers and their application to the analysis of biological samples., J. Sep. Sci. 36 (2013) 3486–3492.

https://doi.org/10.1002/jssc.201300850.

[49] S. Srinivasan, M.W. Lee, M.C. Grady, M. Soroush, A.M. Rappe, Computational study of the self-initiation mechanism in thermal polymerization of methyl acrylate, J. Phys. Chem. A. 113 (2009) 10787–10794. https://doi.org/10.1021/jp904036k.

[50] M. Soroush, A.M. Rappe, Theoretical Insights Into Chain Transfer Reactions of Acrylates, 2019. https://doi.org/10.1016/b978-0-12-815983-5.00005-2.

[51] T. Alizadeh, Molecularly imprinted nanoparticles-based electrochemical sensor for determination of ultratrace parathion in real samples, Int. J. Environ. Anal. Chem. 92 (2012) 1742–1760. https://doi.org/10.1080/03067319.2011.592947.

[52] T. Alizadeh, M. Zare, M.R. Ganjali, P. Norouzi, B. Tavana, A new molecularly imprinted polymer (MIP)-based electrochemical sensor for monitoring 2,4,6-trinitrotoluene (TNT) in natural waters and soil samples, Biosens. Bioelectron. 25 (2010) 1166–1172. https://doi.org/10.1016/j.bios.2009.10.003.

[53] B. Mostafiz, S.A. Bigdeli, K. Banan, H. Afsharara, D. Hatamabadi, P. Mousavi, C.M. Hussain, R. Keçili, F. Ghorbani-Bidkorbeh, Molecularly imprinted polymer-carbon paste electrode (MIP-CPE)-based sensors for the sensitive detection of organic and inorganic environmental pollutants: A review, Trends Environ. Anal. Chem. 32 (2021) e00144. https://doi.org/10.1016/j.teac.2021.e00144.

[54] T. Alizadeh, N. Hamidi, M.R. Ganjali, P. Nourozi, Development of a highly selective and sensitive electrochemical sensor for Bi3+ determination based on nano-structured bismuth-imprinted polymer modified carbon/carbon nanotube paste electrode, Sensors Actuators, B Chem. 245 (2017) 605–614. https://doi.org/10.1016/j.snb.2017.02.024.

[55] T. Alizadeh, M.R. Ganjali, M. Akhoundian, P. Norouzi, Voltammetric determination of ultratrace levels of cerium(III) using a carbon paste electrode modified with nano-sized cerium-imprinted polymer and multiwalled carbon nanotubes, Microchim. Acta. 183 (2016) 1123–1130. https://doi.org/10.1007/s00604-015-1702-6.

[56] D.M. Hawkins, D. Stevenson, S.M. Reddy, Investigation of protein imprinting in hydrogel-based molecularly imprinted polymers (HydroMIPs), Anal. Chim. Acta. 542 (2005) 61–65. https://doi.org/10.1016/j.aca.2005.01.052.

[57] O. Jamieson, T.C.C. Soares, B.A. de Faria, A. Hudson, F. Mecozzi, S.J. Rowley-Neale, C.E. Banks, J. Gruber, K. Novakovic, M. Peeters, R.D. Crapnell, Screen Printed Electrode Based Detection Systems for the Antibiotic Amoxicillin in Aqueous Samples Utilising Molecularly Imprinted Polymers as Synthetic Receptors, Chemosensors. 8 (2019) 5. https://doi.org/10.3390/chemosensors8010005.

[58] K.P. Prathish, R.C. Carvalho, C.M.A. Brett, Highly sensitive poly(3,4-ethylenedioxythiophene) modified electrodes by electropolymerisation in deep eutectic solvents, Electrochem. Commun. 44 (2014) 8–11.

https://doi.org/10.1016/j.elecom.2014.03.026.

[59] K.P. Prathish, R.C. Carvalho, C.M.A. Brett, Electrochemical characterisation of poly(3,4-ethylenedioxythiophene) film modified glassy carbon electrodes prepared in deep eutectic solvents for simultaneous sensing of biomarkers, Electrochim. Acta. 187 (2016) 704–713. https://doi.org/10.1016/j.electacta.2015.11.092.

[60] M. Hirabayashi, B. Mehta, B. Nguyen, S. Kassegne, DNA immobilization on high aspect ratio glassy carbon (GC-MEMS) microelectrodes for bionanoelectronics applications, Microsyst. Technol. 21 (2015) 2359–2365. https://doi.org/10.1007/s00542-014-2332-3.

[61] H.F. El-Sharif, H. Yapati, S. Kalluru, S.M. Reddy, Highly selective BSA imprinted polyacrylamide hydrogels facilitated by a metal-coding MIP approach, Acta Biomater. 28 (2015) 121–127. https://doi.org/10.1016/j.actbio.2015.09.012.

[62] D. Nunes da Silva, H. Leijoto de Oliveira, K.B. Borges, A.C. Pereira, Sensitive Determination of 17β-Estradiol using a Magneto Sensor Based on Magnetic Molecularly Imprinted Polymer, Electroanalysis. 33 (2021) 506–514. https://doi.org/10.1002/elan.202060223.

[63] A. Rachkov, S. McNiven, A. El'skaya, K. Yano, I. Karube, Fluorescence detection of β-estradiol using a molecularly imprinted polymer, Anal. Chim. Acta. 405 (2000) 23–29. https://doi.org/10.1016/S0003-2670(99)00743-6.

[64] X. Liu, Y. Wang, L. Li, R. Li, Synthesis and characterization of

azoxystrobin hydrophilic molecularly imprinted microspheres, J. Macromol. Sci. Part A Pure Appl. Chem. 56 (2019) 907–917. https://doi.org/10.1080/10601325.2019.1607751.

[65] N. Delgado-Mellado, M. Larriba, P. Navarro, V. Rigual, M. Ayuso, J. García, F. Rodríguez, of choline chloride deep eutectic solvents by TGA/FTIR-ATR analysis, J. Mol. Liq. 260 (2018) 37–43. https://doi.org/10.1016/j.molliq.2018.03.076.

[66] N. Fu, X. Liu, L. Li, B. Tang, K.H. Row, Ternary choline chloride/caffeic acid/ethylene glycol deep eutectic solvent as both a monomer and template in a molecularly imprinted polymer, J. Sep. Sci. 40 (2017) 2286–2291. https://doi.org/10.1002/jssc.201700146.

[67] M. Hayyan, A. Abo-Hamad, M.A.H. AlSaadi, M.A. Hashim, Functionalization of graphene using deep eutectic solvents, Nanoscale Res. Lett. 10 (2015). https://doi.org/10.1186/s11671-015-1004-2.

[68] S.M. Chelly, C. Denis, Applying Unsupervised Learning, Med. Sci. Sports Exerc. 33 (2001) 326–333. https://doi.org/10.1111/j.2041-210X.2010.00056.x.

[69] A.C. Ferrari, Raman spectroscopy of graphene and graphite: Disorder, electron-phonon coupling, doping and nonadiabatic effects, Solid State Commun. 143 (2007) 47–57. https://doi.org/10.1016/j.ssc.2007.03.052.

[70] M. Girolami, A. Bellucci, M. Mastellone, V. Serpente, S. Orlando, V. Valentini, A.L. Palma, A. Di Carlo, D.M. Trucchi, Improving the Performance of Printable Carbon Electrodes by Femtosecond Laser

Treatment, C — J. Carbon Res. 6 (2020) 48. https://doi.org/10.3390/c6030048.

[71] Lattice Vibrations and the Phonon Spectrum of Graphite and Graphite-Based Compounds, (1988) 322–409. https://doi.org/10.1016/b978-0-444-87049-0.50017-2.

[72] Y. Yoshimi, K. Sato, M. Ohshima, E. Piletska, Application of the “gate effect” of a molecularly imprinted polymer grafted on an electrode for the real-time sensing of heparin in blood, Analyst. 138 (2013) 5121–5128. https://doi.org/10.1039/c3an00909b.

[73] H. Song, Y. Wang, L. Zhang, L. Tian, J. Luo, N. Zhao, Y. Han, F. Zhao, X. Ying, Y. Li, An ultrasensitive and selective electrochemical sensor for determination of estrone 3-sulfate sodium salt based on molecularly imprinted polymer modified carbon paste electrode, Anal. Bioanal. Chem. 409 (2017) 6509–6519. https://doi.org/10.1007/s00216-017-0598-x.

[74] B. Molinero-Abad, M.A. Alonso-Lomillo, O. Domínguez-Renedo, M.J. Arcos-Martínez, Amperometric determination of sulfite using screen-printed electrodes modified with metallic nanoparticles, Microchim. Acta. 180 (2013) 1351–1355. https://doi.org/10.1007/s00604-013-1074-8.

[75] A.N. Patel, M.G. Collignon, M.A. OConnell, W.O.Y. Hung, K. McKelvey, J. V. MacPherson, P.R. Unwin, A new view of electrochemistry at highly oriented pyrolytic graphite, J. Am. Chem. Soc. 134 (2012) 20117–20130. https://doi.org/10.1021/ja308615h.

[76]. Hasanah, A.N.; Safitri, N.; Zulfa, A.; Neli, N.; Rahayu, D. Factors Affecting Preparation of Molecularly Imprinted Polymer and Methods on Finding Template-Monomer Interaction as the Key of Selective Properties of the Materials. Molecules 2021, 26, 5612.

[77]. Beluomini, M.A.; da Silva, J.L.; de Sá, A.C.; Buffon, E.; Pereira, T.C.; Stradiotto, N.R. Electrochemical sensors based on molecularly imprinted polymer on nanostructured carbon materials: A review. J. Electroanal. Chem. 2019, 840, 343–366.

[78]. Ahmad, O.S.; Bedwell, T.S.; Esen, C.; Garcia-Cruz, A.; Piletsky, S.A. Molecularly Imprinted Polymers in Electrochemical and Optical Sensors. Trends Biotechnol. 2019, 37, 294–309.

[79]. Gui, R.; Guo, H.; Jin, H. Preparation and applications of electrochemical chemosensors based on carbon-nanomaterial-modified molecularly imprinted polymers. Nanoscale Adv. 2019, 1, 3325–3363.

[80]. Gholivand, M.B. and Karimian, N., 2011. Development of piroxicam sensor based on molecular imprinted polymer-modified carbon paste electrode. Materials Science and Engineering: C, 31(8), pp.1844-1851. https://doi.org/10.1016/j.msec.2011.08.019

Chapter 7 General Conclusion

7.1 Conclusions

Research on electrochemical sensors for E2 determination is very active, as evidenced by the number of published works. However, the citation of screen-printed electrochemical sensors (SPE) is still limited when correlated with the number of electrochemical sensor articles obtained from Scopus and other databases. Furthermore, no SPE-based E2 sensors are available on the market. This thesis, therefore, provides a significant contribution by applying screen-printed electrodes as electrochemical sensors for E2 determination. To enhance sensitivity, it delves into carbon-based materials—such as carbon spherical material, graphene, electrolytic exfoliated graphene, and carbon nanotubes. It describes a molecularly imprinted polymer sensor surface to increase selectivity. The first two chapters define and highlight the problems and trends in research in the field. Chapter 3 explores a simple facile hydrothermal synthesis for carbon spherical shell (CSSM) synthesised as a modifier for SPE. Results of CSSM/SPE amperometric measurement show two linear regions in the current versus concentration calibration curve within concentration ranges of 0.83 to 2.49 μM ($8.3 \times 10^{-7} – 2.49 \times 10^{-6}$) and 3.31 to 5 μM ($3.31 \times 10^{-6}$ - 4.98×10^{-6} M) with sensitivity of 0.273 μA $\mu M^{-1} cm^{-2}$ and 0.118 μA $\mu M^{-1} cm^{-2}$. The electrode sensitivity for bare SPE was estimated to be 0.244 μA μM^{-1} cm^{-2}, illustrating that the CSSM/SPE approach did not achieve an improvement. This was because the CSSM has slower electron transfer kinetics compared to the bare electrode surface with graphite, which is known to be conductive.

A further strategy to improve sensor sensitivity, which used direct functionalisation during hydrothermal synthesis, was investigated. This led to the synthesis of graphene via electrolytic exfoliation to produce evenly sized graphene particles, as shown in Chapter 4. Chapter 4 explores the potential use of graphene-based electrodes using amperometric techniques as a straightforward, enzyme-free approach.

Various graphene-based electrodes were examined to mitigate the problems reported by the Unwin and Compton group [104] regarding graphene activity, i.e., that the activity of graphene comes from the basal or edge plane [104, 129, 132, 325]. These were graphene screen-printed electrodes (GHSPE), electrochemically exfoliated graphene-modified electrodes (EEFGHSPE), and 3D graphene foam screen-printed electrodes (3D-GFSPE). The three sensors were tested over the concentration range of 0.83 to 4.98 μM ($(8.3 \times 10^{-7} – 4.98 \times 10^{-6}$ M) E2. The GHSPE, 3D-GFSPE, and EEFGHSPE showed sensitivities of 0.495 μA $\mu M^{-1} cm^{-2}$, 0.121 $\mu A \mu M^{-1} cm^{-2}$, and 0.264 $\mu A \mu M^{-1} cm^{-2}$, respectively. GHPSPE shows better sensitivity for E2 analysis than EEFGH and 3D-GFSPE despite 3D-GFSPE having better electrochemical features in redox probes. These sensors employ commercially available graphite, which is convenient for sensor manufacture. However, it is inconsistent from various sources, and its properties are poorly defined. Further comparison is needed for future research.

Chapter 5 presents the successful application of gold nanoparticle-decorated reduced graphene-oxide to form highly sensitive sensors. Green synthesis at room temperature was used without the need for the harsh oxidants and reductants that are commonly applied. This takes advantage of the reduction

properties of plant extract for in situ fabrication. The optimized estradiol sensor delivered a linear range of concentrations from 0.05 to 1.00 µM, with a LOD of 3 nM. The results were comparable with previously published reports in terms of sensitivity.

Chapter 6 of the thesis examined the application of molecularly imprinted polymer (MIP) techniques for imparting selectivity to the designed sensors using amperometry as the detection technique. The motivation was that carbon paste electrodes and the MIP technique could be used as a simple and cheap disposable approach that offers easy fabrication of screen-printed electrodes. The MIP/NIP, fabricated with carbon paste, shows promise. The sensor sensitivities of 0.0266 µA/µM) for the imprinted and non-imprinted sensor of 0.0183 µA/µM) and the bare carbon paste sensor (sensitivity of 0.0244 µA/µM). Further optimisation is needed to enhance the sensor's performance for the selective detection of E2 in environmental monitoring applications.

Future work

This thesis lays the groundwork for applying screen-printed electrodes to monitor estradiol, and there are some areas where further work would be valuable. However, the sensors described in chapters 3, 4, and 6 use amperometry to detect E2; further performance improvement is still needed. Other analysis methods, such as electrical impedance spectroscopy, could provide a route to achieve this. It is essential to consider optimising different parameters in the fabrication process, such as synthesising CSSM material using various precursors and doping it with metallic nanoparticles in a one-step process. To optimise the methodology, the synthesis of exfoliated graphene should be carried

out at other applied potentials, with different intercalant electrolytes, and using different graphite precursors. Parameters that need to be optimised include 1) the concentration of E2, lower concentrations than those used in this study (< 0.5 mM), 2) the concentration of interferents for selectivity study, 3) the sensor response time to more than 60 s between injection, and 4) the polymerisation technique used for MIP development in chapter 6. Other plant extracts should be tested, optimised, and validated for further studies. It will be strong evidence if X-ray photoelectron spectroscopy (XPS) can confirm a relation between synthesised graphene and particle size. Ultimately, the sensor's performance should be validated using actual water samples and evaluated regarding reproducibility, selectivity, and accuracy. The fabricated sensor based on exfoliated graphene and CSSM represents the direct synthesis of carbon material using the simple one-step technique mentioned earlier. Further studies need to be conducted to evaluate other precursors as a source of graphene using various graphite rods and CSSM, such as using fructose as a carbon source.

7.1.1 Optimization of electrode composition with composites

Achieving reproducibility with modified nanomaterial surfaces remains a challenge in designing electrochemical sensors. While drop casting is a conventional surface modification method, it does not always yield consistent results due to the variability of the drop-casted material. An alternative technique that should be investigated involves using an automatic nano-droplet dispensing system to achieve uniform and repeatable modification of the nanomaterial surface. This method ensures that an equal volume of modifying material is dispensed with high accuracy, improving the measurements' stability and

reproducibility, leading to more consistent and reliable electrochemical sensor performance.

7.1.2 Selectivity enhancement

To develop and improve synthetic materials such as MIPS, working towards a new era of monomers designed in silico for E2 MIP sensors is necessary. Currently, most monomers are derived from petroleum products, which makes them non-renewable and unsuitable for sustainable production of materials. By developing monomers based on in-silico designs, we can create materials that are not only sustainable but also highly functional and tailored to specific applications.

Examining the electrodes' construction is necessary to reduce the capacitive effect further and improve sensor sensitivity. Specifically, the conventional design of electrodes needs to be revised to accommodate potential changes. Metters et al. [18] highlighted the need for back-to-back screen-printing of working electrodes to optimize the sensor's performance. Additionally, implementing the MIP and amperometry flow-injection (FI) flow injection analysis system developed for antibody-based biosensors can help generate high-quality results [83, 84]. Therefore, it is imperative to consider the electrode design and construct them in a way compatible with the screen-printing technique and further analysis.

7.1.3 Real-world applications

From the point of conceptualisation, the protocol for transfer from lab-based to field-based research should be kept in mind. Furthermore, additional chemometric tools must be embedded in the data analysis process to see the “true renaissance in electroanalysis” using SPEs.

APPENDICES

APPENDIX A. A.1 Reprint permission from Elsevier

Auwal Musa

From: Permissions Helpdesk <permissionshelpdesk@elsevier.com>
Sent: 23 November 2021 17:56
To: Auwal Musa
Subject: Re: Permission to re-use Publication content [211122-011531]

ELSEVIER

Dear Auwal Musa,

Thank you for your query.

Please note that, as one of the authors of this article, you retain the right to reuse it in your thesis/dissertation. You do not require formal permission to do so. You are permitted to post this Elsevier article online if it is embedded within your thesis. You are also permitted to post your Author Accepted Manuscript online.

However posting of the final published article is prohibited.

*"As per our Sharing Policy, authors are permitted to post the Accepted version of their article on their institutional repository – as long as it is for **internal institutional use only.***

It can only be shared publicly on that site once the journal-specific embargo period has lapsed. For a list of embargo periods please see: Embargo List.

You are not permitted to post the Published Journal Article (PJA) on the repository."

Please feel free to contact me if you have any queries.

Kind regards,

Anita Mercy Vethakkan
Senior Copyrights Coordinator
ELSEVIER | HCM - Health Content Management

Visit Elsevier Permissions

APPENDIX B. Chapter 3 Detection of Estradiol by Screen-printed Electrode Modified Carbon Spherical Shell Material

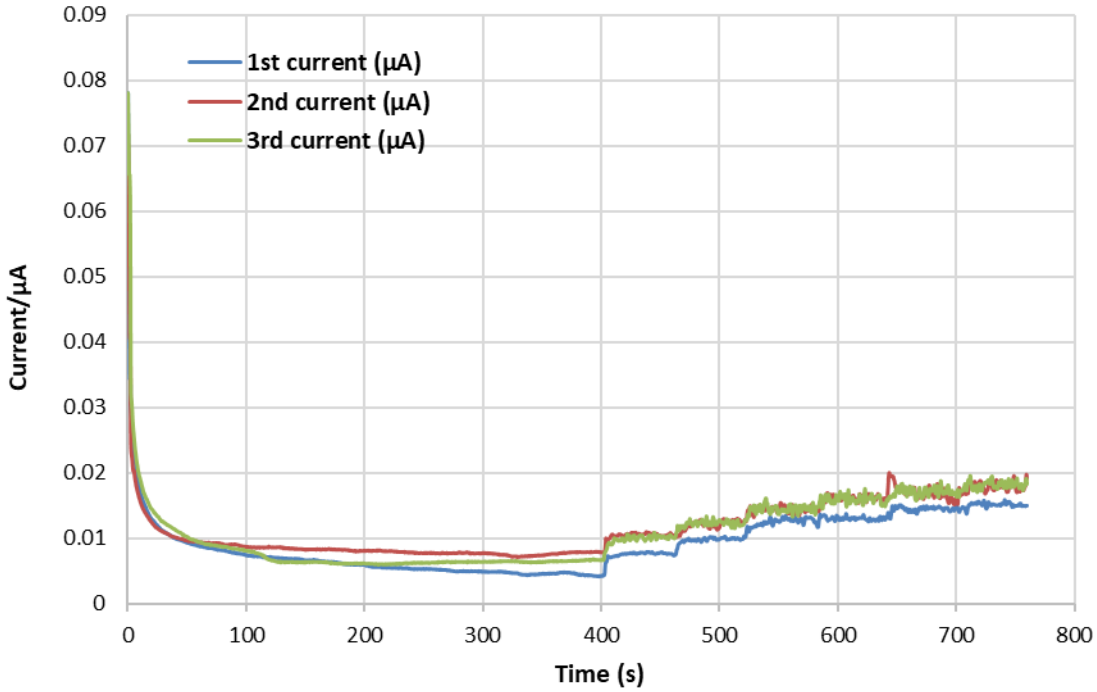

Figure B1. (A) Raw amperometric data for CSSM-SPE without the application of smoothing or baseline correction. 1st current stands for the current from experiment one, the second stands for the current from experiment two, and the third stands for the current from experiment three.

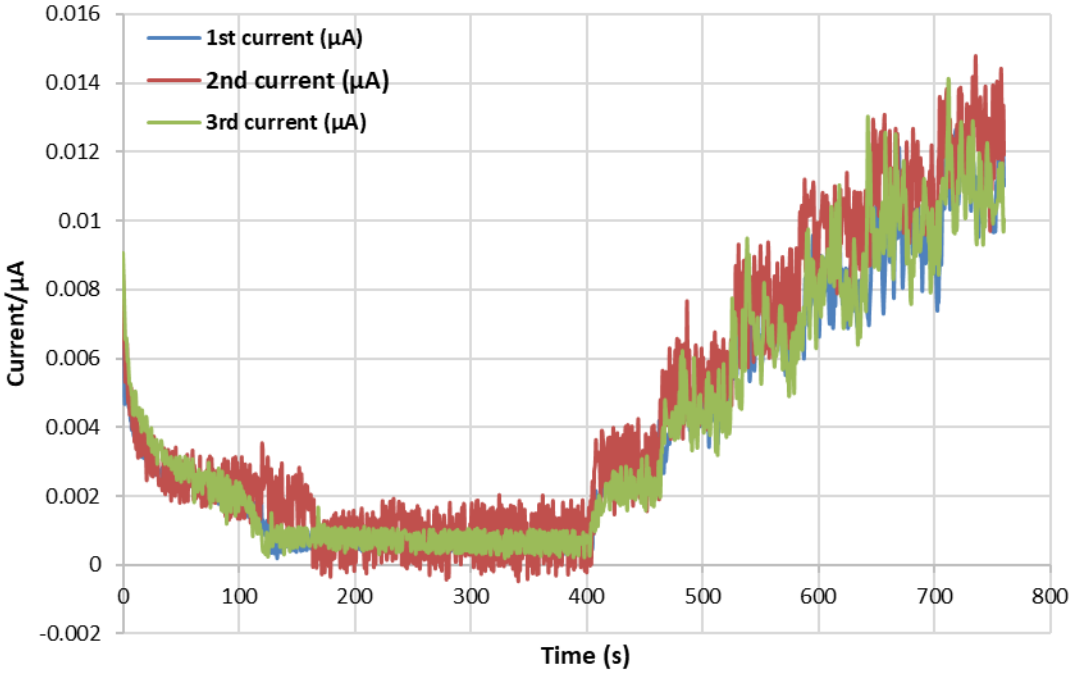

Figure B2. (A) Raw amperometric data for Bare SPE, without smoothing or baseline correction. 1st current stands for the current from experiment one, the second stands for the current from experiment two, and the third stands for the current from experiment three.

APPENDIX C. Chapter 4 Graphene-based electrodes for monitoring of estradiol - Supplemental Figures.

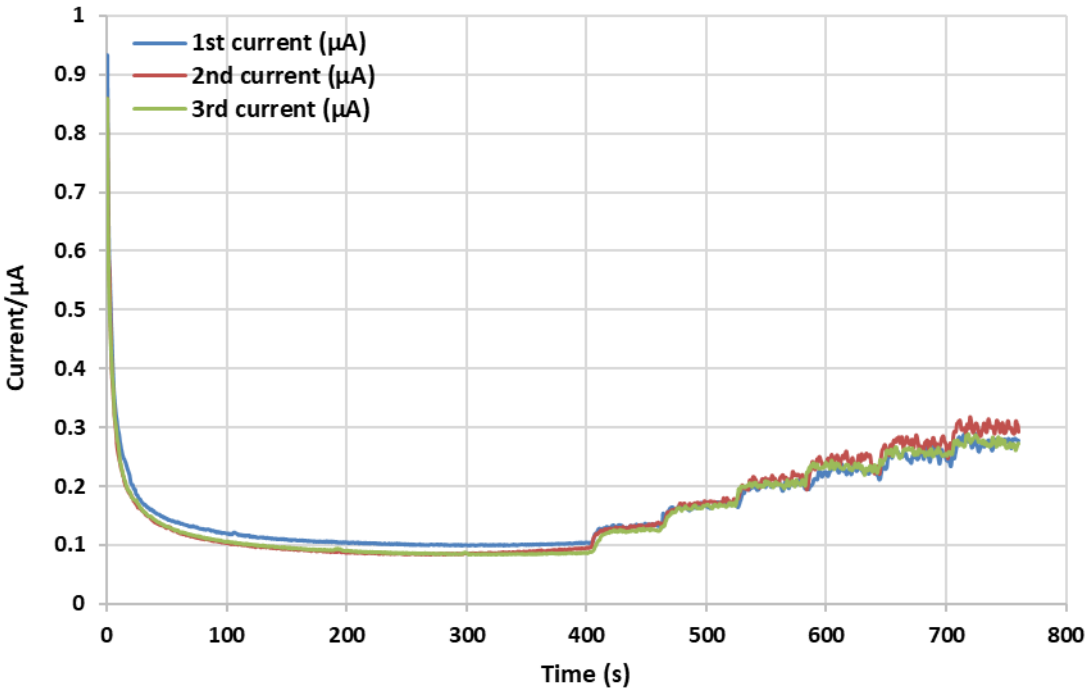

Figure C1. (A) Raw amperometric data for GHPSPE without the application of smoothing or baseline correction. 1st current stands for the current from experiment one, the second stands for the current from experiment two, and the third stands for the current from experiment three.

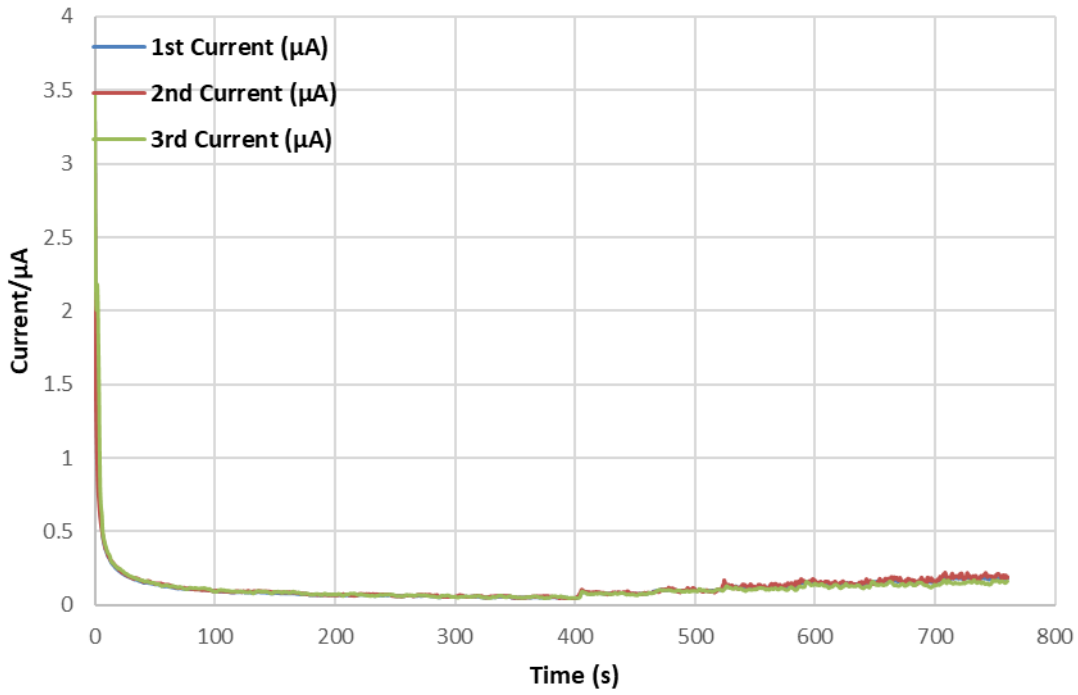

Figure C2. (A) Raw amperometric data for 3D-GFSPE, without smoothing or baseline correction. 1st current stands for the current from experiment one, the second stands for the current from experiment two, and the third stands for the current from experiment three.

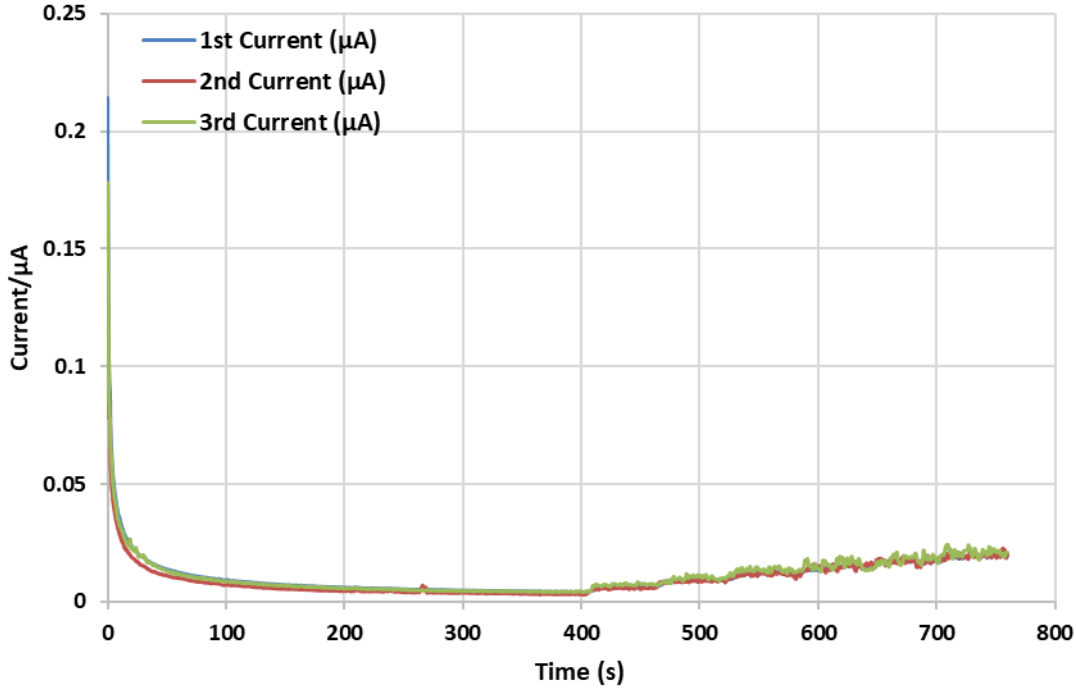

Figure C3. (A) Raw amperometric data for EEFGHSPE without the application of smoothing or baseline correction. 1st current stands for the current from experiment one, the second stands for the current from experiment two, and the third stands for the current from experiment three.

APPENDIX D. Chapter 5 Gold Nanoparticle Decorated Reduced Graphene Oxide Carbon Nanotubes Composites

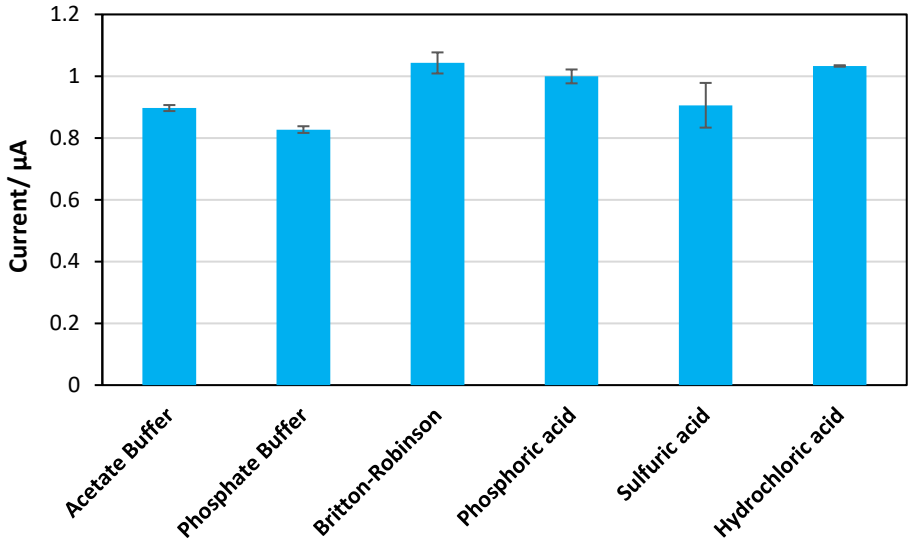

Figure D.1. Shows the peak currents in various supporting electrolytes.

APPENDIX E. Chapter 6 Imparting selectivity with a molecularly imprinted polymers platform

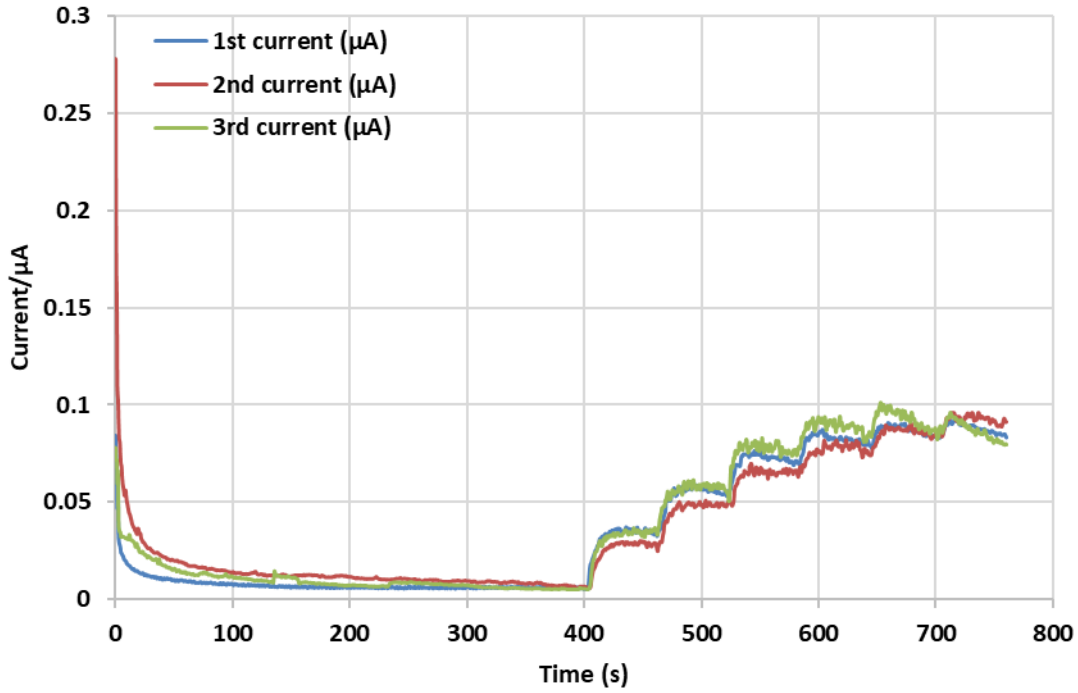

Figure E1. (A) Raw amperometric data for DES-MIP-CP without the application of smoothing or baseline correction. 1st current stands for the current from experiment one, the second stands for the current from experiment two, and the third stands for the current from experiment three.

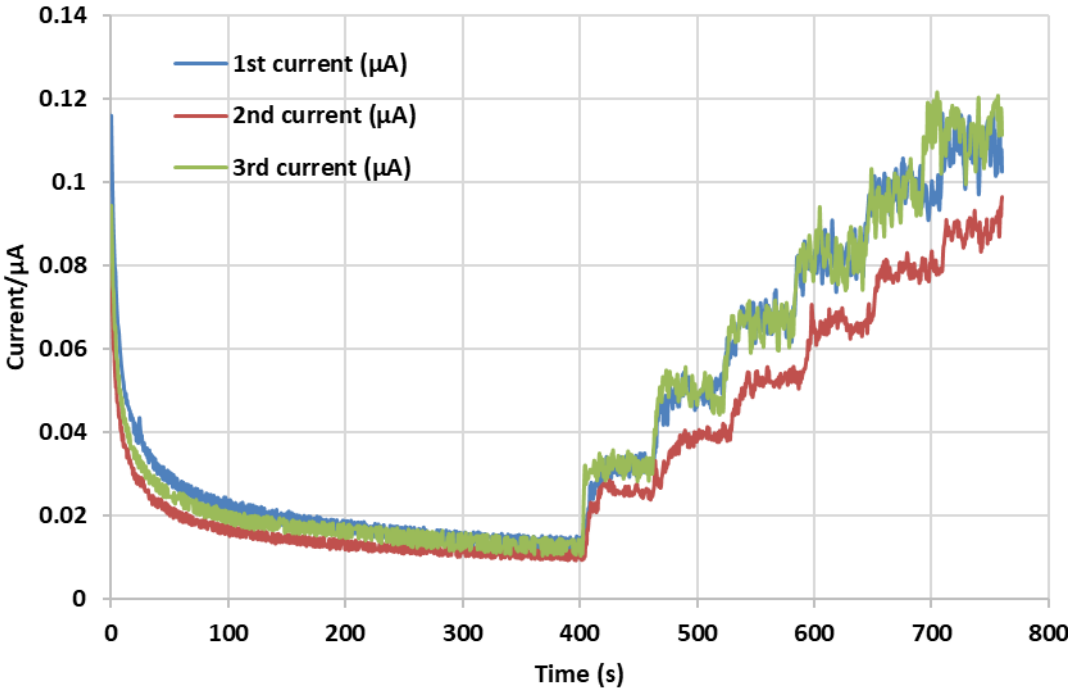

Figure E2. (A) Raw amperometric data for DES-NIP-CP without the application of smoothing or baseline correction. 1st current stands for the current from experiment one, the second stands for the current from experiment two, and the third stands for the current from experiment three.

Data analysis

Data cleaning and preprocessing

Data preprocessing and cleaning are essential components of data analysis to ensure that the data being used accurately represents the oxidation signal from E2 as possible, minimising the effects of noise and other artefacts. Figure 3.24 and the noise characteristics are depicted in Figure B2. It is crucial to highlight the data handling and interpretation process in electrochemical measurements. Raw data obtained from the electrochemical detection of estradiol, particularly at higher concentrations such as 4.98 µM (4.98×10^{-6} M), often exhibit variability

inherent to experimental procedures and measurement techniques. Processing this data is to represent the findings clearly and accurately.

The original raw data consists of the sensor's current response over time, including the actual signal of interest, noise, and potential baseline drifts, standard features in electrochemical measurements (Appendix B-C). Noise reduction techniques were utilised to mitigate environmental and instrumental noise, enhancing the signal-to-noise ratio. Outlier analysis is employed for careful examination and, where scientifically justified, excludes outliers from the dataset to ensure accuracy. Data averaging, using averaged values, presents a more stable and reliable representation of the sensor's response.

This included:

(1) Baseline correction, where a reference signal, typically the average current recorded before the introduction of the analyte, is subtracted from the raw data. The resulting baseline-corrected data demonstrates a more stable starting point, reducing the impact of any drift or systematic bias present in the original data. (2) Moving average was used to smooth the data. This smoothing technique reduces random noise by averaging each data point with neighbouring points without distorting the signal. The following text highlights the utility of the described method in enhancing the clarity of the response curve, particularly in regions exhibiting rapid changes in current. Additionally, the processed data, which has undergone baseline correction and smoothing, serves as the signal for subsequent analysis. This combined approach ensures a more accurate interpretation of the sensor's response, allowing for the distinction of variations resulting from changes in analyte concentration and fouling of the electrode from

confounding noise or instrumental variations. The comparison between the raw and processed data, as depicted in the accompanying figure, unequivocally demonstrates the effectiveness of these methods in isolating the accurate analytical signal from the measured data.

Use of Standard Deviations as Error Bars

Regarding the presentation of error bars, the standard error of the mean (SEM) is customary. To provide a more conservative estimate of the error stemming from the observed variability in three measurements, it was decided to utilise three standard deviations. This approach ensures that the error bars encompass most data points and spread comprehensively around the mean, thereby emphasising the consistency of repeated measurements and the reproducibility of experimental results in the face of noisy data and the application of the cleaning method. The believe is that the most effective way to present the data. Calculated standard error reflect the uncertainty surrounding mean estimates derived from the data. The standard deviation (SD) characterises the typical distance of an observation from the mean. In contrast, the standard Error of the Mean (SEM) estimates the precision with which the sample mean represents the population mean, computed as $SD/\sqrt{n}$.

The methodology adopted in this study involves performing measurements in triplicate for each concentration and using the standard deviation as the measure of error. This approach is based on the technical and in-depth discussion on standard deviation and standard error provided by Barde et al. [116], as well as the report by Ferrier et al. [60] on the use of standard deviation as error bars to show the variability of the data around the mean. The rationale behind using the

standard deviation as an error bar is to describe the variability within the triplicate measurements for each concentration point, with n=3.

The applied approach follows Barde et al.'s more technical and in-depth discussion on standard deviation and standard error [116]. Ferrier et al. reported using standard deviation as error bars to show the variability of the data around the mean [60] and other studies. Figure 3.22. Calibration plot of peak current versus concentration for CSSM/SPE, where error bars depict the standard deviation, representing the variability within triplicate measurements for each concentration point, n = 3.

The calibration plot of peak current versus concentration for CSSM/SPE in Figure 3.22 depicts the standard deviation as error bars, which indicates the variability within the triplicate measurements for each concentration point. The figure illustrates standard deviation as a measure of error in the study. As mentioned earlier, at 4.98 µM, the processed data means and standard deviations from the three measurements were used to ensure an acceptable signal-to-noise ratio. The compatibility between the visual agreement of the processed data and the noise observed in the raw data can be attributed to the methodological approach used to enhance signal clarity. At higher concentrations, such as 4.98 µM, the variance may be more significant due to the electrode response, the nature of the estradiol or both. One potential factor might be the processing of the data. The study's findings contribute to the incremental nature of science and can be further explored in future research. Contributions can be of various types, including conceptual, theoretical, empirical, and methodological, regardless of the magnitude of the study.

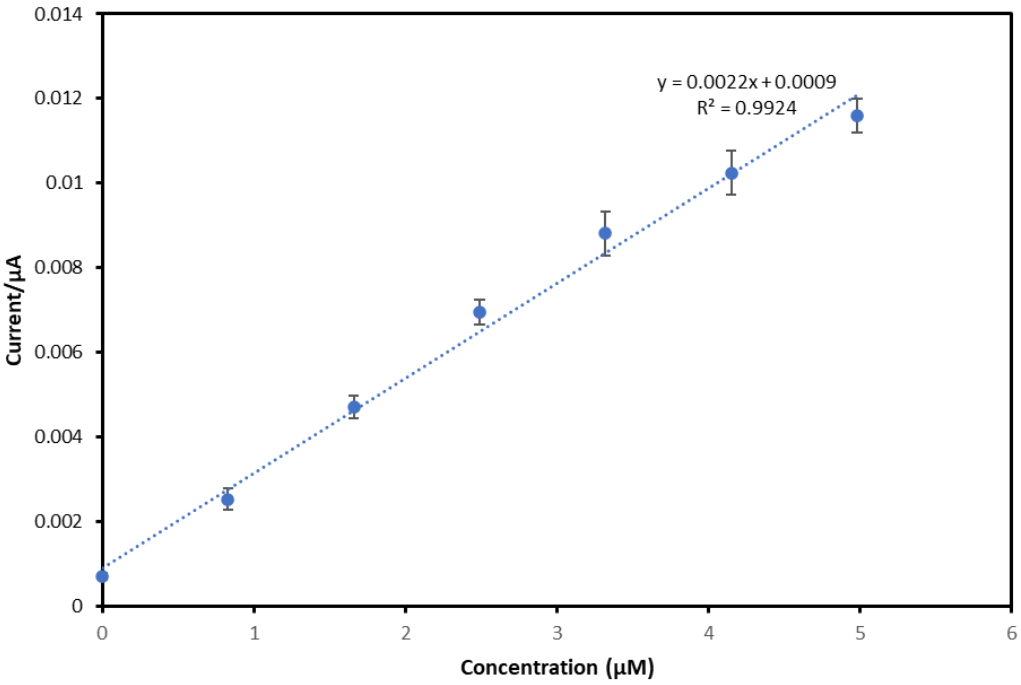

Figure E3. Shows the calibration plot of peak current vs concentration of CSSM/SPE. Error bars represent standard Error of the Mean (SEM), n = 3.

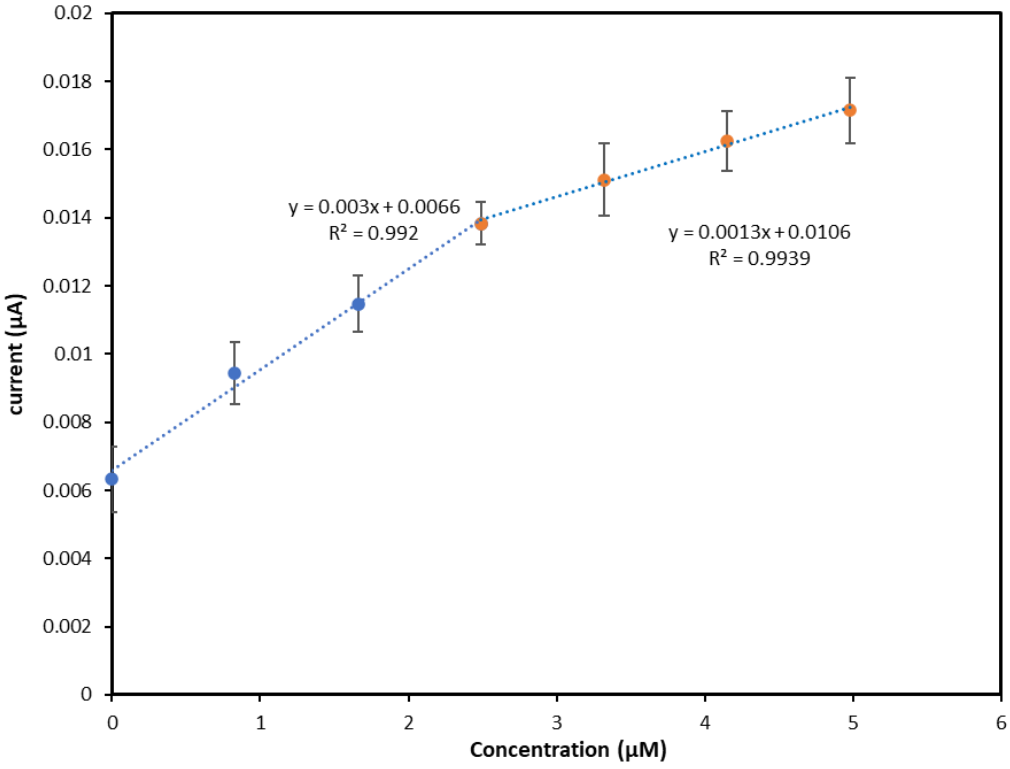

Figure E4 shows the calibration plot of peak current vs concentration of bare SPE. Error bars represent standard Error of the Mean (SEM), n = 3.

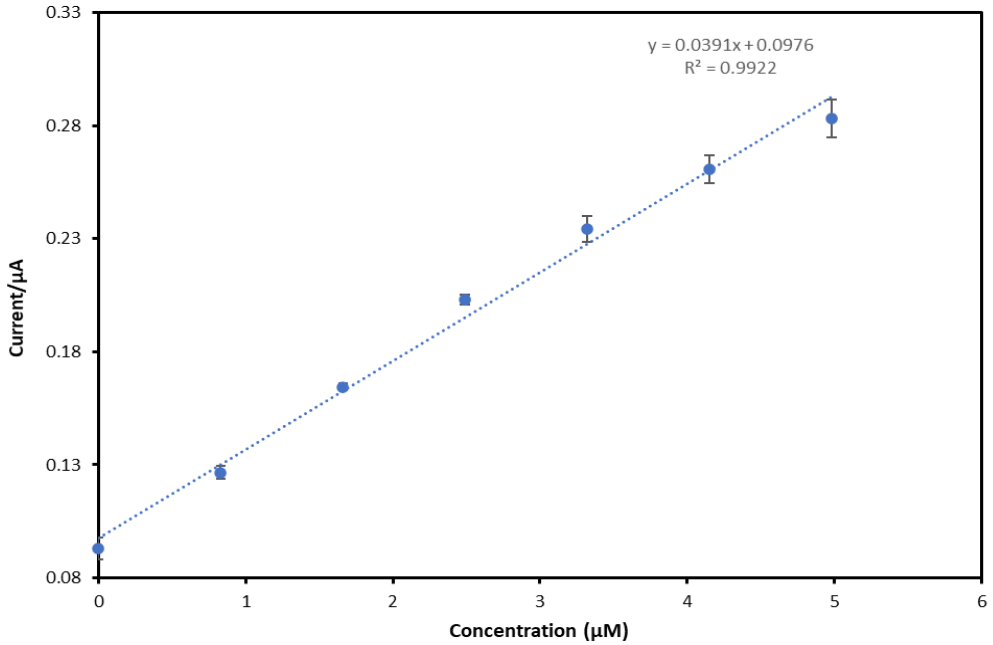

Figure E5. GHPSPE Calibration plot of the average of the current plateau (relative to baseline) against concentration. Error bars represent standard Error of the Mean (SEM), n = 3

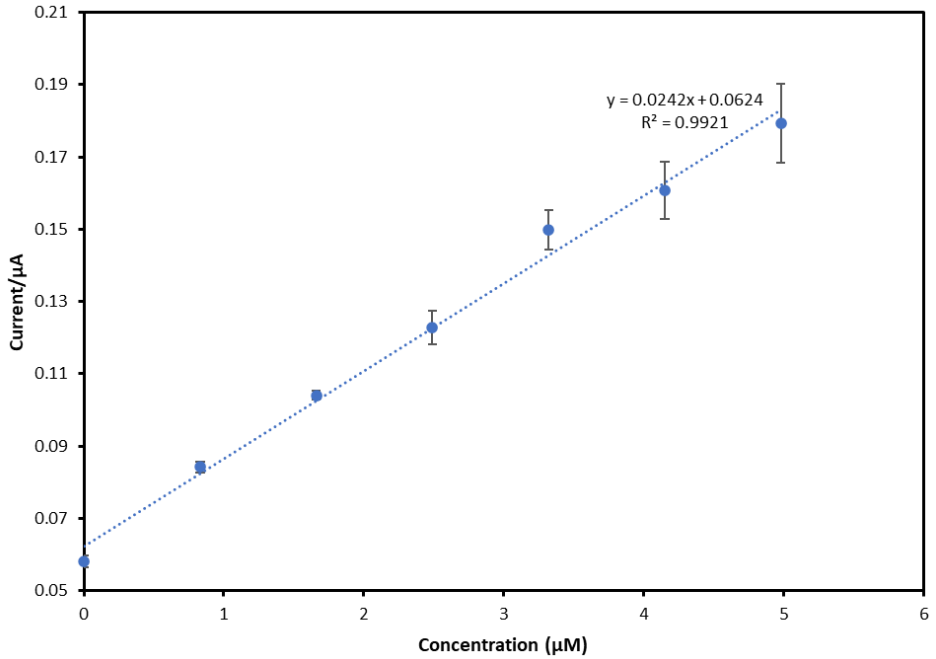

Figure E6. 3D-GFSPE Calibration plot of the average of the current plateau (relative to baseline) against concentration. Error bars represent standard Error of the Mean (SEM), n = 3.

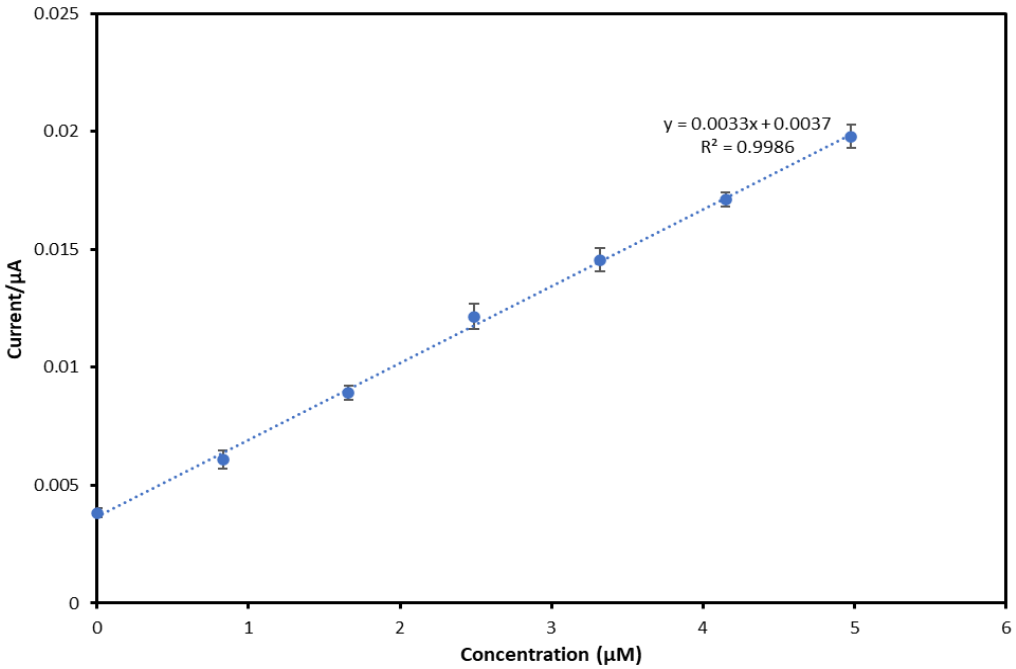

Figure E7. EEFGHSPE Calibration plot of average of the current plateau (relative to baseline) against concentration. Error bars represent standard Error of the Mean (SEM), n = 3.

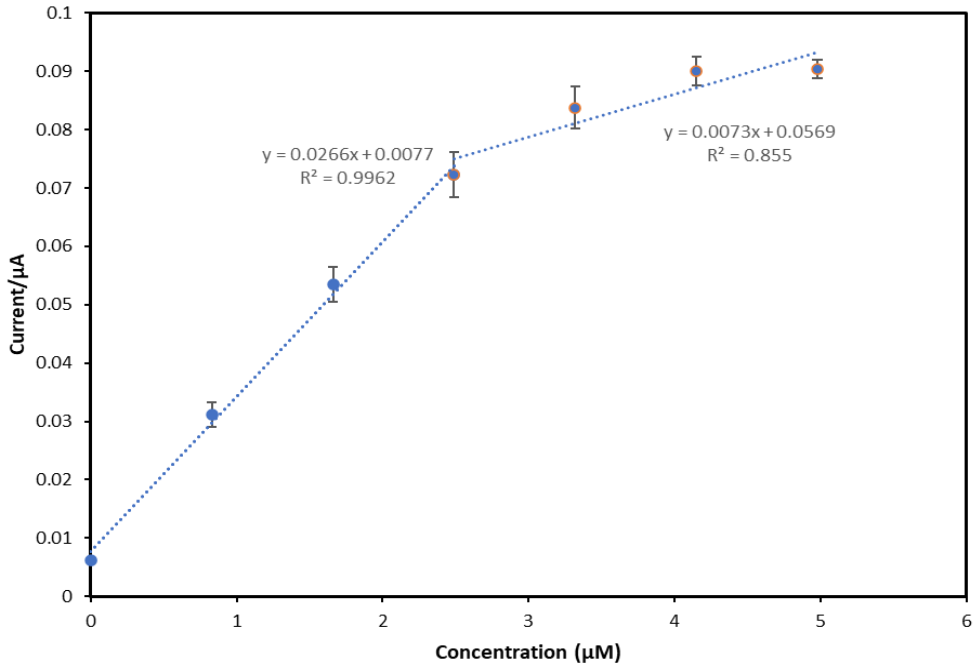

Figure E8. DES-MIP-CP Calibration plot of average of the current plateau (relative to baseline) against concentration. Error bars represent standard Error of the Mean (SEM), n = 3.

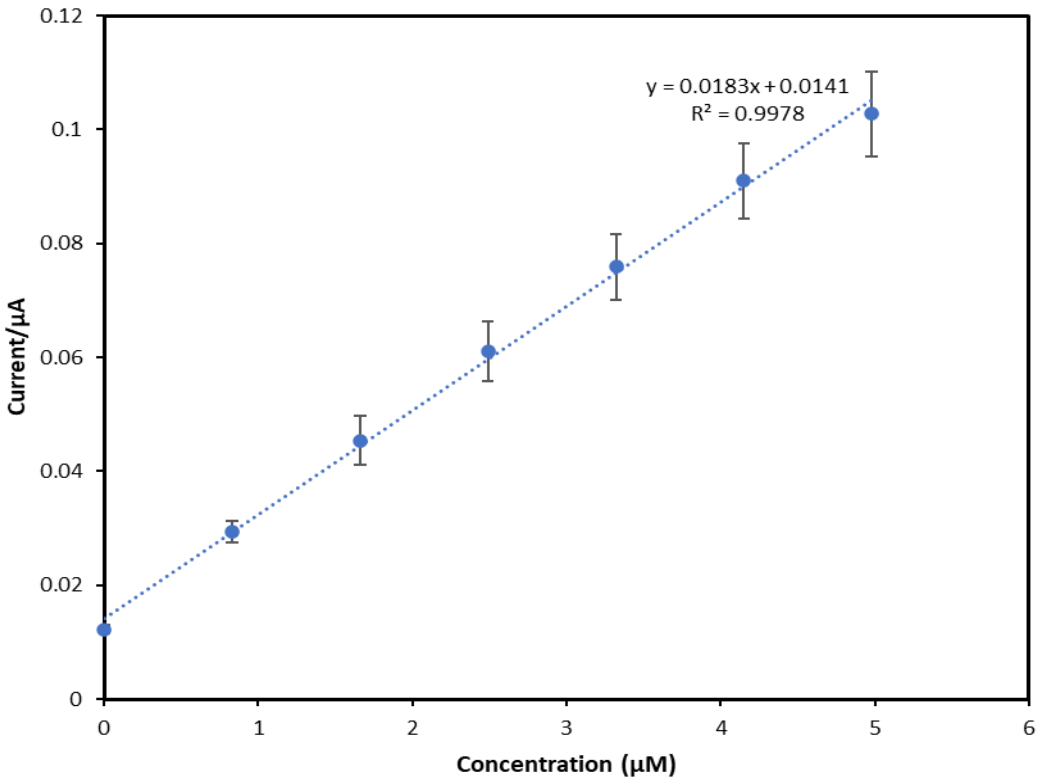

Figure E9. DES-NIP-CP Calibration plot of average of the current plateau (relative to baseline) against concentration. Error bars represent standard Error of the Mean (SEM), n = 3.